

Fifty years of research on the Madden-Julian Oscillation: recent progress, challenges and perspectives

Article

Accepted Version

Jiang, X., Adames, Á. F., Kim, D., Maloney, E. D., Lin, H., Kim, H., Zhang, C., DeMott, C. A. and Klingaman, N. P. ORCID: <https://orcid.org/0000-0002-2927-9303> (2020) Fifty years of research on the Madden-Julian Oscillation: recent progress, challenges and perspectives. *Journal of Geophysical Research: Atmospheres*, 125 (17). e2019JD030911. ISSN 2169-8996 doi: <https://doi.org/10.1029/2019JD030911> Available at <https://centaur.reading.ac.uk/91428/>

It is advisable to refer to the publisher's version if you intend to cite from the work. See [Guidance on citing](#).

To link to this article DOI: <http://dx.doi.org/10.1029/2019JD030911>

Publisher: American Geophysical Union

All outputs in CentAUR are protected by Intellectual Property Rights law, including copyright law. Copyright and IPR is retained by the creators or other copyright holders. Terms and conditions for use of this material are defined in the [End User Agreement](#).

www.reading.ac.uk/centaur

CentAUR

Central Archive at the University of Reading

Reading's research outputs online

1
2 Fifty Years of Research on the Madden-Julian Oscillation: Recent Progress,
3 Challenges, and Perspectives

4 Xianan Jiang^{1,2}, Ángel F. Adames³, Daehyun Kim⁴, Eric D. Maloney⁵, Hai Lin⁶,
5 Hyemi Kim⁷, Chidong Zhang⁸, Charlotte A. DeMott⁵, and Nicholas P. Klingaman⁹
6

7
8 ¹*Joint Institute for Regional Earth System Science & Engineering, University of California, Los*
9 *Angeles, California, USA*

10 ²*Jet Propulsion Laboratory, California Institute of Technology, Pasadena, California, USA*

11 ³*Department of Climate and Space Science and Engineering, University of Michigan, Ann Arbor,*
12 *Michigan, USA*

13 ⁴*Department of Atmospheric Sciences, University of Washington, Seattle, Washington, USA*

14 ⁵*Department of Atmospheric Science, Colorado State University, Fort Collins, Colorado, USA*

15 ⁶*Recherche en prévision numérique atmosphérique, Environment and Climate Change Canada,*
16 *Dorval, Canada*

17 ⁷*School of Marine and Atmospheric Sciences, Stony Brook University, Stony Brook, New York, USA*

18 ⁸*NOAA/Pacific Marine Environmental Laboratory, Seattle, Washington, USA*

19 ⁹*National Centre for Atmospheric Science and Department of Meteorology, University of Reading,*
20 *Reading, UK*

21
22
23
24 Special Collection on “*Grand Challenges in the Earth and Space Sciences*”
25 J. Geophysical Research - Atmosphere

26
27
28 Submitted 02/2020

29 Revised 06/2020

30
31
32
33
34
35

**Corresponding author address: Dr. Xianan Jiang, Jet Propulsion Laboratory, California Institute*
36 *of Technology, MS 233-300, 4800 Oak Grove Drive, Pasadena, CA 91109. Email:*
37 *xianan@ucla.edu. Copyright © 2020. All rights reserved.*
38

Abstract

Since its discovery in the early 1970s, the crucial role of the Madden-Julian Oscillation (MJO) in the global hydrological cycle and its tremendous influence on high-impact climate and weather extremes have been well recognized. The MJO also serves as a primary source of predictability for global Earth system variability on subseasonal time scales. The MJO remains poorly represented in our state-of-the-art climate and weather forecasting models, however. Moreover, despite the advances made in recent decades, theories for the MJO still disagree at a fundamental level. The problems of understanding and modeling the MJO have attracted significant interest from the research community. As a part of the AGU's Centennial collection, this article provides a review of recent progress, particularly over the last decade, in observational, modeling, and theoretical study of the MJO. A brief outlook for near-future MJO research directions is also provided.

Keywords: Madden-Julian Oscillation, tropical convection, climate modeling, seasonal-to-subseasonal prediction

63 1. Introduction

64 Motivated by the desire to explain the newly discovered Quasi-biennial Oscillation (QBO) in
65 the 1960s (*Reed et al.*, 1961), and particularly inspired by Taroh Matsuno’s seminal work on
66 analytical solutions of equatorial waves (*Matsuno*, 1966), Roland Madden and Paul Julian analyzed
67 10-year radiosonde observations collected from Canton Island to find evidence for equatorial
68 synoptic waves. What they found instead was an oscillatory signal in surface pressure and zonal
69 winds with mysterious periodicity of 30-60 days (*Madden and Julian*, 1971). In their follow-up
70 study that analyzed observations collected in 20 stations across the tropics, Madden and Julian
71 (1972) found that this 30-60 day oscillation is part of a slowly eastward propagating ($\sim 5 \text{ m s}^{-1}$),
72 planetary-scale phenomenon that features large-scale convective fluctuations and associated
73 vertically overturning circulation anomalies. This large-scale phenomenon is now widely known as
74 the Madden-Julian Oscillation (MJO; see *Lau and Waliser*, 2012 for details on historical MJO
75 research).

76 Since its discovery, the detailed structure and evolution of the MJO have been extensively
77 characterized, particularly by taking advantage of contemporary observations in recent decades,
78 including those from satellites, in-situ field experiments, and modern reanalysis datasets. For
79 example, as shown in Fig. 1, the recent high-resolution precipitation data from the Tropical Rainfall
80 Measuring Mission (TRMM) satellite provides excellent detail of the MJO’s horizontal structure
81 during its life cycle beyond that depicted by Madden and Julian (1972). These details include the
82 MJO’s asymmetry about the equator associated with the Inter-tropical Convergence Zone (ITCZ)
83 and South Pacific Convergence Zone (SPCZ), and strong disruptions by tropical land masses
84 including the Maritime Continent.

85 Meanwhile, the crucial role of the MJO in Earth’s hydrological cycle has been gradually
86 recognized by numerous studies subsequent to Madden and Julian’s pioneering work. Widespread
87 influences of the MJO on global climate and weather extremes have been documented (see
88 extensive reviews by *Lau and Waliser*, 2012; *Zhang*, 2013), including the onset and demise of
89 global monsoons (e.g., *Lau and Chan*, 1986; *Hendon and Liebmann*, 1990; *Webster et al.*, 1998;
90 *Sultan et al.*, 2003; *Jiang et al.*, 2004; *Wang*, 2006; *Lorenz and Hartmann*, 2006; *Wheeler et al.*,
91 2009; *Mo et al.*, 2012), the genesis and tracks of tropical cyclones (e.g., *Nakazawa*, 1988; *Mo*,
92 2000; *Higgins and Shi*, 2001; *Liebmann et al.*, 1994; *Maloney and Hartmann*, 2000; *Bessafi and*

93 *Wheeler, 2006; Aiyyer and Molinari, 2008; Klotzbach, 2010; Jiang et al., 2012*), the frequency of
94 extreme temperature and precipitation events (e.g., *Zhu et al., 2003; Bond and Vecchi, 2003; Jeong*
95 *et al., 2005; Park et al., 2010; Guan et al., 2012; Zheng et al., 2018; Lin et al., 2019b*), tornadoes
96 (*Tippett, 2018; Gensini et al., 2019*), polar sea ice (*Henderson et al., 2016; Lee and Seo, 2019*), and
97 chemical and biological components in the atmosphere and oceans (e.g., *Waliser et al., 2005; Tian*
98 *et al., 2007; Tian et al., 2011; Li et al., 2010*). The MJO also interacts with other prominent modes
99 of climate variability, including the El Niño / Southern Oscillation (ENSO; e.g., *Takayabu et al.,*
100 *1999; McPhaden, 1999; Kessler and Kleeman, 2000; Hendon et al., 2007*), Arctic Oscillation (AO;
101 *L'Heureux and Higgins, 2008*), North Atlantic Oscillation (NAO; *Cassou, 2008; Lin et al., 2009*),
102 and Indian Ocean Dipole (IOD; *Rao and Yamagata, 2004*). It has also been suggested that the
103 recent rapid warming over the Arctic, a.k.a., Arctic amplification, could be partially attributed to
104 the enhanced moisture transport and warm temperature advection by planetary Rossby waves that
105 are associated with the increase in the frequency of MJO convective activity over the Maritime
106 Continent (MC) and western Pacific (*Yoo et al., 2011; Lee et al., 2011; Yoo et al., 2012; Seo et al.,*
107 *2016*). The MJO influences sudden stratospheric warming events, which can distort or completely
108 reverse the stratospheric polar vortex, thus producing a negative phase of the Northern Annular
109 Mode (*Garfinkel et al., 2014; Garfinkel and Schwartz, 2017; Kang and Tziperman, 2017; 2018a; b*).

110 With its far-reaching impacts on global climate and weather patterns, and its quasi-periodic
111 occurrence on intraseasonal time scales, the MJO provides a primary source of predictability for
112 extended-range weather forecasts, and thereby fills the gap between deterministic weather forecasts
113 and climate prediction (e.g., *Waliser, 2012; Gottschalck et al., 2010; NAS, 2010; Vitart et al., 2012;*
114 *NASEM, 2016*). Motivated by recent coordinated community efforts that target enhancing accuracy
115 and socio-economic utility of seasonal-to-subseasonal (S2S) forecasts (e.g., *Vitart and Robertson,*
116 *2018*), great enthusiasm has developed for improving extended-range prediction of MJO-related
117 extreme weather activity (e.g., *Xiang et al., 2015a; Baggett et al., 2017; Jiang et al., 2018b; Baggett*
118 *et al., 2018; Lee et al., 2018; Mundhenk et al., 2018; Wang et al., 2018d; Lin, 2018; DeFlorio et*
119 *al., 2019; Xiang et al., 2020; Gensini et al., 2019*).

120 Despite its critical role in the global climate system, the MJO remains poorly represented in
121 recent generations of GCMs (*Hung et al., 2013; Jiang et al., 2015; Ahn et al., 2017; Ahn et al.,*
122 *2020b*; see the detailed review in Section 3.3). In the few GCMs that are able to capture the bulk

123 characteristics of the MJO, the reasons for their good MJO simulations are not well understood
124 (e.g., *Klingaman et al.*, 2015a). The improved MJO representation achieved by tuning GCM
125 parameters can occur at the expense of degrading the model mean state and other climate
126 phenomena (e.g., *Kim et al.*, 2011b; *Mapes and Neale*, 2011b). Meanwhile, MJO prediction skill
127 still remains limited in most climate and weather forecasting models (see Section 3.4), with a
128 typical skill of 3-5 weeks (e.g., *Seo et al.*, 2009; *Vitart and Molteni*, 2010; *Rashid et al.*, 2011;
129 *Wang et al.*, 2014; *Neena et al.*, 2014; *Kim et al.*, 2014c; *Xiang et al.*, 2015b; *Kim et al.*, 2018), in
130 contrast to its estimated intrinsic potential predictability of about 5-7 weeks (e.g., *Waliser et al.*,
131 2003; *Neena et al.*, 2014; *Ding et al.*, 2010).

132 The challenges in simulating and predicting the MJO create an urgent demand for improved
133 understanding of its fundamental physics. Since the call for intensified research on MJO physics
134 and dynamics at a Trieste workshop in 2006 (*ICTP*, 2006), the MJO has been a central focus of
135 multinational research projects endorsed by the World Weather Research Program (WWRP), the
136 World Climate Research Program (WCRP), and by International and US CLIVAR (Climate
137 Variability and Predictability) (see a review by *Zhang et al.*, 2013). These international efforts have
138 included the Intraseasonal Variability Hindcast Experiment (*Neena et al.*, 2014), the Year of
139 Tropical Convection (YOTC) virtual field campaign (*Waliser et al.*, 2012; *Moncrieff et al.*, 2012),
140 the Dynamics of the MJO (DYNAMO) field campaign over the Indian Ocean (*Yoneyama et al.*,
141 2013; see Section 3.1.1), the WCRP/WWRP YOTC MJO Task Force (MJOTF, now under the
142 Working Group on Numerical Experimentation, WGNE) and the Global Energy and Water
143 Exchanges (GEWEX) Atmospheric System Study (GASS) MJO model comparison project (*Petch*
144 *et al.*, 2011; *Klingaman et al.*, 2015a), the Subseasonal to Seasonal (S2S) Prediction Project (*Vitart*
145 *et al.*, 2012; 2017), the Years of the Maritime Continent (YMC) field campaign (see Section 3.6.3),
146 and the Subseasonal Experiment (SubX) (*Pegion et al.*, 2019). Meanwhile, to address specific
147 issues related to biases in MJO simulations and predictions, the MJOTF has promoted efforts to
148 develop advanced MJO process-oriented diagnostics (*Waliser et al.*, 2009; *Kim et al.*, 2009;
149 *Gottschalck et al.*, 2010; *Wheeler and Maloney*, 2013; see details in Sections 3.3 and 3.4).

150 Because of the extensive efforts in the weather and climate research community listed above,
151 recent decades have seen significant advances towards improved MJO understanding and
152 prediction, although continued efforts are still warranted as outlined in Section 4. The growing use

153 of models that employ cloud-permitting resolutions either in the form of the super-parameterization
154 (*Randall et al.*, 2003) or global cloud-resolving models (GCRMs; *Miura et al.*, 2007; *Miyakawa et*
155 *al.*, 2014) have provided powerful tools to understand MJO physics and act as a benchmark for
156 conventional GCM parameterization schemes. Theoretical understanding of the MJO has also been
157 significantly advanced in recent decades. In particular, moisture mode theory (*Neelin and Yu*, 1994;
158 *Raymond and Fuchs*, 2009; *Sobel and Maloney*, 2013; *Adames and Kim*, 2016) has provided critical
159 insights into key processes regulating MJO variability in observations and simulations of current
160 and future climate (*Kim et al.*, 2014a; *Kim et al.*, 2017; *Gonzalez and Jiang*, 2019; *DeMott et al.*,
161 2018; *Jiang et al.*, 2018a; *Adames et al.*, 2017a; *Maloney et al.*, 2019a; *Rushley et al.*, 2019) and
162 processes responsible for model deficiencies in simulating and predicting the MJO (*Jiang*, 2017;
163 *Gonzalez and Jiang*, 2017; *Kim*, 2017; *Lim et al.*, 2018; *DeMott et al.*, 2019). New observations
164 from recent in-situ field experiments have meanwhile provided an unprecedented opportunity to
165 document key processes during an MJO life cycle (e.g., *Yoneyama et al.*, 2013). The recently
166 identified strong connection between the MJO and QBO has also inspired great interest in exploring
167 the role of stratosphere-troposphere interactions in shaping the year-to-year variability of MJO
168 activity (e.g., *Yoo and Son*, 2016; *Son et al.*, 2017; *Zhang and Zhang*, 2018).

169 Much of the earlier research on the MJO has been summarized in detail by several previous
170 review articles or books, including *Madden and Julian* (1994), *Zhang* (2005), and *Lau and Waliser*
171 (2012). This article provides a comprehensive review of recent progress on MJO research as a part
172 of the AGU's Centennial collection, motivated by the aforementioned recent exciting developments
173 in MJO research. We mainly focus on progress achieved in the years following those previous
174 reviews, although some important aspects of MJO research earlier in time are included for
175 completeness. In Section 2, several scientific issues related to the essential physics of the MJO are
176 briefly discussed, which provides background for detailed discussion in the following sections.
177 Major progress made over the most recent decade is reviewed in Section 3, including that related to
178 MJO observations (3.1), theoretical understanding (3.2), modeling (3.3), prediction (3.4), air-sea
179 interactions (3.5), MC interactions (3.6), tropical-extratropical interactions (3.7), QBO connections
180 (3.8), and changes under a future climate (3.9). An outlook for future MJO studies is presented in
181 Section 4. A brief summary is given in Section 5.

182 **2. Scientific issues of the MJO**

183 Based on numerous observational studies of MJO structure and evolution, a typical longitude-
184 height profile of the MJO is given by the schematic in Fig. 2 from Kiladis et al. (2009). Vigorous
185 deep convective clouds, enhanced column moisture, and strong upward motion and overturning
186 circulations prevail near the MJO convection center. The region to the east of MJO convection is
187 characterized by enhanced lower-tropospheric moisture anomalies (e.g., *Kemball-Cook and Weare,*
188 *2001; Sperber, 2003; Kiladis et al., 2005; Tian et al., 2010; Johnson and Ciesielski, 2013*), warm
189 sea surface temperature (SST; *Hendon and Glick, 1997; Woolnough et al., 2000; Shinoda et al.,*
190 *1998*), boundary layer (BL) convergence (*Sperber, 2003; Kiladis et al., 2005*), and a bottom-heavy
191 heating structure (e.g., *Lin et al., 2004; Kiladis et al., 2005; Jiang et al., 2011*) dominated by
192 shallow cumuli/congestus clouds (*Johnson et al., 1999; Kikuchi and Takayabu, 2004; Chen and Del*
193 *Genio, 2009b; Tromeur and Rossow, 2010; Powell and Houze, 2013; Xu and Rutledge, 2014*),
194 characteristic of free tropospheric moistening that supports MJO eastward propagation. To the west
195 of MJO convection can be found extensive trailing stratiform-type clouds (*Lin et al., 2004; Kiladis*
196 *et al., 2005*) that interact with atmospheric radiation (*Del Genio and Chen, 2015; Kim et al., 2015*)
197 and enhanced low-level westerly winds that amplify surface turbulent fluxes (*Hendon and Glick,*
198 *1997*). Precipitation from these upper-tropospheric stratiform clouds fall through relatively dry
199 lower levels, cooling the environment through evaporation, leading to a vertical dipole stratiform
200 heating structure, i.e., heating in the upper troposphere and cooling in the lower troposphere (e.g.,
201 *Lin et al., 2004; Benedict and Randall, 2007*).

202 The prominent east-west asymmetry in dynamic and thermodynamic fields of the observed
203 MJO has been one of the key constraints in the development of MJO theories. The fact that the
204 MJO does not appear in the solutions of the dry shallow-water system on an equatorial beta-plane
205 linearized about a resting atmosphere (e.g., *Wheeler and Kiladis, 1999*) has led to the hypothesis
206 that incorporating moisture and its interactions with convection and large-scale dynamics and/or
207 nonlinear interaction among multi-scale waves are key to MJO dynamics. In the following sections,
208 several critical processes associated with the MJO are briefly outlined, which serve as background
209 for the detailed reviews on various MJO aspects in Section 3.

210 ***2.1 Moisture-convection feedback***

211 Observational studies indicate that organized convection over tropical oceans exhibits great
212 sensitivity to tropospheric humidity. In a dry environment, a rising convective parcel can lose its

213 buoyancy quickly due to dilution by turbulent entrainment and resulting evaporative cooling within
214 the parcel, limiting the depth of convective penetration, and favoring shallow cumuli. As a result,
215 heavy area-averaged rainfall associated with oceanic deep convection mostly occurs in moist
216 environments as shown in Fig. 3 (*Bretherton et al., 2004; Peters and Neelin, 2006; Thayer-Calder*
217 *and Randall, 2009; Adames, 2017; Rushley et al., 2018; Kuo et al., 2019*). A particularly strong
218 coupling between moisture and convection is observed for MJO wavenumbers and frequencies
219 (*Yasunaga and Mapes, 2012*), illuminating the crucial role of the convection-moisture feedbacks
220 for the MJO. For example, one measure of convective sensitivity to atmospheric moisture, the
221 convective moisture adjustment time scale, defined as the time it takes for convection to remove a
222 given moisture perturbation (*Bretherton et al., 2004; Sobel and Maloney, 2012*), is highly related to
223 MJO rainfall variability (*Jiang et al., 2016; Adames, 2017*).

224 As shown in Fig. 2, shallow cumulus clouds are prevalent prior to the development of deep
225 MJO convection. These shallow cumuli moisten the atmosphere through detrainment and rain
226 evaporation as well as associated BL convergence, generating a more humid atmosphere that favors
227 the development of deeper convective elements. This recharging process for tropospheric moisture
228 gradually moistens the atmosphere column and favors onset of the deep convective phase of the
229 MJO. Precipitation and compensating convective and mesoscale downdrafts accompany the drying
230 phase of the MJO leading to the suppressed MJO phase. Replicating the interactions between
231 environmental moisture and convection has proven challenging for convection parameterization
232 schemes (e.g., *Derbyshire et al., 2004; Del Genio, 2012; Kim et al., 2014b*). In many GCMs,
233 ubiquitous deep convection still occurs even when the column is relatively dry (*Del Genio et al.,*
234 *2012; Thayer-Calder and Randall, 2009; Rushley et al., 2018*). Therefore, the MJO moistening
235 phase during the shallow-to-deep convective transition is not well depicted, which can lead to a
236 weak model MJO. Indeed, MJO simulations have been improved in many modeling studies by
237 increasing the sensitivity of convection to environmental moisture (see Section 3.3), suggesting that
238 moisture-convection coupling during the transition phase is critical to the MJO.

239 ***2.2 Convection-circulation feedback and the gross moist stability***

240 A growing body of evidence supports the “moisture mode” paradigm of the MJO (see detailed
241 review in Section 3.2), in which MJO convection is tightly coupled to column moisture and the
242 variability of convection is largely regulated by processes that control the variability of column-

243 integrated moisture or moist static energy (MSE). Diagnosis of processes regulating column MSE
244 anomalies have thus been widely applied for understanding the essential physics regulating MJO
245 amplitude and propagation.

246 The MSE budget of the MJO in observations and model simulations suggests that feedbacks
247 between MJO convection and large-scale circulation anomalies play a crucial role for MJO stability
248 and propagation. From the moisture mode perspective, a dominant process regulating MJO
249 eastward propagation is through the horizontal advection of the background lower-tropospheric
250 MSE by the anomalous MJO circulation, which exhibits an east-west asymmetry about MJO
251 convection center associated with a Kelvin wave response to the east and Rossby wave response to
252 the west of MJO convection (*Wang and Li, 1994; Hendon and Salby, 1994; Wang et al., 2018a*).
253 Horizontal MSE advection leads to the build-up of MSE to the east of MJO deep convection and
254 decrease to the west, thus promoting the eastward propagation of the MJO (e.g., *Maloney, 2009;*
255 *Maloney et al., 2010; Andersen and Kuang, 2012; Kim et al., 2014; Sobel et al., 2014; Chikira,*
256 *2014; Adames and Wallace, 2015; Arnold et al., 2015; Jiang, 2017; Gonzalez and Jiang, 2019*).

257 Since a typical profile of mean MSE in the tropics is characterized by a minimum in the mid-
258 troposphere, anomalous low-level convergence and mid-level divergence associated with shallow
259 and congestus clouds to the east of MJO deep convection import high MSE air at low levels, and
260 export low MSE air at mid-levels. This is reflected in a net import of moisture, under which the
261 column MSE will grow and convection will intensify in time. Meanwhile, a top-heavy stratiform
262 heating to the west of MJO deep convection induces a circulation that tends to export MSE, thus
263 effectively drying the column and weakening MJO convection (*Raymond et al., 2009*). The
264 transition from shallow / congestus clouds to deep clouds and then to stratiform clouds as shown in
265 Fig. 2, could therefore also be critical in moistening and supporting convection to the east of the
266 MJO convective center, and drying and suppressing convection to the west, thus promoting the
267 eastward propagation of MJO convection (e.g., *Hsu and Li, 2012; Sobel et al., 2014; Yokoi and*
268 *Sobel, 2015; Wang et al., 2017; Inoue and Back, 2015b*).

269 The efficiency of the large-scale circulation in exporting MSE from a convecting column can
270 be diagnosed with a metric known as the gross moist stability (GMS) (*Neelin and Held, 1987;*
271 *Raymond et al., 2009*), defined as column MSE export through vertical and/or horizontal MSE
272 advection per unit convective activity, and can be used as a metric for MJO instability. It is

273 hypothesized that the GMS should be small or negative in order to sustain strong MJO convection
274 (*Raymond and Fuchs, 2009; Raymond et al., 2009; Hannah and Maloney, 2011; Sobel and*
275 *Maloney, 2012; Benedict et al., 2014; Inoue and Back, 2015a*).

276 **2.3 Cloud-radiation feedbacks**

277 The critical role for cloud-radiative feedbacks to the MJO is now widely recognized (e.g.,
278 *Raymond, 2001; Lee et al., 2001; Sobel and Gildor, 2003; Stephens et al., 2004; Bony et al., 2015;*
279 *Kim et al., 2015*). Reduced column radiative cooling (a positive heating anomaly) dominated by
280 long-wave radiative effects due to increased cloudiness and moisture during periods of active MJO
281 convection (*Lin and Mapes, 2004; Jiang et al., 2011; Ma and Kuang, 2011; Del Genio and Chen,*
282 *2015; Ciesielski et al., 2017*) is considered to be an important anomalous MSE source for
283 destabilizing MJO convection (*Andersen and Kuang, 2012; Arnold and Randall, 2015; Jiang,*
284 *2017*). Even when the GMS is weakly positive by the aforementioned convection-circulation
285 feedback, the MJO can still be destabilized by anomalous column radiative heating, which
286 generates a negative effective GMS (*Sobel and Maloney, 2013; Hannah and Maloney, 2014;*
287 *Adames and Kim, 2016*).

288 Associated with the shallow-to-deep convective transition during an MJO life cycle, a vertical
289 tilting structure in radiative heating is also observed, largely associated with the water vapor effects
290 (*Ciesielski et al., 2017*). While the maximum radiative heating associated with the MJO slightly
291 lags peak MJO convection (*Jiang et al., 2011; Kim et al., 2015; Ciesielski et al., 2017*), various
292 observational and modeling studies report that the column-integrated radiation enhances the
293 convective heating in the context of total apparent heating anomalies by 15-25% (e.g., *Lee et al.,*
294 *2001; Lin and Mapes, 2004; Jiang et al., 2011; Andersen and Kuang, 2012; Johnson et al., 2015;*
295 *Ciesielski et al., 2017*). In the stratiform region, with warm anomalies in the upper-troposphere and
296 cold anomalies in the lower-troposphere, strong top-heavy radiative heating may also destabilize
297 the MJO by the stratiform instability mechanism (*Mapes, 2000; Khouider and Majda, 2006; Kuang,*
298 *2008; Seo and Wang, 2010; Del Genio and Chen, 2015*). The critical role of convection-radiative
299 feedbacks to the MJO will be discussed in detail in Sections 3.2 and 3.3.

300 **2.4 Multi-scale interactions of the MJO**

301 The MJO convective envelope consists of multi-scale elements (e.g., *Nakazawa, 1988;*
302 *Hendon and Liebmann, 1994; Kiladis et al., 2009*), with scales ranging from mesoscale convective

303 systems (MCSs) to synoptic scale waves, with the latter often referred to as the convectively
304 coupled equatorial waves (CCEWs). Figure 4 illustrates the multi-scale structure of convective
305 activity along the equator associated with two MJO events during the 2018/2019 winter. This
306 multiscale structure includes embedded fast eastward-propagating moist Kelvin waves and
307 associated 2-day westward-propagating inertio-gravity waves (Takayabu, 1994; Liebmann et al.,
308 1997; Haertel and Kiladis, 2004; *Hendon and Liebmann*, 1994; Chen and Houze, 1997), westward
309 propagating Mixed Rossby-Gravity waves that are particularly active over the western Pacific, and
310 diurnally-migrating convective signals originated over the MC region (e.g., *Yang and Slingo*,
311 2001a; *Love et al.*, 2011).

312 The dynamical structures and cloud morphology of the MCSs and CCEWs display a large
313 degree of self-similarity to the MJO (Fig. 2), with shallow convection at their leading edge,
314 followed by deep convection and then stratiform precipitation (*Mapes et al.*, 2006; *Kiladis et al.*,
315 2009). Due to these vertical tilting structures, in addition to their contribution to convective heating
316 on the MJO (*Tao et al.*, 2016), these organized MCSs and CCEWs within the MJO envelope affect
317 the MJO circulation through upscale transport of momentum (Moncrieff, 1992; Majda and Biello,
318 2004; Biello and Majda, 2005; *Majda and Stechmann*, 2009; *Tung and Yanai*, 2002a; b; Houze et
319 al., 2000; Khouider et al., 2012; Wang and Liu, 2011; Miyakawa et al., 2014; *Oh et al.*, 2015a; *Oh*
320 *et al.*, 2015b). The MJO-associated anomalous circulation can also regulate MCS and CCEW
321 activities by favoring particular types of convective systems and propagation directions (e.g.,
322 *Straub and Kiladis*, 2003; *Masunaga et al.*, 2006; *Majda and Stechmann*, 2009; 2012; *Han and*
323 *Khouider*, 2010; *Guo et al.*, 2014), although the underlying mechanisms are not fully understood.
324 This feedback represents a two-way interaction between small-scale convective elements and the
325 MJO.

326 Diagnosis based on reanalysis products and models reveal that organized synoptic eddies
327 contribute to MJO eastward propagation through anomalous moistening to the east and drying to
328 the west of MJO convection (e.g., Maloney, 2009; Andersen and Kuang, 2012; Benedict et al.,
329 2015; Jiang, 2017). The moistening and drying are largely considered to be driven by anomalous
330 poleward moisture transport by synoptic eddies. To the east of MJO convection, synoptic eddy
331 activity tends to be reduced within anomalous MJO easterlies possibly through the barotropic
332 kinetic energy conversion processes (Maloney and Hartmann 2001; Maloney and Dickinson 2003;

333 *Andersen and Kuang, 2012*). This reduction in eddy activity suppresses the entrainment of dry air
334 into the Tropics by these eddies, representing an anomalous moistening. However, further
335 investigation is needed to fully understand the importance of synoptic eddies to the MJO.

336 Lastly, the build-up of moisture during the MJO preconditioning phase is often accompanied
337 by the emergence of an early-afternoon secondary peak in the diurnal cycle of oceanic convection
338 (e.g., *Ruppert and Johnson, 2015*). The early afternoon peak is thought to arise from a reduction of
339 convective inhibition due to enhanced heat and moisture fluxes in response to oceanic diurnal warm
340 layers (*Bernie et al., 2005; Bellenger and Duvel, 2009; Moum et al., 2014a; Ruppert and Johnson,*
341 *2015; Section 3.5*). The diurnal cycle over MC islands is also considered important for the so-called
342 “barrier” effect of the MC on MJO propagation (*Section 3.6*).

343 **3. Recent progress in understanding, modeling, and predicting the MJO**

344 **3.1 Observation of key MJO processes**

345 *3.1.1 Recent results from in situ observations*

346 In situ observations help advance our fundamental understanding of the MJO. Our ability of
347 numerically simulating and predicting the MJO critically depends on our knowledge of detailed
348 physical processes that can be gained only through in situ observations. Sustained observing
349 systems, such as the tropical mooring arrays in the Pacific and Indian Ocean (*Hayes et al., 1991*)
350 and the Department of Energy Atmospheric Radiation Measurement (ARM) Program tropical sites
351 at Manus and Nauru (*Long et al., 2013*), have provided large samples for robust statistics. Special
352 field campaigns provided comprehensive in situ observations for the MJO study. The Tropical
353 Ocean Global Atmosphere Coupled Ocean-Atmosphere Response Experiment (TOGA COARE,
354 *Webster and Lukas, 1992*) covered for the first time several MJO events in the equatorial western
355 Pacific. Dynamics of the MJO (DYNAMO), designed specifically for the study of MJO initiation
356 over the Indian Ocean (*Yoneyama et al., 2013*), covered three MJO events (*Gottschalck et al.,*
357 *2013*). (Note the DYNAMO field campaign was joined by three other projects: The Cooperative
358 Indian Ocean Experiment on Intraseasonal Variability in the Year 2011, the ARM MJO
359 Investigation Experiment, and the Littoral Air-Sea Process). YMC is a multi-year project with
360 broad scientific scopes related to the Indo-Pacific MC, and will be discussed in Section 3.6.

361 Results from most studies on the MJO using in situ observations from TOGA COARE and the
362 tropical mooring arrays were summarized by *Zhang (2005)* and *Demott et al (2015)*. The following

363 discussions cover physical processes related to the MJO gained from in situ observations of the
364 ARM tropical sites and DYNAMO.

365 The new capability of advanced polarimetric radars can detect hydrometeor distributions within
366 clouds. The radar observations made during DYNAMO were used to document the characteristics
367 of cloud hydrometers at certain stages of the MJO: graupel near the melting level (~5 km) in
368 actively convective towers, dry aggregates between 7-9 km increasing as convective clouds deepen,
369 wet aggregates almost exclusively in the stratiform regions of MCSs, and small ice particles at
370 altitudes of 9-10 km (*Barnes and Houze, 2014; Rowe and Houze, 2015*). Drop size distribution
371 spectra of liquid water content and median diameter are distinct between convective and stratiform
372 regions (*Thompson et al., 2015*). These hydrometeor distributions can be related to lightning
373 frequencies of the MJO (*Stolz et al., 2017*).

374 Radar observations of shallow clouds in conjunction with sounding observations have led to
375 several new discoveries. During suppressed periods of the MJO, shallow convective clouds first
376 moisten the environment (*Bellenger et al., 2015b*). Once they start to precipitate, small cold pools
377 form below the showers, and as the suppressed environment gained moisture, clouds are able to
378 grow, with the deepest precipitating clouds occurring in clusters at intersections of cold pool
379 boundaries by afternoon (*Rowe and Houze, 2015*). From the suppressed to pre-onset stage of the
380 MJO as lower-tropospheric moisture increases, shallow/isolated convection undergoes remarkable
381 growth (*Xu and Rutledge, 2014*). They produce about 30% of all rain events and 15% of total rain
382 volume in the warm pool (*Thompson et al., 2015*) because they exist in all phases of the MJO and
383 non-MJO periods (*Zermeño-Díaz et al., 2015*). Over the Indian Ocean, the contribution from
384 shallow convection to total precipitation is larger in the ITCZ south of the equator than in the
385 equatorial region where MJO deep convection is more prominent (*Xu et al., 2015*).

386 During the transition from pre-convective initiation to initiation stages of the MJO, the
387 oceanic diurnal warm layer drives a daytime increase of the air-sea fluxes of heat and moisture. In
388 consequence, a daytime growth of cumulus clouds in both depth and areal coverage invigorates
389 convective clouds and cumulus moistening each day leading to convective initiation of the MJO
390 (*Ruppert and Johnson, 2015*). This shallow-to-deep convective transition can take place within a
391 wide range of 2–20 days (*Xu and Rutledge, 2016*). During the transition, sub-MCS rainfall fraction
392 declines from its maximum as MCS precipitation increases (*Xu and Rutledge, 2015*). The transition

393 from shallow, non-precipitating cumulus before initiation, to increasing cumulus congestus, then
394 deep convection during the initiation, to later stratiform precipitation can be consistently seen from
395 the evolution in apparent heat sources and sinks derived from sounding observations (*Johnson et*
396 *al.*, 2015). A reduction in vertical wind shear and enhanced low-level convergence induced by the
397 equatorial low-pressure system can lead to an explosive large MCS during MJO initiation (*Judt and*
398 *Chen*, 2014).

399 During rain events of 2-4 days after convective initiation, cloud evolutions follow the same
400 pattern, from shallow convection to deep convection, then wide convective systems with maximum
401 rainfall followed by broad stratiform clouds (*Zuluaga and Houze*, 2013). The cloud radiative
402 forcing, was approximately 20% of the column-integrated convective heating (*Johnson and*
403 *Ciesielski*, 2013). MCSs over the Indian Ocean were linearly organized more parallel to the low-
404 level shear with weaker but deeper updrafts and weaker cold pools than over the western Pacific
405 (*Guy and Jorgensen*, 2014). The number of cold pools, and their contribution to BL heat and
406 moisture, nearly double after convective initiation of the MJO (*de Szoeke et al.*, 2017).

407 The contrast between tropical moist air and extratropical dry air observed by aircraft
408 dropsonde data is much sharper than those in any other data (*Chen et al.*, 2016). Such contrast is a
409 result of synoptic-scale dry air intrusion from the extratropics, which can be instrumental to
410 convective initiation of the MJO (*Kerns and Chen*, 2014). At the convective initiation stage of the
411 MJO, the lower-tropospheric moistening by shallow convection is accompanied by advection as
412 low-level wind switch from westerlies to easterlies (*Sobel et al.*, 2014). After the initiation, low-
413 level dry advection by off-equatorial cyclonic gyres may act to push MJO convection moving
414 eastward (*Kerns and Chen*, 2014). Rapid increases in areal coverage of precipitating radar echo,
415 convective echo-top height, and tropospheric humidity above 850 hPa can happen over 3-7 days
416 close to MJO initiation before low-tropospheric moistening (*Powell and Houze*, 2013). Upper-
417 tropospheric moisture increases as large-scale subsidence is reduced in association with eastward
418 circumnavigating dry planetary perturbations (*Powell and Houze*, 2015). Moisture variability can
419 also be instigated by Mixed Rossby Gravity waves (*Muraleedharan et al.*, 2015) that may origin
420 from the MC (*Kubota et al.*, 2015) and Kelvin waves (*DePasquale et al.*, 2014).

421 Using sounding data to observe atmospheric BL variability, especially that of turbulence, is
422 very difficult because of uncertainties in estimating key parameters such as the eddy diffusivity

423 coefficient (*Bellenger et al.*, 2015a). Limited high-quality turbulence measurement has shed new
424 lights on interactions between the BL and troposphere. Entrainment and downdraft fluxes export
425 equal shares of moisture from the BL to the lower troposphere before MJO initiation; downdraft
426 fluxes are found to increase by 50% and entrainment to decrease after the initiation (*de Szoeko*,
427 2018).

428 Fluctuations in air-sea heat fluxes associated with the MJO are insufficient to supply needed
429 moisture for MJO convection after its initiation (*de Szoeko et al.*, 2015). They can be induced by, in
430 addition to large-scale wind, perturbations in surface air temperature and local wind associated with
431 convective cold pools (*Yokoi et al.*, 2014) and synoptic perturbations, such as Kelvin waves
432 (*Baranowski et al.*, 2016). An unanticipated consequence of air-sea interaction associated with the
433 MJO over the equatorial Indian Ocean is the transition from dominant BL aerosol of industrial
434 carbon-based fine particles prior to MJO initiation to coarse particles of sea spray after initiation
435 (*DeWitt et al.*, 2013).

436 Before MJO initiation, a diurnal warm layer of about 4-5 m deep forms in days of low wind
437 ($< 6\text{ms}^{-1}$) and high solar radiation flux ($> 80\text{Wm}^{-2}$), with their amplitude in SST perturbations
438 greater than 0.8°C in the afternoon (*Matthews et al.*, 2014). Stratification caused by penetrating
439 solar radiation initiates a decrease in turbulence dissipation rates by two orders of magnitude over
440 1–2 hours immediately after sunrise, leading to the change in net surface heat flux from cooling to
441 warming (*Moulin et al.*, 2018). The entire mixed layer temperature also increases, as net surface
442 warming becomes larger than turbulent cooling at the bottom (*Pujiana et al.*, 2018). The strength of
443 a barrier layer can be measured by its potential energy, which is defined by the thickness of the
444 barrier layer, the thickness of the surface mixed layer, and the density stratification across the
445 isothermal layer (*Chi et al.*, 2014).

446 Ocean turbulence measurement has brought new perspectives to MJO air-sea interaction
447 (*Moum et al.*, 2014b; *Pujiana et al.*, 2015; *Moum et al.*, 2016; *Pujiana et al.*, 2018). Over the Indian
448 Ocean, the Yoshida-Wyrtki Jet at the equator accelerates from less than 0.5 m s^{-1} to more than 1.5
449 m s^{-1} in 2 days because of surface westerlies after MJO initiation. The jet energizes shear-driven
450 entrainment at its base near the 100 m depth and advects salty water from the west. Subsurface
451 mixing is sufficient to increase the mixed layer salinity, despite heavy precipitation after MJO
452 initiation, by entraining salty water from the pycnocline. The turbulent salt flux across the mixed

453 layer base is, on average, 2 times as large as the surface salt flux. Subsurface turbulent heat fluxes
454 related to the surface jet are comparable to atmospheric surface fluxes. The related turbulent stress,
455 roughly 65% of the mean surface wind stress, is responsible for decelerating the jet. Nevertheless,
456 the jet is able to sustain itself and its subsurface mixing continues reducing the heat content in the
457 mixed layer by an amount significantly greater than atmospheric surface cooling for several weeks
458 after an MJO event moves out of the region to the east. The resulting cooler upper ocean might
459 affect initiation of the next MJO event.

460 These individual studies provided detailed perspectives of physical processes during MJO
461 initiation using observations from different instruments. Some of these processes may be found
462 during transitions from convectively suppressed to active periods for the mature MJO, others are
463 unique to MJO initiation. More studies are needed to synthesize these processes and determine the
464 degree to which these processes are critical to MJO initiation and must be adequately represented in
465 prediction models.

466 *3.1.2 Recent satellite observations of the MJO*

467 Satellite observations have provided unprecedented datasets in characterizing three-
468 dimensional structures of the MJO with a global coverage. For example, the TRMM rainfall
469 observations has been extensively used to identify convective signals associated with the MJO (e.g.,
470 Fig. 1). The latent and radiative heating products based on the TRMM (*Masunaga et al.*, 2006; *Tao*
471 *et al.*, 2006; *Jiang et al.*, 2009; *Jiang et al.*, 2011; *Ling and Zhang*, 2011), moisture and temperature
472 estimates based on the Atmospheric Infrared Sounder (AIRS; *Tian et al.*, 2006b; *Tian et al.*, 2010),
473 cloud products from the International Satellite Cloud Climatology Project (*Chen and Del Genio*,
474 2009a; *Tromeur and Rossow*, 2010), and cloud water and water vapor from the Microwave Limb
475 Sounder (*Schwartz et al.*, 2008), among others, have been applied toward a comprehensive
476 depiction of MJO structures as previously discussed (see a review by *Zhang*, 2012 for these earlier
477 studies). In this subsection, we provide a brief update on observational studies of the MJO using
478 satellite data since *Zhang* (2012).

479 Taking advantage of the explicit observations of vertical cloud structure by CloudSat, *Riley et al.*
480 (2011) examined evolution of cloud types during the MJO life cycle. Largely in agreement with
481 many previous results based on reanalyses and field observations, a transition from shallow clouds
482 along with deep, narrow, less-organized convection in the growing stage, to widespread and more

483 organized convection during active phases, then to more anvil and stratiform in the mature phases
484 of the MJO is observed by CloudSat. By using a combined data from CloudSat and the Cloud-
485 Aerosol Lidar and Infrared Pathfinder Satellite Observations (CALIPSO), Del Genio et al. (2012)
486 also detected the deepest, tropopause-penetrating convective events during the MJO onset stage
487 about one week before the MJO peak in convection.

488 Vertical temperature and specific humidity profiles associated with the MJO are also derived
489 by the Constellation Observing System for Meteorology, Ionosphere, and Climate (COSMIC) radio
490 occultation (RO) measurements (*Zeng et al., 2012; Tian et al., 2012*), and compared to previous
491 results based on the AIRS observations (*Tian et al., 2006b; Tian et al., 2010*). Compared to the RO
492 observations, MJO temperature anomalies in the upper-troposphere are underestimated by 40% in
493 the AIRS estimates (*Tian et al., 2012*). With a much higher vertical resolution of RO data, the RO-
494 based results better capture the sharp temperature anomaly structures near the tropopause.
495 Particularly, the eastward tilting of negative temperature anomalies with height in the tropopause
496 transition layer (TTL) above the enhanced MJO convective region is well captured in RO, which is
497 thought to be associated with the Kelvin waves excited by the “convective cold top” above the MJO
498 convective heating as previously reported (*Kiladis et al., 2005; Holloway and Neelin, 2007; Tian et*
499 *al., 2010; Virts and Wallace, 2010; Virts and Wallace, 2014*). These negative temperature
500 anomalies in the TTL ahead of MJO convection can lead to increased cirrus clouds (*Del Genio et*
501 *al., 2012; Virts and Wallace, 2014*), indicative of a potential positive radiative feedback on the MJO
502 (*Del Genio and Chen, 2015; Ciesielski et al., 2017*).

503 Characteristics of separated MCSs (SMCSs) and connected MCSs (CMCSs) associated with
504 the MJO, identified by combined data from the Moderate Resolution Imaging Spectroradiometer
505 (MODIS) and the Advanced Microwave Scanning Radiometer for Earth Observing System
506 (AMSR-E), were investigated by Yuan and Houze (2010; 2012). It was shown that variability in
507 precipitation contribution from CMCSs largely matches the overall MJO precipitation variability.
508 Meanwhile, greater occurrence frequency of CMCSs associated with enhanced large-scale MJO
509 convection was found to be closely associated with increased mid-troposphere moisture (*Yuan and*
510 *Houze, 2012*).

511 Using the TRMM Precipitation Radar data over the Indian Ocean and western Pacific, Barnes
512 and Houze (2013) examined variability of precipitating cloud population associated with the MJO.

513 The broad stratiform regions (BSRs), which occur in connection with well-developed MCSs, are
 514 found to dominate the variability of precipitating cloud population in terms of areal coverage, and
 515 are most prevalent during the active stage of the MJO. These BSRs are favored in a large-scale
 516 environment with strong low-level shear, moderate mid-level shear, and a moist mid-to-upper
 517 troposphere.

518 By analyzing lightning occurrence by the World-Wide Lightning Location Network, Virts and
 519 Houze (2015) found that lightning frequency density in an MCS maximizes during the MJO
 520 transition periods at or just after the time of minimum MJO rainfall; during the MJO active periods,
 521 the zone of lightning is contracted around the centers of MCSs, and flashes are less frequent. These
 522 results are largely consistent with previous findings of an out-of-phase relationship between
 523 lightning and MJO precipitation by the TRMM-Lightning Image Sensor (Kodama *et al.*, 2006;
 524 Morita *et al.*, 2006).

525 **3.2 Modern theories of the MJO**

526 In this section, we review several theories that are currently being used to understand the
 527 MJO. Emphasis will be placed on the mechanisms in which the theory explains two salient features
 528 of the MJO: (1) its slow eastward propagation and (2) planetary scale. The major caveats of each
 529 theory will also be highlighted. Four of the theories discussed here are discussed in detail in recent
 530 reviews by Zhang *et al.* (2020) and Yang *et al.* (2020). The reader is referred to these review papers,
 531 as well as the original publications on these theories, for the mathematical formulation,
 532 assumptions, and comparisons with observations. Following Kim and Maloney (2017), a summary
 533 of each theory, and its essence and supporting references are shown in Table 1.

534 Table 1: Summary of each theory discussed in this section.

<i>Theory</i>	<i>Essence</i>	<i>Observational/Modeling Evidence</i>
WTG Moisture Mode+ <i>Sobel and Maloney, (2012, 2013), Adames and Kim (2016)</i>	Moisture-convection coupling is key. Moisture advection important for propagation. Cloud-radiative feedbacks cause growth and determine horizontal scale.	<i>Andersen & Kuang (2012), Chikira (2014), Pritchard & Bretherton (2014), Wolding & Maloney (2015), Jiang (2017), Adames et al. (2017b), Kim et al. (2017), Janiga et al. (2018), Rushley et al. (2019), Pritchard & Yang (2016)*, Kacimi & Khouider (2018)*, Chen & Wang (2018a)*</i>
WISHE Moisture Mode+ <i>Fuchs and Raymond (2005, 2007, 2017)</i>	Moisture-convection coupling is key. WISHE determines propagation, growth and scale selection. Cloud-radiative feedbacks provide additional growth.	<i>Maloney and Sobel (2004), Shi et al. (2018), Sobel et al. (2008, 2010), Wang (1988)*, Zhang (1996)*, de Szoeke et al. (2015)*</i>
BLQE Model <i>Khairoutdinov and Emanuel (2018; Emanuel, 2019)</i>	Convection adjusts to maintain BL quasi-equilibrium (BLQE). MSE evolution is key. Cloud-radiation feedback determines growth, WISHE propagation.	<i>Maloney & Sobel (2004), Khairoutdinov & Emanuel (2018), Arnold & Randall (2015), de Szoeke (2018), Wang (1988)*, Zhang (1996)*, de Szoeke et al. (2015)*</i>
Trio Interaction	BL frictional moisture convergence to the east of MJO	<i>Maloney & Hartmann (1998), Lee et al. (2001),</i>

<i>(Wang and Rui, 1990; Wang et al., 2016a)</i>	convection center determines propagation and growth. Moisture-convection coupling slows down the MJO.	<i>Benedict & Randall (2007), Adames & Wallace (2014), Salby et al. (1994), Hendon and Salby (1994), Chao & Chen (2001)*, Shi et al. (2018)*, Kim et al. (2011a)*</i>
Skeleton <i>Majda and Stechman (2009, 2011), Thual et al. (2014)</i>	MJO is an envelope of synoptic waves and mesoscale systems. MJO propagation due to interaction between low-level moisture and synoptic-scale wave activity.	<i>Deng and Wu (2010, 2011), Dias et al. (2013, 2017), Guo et al.(2015), Chen and Wang (2017)*, Miyakawa and Kikuchi (2018)*</i>
Gravity Wave <i>Yang and Ingersoll (2013, 2014)</i>	MJO is an envelope of eastward and westward-propagating inertio-gravity waves. Horizontal scale is determined by interaction of waves and convection. Asymmetry between waves due to beta effect determines propagation.	<i>Kikuchi (2014), Pritchard & Yang (2016), Guo et al.(2015), Dias et al., (2013)*, Miyakawa and Kikuchi (2018)*</i>
Nonlinear Solitary Wave <i>Yano and Tribbia (2017), Rostami and Zeitlin (2019)</i>	MJO is a strongly nonlinear solitary Rossby wave. MJO is explained by dry dynamics to first order. Nonlinear vorticity advection explains propagation. Large-scale modons exhibit the longest duration.	<i>Wang et al. (2019b), Zhang and Ling (2012)*</i>
Large-scale Convective Vortex <i>Hayashi and Itoh (2017)</i>	MJO is an eastward-propagating pair of Rossby gyres. Propagation is due to strong low-level vortex stretching from deep convection to the east of the cyclones.	<i>Benedict and Randall (2009), Zhang et al. (2010), Lin et al. (2004)*</i>

535 * Results contradict or are not consistent with theory.
536 + These two theories offer different perspectives of a more general “moisture mode” theory.

537 *3.2.1 Early work and observations leading to modern theories*

538 The first attempt to understand the MJO was made by Chang (1977). His work showed that
539 convection can slow convectively-coupled waves, although not enough to match observations.
540 Subsequent attempts to understand the MJO include the use of a wave-driven version of the
541 convective instability of the second kind (wave-CISK) (Lau and Peng, 1987; Chang and Lim,
542 1988), wind-induced surface heat exchange (WISHE) (Emanuel, 1987; Neelin et al., 1987), and a
543 version of the wave-CISK model that includes a BL convergence feedback (frictional CISK; Wang,
544 1988; Wang and Rui, 1990). While many of these theories succeeded at describing some aspects of
545 the MJO, they were unable to fully explain all of its key features. The simulated variability
546 exhibited faster eastward propagation than observed, and often lacked the Rossby wave structures
547 seen when the MJO is active over the warm pool. Both characteristics are more consistent with
548 convectively-coupled Kelvin waves than the MJO. Nonetheless, many of these early theories form
549 the building blocks of several of the modern theories discussed herein (Sections 3.2.2-3.2.4).

550 Observations arising from field campaigns such as TOGA-COARE (Webster and Lukas,
551 1992) indicate that tropical precipitation is highly sensitive to the thermodynamic environment.
552 Precipitation occur when the free troposphere is humid, or when convective available potential
553 energy (CAPE) is increased, or convective inhibition (CIN) is reduced (Mapes, 2000). These
554 observations led to most of the modern theories of the MJO, where moist thermodynamics interact
555 with both deep convection and the large-scale circulation. With only one exception (section 3.2.7),
556 all of the views discussed here emphasize the role of moist thermodynamics in the MJO.

3.2.2 Moisture mode theory

The role that water vapor plays in regulating tropical convection was further developed into a theory of the MJO, known as “moisture mode theory”. A “moisture mode” can be defined as an atmospheric disturbance where the evolution of moisture (i.e. inclusion of prognostic moisture) plays a dominant role in its dynamics. The term was coined by Yu and Neelin (1994), who analyzed a system of equations in the equatorial belt and found wave solutions driven by moisture fluctuations that were unlike any previously documented wave. While Neelin and Yu (1994) and Yu and Neelin (1994) documented the analytical existence of moisture modes, they did not attribute the MJO to such a wave. The first studies indicating that the MJO may be a moisture mode were Raymond (2001) and Sobel et al. (2001). Raymond (2001) argued that MJO-related precipitation anomalies are predominantly caused by moisture fluctuations, and are destabilized by cloud-radiative feedbacks, as in Hu and Randall (1995). Surface latent heat fluxes drive the propagation of the disturbance. Sobel et al. (2001) obtained balanced moisture wave solutions under weak temperature gradient (WTG) balance that propagated due to horizontal moisture advection. They argued that the MJO may be characterized as a type of moisture wave.

The moisture mode framework gained further attention as studies like Grabrowski and Moncrieff (2004) showed that simulating strong moisture-convection feedbacks are central to simulating strong MJO activity. Subsequent studies showed that MJO simulations can be improved by increasing convection’s sensitivity to free tropospheric water vapor (*Kim and Kang, 2012; Kim et al., 2012; Del Genio et al., 2012; Zhu and Hendon, 2015; Arnold et al., 2015; Kim and Maloney, 2017*). Furthermore, several studies have found a link between the concentration and distribution of water vapor and the ability of models to simulate the MJO (*Gonzalez and Jiang, 2017; Jiang, 2017*). Fast drying of the troposphere in forecast models has also been linked with models’ tendency to dissipate the MJO (*Kim et al., 2016, 2017; Weber and Mass, 2017; Kim et al., 2019*). Due to the well-documented importance of moisture-convection feedbacks in the representation of intraseasonal rainfall variability, the moisture mode framework is now one of the most well-known theories of the MJO. However, even within this theory differing views exist as to which moist processes determine the MJO’s eastward propagation and planetary scale. Two of these views are discussed here.

a. Moisture mode under WTG balance

One type of moisture mode model focuses on the role that moisture evolution alone plays in the MJO. This model assumes that the MJO-related wind field instantaneously adjusts to an

589 equatorial heat source in the form of the Matsuno-Gill steady-state response, and that the
590 intraseasonal heating anomalies are in WTG balance. We will refer to this model as the WTG
591 moisture mode model. The foundations of this model were originally conceived by Sobel and
592 Maloney (2012, 2013). They diagnosed precipitation anomalies from moisture anomalies using a
593 simplified Betts-Miller scheme and obtained a dispersion relation using a 1-D model. Adames and
594 Kim (2016) further developed their framework by treating the meridional and vertical structure of
595 the MJO explicitly, and adjusted several key parameters to be more consistent with observations.
596 Through this revision, they found that the wind anomalies in the MJO explain its eastward
597 propagation through horizontal moisture advection, frictional convergence, and modulation of
598 surface fluxes. The propagation mechanism also results in a westward group velocity (the extrema
599 in the moisture/rainfall anomalies drift westward with time). Lastly, Adames and Kim (2016)
600 showed that planetary-scale selection in the MJO can occur through a non-local feedback between
601 convection and longwave radiative heating. Upper level clouds that spread away from regions of
602 precipitation reduce outgoing longwave radiation. The anomalous radiative heating that results
603 from these clouds is balanced by anomalous upward motion and adiabatic cooling. The anomalous
604 upward motion moistens the free troposphere, which favors the development of convection.

605 There are several caveats to this moisture mode model. While assuming that moisture is the
606 only prognostic variable lends analytical tractability and physical interpretation to the theory, it is
607 unlikely that these approximations are adequate during all times in the MJO life cycle (*Kacimi and*
608 *Khouider, 2018*). Several processes, such as BL moisture convergence, are parameterized based on
609 observations. While the scale-selecting role of radiation has been demonstrated by some studies
610 (*Shi et al., 2018; Khairoutdinov and Emanuel, 2018*), the way it is incorporated into this model is
611 based on empirical evidence, rather than first principles. It is also noteworthy that while some
612 studies suggest that cloud-radiation feedbacks are essential to the MJO (*Andersen and Kuang,*
613 *2012; Shi et al., 2018*), eliminating these feedbacks weakens but does not eliminate the MJO
614 (*Arnold and Randall, 2015*), which suggests that it may not be the only instability mechanism.
615 Lastly, while some studies support the notion that the MJO has a westward group velocity (*Janiga*
616 *et al., 2018*), a study based on observations does not support this type of dispersion (*Chen and*
617 *Wang, 2018a*).

618 b. WISHE moisture mode

619 Another relevant moisture mode model was developed by Fuchs and Raymond (2005, 2017).
620 Unlike the WTG-based moisture mode model, this model does not use WTG strictly and the

621 tendency in momentum is also included. Additionally, while the WTG moisture mode model
622 includes multiple processes that can induce eastward propagation, this model incorporates WISHE
623 as the only process that drives propagation. In this model, WISHE not only results in MJO eastward
624 propagation, but also induces a planetary-scale instability. A salient feature of this model is the
625 exclusion of the meridional wind as a fundamental feature of the MJO, with the horizontal structure
626 of this moisture mode resembling that of a convectively coupled equatorial Kelvin wave.

627 There are several caveats to this model. First, while it is true that the mean tropical zonal wind
628 is easterly, the mean zonal winds over the Indo-Pacific warm pool are weakly westerly near the
629 equator. As a result, surface latent heat fluxes to the east of the region of enhanced MJO convection
630 are suppressed, rather than enhanced (*Zhang, 1996; Kiranmayi and Maloney, 2011; de Szoeke et al.,*
631 *2015*). This distinction may be important since suppressing WISHE eliminates MJO-like activity in
632 aquaplanet simulations (*Shi et al., 2018; Khairoutdinov and Emanuel, 2018*), but not in most
633 simulations with realistic topography (e.g., *Kim et al., 2011a; Ma and Kuang, 2016*). It is possible
634 that MJO propagation may instead be explained by a nonlinear WISHE mechanism over the warm
635 pool (*Maloney and Sobel, 2004*).

636 3.2.3 Boundary layer quasi equilibrium (BLQE) model

637 Boundary layer quasi-equilibrium (BLQE, *Raymond, 1995; Emanuel, 1995*) assumes that
638 regions of deep convection exhibit a balance in the BL where the net gain of MSE through surface
639 fluxes is balanced by the import of low MSE air from the free troposphere that result from
640 convective downdrafts. The intensity of the downdrafts are in turn related to updrafts through a
641 precipitation efficiency parameter (*Emanuel, 1991*). When this concept is applied to the MJO
642 (*Khairoutdinov and Emanuel, 2018; Emanuel, 2019*), it is found that planetary-scale instability is
643 the result of longwave radiative heating. Like the WISHE moisture mode discussed in the previous
644 subsection, eastward propagation of the MJO in the BLQE model is due to WISHE. To some
645 extent, this theory can also be thought as a moisture mode model since the strict application of
646 WTG balance still yields unstable planetary-scale modes, which indicates that the evolution of
647 moisture may be of critical importance in this model. This is somewhat evident in the dispersion
648 relation of this mode, which is reminiscent of the moisture mode models discussed above (*Adames*
649 *and Kim, 2016; Fuchs and Raymond, 2017*). However, the use of BLQE does yield results that
650 differ from the WISHE-moisture mode model. For example, in this model WISHE actually reduces
651 the growth rate, whereas in the WISHE moisture mode model WISHE is the leading cause of
652 instability.

653 While the assumption of BLQE is central to this model, it is unclear how these results would
654 be affected if the assumption of BLQE were relaxed and BL MSE were allowed to evolve in time.
655 Furthermore, as in all theories that rely on WISHE as a mechanism of eastward propagation, it is
656 unclear whether this mechanism is truly applicable to the MJO when its convection is in the warm
657 pool (*Wang, 1988*).

658 *3.2.4 Trio interaction theory*

659 The “trio interaction theory” can be considered to be an update to the original frictionally-
660 coupled Kelvin-Rossby wave theory of Wang and Rui (1990), modified to include water vapor as a
661 prognostic variable. The essence of this theory is rooted in BL convergence, equatorial wave
662 dynamics, moisture, and diabatic heating. Cloud-radiation feedbacks, while not essential, are also
663 included in the theory for completeness. In the trio interaction model, BL friction causes wave-
664 driven convergence to occur to the east of the main region of convection (*Maloney and Hartmann,*
665 *1998; Hendon and Salby, 1994; Salby et al., 1994; Wang and Li, 1994; Adames and Wallace,*
666 *2014*). This convergence results in upward motion, which moistens the atmosphere and generates
667 available potential energy, resulting in eastward propagation and planetary-scale instability. The
668 inclusion of moisture along with the use of a Betts-Miller parameterization scheme results in even
669 slower eastward propagation in the most unstable mode at values that are more consistent with
670 observations (*Wang et al., 2016a*). The “trio” in the name is suggestive of the three-way interaction
671 among convective heating, moisture and boundary layer dynamics. According to this theory, MJO
672 simulations can be improved if the interactions between BL processes, moisture and large-scale
673 waves are improved.

674 It is important to note that the literature is currently divided on the role of frictional
675 convergence in the MJO. Some studies have supported its central importance using a suite of
676 observations and modeling (*Wang and Lee, 2017; Wang et al., 2018a*). Other studies indicate that
677 removing BL friction in GCMs does not negatively impact the MJO, casting doubt on the
678 fundamental processes of this theory (*Kim et al., 2011a; Shi et al., 2018*). It may be difficult to fully
679 test this theory given the sensitivity of the mean state to surface friction. Furthermore, BL friction
680 may not only be due to surface roughness, but due to other processes such as momentum damping
681 due to turbulent entrainment (*Stevens, 2002*).

682 *3.2.5 Skeleton model*

683 The MJO skeleton model was originally proposed by Majda and Stechmann (2009). The
684 theory describes the MJO as a neutrally-stable envelope of higher-frequency synoptic and

685 mesoscale systems. The heating driven by convection in these high-frequency systems maintain the
686 MJO through an upscale transport of momentum. In turn, the evolution of these synoptic and
687 mesoscale systems is driven by a planetary-scale envelope of low-level moisture. This interaction
688 between low-level moisture and high-frequency wave activity is the essence of the skeleton model
689 and is the basis of their representation of convective processes. This “wave activity” and low-level
690 moisture are in quadrature, resulting in the propagation of the convective anomalies. An eastward-
691 propagating and a westward-propagating solution arise from a shallow-water system of equations.
692 Of these two, only the eastward propagating solution exhibits a quadrupole vortex structure
693 consisting of Kelvin and Rossby waves, similar to what is observed during the MJO phases where
694 there is both enhanced and suppressed convection over the warm pool. The planetary-scale
695 disturbance propagates eastward at $\sim 5 \text{ m s}^{-1}$ and exhibits a dispersion relation that is approximately
696 independent of wavenumber (i.e. constant), yielding a group velocity of zero. A study by Chen and
697 Wang (2018a) indicates that the MJO may exhibit this type of dispersion.

698 There are some limitations to this view of the MJO. First, it is unclear how the formulation of
699 the wave activity function can be quantitatively evaluated using observations. Observations also
700 reveal that, while low-level moisture does lead MJO convection, it is not in spatial quadrature.
701 Instead, low-level moisture is observed to slightly lead precipitation ($\sim 30^\circ$ shift in phasing) (*Chen*
702 *and Wang*, 2017). The literature is also divided on the role of upscale interactions in the MJO, with
703 some studies suggesting that the MJO’s momentum generation occurs at the planetary,
704 intraseasonal scale (*Zhou et al.*, 2012a; *Dubey et al.*, 2018), while others suggest it comes from the
705 synoptic and mesoscale (*Khouider et al.*, 2012; *Yang et al.*, 2019).

706 3.2.6 Gravity wave model

707 The gravity wave model was originally proposed by Yang and Ingersoll (2013, 2014). This
708 view of the MJO was motivated by observations of the intermittency of convection in the tropics
709 (*Zuluaga and Houze*, 2013). In this model, the MJO is conceived to be the result of an interference
710 pattern between eastward and westward-propagating inertia-gravity waves. The eastward
711 propagation is the result of the difference in propagation speed between the two inertio-gravity
712 waves. Eastward inertia gravity waves exhibit slightly faster eastward propagation than their
713 westward counterparts. This small difference is attributed to the gradient in planetary vorticity
714 (β). Thus, the eastward-propagation of the MJO can only occur in the equatorial belt of a rotating
715 planet. The planetary scale of the MJO results from the distance that the inertia-gravity waves
716 propagate without being dissipated by a convective storm (*Yang and Ingersoll*, 2014). This distance

717 is qualitatively determined by the phase speed of convectively-coupled gravity waves divided by
718 the density of convective events.

719 Like the skeleton model, this model suggests that multi-scale interactions are essential to the
720 MJO. However, unlike the skeleton model, where only the net upscale impact of these systems are
721 important, here the details of the interactions between the inertio-gravity waves are critical. As a
722 result, the gravity wave theory is arguably the only theory described here where the details of
723 convective organization and its interaction with the synoptic scale are of critical importance.
724 Additionally, this model treats convection as a triggered process and it is inherently nonlinear.

725 While spectral analysis reveals that gravity wave energy co-varies with the MJO (Kikuchi,
726 2014), observations have currently not observed inertio-gravity waves propagating in both eastward
727 and westward directions during an MJO life cycle (*Dias et al.*, 2017). It is unclear whether this is a
728 result of insufficient temporal resolution to fully resolve these fast waves or if these waves are not
729 central to MJO dynamics.

730 *3.2.7 Nonlinear Solitary Rossby Wave*

731 The solitary wave framework was originally proposed by Yano and Tribbia (2017), and
732 further developed by Rostami and Zeitlin (2019). The essence of this theory is that the MJO is a
733 pair of equatorially-symmetric Rossby wave vortices whose propagation is due to nonlinear
734 potential vorticity advection. This framework differs from other theories in that it completely
735 eliminates the need for deep convection as a first-order process. Their justification of a dry
736 framework arise from results such as those from Holloway et al. (2013) and Monier et al. (2010),
737 who found strong intraseasonal variations in wind even when intraseasonal fluctuations in
738 convection are weak.

739 The most unstable mode solution in this theory exhibits a scale of ~ 3000 km and a phase
740 speed that ranges from $8\text{--}18$ m s⁻¹. This scale is slightly smaller with larger phase speed than what
741 is observed in composite MJOs. Furthermore, a potential vorticity (PV) budget analysis by Zhang
742 and Ling (2012) suggests that PV evolution in the MJO is predominantly driven by diabatic
743 processes, rather than horizontal advection of the PV field. Nonetheless, it is remarkable that a dry
744 theory for the MJO can be conceived, and more work is needed to evaluate this theory.

745 *3.2.8 Large-scale convective vortex*

746 The large-scale vortex theory was initially proposed by Hayashi and Itoh (2017) to explain the
747 eastward propagation of the MJO. They proposed that the MJO is a pair of cyclonic Rossby gyres

748 that are strongly coupled to convection. The eastward propagation can be explained by strong
 749 vortex stretching that occurs in the regions of deep convection associated with strong westerly
 750 winds. This mechanism exceeds the advection of planetary vorticity that would cause Rossby gyres
 751 to otherwise propagate westward, a mechanism that is often disregarded in MJO theories such as
 752 that of Adames and Kim (2016). This framework may serve not only as an explanation for the
 753 propagation of the MJO, but may also be used as a basis to understand westerly wind bursts (*Fu*
 754 *and Tziperman, 2019*).

755 3.2.9 Overlap between the theories

756 The diversity of the theories presented in this subsection could easily lead the reader to
 757 conclude that our understanding of the MJO remains very poor. Such a conclusion is misguided. In
 758 the last decade simulation of the MJO has vastly improved to the extent that many models can
 759 reproduce many of its observed features (see Section 3.3). Many of the improvements have been the
 760 result of a greater understanding of the processes that drive tropical convection. In particular, the
 761 role that water vapor plays in the convective organization of the MJO has been especially critical.
 762 An examination of each theory (Table 2) quickly reveals that moist processes are the centerpiece to
 763 the majority of the theories. For example, the majority of theories include moisture as a prognostic
 764 variable and consider moist processes to be crucial for understanding the propagation and growth of
 765 the MJO. Additionally, the majority of the theories emphasize interactions between moisture and
 766 convection in the growth and propagation of the MJO. Half of the models discussed here also
 767 include cloud-radiative feedbacks, although this process has varying degrees of importance across
 768 models. Out of the eight theories discussed, two can be considered to be moisture mode theories,
 769 and two others (BLQE and trio interaction) contain essential elements of moisture mode theory.
 770 Only the solitary Rossby wave model has its fundamental elements rooted in dry dynamics.

771 Table 2: Comparison of the role of moist processes in each of the theories discussed here.

Theory	Conv coupling is essential	Prognostic moisture is key	Moist processes key to propagation	Moist processes key to MJO growth	Cloud- radiative heating is included
WTG moisture mode	yes	yes	yes	yes	yes
WISHE moisture mode	yes	yes	yes	yes	yes
BLQE model	yes	yes ¹	yes	yes	yes
Trio Interaction model	yes	yes	yes	yes	yes
Skeleton model	yes	yes	yes	no	no
Gravity Wave model	yes	no	no ²	no ²	no
Nonlinear Solitary wave	no	no	no	no	no

Large-scale Convective	yes	no	yes	yes	no
Vortex					

772 1. This model does not have an explicit moisture equation, but a moist static energy equation. Nonetheless, they make use of the WTG
773 approximation, which makes MSE effectively a moisture equation.
774 2. In this model, deep convection plays a key role in MJO propagation and scale. The “no” is because moisture-convection feedbacks are not explicit
775 in this model.

776

777 **3.3 Modeling the Madden-Julian Oscillation**

778 In this section, we highlight recent development and activity toward process-level
779 representation and understanding of the MJO in GCMs. These include new model intercomparison
780 studies, development of new modeling framework and diagnostics, and an emerging area of active
781 research – understanding the role of the mean state. The interaction of the MJO with the MC islands
782 is another theme of active modeling studies, which are summarized in Section 3.6. Readers are
783 referred to Sperber et al. (2012) and Kim and Maloney (2017) for a detailed summary and
784 discussion of the achievement in MJO modeling during the earlier period.

785 *3.3.1 Process-oriented diagnostics*

786 Since the early 2010s, the concept of “process-oriented” diagnostics, which are distinguished
787 from the traditional performance-oriented diagnostics by their ability to more directly guide model
788 development, was put forward within the MJO community. In GCMs, the MJO is one of the
789 “emerging” systems that are internally generated through the interactions among resolved and
790 parameterized processes. The main goals of the process-oriented diagnostics are to identify
791 processes that are key to the MJO and to provide insights into specific aspects of the model that
792 affects the identified key processes. Various process-oriented MJO diagnostics have been
793 developed and tested based on the processes that had been suggested to be important in the MJO
794 dynamics: the moisture-precipitation coupling (e.g., Kim et al., 2014b; Jiang et al., 2015; Section
795 2.1), the mean GMS (e.g., Benedict et al., 2014; Section 2.2), the cloud-radiation feedbacks (e.g.,
796 Kim et al., 2015; Section 2.3). It was found that models with tighter moisture-convection coupling,
797 stronger cloud-radiation feedbacks, and lower mean GMS tend to simulate a stronger MJO. Readers
798 are referred to Jiang et al. (2020) for a more detailed review on the development of the process-
799 oriented MJO diagnostics.

800 *3.3.2 Recent model intercomparison studies*

801 Model intercomparison studies have been a useful framework to gauge the overall model
802 fidelity and to identify systematic biases that are common to many models. Prior to 2010, Slingo et

803 al. (1996) and Lin et al. (2006) conducted an intercomparison study focused on the MJO with more
804 than a dozen GCMs. Slingo et al. (1996) found that all participating AMIP (Atmospheric Model
805 Intercomparison Project) models failed to capture the observed intraseasonal spectral power in the
806 upper level velocity potential field. Lin et al. (2006) analyzed 14 coupled GCMs participating in the
807 3rd coupled model intercomparison project (CMIP3) and found that the intraseasonal spectral peak
808 in equatorial precipitation is realistically captured in only one model. The daunting conclusions of
809 the earlier intercomparison studies - almost all models cannot simulate even the most basic features
810 of the MJO - highlighted the need to better understand the phenomenon, for example, by making
811 observations of key processes (Section 3.1) and via theoretical considerations (Section 3.2).

812 In the early 2010s, jointly led by the MJOTF and the GEWEX GASS Project, a large GCM
813 intercomparison project that specifically focused on the MJO was successfully carried out with 27
814 participating models (*Petch et al., 2011; Jiang et al., 2015; Klingaman et al., 2015b; Xavier et al.,*
815 *2015*). The model simulation data collected during the activity has been widely used for MJO
816 studies (*Jiang et al., 2016; Ling et al., 2019; Wang and Lee, 2017; Wang et al., 2017; Jiang, 2017;*
817 *Gonzalez and Jiang, 2017*) and for developing process- and dynamics-oriented MJO diagnostics
818 (e.g., *Wang et al., 2018a; Jiang et al., 2016; Maloney et al., 2019b*). In terms of MJO simulation
819 fidelity, Jiang et al. (2015) found that about one fourth of the participating models represented the
820 eastward propagation of the MJO realistically (Fig. 5). For the first time, a large model
821 intercomparison study concluded that a significant fraction (25%) of participating models simulated
822 a reasonable MJO.

823 By providing standardized output variables at the daily frequency, the CMIP activity has
824 provided an invaluable resource for MJO performance assessment. Hung et al. (2013) and Ahn et
825 al. (2017) examined CMIP5 models in terms of their MJO simulation capability. By applying the
826 same diagnostics that were applied to the CMIP3 models by Lin et al. (2006), Hung et al. (2013)
827 noted a slight improvement in the performance of CMIP5 models over the CMIP3 models. Ahn et
828 al. (2017) showed that MJO amplitude in the upper level velocity potential field in the CMIP5
829 models are stronger than that in the AMIP models examined in Slingo et al. (1996). Ahn et al.
830 (2020b) analyzed the latest CMIP6 models with a focus on MJO propagation over the MC and
831 compared them with their predecessors. They found that the CMIP6 models as a group better
832 simulate the MJO eastward propagation over the MC, which they attributed to a reduction of dry

833 mean state bias near the equator. With a weaker equatorial dry bias, the CMIP6 models show a
834 steeper mean meridional moisture gradient in the MC, which leads to a greater moisture recharging
835 to the east of MJO convection, and provide a favorable condition for MJO eastward propagation.

836 3.3.3. Modeling the MJO with and without parameterized convection

837 It has long been known that the cumulus parameterization schemes greatly affect the
838 simulation of tropical intraseasonal oscillations (e.g., Tokioka *et al.*, 1988; Park *et al.*, 1990).
839 GCMs tend to produce stronger intraseasonal oscillations in the tropics as triggering of deep
840 convection is more severely inhibited in dry conditions (e.g., Maloney and Hartmann, 2001; Lee *et*
841 *al.*, 2003; Zhang and Mu, 2005; Lin *et al.*, 2008; Bechtold *et al.*, 2008; Ling *et al.*, 2009; Zhang and
842 Song, 2009; also see Kim and Maloney, 2017 for a review). Also, it was noted that the version of
843 convection scheme that improves the MJO does not necessarily improve the mean state (e.g., Kim
844 *et al.*, 2011b). Efforts of improving MJO in GCMs via changes in the cumulus parameterization
845 scheme continued during the recent decades. Most recent modeling studies that examined the effect
846 of cumulus parameterization on the simulation of the MJO emphasized the sensitivity of
847 parameterized convection to environmental moisture (e.g., Chikira and Sugiyama, 2010; Deng and
848 Wu, 2010; Kim and Kang, 2012; Kim *et al.*, 2012; Del Genio, 2012; Zhou *et al.*, 2012a).

849 What has also long been known is that the same changes in the convection scheme that
850 improves the MJO tend to affect the mean state significantly, often in a negative way (e.g., Wang
851 and Schlesinger, 1999; Kim *et al.*, 2011b; Mapes and Neale, 2011a). For example, if the fractional
852 entrainment rate in the convection scheme is increased, the convection scheme becomes more
853 sensitive to environmental moisture, giving the parent model an enhanced variability in the tropics,
854 including the MJO. Another consequence of increasing the fractional entrainment rate is that
855 convective plumes become shallower and seldom reach the tropopause. The overall shoaling of
856 convective plumes means convection becomes less efficient in removing instability from the
857 column and therefore excessive convective activity is required. The excessive precipitation
858 especially over the warmest part of the globe tends to distort the tropical mean climate (e.g., Kim *et*
859 *al.*, 2011b). Recent modeling studies suggested that the apparent mean state-MJO trade off can be
860 mitigated by explicitly representing mesoscale organization of convection in the convection
861 schemes (Mapes and Neale, 2011a; Chen and Mapes, 2018; Ahn *et al.*, 2019). For example, Ahn *et*
862 *al.* (2019) examined the mean state and MJO in a series of simulations using a GCM with a unified

863 convection scheme (UNICON, *Park, 2014*) in which the degree of mesoscale organization of
864 convection is a prognostic variable whose main source is convective downdraft. They found that the
865 GCM represented both the mean state and the MJO realistically. It was suggested that the key to the
866 success of UNICON in mitigating the MJO-mean state tradeoff is that the plume properties (e.g.,
867 entrainment rate) are situation-adaptive: the effective entrainment rate is high for plumes in an
868 undisturbed region (e.g., during the suppressed phase of the MJO), as the degree of organization
869 would be lower, while it is low for the plumes within the mature systems (e.g., those embedded in
870 the active MJO). More work is warranted in the area of developing parameterizations of mesoscale
871 organization and its impacts on MJO simulation (e.g., *Moncrieff, 2019*; see Section 4.3).

872 Recently, new modeling tools that do not rely on the cumulus parameterization schemes were
873 developed and have been used in modeling the MJO. In the so-called “superparameterization”
874 approach, the cumulus parameterization schemes were replaced by a 2-D cloud-resolving models
875 (CRMs) in each grid column (*Grabowski, 2001; Khairoutdinov and Randall, 2003*). The mesoscale
876 organization of convection, therefore, is explicitly resolved within the 2-D CRMs. Studies have
877 shown that the models with superparameterized convection largely showed a better performance in
878 MJO simulation than the corresponding model with a conventional parameterization scheme
879 (*Khairoutdinov et al., 2005; Thayer-Calder and Randall, 2009; Benedict and Randall, 2009; Kim et al., 2009; Zhu et al., 2009*). It is worthwhile to note that while the models with superparameterized
880 convection have shown to perform well in model intercomparison studies (*Kim et al., 2009; Jiang et al., 2015*), they often suffer from the same mean state biases as in the models with parameterized
881 convection (e.g., *Kim et al., 2011b*) and tend to exhibit too strong MJO variability (e.g., *Zhu et al., 2009*). Moreover, not every model that employs superparameterized convection simulates a decent
882 MJO, suggesting that employing high-resolution and resolving convective motions do not
883 automatically improve MJO simulations.

887 With the aid of increasing computational power, the GCRMs became available for MJO
888 studies (*Miura et al., 2007; Liu et al., 2009; Nasuno et al., 2009*), although in most cases the use of
889 GCRM was limited by a relatively short integration period. Nonetheless, *Miura et al. (2007)*
890 demonstrated that a GCRM reproduced an observed MJO event quite realistically. After the
891 DYNAMO field campaign (Section 3.1), many modeling studies were conducted with a focus on
892 understanding the observed MJO events during the field campaign. The new modeling tools -

893 superparameterized GCMs and GCRMs – as well as regional CRMs were actively used to study the
894 initiation and subsequent eastward propagation of the DYNAMO MJO events in the form of
895 hindcast experiments. It was found that the models that explicitly resolves convective systems
896 realistically represent the DYNAMO MJO events (e.g., *Hannah et al.*, 2015; *Weber and Mass*,
897 2019; *Miyakawa and Kikuchi*, 2018; *Hagos et al.*, 2014; *Wang et al.*, 2015).

898 New modeling strategies that recently emerge towards improved MJO simulations will be
899 further discussed in Section 4.3.

900 3.3.4. Role of the basic state

901 From a point of view that defines the MJO as perturbations from the climatological seasonal
902 cycle of the mean climate, whether and to what extent the basic state affects the salient features of
903 the MJO has been a central question to many modeling and theoretical studies. Studies have
904 examined the relationship between aspects of the mean state and MJO simulation capability in
905 ensembles of GCM simulations. Such efforts recently revealed that horizontal gradient of the mean
906 moisture is a key factor that determines models' MJO simulation fidelity (*Gonzalez and Jiang*,
907 2017; *Jiang*, 2017; *DeMott et al.*, 2018; *Ahn et al.*, 2020b). In particular, GCMs that show a sharper
908 meridional mean moisture gradient in the vicinity of the MC tend to better represent the eastward
909 propagation of the MJO with a more realistic moisture recharging and discharging pattern to the
910 east and west of MJO convection (*Jiang*, 2017; *Ahn et al.*, 2020b). It is worthwhile to note that
911 earlier studies also reported that models that simulate a relatively strong MJO tend to have mean
912 precipitation confined within the area of warm sea surface temperature (*Slingo et al.*, 1996; *Wang*
913 *and Schlesinger*, 1999), indicating strong MJO is preferred in a mean state with a greater contrast
914 between moist and dry areas, i.e., a steeper horizontal mean moisture gradient (see Fig. 3 in *Wang*
915 *and Schlesinger*, 1999).

916 While the empirical relationship between the mean moisture gradient and MJO variability
917 emphasizes the central role of moisture in the MJO dynamics, supporting the moisture mode theory
918 for the MJO, isolating the role of the mean state from the effect of the convection scheme is a non-
919 trivial task in multi-model studies (*Jiang*, 2017; *Ahn et al.*, 2020b) because the convection scheme
920 affects both the mean state and the MJO. Kang and Kim (2020, Role of background meridional
921 moisture gradient on the ensemble spread of MJO simulation in CESM2, GRL, submitted
922 manuscript) analyzed a 10-member ensemble of simulations made with a single model (CESM2)

923 and found a marked spread among the ensemble members in their ability to represent MJO
924 propagation over the MC. The ensemble members with a stronger MJO propagation showed
925 enhanced moistening to the east of MJO convection that is associated with a steeper mean state
926 meridional moisture gradient in the southern MC, highlighting the effects of background state that
927 is independent of the effects of the convection scheme.

928 **3.4 Predicting the MJO**

929 Advances in theoretical understanding, improved numerical models, and collaborative
930 international activities, such as field campaigns and multi-model ensemble prediction projects (e.g.,
931 ISVHE, S2S, SubX), have promoted remarkable improvements in MJO prediction during the past
932 decade. Through the perfect-model assumption, the MJO predictability reaches up to 7 weeks (e.g.,
933 *Waliser et al.*, 2003; *Neena et al.*, 2014). In reality though, errors originating from the imperfect
934 model and initial conditions make the actual prediction skill lower than the predictability;
935 reforecasts from the recent operational and research models exhibit MJO prediction skill varying
936 widely between 2-4.5 weeks (*Kim et al.*, 2019; *Lim et al.*, 2018). Figure 6 compares the MJO
937 prediction skill during boreal winter from the S2S and SubX reforecasts assessed by the Real-time
938 Multivariate MJO (RMM, *Wheeler and Hendon*, 2004) index.

939 To make a consistent evaluation of MJO prediction skill and fair comparison among multi-
940 models, the majority of the studies on MJO prediction and operational forecasts use the RMM
941 indices as a measure of the MJO. It is relatively simple to calculate and easy to implement for real-
942 time monitoring and forecasting of the MJO. However, interpretation of the MJO prediction skill
943 with the RMM index often needs careful consideration. It mainly reflects the skill of the predicted
944 wind anomalies but not necessarily the predicted convective anomalies associated with the MJO
945 (*Straub*, 2013). High prediction skill based on the RMM indices may therefore lead to an optimistic
946 conclusion regarding our MJO prediction capabilities. A common benchmark to measure the MJO
947 prediction skill has been scalar metrics, such as the bivariate anomaly correlation coefficient or
948 bivariate root-mean-squared error using two RMMs which represents the skills as a function of
949 forecast lead times (e.g., *Lim et al.*, 2018; *Rashid et al.*, 2011).

950 MJO prediction skill is generally higher when a model is initialized with a stronger MJO
951 signal than with weaker or with no signal, and thus tends to be higher in boreal winter (e.g., *Rashid*
952 *et al.*, 2011). During boreal winter, MJO prediction skill varies with the stratospheric low-frequency

953 mean state, for example during different QBO phases, which will be discussed in Section 3.8. MJO
954 prediction skill becomes higher when the extratropical influence on the tropics is reasonably
955 simulated (*Vitart and Jung, 2010; Ray and Li, 2013*). Recent studies have clearly shown that
956 averaging multi-ensembles or multi-models extends the MJO prediction skill (e.g., *Neena et al.,*
957 *2014; Pegion et al., 2019*), although including a low-performance model in the mean degrades the
958 skill (*Green et al., 2017*). Therefore, individual model needs to be improved in tandem with
959 developing an optimal strategy to maximize the benefit of the multi-model mean. The importance
960 of ocean feedback and varying SST to MJO prediction has been demonstrated (e.g., *Woolnough et*
961 *al., 2007; Seo et al., 2014*), although the role of the ocean varies for individual MJO cases (*Fu et*
962 *al., 2015*) and by model configuration (e.g., *Crueger et al., 2013; Wang et al., 2014*). Ocean-
963 atmosphere coupling may even degrade the MJO simulation due to the mean bias (*Hendon, 2000*).
964 Understanding the role of mean state bias on MJO prediction (*Lim et al., 2018; Kim et al., 2019*)
965 and improving the mean state is crucial to extending MJO prediction skill, since the quickly
966 developing mean state biases over the tropics can distort the further development of the MJO
967 (*Hannah et al., 2015; Kim et al., 2019*).

968 Although research and operational models have shown continuous improvement of MJO
969 prediction, various challenges remain. Ensemble prediction systems have shown a lack of ensemble
970 spread (i.e., under-dispersive) in MJO prediction (*Kim et al., 2014c; Neena et al., 2014; Vitart,*
971 *2017; Lim et al., 2018*). Improving the representation of uncertainty in the model physics schemes
972 has improved the MJO simulation (*Weisheimer et al., 2014*) and the spread-error relationship
973 (*Palmer et al., 2009; Leutbecher et al., 2017; Subramanian and Palmer, 2017*), indicating that
974 devising ensemble generation approaches tailored for the MJO may have a considerable impact on
975 MJO prediction. Better quality of atmospheric and ocean analyses and reanalyses for initial
976 conditions are conducive to extending MJO prediction skill as well (*Vitart et al., 2007; Dee et al.,*
977 *2011; Fu et al., 2011; Liu et al., 2017*).

978 Due to the huge computational costs for a long record of extended range reforecast
979 experiment, only a handful of studies have performed sensitivity tests of MJO prediction skill to
980 model physics or resolution. Studies have shown extended skill via an enhancement to the
981 entrainment rate for deep convection, which makes the MJO amplitude stronger (*Bechtold et al.,*
982 *2008; Hannah and Maloney, 2011; Klingaman and Woolnough, 2014*), although the improvement

983 of the MJO often leads to degradation of the mean state (e.g., *Kim et al.*, 2011b). Using super-
984 parameterized GCMs or GCRMs has been shown to improve the MJO skill compared to
985 conventional cumulus parameterization (*Miyakawa et al.*, 2014; *Hannah et al.*, 2015), while the
986 physical reasons for the improvement remain elusive. Compared to the impact of model physics or
987 ocean-atmosphere coupling, the influence of model resolution seems to be marginal (*Vitart et al.*,
988 2007).

989 The MJO prediction skill decline after 2-3 weeks is mostly attributed to MJO phase errors,
990 indicating that the phase change (i.e., the location) of the MJO is not accurately predicted (*Vitart*,
991 2017; *Lim et al.*, 2018; *Kim et al.*, 2019). In most contemporary models, the predicted MJO signal
992 does not persist as long as it does in observations, especially when the MJO propagates across the
993 MC, which is referred to as the MC MJO prediction barrier (e.g., *Vitart*, 2017). This MC barrier is
994 exaggerated in forecasts; the percentage of predicted MJO events starting from the Indian Ocean
995 and not crossing the MC is significantly higher in models compared to that in observations. This
996 indicates the shortcoming of models to maintain MJO propagation through the MC (*Neena et al.*,
997 2014; *Kim et al.*, 2014c, *Kim et al.*, 2018, *Kim et al.*, 2019; *Wang et al.*, 2014; *Xiang et al.*, 2015b;
998 *Liu et al.*, 2017; *Vitart*, 2017; *Wang et al.*, 2019c). MC-MJO interactions are further discussed in
999 Section 3.6.

1000 To better understand the sources of model errors in MJO propagation processes, several
1001 studies have applied the moisture mode hypothesis to the S2S and SubX reforecasts (*Lim et al.*,
1002 2018; *Kim*, 2017; *Kim et al.*, 2019). Models generally struggle to predict MJO convection, its
1003 associated circulations, and especially the horizontal moisture advection which is a key process for
1004 eastward propagation when crossing the MC (*Kim et al.*, 2019). The error in the MJO propagation
1005 processes and the weaker moisture advection process can be partly associated with the following
1006 mean biases across the Indo-Pacific: a too-dry lower troposphere, excess surface precipitation, more
1007 frequent occurrence of light precipitation rates, and a transition to stronger precipitation rates at
1008 lower humidity than in observations (*Kim et al.*, 2019). However, errors emanating from other
1009 processes (vertical moisture advection, cloud-radiation feedback, air-sea coupling, and diurnal
1010 cycle) may also play an important role in degrading MJO propagation and prediction skill.
1011 Therefore, improved process-level understanding of model errors in MJO prediction is crucial for
1012 improving MJO prediction skill. The ongoing international projects, such as the YMC Project

1013 (Section 3.6.3), will help improve our understanding of the critical processes involved with the MC
1014 prediction barrier issue. Also, saving 3D output fields from multi-model prediction systems will
1015 provide an opportunity to study which physical processes in the forecast models require better
1016 representation for better MJO predictions. In addition to metrics based solely on forecast skill, more
1017 focus on the process-based skill metrics could help illuminate addressable model shortcomings,
1018 which is necessary to advance MJO prediction towards its theoretical predictability.

1019 This concise review of the latest progress on MJO prediction and predictability is largely
1020 based on the extensive review by Kim et al. (2018) where more detailed discussions can be found.

1021 ***3.5 Atmosphere-ocean coupled feedbacks within the MJO***

1022 MJO convection is most often observed over SSTs greater than 28°C throughout the Indo-
1023 Pacific Warm Pool, with a secondary maximum over the eastern tropical Pacific (*Salby and*
1024 *Hendon, 1994*). Krishnamurti et al. (1988) first proposed that air-sea interactions over these warm
1025 waters provide energy for 30-50 day convective motions, noting that the typical intraseasonal SST
1026 fluctuations of ~0.25°C could alter fluxes by 10-15% to regulate MJO convective intensity. Ocean
1027 “coupled feedbacks” comprise the SST response to atmospheric forcing, its modulation of surface
1028 fluxes, and the effects of the modified fluxes on the atmosphere.

1029 Understanding the role of ocean feedbacks to the MJO is beset with several challenges. The
1030 observed MJO always develops in a coupled system, but some MJO events appear more sensitive to
1031 ocean feedbacks than others (e.g., *Gottschalek et al., 2013; Fu et al., 2015*). Furthermore, the
1032 seasonal cycle (*Zhang and Dong, 2004; Jiang et al., 2018a*) and modes of interannual variability,
1033 including the IOD (*Wilson et al., 2013*), ENSO (*Pohl and Matthews, 2007; DeMott et al., 2018*),
1034 and the QBO (e.g., *Nishimoto and Yoden, 2017; Son et al., 2017*), influence MJO intensity and
1035 propagation.

1036 Given the complex, multi-scale and coupled nature of the MJO, model experiments are
1037 required to test hypotheses of ocean feedbacks to the MJO. Analysis typically compares MJO
1038 behavior in coupled (CGCMs) and atmosphere-only (AGCMs) models. While coupled feedbacks
1039 almost always improve MJO simulation (*DeMott et al., 2015* and references therein), biases in
1040 simulated atmospheric and oceanic processes may strengthen or weaken coupled interactions in
1041 CGCMs relative to those observed, erroneously supporting or refuting the tested hypotheses. More
1042 importantly, mean-state SST biases in CGCMs alter tropical mean moisture and circulation (*Zhang*

1043 *et al.*, 2006) and may lead to incorrect conclusions about the MJO sensitivity to coupled feedbacks
1044 (*Klingaman and Woolnough*, 2014).

1045 In this section, we review MJO coupled feedbacks, report recent advances in understanding
1046 how ocean feedbacks affect the MJO, interpret these results in terms of MJO scientific issues
1047 (Section 2) and theory (Section 3.2), and conclude with recommended experimental protocols to
1048 further advance our understanding. For simplicity, we limit our discussion to extended boreal
1049 winter (November-April).

1050 *3.5.1 Summary of coupled processes within the MJO*

1051 MJO coupled feedbacks can be thought of as a cycle of atmospheric forcing of the ocean, the
1052 oceanic response to that forcing, and the atmospheric response to the resulting SST anomalies.
1053 DeMott *et al.* (2015) discuss these processes in detail; a brief synopsis is presented here. The
1054 atmosphere forces the ocean through fluxes of heat, fresh-water, and momentum. Reduced
1055 cloudiness and calm winds during an MJO suppressed phase increase solar heating and reduce
1056 wind-driven upper-ocean mixing, and reduce evaporative surface cooling (Fig. 7), which stabilize
1057 and thin (or shoal) the oceanic mixed layer (5~20 m deep; *Drushka et al.*, 2012). The shallower
1058 mixed layer effectively reduces upper-ocean heat capacity, yielding a larger warming per unit
1059 heating than for a deeper mixed layer. Under strongly suppressed conditions, a thin ocean mixed
1060 layer combined with intense diurnal surface heating can induce diurnal SST perturbations of 1-3 K.
1061 Nighttime surface cooling drives convective overturning of the ocean mixed layer, mixing some of
1062 the daytime-accumulated heat below the mixed layer; the remaining heat yields a warmer upper
1063 ocean at the next day's sunrise than the previous day's sunrise (*Anderson et al.*, 1996). Thus, the
1064 SST diurnal cycle rectifies onto the intraseasonal scale (e.g., *Bernie et al.*, 2005; *Zhao and Nasuno*,
1065 2020).

1066 For sufficiently strong MJO events, low-level MJO-induced easterlies may exceed low-level
1067 mean state westerlies, resulting in a net westward momentum flux into the upper ocean. As with
1068 surface heat fluxes, the strongly stratified upper ocean limits the momentum flux to the upper
1069 ocean, yielding westward surface currents, especially within about 2.5°S-2.5°N. The resulting
1070 warm-water advection augments flux-driven surface warming. Poleward of 2.5° latitude, Coriolis
1071 deflection of surface currents excites anticyclonic (downwelling) oceanic equatorial Rossby waves,

1072 their Ekman transport forces surface water to the circulation center, suppressing the local
1073 thermocline and further maintaining the local warm SST anomaly by limiting deep-ocean mixing.

1074 During an MJO convective transition phase, reduced subsidence and low-level easterlies
1075 promote more frequent and deeper convection and enhance evaporation, which tempers upper-
1076 ocean warming. By the onset of an MJO active phase, cloud shielding of surface solar heating and
1077 strong low-level westerlies that typically follow MJO convection (e.g., *Lin and Johnson, 1996; Puy*
1078 *et al., 2016*) transfer accumulated upper ocean energy to the atmosphere via surface fluxes (*Zhang*
1079 *and McPhaden, 2000*), where it helps maintain anomalous convective heating (*Riley Dellaripa and*
1080 *Maloney, 2015; DeMott et al., 2016*).

1081 Fresh-water and momentum fluxes during an MJO active phase substantially affect upper-
1082 ocean stratification and surface currents. Widespread freshening from rainfall stabilizes the upper
1083 ocean, yielding a shallower salt-stratified layer over a deeper temperature-stratified layer (e.g.,
1084 *Drushka et al., 2016; Pei et al., 2018*) separated by an isothermal “barrier layer” (*Sprintall and*
1085 *Tomczak, 1992*) that resists mixing both from above and below. Sufficiently strong barrier layers
1086 can inhibit vertical mixing of MJO-driven surface momentum fluxes, limiting them to the
1087 uppermost ocean, where they may drive anomalous surface currents that persist long after the wind
1088 forcing subsides, limiting further upper-ocean stabilization and warming before the next MJO event
1089 (*Moum et al., 2016; Hong et al., 2017b*). Equatorial current-driven Ekman transports and sea
1090 surface height anomalies forced by strong low-level westerly winds project onto oceanic shallow-
1091 water wave modes, such as oceanic upwelling Rossby and downwelling Kelvin waves. In the
1092 Indian Ocean, the downwelling Kelvin wave is partially reflected by the Sumatra coast as
1093 downwelling Rossby waves that propagate to the western Indian Ocean in roughly 70 days (*Nagura*
1094 *and McPhaden, 2012*), whereas in the Pacific, the downwelling Kelvin wave may initiate
1095 (*McPhaden, 2004*) or maintain (*Kapur and Zhang, 2012; Lopez et al., 2013*) El Niño conditions. In
1096 less stable conditions, momentum fluxes promote mixing to the deeper ocean (e.g., *Han, 2005*).

1097 3.5.2 Recent Progress: Direct vs indirect ocean feedbacks to the MJO

1098 While there are event-to-event differences in MJO-linked SST anomalies, the canonical view
1099 of the ocean-atmosphere system during MJO active phases includes warm SST anomalies to the
1100 east, maximum ocean-to-atmosphere surface turbulent fluxes roughly collocated with MJO
1101 convection, and cold SST anomalies to the west (Fig. 8). Variations in surface fluxes arise from

1102 variations in low-level winds (wind-driven fluxes) and near-surface vertical gradients of moisture
1103 or temperature (SST-driven fluxes). Since SST-driven fluxes communicate SST anomalies to the
1104 atmosphere, the most direct ocean feedbacks to the MJO are enhanced total surface flux before
1105 convective maximum, and reduced total surface flux afterward.

1106 DeMott et al. (2016) estimated that direct SST-driven ocean feedbacks contribute up to 10%
1107 of the change in column moisture associated with MJO propagation, and roughly $2\% \text{ day}^{-1}$ of the
1108 column moistening or heating that sustains MJO convection. Since SST-driven surface fluxes tend
1109 to offset wind-driven fluxes, the *direct* effect of coupled feedbacks *reduces* the amplitude of
1110 anomalous surface fluxes within the MJO lifecycle, which seems at odds with numerous studies
1111 that report coupled feedbacks improve MJO simulation. Furthermore, MJO MSE budget analyses
1112 (Section 3.9) confirm that surface fluxes are secondary to cloud radiative feedbacks and mid-level
1113 moisture advection for MJO maintenance and propagation, respectively. It is unlikely that direct
1114 coupled feedbacks are the primary means by which ocean processes influence the MJO and its
1115 propagation.

1116 The limited role of direct feedbacks suggests that more complex *indirect* ocean feedbacks--
1117 those that regulate an intermediate process that more effectively interacts with the MJO, or operate
1118 on temporal scales other than intraseasonal--may be important. Examples of intermediate processes
1119 include stronger MJO convection with larger anvil clouds that amplify radiative feedbacks to MJO
1120 convection (*Del Genio and Chen, 2015*); low-level convergence forced by MJO-associated sharp
1121 SST gradients (*Hsu and Li, 2012; Li and Carbone, 2012*); or amplified low-level convergence east
1122 of MJO convection through lower-tropospheric destabilization (*Marshall et al., 2008; Benedict and*
1123 *Randall, 2011; Wang and Xie, 1998; Fu et al., 2015*).

1124 DeMott et al. (2019) explored direct and indirect ocean feedbacks to the MJO in four pairs of
1125 CGCMs and AGCMs. For each model, monthly mean SSTs from the CGCMs were prescribed to
1126 the AGCMs, to ensure that they had identical SST mean states and low-frequency variability.
1127 Consistent with previous studies, the CGCMs showed significantly enhanced MJO propagation
1128 compared to the AGCMs. However, ocean feedbacks did not uniformly (across models) improve
1129 metrics of MJO circulation or cloudiness structure (e.g., *Wang et al., 2018a*). The CGCMs showed
1130 mixed effects of *direct* coupled feedbacks to the MJO: maintenance of the MJO heating anomalies
1131 by surface fluxes increased in two models, but decreased or unchanged in the other two. Surface

1132 flux feedbacks to MJO propagation decreased in all four CGCMs, despite warm SST anomalies
1133 during MJO convective development, which strongly supports the role of *indirect* ocean feedbacks
1134 to MJO propagation in models.

1135 DeMott et al. (2019) also found inconsistent evidence for “intermediate” coupled feedback
1136 processes. Coupling enhanced longwave heating and MJO maintenance in only one GCM; BL
1137 convergence east of MJO convection (akin to frictional wave-CISK; Section 3.2) was enhanced in
1138 two GCMs. In one GCM, MJO propagation improved despite weakening of both these intermediate
1139 processes.

1140 An MSE budget analysis showed that coupled feedbacks improved MJO propagation in all
1141 CGCMs through stronger mid-level horizontal moisture advection, driven by sharper mean near-
1142 equatorial meridional moisture gradients (Fig. 9). Similar experiments with at least two other
1143 models have produced similar results (D. Kim, X. Jiang; personal communications). This implies
1144 that relatively high-frequency (<30 days) SST perturbations affect MJO propagation through the
1145 background moisture distribution, even under identical SST mean state and low-frequency
1146 variability.

1147 Other recent studies have revealed different flavors of cross-timescale or “intermediate
1148 process” MJO coupled feedbacks. Rydbeck and Jensen (2017) found that warm SST anomalies
1149 from oceanic equatorial Rossby waves in the western Indian Ocean (generated by coastal reflection
1150 of downwelling Kelvin waves forced by earlier MJO westerly winds) create sharp SST gradients,
1151 which are responsible for up to 45% of boundary layer convergence prior to MJO convective onset.
1152 Shinoda et al. (2017) note that the reflected Rossby waves may modulate the near-Equator Somali
1153 Current or alter the thermal structure of the Seychelles thermocline ridge. Zhou and Murtugudde
1154 (2020) found that SST anomalies up to +0.6 K northwest of Australia during MJO suppressed
1155 conditions generate anomalous cyclonic circulations and moisture advection that promote the MJO
1156 convective “detour” south of the MC. In regional coupled simulations, Zhao and Nasuno (2020)
1157 found that the rectification of diurnal SST variability associated with ocean mixed-layer shoaling
1158 onto intraseasonal SST perturbations was more important for MJO propagation than the diurnal
1159 SST itself.

1160 Advances in understanding MJO interactions with lower-frequency variability in SST and
1161 moisture have refocused efforts to understand ENSO modulation of MJO activity. ENSO-driven

1162 Warm Pool SST anomalies modulate MJO variance, such that seasonal-scale MJO activity is
1163 enhanced near warm ENSO SST anomalies and suppressed near cold SST anomalies. Wang et al.
1164 (2018c) highlighted that western Pacific MJO activity is weaker during East Pacific (EP) El Niños
1165 and stronger during Central Pacific (CP) El Niños, associated with greater meridional advection of
1166 mean state moisture by stronger intraseasonal wind anomalies during CP events. CP events also
1167 drive stronger MJO diabatic heating anomalies (e.g., *Marshall et al.*, 2016), which may be related
1168 to the aforementioned stronger wind anomalies, MJO propagation is faster in CP events than in EP
1169 events, associated with enhanced low-level convergence east of MJO convection (Wang et al.,
1170 2019).

1171 Klingaman and DeMott (2020) demonstrated that the MJO response to ENSO in a CGCM
1172 may lead to incorrect perceptions of how intraseasonal coupled feedbacks affect MJO. In the full
1173 CGCM, the MJO improved substantially with coupling, compared to the corresponding AGCM
1174 with prescribed CGCM SSTs (*DeMott et al.*, 2014). The authors coupled the same AGCM to a one-
1175 dimensional (1D) mixed-layer ocean model to control the background SST while retain
1176 intraseasonal coupled feedbacks. The MJO was robust when background SST was constrained to an
1177 observed climatology, but weakened substantially when background SST was constrained to the
1178 CGCM climatology, in contrast to the strong MJO in the CGCM itself. The AGCM-1D ocean
1179 model produced an MJO that resembled the CGCM MJO only when background SST was
1180 constrained to the CGCM climatology plus a repeating ENSO cycle derived from the CGCM. In
1181 both this AGCM-1D and the CGCM simulations, MJO was stronger in El Niño years, but weaker
1182 or absent in neutral or La Niña years, respectively. The El Niño background SST and moisture
1183 gradients mitigated CGCM mean-state biases, including a cold and dry equatorial Pacific. The
1184 simulated MJO is sensitive not only to intraseasonal coupled feedbacks, as often assumed, but also
1185 to (potentially erroneous) longer-scale feedbacks. Changes to model physics may affect the MJO
1186 directly, or via direct coupled feedbacks, or via indirect coupled feedbacks on scales shorter or
1187 longer than the MJO. Isolating these effects requires investing in detailed sensitivity experiments.

1188 *3.5.3 Ocean feedbacks to the MJO in the context of critical issues and existing theories*

1189 Recent studies provide the context for critical issues (Section 2) and prevailing theories
1190 (Section 3.2) of the MJO. The coupled feedbacks analyzed in DeMott et al. (2019) and Klingaman
1191 and DeMott (2020) and their effects on the mean moisture distribution strongly support the WTG

1192 moisture mode theory of the MJO. The increased boundary-layer moisture export east of MJO
1193 convection in two CGCMs in DeMott et al. (2019) supports the trio-interaction theory; the
1194 surprising result that the two other CGCMs exhibited weaker boundary-layer moisture export,
1195 despite improved MJO propagation, suggests a need for greater scrutiny of boundary layer-
1196 moisture-convection feedbacks in models and observations. These latter models used 1D ocean
1197 mixed-layer models constrained to climatological SSTs. This eliminates ENSO and may limit MJO
1198 improvement with coupling, either through missing El Niño-induced zonal moisture gradients, the
1199 absence of an extended Warm Pool (e.g., *Pohl and Matthews, 2007*), or the lack of central Pacific
1200 warm SST anomalies to promote boundary-layer moisture export east of MJO convection
1201 (*Marshall et al., 2008; Wang et al., 2019a*). Support for skeleton model or gravity wave
1202 interference MJO theories are unclear in these studies. The results of DeMott et al. (2019) argue
1203 against the BLQE theory, as all four CGCMs show improved MJO propagation despite
1204 significantly reduced surface fluxes east of MJO convection.

1205 *3.5.4 Recommendations for future progress*

1206 Recent progress in understanding the role of ocean coupling to the MJO suggests that ocean
1207 feedbacks on scales both shorter and longer than intraseasonal are important for MJO propagation.
1208 Improved understanding of oceanic processes that affect high-frequency SST fluctuations, and how
1209 low-level atmospheric stability and free-tropospheric moisture regulate the convective response to
1210 those SST fluctuations, is essential to improve MJO in models. This objective involves two of the
1211 longest-standing challenges in atmospheric and oceanic modeling: the parameterizations of
1212 atmospheric convection and oceanic mixing, respectively. For longer scales, process-level
1213 diagnostics can shed light on how ENSO regulates MJO behavior, as well as synergistic ENSO-
1214 MJO feedbacks.

1215 Recent work has led to a few “best practices” for related model sensitivity studies. First, the
1216 MJO in a CGCM should not be compared to that in an AGCM with prescribed CGCM daily mean
1217 SSTs, as the inability of the AGCM SST to vary in response to surface fluxes leads to strong
1218 simultaneous rainfall-SST correlations, instead of the lead-lag relationship from observations and
1219 CGCMs (e.g., *Pegion and Kirtman, 2008*). Second, CGCM and AGCM simulations should be
1220 performed with the same mean SST and low-frequency SST variability, as any differences may
1221 affect the MJO more strongly than intraseasonal or higher-frequency ocean feedbacks. It is best

1222 practice to force the AGCM with CGCM monthly mean SSTs. Klingaman and DeMott (2020)
1223 demonstrated that it is then helpful to diagnose MJO sensitivity to ENSO. Finally, thermodynamic
1224 ocean feedbacks to the MJO are best understood in an AGCM coupled to a 1D ocean mixed-layer
1225 model constrained to observed, CGCM, or ENSO states. This framework minimizes SST mean-
1226 state changes, includes feedbacks from high-frequency SST perturbations, and maintains the
1227 observed SST-rainfall phase relationship. Furthermore, this framework can help reveal the
1228 sensitivity of the MJO, and convection in general, to diurnal SST fluctuations (e.g., *Matthews et al.*,
1229 2014) that are captured only with fine oceanic vertical resolution (~1 m in the upper ocean) and
1230 frequent (~hourly) ocean-atmosphere coupling (e.g., *Li et al.*, 2013; *Hsu et al.*, 2019; *Zhao and*
1231 *Nasuno*, 2020). A collection of simulations, including fully coupled, atmosphere-only, and 1D-
1232 ocean coupled can help identify the timescales of coupled feedbacks that most strongly enable or
1233 inhibit MJO fidelity, and focus efforts to improve oceanic or atmospheric processes most relevant
1234 to those scales during model development cycles.

1235 **3.6 MJO propagation over the Maritime Continent**

1236 Situated in the heart of the Indo-Pacific warm pool between the Indian and Pacific Oceans,
1237 the MC has been recognized as a major source of heat and moisture that plays a pivotal role in
1238 driving global atmospheric circulation (*Ramage*, 1968; *Neale and Slingo*, 2003; *Slingo et al.*, 2003).
1239 Due to land-ocean contrasts and to complex topography over the mountainous MC islands, most of
1240 the total annual rainfall over the MC occurs via a vigorous diurnal cycle that is strongly coupled
1241 with land-sea breezes (e.g., *Yang and Slingo*, 2001b; *Nesbitt and Zipser*, 2003; *Mori et al.*, 2004;
1242 *Qian*, 2008; *Kikuchi and Wang*, 2008; *Love et al.*, 2011; *Peatman et al.*, 2014). Observations show
1243 that the MJO tends to be significantly weakened when propagating eastward into the MC region;
1244 the MJO also often detours around the MC via an oceanic pathway south of Sumatra Island and
1245 over the Java Sea in austral summer (*Wu and Hsu*, 2009; *Kim et al.*, 2017). Often, the MJO even
1246 completely dissipates over the MC and fails to propagate into the western Pacific, known as the MC
1247 barrier effect for MJO propagation (e.g., *Salby and Hendon*, 1994; *Seo and Kim*, 2003; *Kim et al.*,
1248 2014a; *Kerns and Chen*, 2016; *Zhang and Ling*, 2017). About 50% of the total MJO events during
1249 the boreal winter are disrupted over the MC (*Zhang and Ling*, 2017). Due to the MJO's significant
1250 impacts on downstream high-impact weather and climate events in both the tropics and extratropics

1251 (see Section 3.8), determining whether the MJO will propagate through the MC is crucial for
1252 climate prediction.

1253 The MC barrier effect, however, is poorly simulated in current GCMs (e.g., *Jiang et al.*, 2015;
1254 *Ahn et al.*, 2017; *Ahn et al.*, 2020b); and most forecast systems exhibit large deficiencies in
1255 predicting the MJO propagation through the MC (see Section 3.4). These model shortcomings in
1256 simulating and predicting the MJO propagation through the MC are partially due to our poor
1257 understanding of the underlying physics responsible for the MC barrier effect (see also a recent
1258 review by *Kim et al.*, 2020a). In this subsection, we briefly review recent progress on studies of the
1259 interactions between the MC and the MJO.

1260 *3.6.1 The barrier effect of the Maritime Continent on the MJO propagation*

1261 Several factors have been proposed for the weakening of MJO amplitude over the MC, which
1262 include the topographic effect and land surface processes over the MC, upscale impacts of the local
1263 diurnal cycle, and regional and large-scale mean moisture distributions.

1264 a. Orographic effects of MC

1265 Hsu and Lee (2005) illustrated that the lifting and frictional effects caused by the steep
1266 topography over the major MC islands will induce near-surface moisture convergence east of the
1267 topography, where a new deep-convection region develops. This leads to a sudden shift in the deep
1268 convection from the Indian Ocean to the western Pacific. Wu and Hsu (2009) further showed that
1269 the blocking effect, as well as the mountain-wave-like structures induced by the MC topography,
1270 will lead to a southward detour of the eastward propagating MJO away from the MC mountains and
1271 a sudden shift of deep convection. In an aqua-planet AGCM study, Inness and Slingo (2006) also
1272 suggested that the topographic blocking effect on the low-level Kelvin wave leads to the observed
1273 weakening of the MJO over MC. In particular, the representation of Sumatra in the GCM, as a
1274 north-south oriented ridge straddling the equator, seems to be particularly effective at blocking the
1275 Kelvin wave signal, and thus weakening or even completely destroying the MJO signal east of the
1276 MC.

1277 By using a full atmosphere-ocean coupled GCM that realistically simulates the major
1278 observed MJO characteristics, Tseng et al. (2017) found that the MC orography and land-sea
1279 contrast can lead to the southward detour during the eastward propagation of MJO convection. The
1280 authors also found the MC orography and land-sea contrast distorted the coupled Kelvin-Rossby

1281 wave structure as previously hypothesized, but amplified the MJO over the MC, in contrast to the
1282 general notion of the MC damping effect on the MJO. It is argued that the MC islands strengthen
1283 the mean low-level westerlies in the eastern Indian Ocean and the western MC, which strengthens
1284 the eastward-propagating MJO. This will be further discussed.

1285 b. MC land surface processes

1286 Motivated by the observational and modeling evidence that the surface latent heat flux is
1287 critical to sustain MJO variability (e.g., *Maloney and Sobel, 2004; Kim et al., 2011a*), the reduced
1288 MJO amplitude over the MC could be ascribed to the weak surface heat flux associated with
1289 enhanced MJO convection over the MC land, because of finite land-surface moisture holding
1290 capacity relative to ocean regions (*Sobel et al., 2008; Sobel et al., 2010*). On the other hand, an
1291 AGCM simulation suggests that transpiration in the tropical forests over the MC may play a critical
1292 role in weakening local MJO variability (*Lee et al., 2012*). By turning off transpiration in the
1293 AGCM, the simulated precipitation variability increases substantially compared to the control
1294 experiment. It is argued that surface turbulent fluxes over tropical rainforests are highly correlated
1295 with incoming solar energy rather than wind speed as is the case over the ocean, which possibly
1296 decouples the land precipitation and large-scale disturbances like the MJO. In contrast, in the
1297 absence of transpiration, the simulated surface latent heat flux dependence on incoming solar
1298 energy decreases, while its dependence on wind increases, making land areas more coupled to
1299 MJO-like disturbances (*Lee et al., 2012*).

1300 c. Diurnal cycle

1301 It has been hypothesized that reduced MJO amplitude over the MC region could result from a
1302 competition for moist energy between the diurnal cycle of convection and low-frequency variability
1303 (e.g., *Wang and Li, 1994; Zhang and Hendon, 1997; Neale and Slingo, 2003; Oh et al., 2012; Oh et*
1304 *al., 2013*). Therefore, vigorous diurnal variability over MC land limits the moist energy to support
1305 MJO convection. This dynamical link between the diurnal cycle and the MJO, however, needs to be
1306 corroborated further, as results vary on the relationship between the MJO and the diurnal rainfall
1307 rate over MC land. While several studies suggested that the amplitude of the diurnal rainfall cycle
1308 over MC islands tends to weaken during enhanced MJO convection (*Oh et al., 2012; Peatman et*
1309 *al., 2014; Sui and Lau, 1992; Rauniyar and Walsh, 2011*), Sakaeda et al. (2017) suggested that such
1310 a relationship is statistically insignificant, particularly over land regions away from the coasts. Jiang

1311 et al. (2019) also suggested that the MJO does not significantly change the amplitude of diurnal
1312 rainfall cycle over MC land, but rather increases its daily mean value. Meanwhile, Tian et al.
1313 (2006a) illustrated that the diurnal cycle of tropical deep convective clouds tends to be enhanced
1314 over both MC land and ocean during the convectively active phase of the MJO.

1315 On the other hand, several modeling studies support the hypothesis that the diurnal cycle over
1316 the MC damps the MJO amplitude as previously hypothesized. Oh et al. (2013) showed that in
1317 simulations where the diurnal cycle was suppressed by nudging toward daily averaged TRMM rain
1318 rates and reanalysis prognostic variables, the MJO amplitude is maintained rather than weakened as
1319 it moves over the MC. In an idealized modeling study, Majda and Yang (2016) proposed that the
1320 MJO temperature anomaly is cancelled by that from the upscale impact by the diurnal cycle, which
1321 suppresses MJO deep convection when it propagates into the MC. Based on CRM simulations,
1322 Hagos et al. (2016) demonstrated that the eastward propagation of an MJO event over the MC can
1323 be significantly enhanced after switching off the diurnal cycle of insolation in the model, while the
1324 model MJO is quickly damped over the MC when the diurnal effect is present.

1325 d. Regional and large-scale mean moisture distribution

1326 From the perspective of the moisture mode framework, Kim et al. (2017) illustrates that the
1327 southward detour of MJO convection during its propagation over the MC is primarily ascribed to
1328 stronger moistening ahead of the MJO convection over the southern MC, rather than the central
1329 MC, due to horizontal moisture advection by MJO perturbation winds acting upon the background
1330 moisture gradient. Both zonal and meridional moisture advection are greater in the southern MC
1331 region because of a stronger zonal gradient of background moisture for the former, and more
1332 organized northerly MJO wind anomalies that bring near-equatorial moist air southward for the
1333 latter (*Kim et al.*, 2017).

1334 Meanwhile, by using high-resolution reanalysis data, it is shown that the interruption of
1335 lower-tropospheric moistening over the MC islands ahead of the MJO convection is closely
1336 associated with the topographically phase-locked mean moisture pattern over the MC (*Hung and*
1337 *Sui*, 2018; *Jiang et al.*, 2019). Strongly shaped by the local diurnal cycle, the low-level winter-mean
1338 moisture pattern over the MC is characterized by moisture maxima over local mountain peaks
1339 (*Jiang et al.*, 2019). Given this mean moisture distribution, the moisture advection by anomalous
1340 easterly MJO winds corresponding to the active MJO convection over the eastern Indian Ocean will

1341 lead to a drying (moistening) effect to the east (west) of the mountain peaks, which disrupts the
1342 organization of large-scale MJO convection over the MC area.

1343 *3.6.2 Propagating versus non-propagating MJO events over the Maritime Continent*

1344 While several plausible processes responsible for the reduced MJO amplitude over the MC
1345 are described above, they do not address the question of why some MJO events pass through the
1346 MC and propagate into the western Pacific, while others are interrupted over the MC region. As
1347 previously mentioned, accurate forecasts of whether the MJO can pass over the MC is critical for
1348 prediction of downstream climate and weather extremes influenced by the MJO. This has motivated
1349 many recent studies to identify key processes underlying the propagating and non-propagating MJO
1350 events over the MC.

1351 Kim et al. (2014a) suggested that whether MJO convection over the eastern Indian Ocean can
1352 cross over the MC is closely associated with the suppressed convective conditions over the western
1353 Pacific. The low-level off-equatorward Rossby wave circulation in response to the negative
1354 convective heating over the western Pacific induces strong moistening over the MC, which helps
1355 MJO eastward propagation over the MC. The importance of the leading suppressed convection
1356 (LSC) for Indian Ocean MJO convection to cross the MC is also suggested by Chen and Wang
1357 (2018b). The LSC enhances the low-level anomalous easterly winds, and thus increases BL
1358 convergence and promotes eastward propagation of the MJO. Higher predictive skill is also found
1359 for Indian Ocean MJO events when the LSC is present in the forecast initial conditions (Kim,
1360 2017). A systematic relationship between propagating MJO events crossing the MC and suppressed
1361 convective conditions over the west Pacific, however, is not evident in the analysis by Feng et al.
1362 (2015), although MJO cases with strong LSC tend to exhibit more coherent eastward propagation
1363 than those with weak LSC. It is questionable, however, whether the LSC is independent from the
1364 enhanced MJO convection over the Indian Ocean. And what controls the strength of the LSC? The
1365 enhanced MJO convection over the Indian Ocean and the LSC over the western Pacific may be
1366 modulated by the same large-scale factors.

1367 By using a precipitation-tracking method, Zhang and Ling (2017) also examined distinctions
1368 between MJO events that propagate across the MC and those blocked by the MC. The authors
1369 found that precipitation of propagating MJO events mainly occurs over the MC ocean area, while
1370 land precipitation dominates for the blocked MJO events. It is thus hypothesized that the strong

1371 diurnal cycle over the MC land may inhibit convective development over the ocean and thus be a
1372 possible mechanism for the barrier effect of the MC. Ling et al. (2018) further illustrates that
1373 propagating MJO events over the MC region are characterized by a stronger vanguard of
1374 precipitation, namely, enhanced precipitation over the MC islands one week prior to the peak MJO
1375 convection, when convection over the surrounding seas is still suppressed (*Peatman et al., 2014*;
1376 see Fig. 1b). This stronger land precipitation increases soil moisture, thus reducing the diurnal
1377 amplitude of land convection and the dominance of oceanic precipitation as the MJO convection
1378 moves over the MC, which is conducive for propagating MJO events over the MC as discussed by
1379 Zhang and Ling (2017). This process also plays a role for the more coherent model MJO eastward
1380 propagation over the MC when the diurnal cycle is turned off in Hagos et al. (2016). Weakening of
1381 MJO propagation by enhanced land convection over the MC is also illustrated by recent GCM
1382 experiments (*Ahn et al., 2020a*), although the strong MC influences on the MJO propagation in this
1383 study are found to be associated with changes of the mean moisture distribution.

1384 Additionally, the termination of many MJO events (~ 50%) over the MC region could result
1385 from the interruption of MJO moistening over the MC by westward propagating Rossby wave-like
1386 dry anomalies, or the so-called transient dry precursor (TDP), from the eastern / central Pacific
1387 (*Feng et al., 2015a; DeMott et al., 2018*). These TDPs tend to be more frequent during La Niña
1388 winters (*DeMott et al., 2018*). The origin of these westward propagating TDPs, however, is not well
1389 understood. Other non-propagating MJO events over the MC that are not linked to TDPs are
1390 associated with weak moistening over the southern MC by horizontal moisture advection, due to
1391 both weak mean moisture gradients (zonal and meridional) associated with the Australian
1392 Monsoon, and easterly wind anomalies due to weak LSC over the western Pacific, largely in
1393 agreement with several previous studies (*Kim et al., 2014a; Feng et al., 2015a; Kim et al., 2017*;
1394 *Chen and Wang, 2018b*).

1395 In a recent observational study, Gonzalez and Jiang (2019) identified two prevailing
1396 intraseasonal variability modes over the western Pacific during boreal winter. In addition to the
1397 eastward propagating MJO as the leading mode, the second mode is characterized by a westward
1398 propagating intraseasonal mode (WPIM). The MJO eastward propagation tends to be largely
1399 interrupted over the MC when the WPIM is active over the western Pacific, which typically occurs
1400 under a La Niña-like condition, as for the TDPs discussed above, although the link between the

1401 WPIM and TDP is not clear. Propagation of both the MJO and WPIM are regulated by horizontal
1402 MSE advection; their distinct propagation behaviors are largely defined by substantial differences
1403 in mean background moisture and zonal winds (*Gonzalez and Jiang, 2019*). It is thus hypothesized
1404 that the WPIM could also be a moisture mode like the MJO, but is dominated by westward
1405 propagation under a unique environment over the western Pacific, such as a typical La Niña
1406 condition with a sharp reduction in the mean moisture towards the east of the MC. Therefore,
1407 improved understanding of large-scale controls on tropical climate variability modes is needed to
1408 better understand whether MJO convection can propagate through, or get interrupted over, the MC.

1409 On the other hand, a possible role of air-sea coupling has also been suggested for the MJO
1410 propagation over the MC. Timor Sea SSTs are observed to be warmer for propagating MJO events
1411 over the MC than for non-propagating MJO events (*Zhang and Ling, 2017*). Hirata et al. (2013)
1412 also showed that pronounced eastward propagation of the MJO across the MC is associated with
1413 locally warmer SST anomalies over the MC region associated with the subsiding Rossby wave that
1414 precedes the convective phase.

1415 While various processes have been proposed to influence propagation of the MJO over the
1416 MC, these processes are not mutually exclusive. As the strong diurnal cycle over the MC land is
1417 proposed to damp the MJO during its passage over the MC, the diurnal cycle over MC itself is
1418 subject to strong modulations by large-scale climate variability modes, such as El Niño and La Niña
1419 (*Rauniyar and Walsh, 2013*). Therefore, the plausible impacts of the diurnal cycle on the MJO
1420 propagation could also reflect influences from large-scale conditions. Also, in the model
1421 experiments with disabled diurnal cycles or modified MC topography, the simulated changes to
1422 MJO propagation behavior are not only due to the diurnal cycle and MC topography, but also to
1423 associated changes in the large-scale mean state. For example, as previously discussed, the strong
1424 topographically phase-locked mean moisture pattern over the MC, which strongly interrupts MJO
1425 moist preconditioning over the eastern part of the MC mountains, is largely defined by the diurnal
1426 cycle (*Jiang et al., 2019*). If the diurnal cycle is disabled in a model, the regional mean moisture
1427 gradient will be significantly weakened, which favors a smooth eastward MJO propagation over the
1428 MC (*Oh et al., 2013; Hagos et al., 2016*). The reduced MJO amplitude over the MC in Tseng et al.
1429 (2017), in which the MC orography is removed or MC land is replaced by ocean, may also result
1430 from dramatic changes in the model mean state, including the lower-tropospheric mean moisture

1431 distribution, which have been suggested to play a critical role in regulating MJO propagation
1432 (*Gonzalez and Jiang, 2017*).

1433 *3.6.3 The Years of the Maritime Continent (YMC) Field Observations*

1434 As discussed above, MJO propagation over the MC is regulated by both large-scale conditions
1435 and regional processes over the MC, including the diurnal cycle and land-sea breezes, due to local
1436 land coverage and elevated terrain. The intricate interactions between the MJO and MC remain
1437 poorly represented in weather and climate models even at very high resolutions (e.g., cloud
1438 permitting; *Hagos et al., 2016; Peatman et al., 2015; Birch et al., 2016; Baranowski et al., 2019*).
1439 With an overarching goal to expedite improved understanding and prediction of local multi-scale
1440 variability of the MC weather-climate systems and its global impact, through observations and
1441 modeling exercises, the YMC field observations have been organized through international
1442 collaboration and coordination (*Yoneyama and Zhang, 2020*). One YMC focus is the barrier effect
1443 of the MC on MJO propagation.

1444 With few YMC field campaigns conducted and others still pending, the limited in situ
1445 observations available from YMC start to provide detailed depictions of MJO modulations of the
1446 local diurnal cycle (*Wu et al., 2017; Yokoi et al., 2017; Yokoi et al., 2019; Wu et al., 2018*), oceanic
1447 barrier layers (*Moteki et al., 2018*), and CCEWs (*Kubokawa et al., 2016; Takasuka et al., 2019*)
1448 over the MC region. With the progress of YMC, these observations will provide unprecedented
1449 datasets to identify model deficiencies in representing MC-MJO interactions, and to advance our
1450 understanding and prediction of MC weather-climate systems and their remote teleconnections.

1451 ***3.7 Tropical-extratropical interaction associated with the MJO***

1452 In addition to the direct impact on the weather and climate in the tropics, the MJO influences
1453 a broad range of phenomena, including high impact weather events, in the extratropical regions
1454 (e.g., *Higgins et al., 2000; Bond and Vecchi, 2003; Jones et al., 2004b; Donald et al., 2006; Lin and*
1455 *Brunet, 2009; Alvarez et al., 2016*). Such global impacts of the MJO likely provide an important
1456 source of skill for subseasonal climate predictions (e.g., *NASEM, 2016*). On the other hand, the
1457 tropical MJO variability can be induced or influenced by extratropical disturbances (e.g., *Lin et al.,*
1458 *2007; Ray and Zhang, 2010; Vitart and Jung, 2010*). The coherent variability between the
1459 extratropical atmosphere and the organized tropical convection, therefore, indicates a tropical-
1460 extratropical interaction on the subseasonal time scale (see a review by *Stan et al., 2017*).

1461 3.7.1 MJO influences on the extratropical circulation

1462 An increasing number of studies have shown that the variability of tropical convection
1463 associated with the MJO has a considerable influence on a wide range of extratropical weather and
1464 climate events. For example, the tropical convection associated with the MJO was found to be
1465 correlated with the precipitation anomaly in the North American west coast (*Higgins et al.*, 2000;
1466 *Mo and Higgins*, 1998; *Bond and Vecchi*, 2003; *Lin et al.*, 2010; *Becker et al.*, 2011). A near-global
1467 impact of the MJO on precipitation was reported in *Donald et al.* (2006). Extreme rainfall over the
1468 contiguous United States was found more likely to happen when the MJO is active than inactive
1469 and most frequently when the MJO convection center is over the Indian Ocean (*Jones and*
1470 *Carvalho*, 2012; *Barrett and Gensini*, 2013). A modulation of U.S. West Coast atmospheric river
1471 activity is responsible for the MJO's effect on extreme rainfall there (*Guan et al.*, 2012; *Baggett et*
1472 *al.*, 2017; *Mundhenk et al.*, 2018). A significant influence of the MJO on subseasonal variability in
1473 wintertime surface air temperature in North America was observed (*Lin and Brunet*, 2009; *Zhou et*
1474 *al.*, 2012b; *Baxter et al.*, 2014; *Zheng et al.*, 2018). Surface air temperature over Canada and the
1475 eastern United States in winter tends to be anomalously warm (cold) 10-20 days following the MJO
1476 phase 2-3 (6-7), which according to *Wheeler and Hendon* (2004) corresponds to enhanced
1477 (reduced) convection in the tropical Indian Ocean and suppressed (enhanced) convection in the
1478 equatorial western Pacific (*Lin and Brunet*, 2009; *Lin et al.*, 2019a). It was reported that the phase
1479 of the MJO has a substantial systematic and spatially coherent effect on subseasonal variability in
1480 wintertime surface air temperature in the Arctic region (*Vecchi and Bond*, 2004; *Yoo et al.*, 2012),
1481 which contributes to the subseasonal forecast skill (*Lin*, 2020).

1482 The influence of the MJO also extends to the Southern Hemisphere extratropics. The winter
1483 temperature and precipitation variability in southeastern South America was observed to have a
1484 coherent signal associated with different MJO phases (*Naumann and Vargas*, 2010; *Barrett et al.*,
1485 2011). *Alvarez et al.* (2016) documented the influence of the MJO in South America and their
1486 marked seasonal variations. *Chang and Johnson* (2015) reported that several Southern Hemisphere
1487 teleconnection patterns in June-August exhibit oscillatory behavior on time scales of 20-30 days
1488 and with the frequency of occurrence modulated by the MJO phases. *Flatau and Kim* (2013)
1489 demonstrated that enhanced MJO convection in the Indian Ocean precedes changes in the Antarctic
1490 Oscillation (AAO). The impact of the MJO on Australian rainfall, circulation, and temperature was

1491 also reported (*Wheeler et al.*, 2009; *Marshall et al.*, 2014). Fauchereau et al. (2016) suggested that
1492 the MJO directly impacts regional circulation and climate in the New Zealand region, potentially
1493 through extratropical Rossby wave response to tropical diabatic heating. Whelan and Frederiksen
1494 (2017) found that tropical-extratropical interactions associated with the MJO contributed to the
1495 extreme rainfall and flooding in northern Australia during January 1974 and January 2011.

1496 The MJO influence on extratropical weather and climate events is largely through its
1497 modulation of atmospheric circulation patterns. Of particular interest is the modulation of the
1498 dominant modes of variability in the wintertime Northern Hemisphere by the MJO, as these modes
1499 account for a large portion of variance on the S2S time scale and have a significant impact on
1500 extratropical weather and climate. The PNA pattern is known to be closely associated with ENSO
1501 variability on the interannual time scale (*Wallace and Gutzler*, 1981; *Horel and Wallace*, 1981).
1502 Hsu (1996) suggested that the PNA variability on the intraseasonal time scale is linked to the
1503 convective activity over the eastern Indian Ocean. Mori and Watanabe (2008) found that the
1504 development of the PNA can be triggered by the MJO convection activity in the tropical Indian
1505 Ocean and western Pacific. Seo and Lee (2017) explicitly demonstrated three different propagation
1506 ways of waves emanating from the Rossby wave source to the PNA region. Tseng et al. (2019)
1507 showed that the PNA pattern is optimally triggered when the MJO has a dipole heating structure
1508 with opposite signed convection anomalies in the west Pacific and Indian Ocean.

1509 The NAO is another important mode of variability that influences the Northern Hemisphere
1510 weather, especially in eastern North America and Europe (e.g., *Hurrell et al.*, 2013). The NAO is
1511 usually considered as a regional expression of the Arctic Oscillation (AO), or the Northern Annular
1512 Mode (NAM; e.g., *Thompson and Wallace*, 1998; 2000). Earlier studies found that the AO/NAO
1513 variability is associated with wave-mean flow interactions and wave breaking in the extratropics
1514 (e.g., *Limpasuvan and Hartmann*, 1999; *Franzke et al.*, 2004). This indicates that the atmospheric
1515 internal dynamics of the extratropical circulation is likely the primary mechanism for the AO/NAO
1516 variability, and implies a lack of predictability for this mode beyond the synoptic weather time
1517 scale (e.g., *Greatbatch*, 2000). However, recent studies have provided evidence that part of the
1518 AO/NAO variability is associated with the tropical forcing of the MJO. The eastward progression
1519 of the convectively active phase of the MJO was found to be associated with changes in tendency
1520 and sign of the AO (*L'Heureux and Higgins*, 2008). Through time-lagged composites and

1521 probability analysis of the NAO index with respect to different phases of the MJO, Lin et al. (2009)
1522 revealed a robust lagged connection between the MJO and NAO. About 10-15 days after the
1523 occurrence of MJO phase 2-3 (6-7), the probability of a positive (negative) NAO is significantly
1524 increased. Based on the definition of Wheeler and Hendon (2004), MJO phases 2-3 (6-7)
1525 corresponds to a dipole structure of tropical convection anomaly with enhanced convection in the
1526 tropical Indian Ocean (western Pacific) and reduced convection in the tropical western Pacific
1527 (Indian Ocean). Similar results of the association between the MJO and NAO were reported in
1528 Cassou (2008). Many S2S models are able to capture such MJO-NAO teleconnection to some
1529 extent (e.g., Vitart, 2017).

1530 To illustrate the influence of the MJO on the PNA and NAO teleconnection patterns, shown
1531 in Fig. 10 are lagged composites of 500-hPa geopotential height anomalies following MJO phase 2
1532 (Figs. 10a-c) and phase 6 (Figs. 10d-f). The calculation is performed on pentad (5-day average) data
1533 derived from the NCEP/NCAR reanalysis (Kalnay et al., 1996) for extended boreal winter of
1534 November to April and the MJO phases are determined from the RMM index of Wheeler and
1535 Hendon (2004). The analysis procedure is the same as that described in Lin et al. (2009), except
1536 that data of 40 winters (1979/80-2018/19) are used here compared to 25 years (1979/80-2003/04) in
1537 the previous study. Lag n indicates that the 500-hPa height anomaly lags the MJO phase by n
1538 pentads. Indicated on the lower left and upper right corners of each panel in Fig. 10 are composite
1539 PNA and NAO indices. The results show that the MJO phases corresponding to a dipole tropical
1540 convection anomaly tend to influence the amplitude of both the PNA and NAO. A negative
1541 (positive) PNA and then a positive (negative) NAO develop following MJO phase 2 (phase 6).

1542 The mechanism for MJO influence on the middle and high latitudes is related to atmospheric
1543 response to tropical forcing. Enhanced vertical motion associated with large-scale tropical deep
1544 convection leads to divergence in the upper tropical troposphere. The upper divergent flow near the
1545 subtropical westerly jet regions creates a source for extratropical Rossby waves (Sardeshmukh and
1546 Hoskins, 1988) that propagate in the middle latitude westerlies bounded by the pole and the critical
1547 latitude where the climatological zonal wind becomes easterlies (e.g., Webster and Holton, 1982;
1548 Hoskins and Ambrizzi, 1993).

1549 The general features of extratropical atmospheric response to the MJO can be simulated using
1550 simple numerical models with idealized tropical thermal forcing (e.g., Matthews et al., 2004; Lin et

1551 *al.*, 2010; *Seo and Son*, 2012; *Tseng et al.*, 2019). One important aspect of these numerical model
1552 studies is the use of realistic three-dimensional wintertime climatological mean flow. It was
1553 demonstrated that a large portion of the MJO-related teleconnection is a direct response to tropical
1554 heating and can be explained by linear dynamics. These numerical studies also show that the
1555 extratropical response pattern is established in about two weeks. A dipole tropical forcing which
1556 corresponds to MJO phases 2-3 or 6-7 is the most effective in exciting extratropical circulation
1557 anomalies (*Lin et al.*, 2010; *Tseng et al.*, 2019), consistent with several earlier studies (e.g.,
1558 *Simmons et al.*, 1983; *Lau and Phillips*, 1986; *Ferranti et al.*, 1990).

1559 Besides the Rossby wave propagation discussed above, other dynamical processes in the
1560 extratropics likely contribute to the atmospheric response to tropical heating as well. The centers of
1561 action of teleconnection patterns tend to appear in preferred locations, e.g., the eastern North
1562 Pacific and the North Atlantic. Disturbances on the time scale of 10-90 days at these locations can
1563 grow by extracting kinetic energy from the zonally asymmetric climatological flow through
1564 barotropic conversion (e.g., *Simmons et al.*, 1983; *Branstator*, 1985). The effect of synoptic-scale
1565 transients of the 2-10-day time scale is another factor that contributes to the extratropical
1566 atmospheric response to the tropical forcing. When interactions between different frequencies
1567 become strong, the nonlinear component of extratropical response becomes important. For
1568 example, *Cassou* (2008) noticed that the positive and negative NAO events following MJO phases
1569 3 and 6 evolve differently. Some nonlinear aspects of the extratropical response to the MJO were
1570 discussed in *Lin and Brunet* (2018).

1571 As Rossby wave propagation is dependent on the strength of the westerly mean wind
1572 (*Hoskins and Ambrizzi*, 1993; *Ting and Sardeshmukh*, 1993), the MJO teleconnection is sensitive to
1573 the background mean flow. This is reflected by the fact that the MJO teleconnection in the Northern
1574 Hemisphere extratropics is stronger in winter than in summer. Another indication of this sensitivity
1575 is that the extratropical patterns associated with the MJO vary in phase and amplitude in different
1576 phases of ENSO (*Roundy et al.*, 2010). The characteristic of the tropical thermal forcing related to
1577 the MJO is likely another important factor that influences the extratropical response. *Yadav and*
1578 *Straus* (2017) demonstrated that slow MJO events tend to have a stronger impact on NAO than fast
1579 MJO events. *Henderson et al.* (2017) found that GCMs with significant biases in basic state and
1580 those with poorly represented MJO forcing simulate poor MJO teleconnection patterns.

1581 Recent studies have shown that the stratosphere may play a role in the MJO teleconnection.
1582 The MJO is observed to influence the state of the stratospheric polar vortex (e.g., *Garfinkel et al.*,
1583 2012, 2014; *Liu et al.*, 2014; *Kang and Tziperman*, 2018b). The signal in the stratospheric polar
1584 vortex can then descend to affect the AO / NAO in a way as described in Baldwin and Dunkerton
1585 (2001). The stratospheric polar vortex may also condition the background flow of the extratropical
1586 Northern Hemisphere for the MJO-related wave propagation. Such a stratospheric pathway for the
1587 MJO-NAO connection was demonstrated in Barnes et al. (2019). Another stratospheric influence is
1588 through the QBO in the tropical stratosphere, which will be discussed in Section 3.8.

1589 3.7.2 Extratropical influences on the MJO and the global intraseasonal variability

1590 Many previous studies have provided evidence that there is considerable extratropical
1591 influence on the tropics. Extratropical waves propagate into the tropics through regions of westerly
1592 zonal wind (e.g., *Webster and Holton*, 1982), and influence tropical convection (e.g., *Kiladis and*
1593 *Weickmann*, 1992; *Matthews and Kiladis*, 1999). Tropical waves can be forced by lateral forcing
1594 from the middle latitudes (e.g., *Yanai and Lu*, 1983; *Zhang and Webster*, 1989; *Hoskins and Yang*,
1595 2000).

1596 On the intraseasonal time scale, the extratropical influence on the tropical variability is also
1597 observed. Liebmann and Hartmann (1984) found that energy propagates from the middle latitudes
1598 to the tropics especially over the eastern Pacific. Localized intraseasonal tropical convection near
1599 the dateline and to the east was found to be forced by extratropical circulation anomalies in Lau and
1600 Phillips (1986). Again over the tropical eastern Pacific was observed the largest extratropical
1601 impact of the non-divergent component of the wind by Ferranti et al. (1990). The large extratropical
1602 impact occurs in the eastern Pacific where the extratropical westerly flow in the upper troposphere
1603 extends into the tropics, which can possibly be explained by the wave propagation mechanism as
1604 discussed in Webster and Holton (1982).

1605 There is evidence of extratropical influence on the MJO. Lin et al. (2007) demonstrated that a
1606 tropical MJO-like wave can be generated in a long integration of a dry atmospheric model with
1607 time-independent forcing. Hong et al. (2017a) observed that the southward penetration of northerly
1608 wind anomalies associated with extratropical disturbances in the extratropical western North Pacific
1609 triggered the tropical convective instability that led to the onset of the MJO to the west of the
1610 dateline. Ray and Zhang (2010) investigated the initialization of MJO events, and found that a

1611 critical factor to the reproduction of the MJO initiation is time-varying lateral boundary conditions
1612 from the reanalysis. Hall et al. (2017) performed several experiments with different lateral
1613 boundary conditions and concluded that about half of the intraseasonal variance in the tropics can
1614 be attributed to the boundary influence of middle latitudes. The NAO variability on the subseasonal
1615 time scale was observed to influence the tropical MJO (*Lin et al., 2009; Lin and Brunet, 2011*).

1616 The instability theory of Frederiksen and Frederiksen (1993,1997) and Frederiksen (2002)
1617 provides a possible explanation for the global intraseasonal variability. Based on a linearized two-
1618 level primitive equation model and simplified tropical convection representation in a three-
1619 dimensional basic state of boreal winter, the instability analysis revealed that some of the unstable
1620 modes couple the extratropics with a tropical 40-60 day disturbance, which is similar to the MJO
1621 (*Frederiksen, 1982; 1983*). The development of extratropical teleconnection patterns including the
1622 PNA and NAO is captured in this framework (*Frederiksen and Lin, 2013*). Simmons et al. (1983)
1623 calculated the most unstable normal mode of the linearized vorticity equation with a zonally
1624 varying basic state of wintertime 300-hPa flow. This mode was found to have a period of 45 days,
1625 and two of its phases project significantly onto the PNA and NAO respectively. The adjoint normal
1626 mode analysis of Ferranti et al. (1990) revealed that the tropical forcing that is optimal to excite the
1627 extratropical unstable normal mode is related to the MJO. This indicates that the atmospheric
1628 barotropic process likely plays an important role in the intraseasonal variability linking the tropical
1629 and extratropical atmosphere. The baroclinic process, on the other hand, was found to enhance the
1630 growth rate of the unstable modes (*Frederiksen, 1983*).

1631 3.7.3 Remarks

1632 Improved understanding of the MJO-related teleconnection and tropical-extratropical
1633 interaction is important for subseasonal to seasonal predictions (e. g., *NASEM, 2016; Vitart et al.,*
1634 *2015*). However, there remain tremendous challenges. Numerical models have great difficulties in
1635 simulating the MJO (Section 3.3). Most S2S models have significant biases in predicting the pattern
1636 and amplitude of the MJO teleconnection (e.g., *Vitart, 2017; Section 3.4*). Reducing model
1637 systematic errors, to have a realistic three-dimensional basic flow, probably is one of the most
1638 important steps to improve the MJO teleconnection simulation, although many challenges remain
1639 (e.g., *Zadra et al., 2018*). Other aspects to explore include the role of synoptic-scale transients in
1640 generating and maintaining the MJO teleconnection. It is of interest to better understand the

1641 processes involved in the initiation of tropical intraseasonal convection by extratropical waves.
1642 Further studies are also required to understand the role of the stratosphere in the tropical-
1643 extratropical interactions on the subseasonal time scale.

1644 **3.8 The Quasi-biennial Oscillation (QBO) - MJO connection**

1645 **3.8.1 QBO influences on MJO activity**

1646 The MJO activity exhibits pronounced year-to-year variability, which has been attributed to
1647 influences by ENSO (*Hendon et al., 1999; Hendon et al., 2007; Marshall et al., 2016*) in addition to
1648 the internal variability of the MJO (*Slingo et al., 1999; Lin et al., 2015*). For example, the MJO
1649 activity tends to extend farther eastward to the date line during El Niño winters. The overall level of
1650 MJO activity across the MC, however, does not change significantly in response to ENSO (*Hendon*
1651 *et al., 1999; Son et al., 2017*). Most recently, a strong connection between the QBO, a prevailing
1652 interannual variability mode in the tropical stratosphere, and MJO activity during boreal winter
1653 season was identified (*Liu et al., 2014; Yoo and Son, 2016*), which spurred great interest in many
1654 active studies on this topic (e.g., *Son et al., 2017; Nishimoto and Yoden, 2017; Marshall et al.,*
1655 *2017; Hendon and Abhik, 2018; Wang et al., 2018b; Zhang and Zhang, 2018; Kim et al., 2020c*).

1656 The QBO is an oscillation of the equatorial stratospheric zonal winds between easterlies and
1657 westerlies with an average period of 28 months. These alternating easterlies and westerlies of the
1658 QBO propagate downward with a near-constant amplitude of 20 m s^{-1} between 5 and 40 hPa (e.g.,
1659 *Baldwin et al., 2001*). It is found that about 40-50% of interannual variations of boreal winter MJO
1660 activity is attributed to the QBO (*Marshall et al., 2017; Son et al., 2017*), in contrast to only a
1661 modest (less than 10%) variance of interannual MJO activity explained by the (*Hendon et al., 1999;*
1662 *Hendon and Abhik, 2018; Son et al., 2017*). In general, boreal winter MJO activity is enhanced
1663 when the equatorial lower stratospheric winds at 50hPa are in the easterly phase of the QBO
1664 (hereafter EQBO) and decreased during the westerly phase of the QBO (WQBO; *Yoo and Son,*
1665 *2016; Son et al., 2017; Densmore et al., 2019; Nishimoto and Yoden, 2017; Marshall et al., 2017*).
1666 Moreover, during EQBO MJO propagates more slowly eastward with a prolonged period of active
1667 convection farther into the western Pacific, whereas the MJO convection is largely confined to the
1668 west of the MC during WQBO (*Nishimoto and Yoden, 2017; Son et al., 2017; Zhang and Zhang,*
1669 *2018; Wang et al., 2019d*). The slower eastward propagation of the MJO during the EQBO phase is
1670 possibly resulted from a stronger convection-circulation coupling associated with the MJO,

1671 particularly, due to more coherent MJO eastward propagation over the MC (*Son et al.*, 2017;
1672 *Hendon and Abhik*, 2018). In contrast, activity in CCEWs is found to be insensitive to QBO phases
1673 (*Abhik et al.*, 2019).

1674 Whether MJO events are stronger during EQBO than WQBO or not depends on the MJO
1675 metrics used. Most studies using RMM or the outgoing longwave radiation (OLR)-based MJO
1676 index (OMI; *Kiladis et al.*, 2014) concluded that the MJO is stronger in EQBO than WQBO. By
1677 applying a precipitation tracking method to select individual MJO events and exclude non-MJO
1678 signals, Zhang and Zhang (2018) provided a minority opinion: stronger MJO activities during
1679 EQBO than WQBO are due to a greater number of MJO days during EQBO than WQBO, rather
1680 than stronger individual MJO events. While the strongest MJO events tend to occur during EQBO,
1681 the overall correlation between the strength of all tracked MJO events and a QBO index is
1682 statistically insignificant but the correlation between the number of MJO days and the QBO index is
1683 significant. The more MJO days during the EQBO period is due to more frequent initiation of MJO
1684 events over the Indian Ocean and their longer durations as a result of a weaker barrier effect of the
1685 MC on MJO propagation. The discrepancy on this issue because of different metrics used needs to
1686 be reconciled to provide solid observational evidence for understanding of the mechanism for the
1687 QBO-MJO connection.

1688 *3.8.2 QBO influences on MJO teleconnection patterns*

1689 The MJO teleconnection patterns over the North Pacific is also subject to strong modulations
1690 by the QBO. During EQBO winters, the PNA-like Rossby wave teleconnection pattern over the
1691 North Pacific is more pronounced than the WQBO winters (*Son et al.*, 2017; *Wang et al.*, 2018b;
1692 *Toms et al.*, 2020). The MJO-related North Pacific storm track (NPST) variability exhibits larger
1693 amplitude during EQBO than WQBO. Meanwhile, significant differences in the spatial distribution
1694 of the NPST change between the two QBO phases are also noticed with a zonally elongated pattern
1695 during EQBO winters but separated into two centers during WQBO winters (*Wang et al.*, 2018b).
1696 Further analysis indicates that these differences in NPST activity between the two QBO phases
1697 could be primarily caused by the baroclinic energy conversion and downstream energy propagation,
1698 possibly due to stronger MJO convection and thus associated Rossby wave sources in EQBO
1699 winters (*Wang et al.*, 2018b).

1700 Meanwhile, over the Atlantic sector, the QBO also strongly modulates the MJO-induced NAO
1701 pattern (*Feng and Lin, 2019*). The positive (negative) NAO pattern, which usually occurs after 10
1702 days of the MJO Phase 3 (7) as previously observed (*Lin et al., 2009; Cassou, 2008*), tends to be
1703 much stronger and longer lasting during WQBO than EQBO, possibly by modulating the
1704 extratropical mean flow. During the WQBO winters, anomalous westerly winds are observed over
1705 the extratropical North Pacific as well as high-latitude over the North Atlantic, which could favor
1706 poleward propagation of extratropical Rossby waves and enhance troposphere-stratosphere
1707 interaction that promote development of the NAO (*Feng and Lin, 2019*).

1708 3.8.3 Physical mechanisms for the QBO-MJO connection

1709 While the physical mechanism of the QBO-MJO connection is not completely understood, it
1710 is generally considered through the QBO-related changes in the upper tropospheric static stability
1711 and the vertical zonal wind shear across the tropopause (*Son et al., 2017; Nishimoto and Yoden,*
1712 *2017; Yoo and Son, 2016*). During the EQBO phase, easterlies in the lower stratosphere are
1713 associated with cold temperature anomalies in the lower stratosphere and upper troposphere, in
1714 accord with the thermal wind balance (*Son et al., 2017; Nishimoto and Yoden, 2017*). This is
1715 thought to reduce static stability near the tropopause, and destabilize tropical deep convection as
1716 supported by the recent modeling study (*Nie and Sobel, 2015; Martin et al., 2019*), and thus
1717 promote stronger MJO activity (*Son et al., 2017; Nishimoto and Yoden, 2017; Hendon and Abhik,*
1718 *2018; Martin et al., 2019*).

1719 Hendon and Abhik (2018) further suggested that both positive temperature anomalies in the
1720 upper troposphere and cold anomalies near tropopause at 100hPa are stronger and more in-phase
1721 with the MJO convection during EQBO. Acting together with the reduced static instability during
1722 the EQBO phase, these MJO-induced temperature anomalies can further weaken static instability
1723 near the tropopause, and promote stronger MJO convection during EQBO, which extends further
1724 eastward past the MC (*Hendon and Abhik, 2018*).

1725 Additional evidence of the influences of the QBO-related static stability on the MJO is
1726 provided by examining the QBO-MJO connection during the 11-year solar cycle (*Hood, 2017*). It is
1727 illustrated that the largest amplitudes and occurrence rates of the MJO during boreal winter tend to
1728 occur during EQBO under solar minimum conditions, in concert with the weakest static stability in
1729 the tropical lower stratosphere (*Hood, 2017*). It is also hypothesized that the observed strongest

1730 QBO-MJO connection during boreal winter could be explained by the strongest influences of the
1731 tropopause by the QBO, since the tropical tropopause is highest during this season, particularly
1732 over the MC region (*Kim and Son, 2012; Son et al., 2017; Abhik et al., 2019; Klotzbach et al.,*
1733 *2019*).

1734 Note that enhanced tropical mean convection during the EQBO phase have also previously
1735 been reported (e.g., *Collimore et al., 2003; Liess and Geller, 2012*). In addition to changes in static
1736 stability, strong vertical wind shear of the QBO could also play a role in affecting deep convection
1737 by disrupting the coherent structure of deep convective plumes (*Gray et al., 1992; Collimore et al.,*
1738 *2003; Nie and Sobel, 2015*). The observed QBO-MJO connection, particularly the relative role of
1739 the QBO-related static instability and vertical wind shear near the tropopause, was investigated by a
1740 limited-area CRM with idealized QBO states imposed (*Martin et al., 2019*). In experiments only
1741 forced by the QBO temperature anomalies, stronger MJO convection during EQBO compared to
1742 WQBO is simulated although weaker than the observed. In contrast, experiments with only
1743 imposed QBO wind anomalies show much weaker effects on the MJO, suggesting that temperature
1744 anomalies could be a key pathway through which the QBO can modulate the MJO (*Martin et al.,*
1745 *2019*). Sensitivity experiments also suggest that the QBO influences on MJO tend to depend on
1746 both the amplitude and the height of the QBO temperature anomalies (*Martin et al., 2019*).

1747 Meanwhile, it has also been suggested that the QBO's influences on MJO convective activity
1748 can also be through the cloud-radiation feedback by changing cirrus clouds near the tropopause
1749 (*Son et al., 2017; Hendon and Abhik, 2018*). During EQBO, associated with reduced tropopause
1750 stability, cirrus clouds tend to form more frequently near the tropopause, especially across the MC
1751 and central Pacific (*Son et al., 2017*). These cirrus clouds will lead to a net radiative cooling in the
1752 lower stratosphere and warming in the troposphere (e.g., *Hartmann et al., 2001; Yang et al., 2010*),
1753 thus further destabilize the tropical upper troposphere and help to amplify the MJO (*Son et al.,*
1754 *2017*).

1755 3.8.4 *The QBO-MJO connection in climate model simulations and predictions*

1756 Despite the evidence on the QBO-MJO connection from both observations and idealized
1757 CRM simulations, our latest GCMs have great difficulty in representing this relationship. Lee and
1758 Klingaman (2018) illustrated that while both the QBO and MJO can be well simulated in the
1759 MetUM Global Ocean Mixed Layer coupled model (MetUM-GOML1), a rather weak QBO-MJO

1760 connection is captured in this model compared to the reanalysis. The biased QBO-MJO relationship
1761 in MetUM-GOML1 is considered to be associated with weak QBO-induced temperature anomalies
1762 in the tropical tropopause, or to errors in MJO vertical structure (*Lee and Klingaman, 2018*). By
1763 comparing the 30 CMIP6 models, it is shown that none of the models are able to capture the
1764 observed QBO-MJO connection (*Kim et al., 2020b*).

1765 Due to the inability of GCMs in realistically depicting the QBO-MJO interaction, as an
1766 alternative, model representation of the QBO influences on MJO has been examined using
1767 initialized predictions based on operational models including those participated in the S2S and
1768 SubX Projects. Differences in the predicted MJO under the EQBO and WQBO phases with the
1769 forecast lead time can be examined in these hindcasts. In general, models show a higher MJO
1770 prediction skill during EQBO winters than WQBO winters. For the bivariate anomaly correlation
1771 coefficient of 0.5 or 0.6, the MJO prediction skill during EQBO winters is enhanced by up to 10
1772 days (*Lim et al., 2019; Wang et al., 2019d; Marshall et al., 2017; Abhik and Hendon, 2019*). This
1773 enhancement is found to be insensitive to the initial MJO amplitude, indicating that the improved
1774 MJO prediction skill is not simply the result of an initially stronger MJO during EQBO. Instead, a
1775 longer persistence of the MJO during EQBO winters, is likely responsible for a higher prediction
1776 skill (*Lim et al., 2019; Marshall et al., 2017; Wang et al., 2019d*).

1777 Particularly noteworthy is that the improved MJO predictive skill during EQBO is found even
1778 in low-top models with stratospheric processes poorly resolved (*Marshall et al., 2017; Abhik and
1779 Hendon, 2019; Wang et al., 2019d*). This leads to the implication that the improved MJO predictive
1780 skill during EQBO is not directly resulted from the model-predicted QBO state, or the effect of the
1781 QBO can still be felt in low-top models during the first two weeks of hindcasts. This notion is
1782 further confirmed by the higher MJO prediction skill during EQBO than WQBO in statistical
1783 models that does not contain explicit information about the stratosphere (*Wang et al., 2019d;
1784 Marshall et al., 2017*). Instead, the MJO skill dependence on QBO phases is suggested to be
1785 associated with the initial state of the MJO and/or the regularity of its propagation in the verifying
1786 observations (*Wang et al., 2019d*).

1787 On the other hand, by evaluating reforecasts from nine models participating in the S2S and
1788 SubX Projects, Kim et al. (2020c) illustrated that while generally higher MJO prediction skill
1789 during EQBO than WQBO is also found as in previous studies, the MJO skill difference between

1790 the QBO phases is not statistically significant for most models. This insignificant QBO-MJO skill
1791 relationship is further confirmed by comparing two experiments by using both a high-top and low-
1792 top version of the same GCM. While there are clear differences in the forecasted QBO between the
1793 two experiments, a negligible change is shown in the MJO prediction, indicating that the QBO in
1794 this model may not directly control the MJO prediction. The insignificant QBO-MJO skill
1795 relationship could be due to model deficiencies in representing the QBO signals in tropopause static
1796 stability and vertical wind shear or the vertical structures of the MJO (*Kim et al., 2020c; Lee and*
1797 *Klingaman, 2018; Abhik and Hendon, 2019*). Also, smaller sample size of QBO and MJO events in
1798 the reforecasts relative to the observation could be a reason for the insignificant QBO-MJO
1799 relationship.

1800 Since MJO teleconnection is also strongly modulated by QBO, this thus offers an opportunity
1801 to improve the prediction skill of the MJO-related mid-latitude circulations. Based on the ECMWF
1802 reforecast ensemble system, *Baggett et al. (2017)* found notable differences in the prediction skill
1803 for atmospheric river (AR) activity in mid-latitude during different phases of the MJO and QBO.
1804 Particularly, it is indicated that ARs have the potential to be forecasted more accurately at lead
1805 times of 3 to 5 weeks when the phases of both the MJO and the QBO are considered (*Baggett et al.,*
1806 *2017*). Therefore, future investigations are warranted for improved understanding of the QBO-MJO
1807 interaction when exploiting the untapped source of subseasonal predictability that can provide a
1808 window of opportunity for improved prediction of global climate.

1809 **3.9 MJO structure and teleconnections under a changing climate** 1810

1811 A future climate that is warmed by increasing greenhouse gas concentrations is expected to
1812 produce fundamental changes to the tropics including warmer SSTs, an increased lower
1813 tropospheric vertical moisture gradient, and increased static stability (e.g. *Held and Soden, 2006;*
1814 *Knutson and Manabe, 1995*; see Figure 11). Given the strong dependence of MJO dynamics on the
1815 basic state (e.g. Section 3.2), it is natural to expect that MJO characteristics and associated
1816 teleconnections may be affected by these future climate changes (see *Maloney et al., 2019a* for an
1817 extended review). A general, but not universal, finding from climate models is for the increased
1818 SST and stronger lower tropospheric vertical moisture gradient associated with climate warming to
1819 result in increased MJO precipitation variance (e.g. *Takahashi et al., 2011; Arnold et al., 2015;*
1820 *Wolding et al., 2017; Bui and Maloney, 2018; Haertel, 2018; Rushley et al., 2019*, and Figure 12).

1821 Preferential SST warming in the eastern tropical Pacific (e.g. *Xie et al.*, 2010) may result in
1822 proportionally greater increases in MJO precipitation variance in those regions, although the
1823 tendency for models to preferentially warm the east Pacific with increasing greenhouse gas forcing
1824 does not yet have observational support (*Coats and Karnauskas*, 2017). Increased MJO
1825 precipitation amplitude in a warmer climate is consistent with reduced gross moist stability that
1826 produces a stronger MJO (e.g. *Adames et al.*, 2017a). At the end of the 21st Century under business
1827 as usual warming scenarios, some CMIP3 and CMIP5 models do indicate decreases in MJO
1828 precipitation variance (*Takahashi et al.*, 2011; *Bui and Maloney*, 2018). The modest or even
1829 decreased MJO precipitation amplitude change in some models may be due to a different SST
1830 warming pattern, or a particularly pronounced change toward top-heavy MJO heating structure with
1831 warming (*Takahashi et al.*, 2011; *Bui and Maloney*, 2019a). The latter effect would shift the
1832 vertical profile of MJO convection and associated vertical motion away from the region of strongest
1833 lower tropospheric moisture gradient, making large-scale vertical motion associated with MJO
1834 precipitation less efficient at moistening the column and hence weakening the MJO (*Bui and*
1835 *Maloney*, 2019a; *Wolding et al.*, 2017). Other factors that have been proposed as affecting MJO
1836 amplitude with climate warming include weaker cloud-radiation feedbacks (*Arnold et al.*, 2013;
1837 *Arnold and Randall*, 2015; *Carlson and Caballero*, 2016; *Wolding et al.*, 2017; *Adames and Kim*,
1838 2016), stronger surface flux feedbacks (*Arnold and Randall*, 2015; *Wolding et al.*, 2017), and the
1839 onset of equatorial superrotation that reduces the equator to pole humidity gradient and weakens
1840 dry air advection into the tropics that can damp the MJO (*Carlson and Caballero*, 2016).

1841 Even if MJO precipitation variability increases in a warmer climate, most models indicate that
1842 MJO circulation amplitude decreases more modestly or can even decrease in amplitude relative to
1843 historical conditions (*Bui and Maloney* 2018). This result can be explained by WTG
1844 thermodynamic energy balance. In the presence of increased static stability in a warmer climate
1845 that is consistent with a tropical temperature profile approximately determined by moist adiabatic
1846 adjustment (e.g. Figure 11; *Knutson and Manabe*, 1995), MJO apparent heating anomalies are
1847 balanced by weaker vertical motion (*Maloney and Xie*, 2013; *Bui and Maloney*, 2018). Through
1848 continuity this implies weaker MJO horizontal wind anomalies. Multimodel mean MJO wind
1849 anomalies from CMIP5 are projected to decrease in amplitude at the end of the 21st Century
1850 (Figure 12), although multimodel mean precipitation anomalies are projected to increase (*Bui and*

1851 *Maloney, 2018*). A weakening of MJO wind anomalies at the end of the 21st Century would have
1852 important implications for S2S prediction of extratropical weather, given that Rossby wave
1853 generation associated with MJO teleconnections is forced by divergent flow anomalies produced by
1854 MJO heating (e.g. *Sardeshmukh and Hoskins, 1988; Wolding et al., 2017; Section 3.7*).

1855 Recent work has examined the transient response of the MJO over the 21st Century under
1856 RCP8.5 in CMIP5 models, and has provided mixed results regarding the detectability of MJO
1857 precipitation and wind amplitude changes before the end of the 21st Century. *Rushley et al. (2019)*
1858 examined five CMIP5 models that exhibit good MJO performance in current climate to demonstrate
1859 monotonic increases in MJO precipitation amplitude over consecutive 20 years periods of the 21st
1860 Century, although the increases in MJO precipitation amplitude changes are not distinct from
1861 increases in the background spectrum. *Bui and Maloney (2019b)* used a compositing technique to
1862 examine MJO precipitation and wind amplitude changes over the 21st Century in eleven
1863 simulations from models assessed to have a realistic MJO, including three ensemble members from
1864 one model. Defining a detectable change in MJO activity as the multi-model mean change being
1865 larger than the standard deviation across models (e.g. *Kirtman and coauthors, 2013*), increases in
1866 MJO precipitation amplitude and decreases in MJO circulation amplitude do not become
1867 individually detectable until the last two decades of the 21st Century (Figure 12). Even different
1868 ensemble members from the same model can disagree on the sign of MJO precipitation change for
1869 a given 20-year period, consistent with substantial decadal variability in the climate system.
1870 However, decreases in the relative strength of MJO wind to precipitation anomalies can be detected
1871 as early as 2020-2040, consistent with tropical mean temperature warming and increases in static
1872 stability resulting from such warming (Figure 12). These results suggest that MJO impacts such as
1873 Rossby wave teleconnections that are initiated by divergent flow anomalies may be weaker per unit
1874 MJO precipitation anomaly over the next several decades, and also suggest the robustness of WTG
1875 theory for regulating MJO dynamics. Models from the upcoming CMIP6 database might help to
1876 resolve discrepancies between the *Rushley et al. (2019)* and *Bui and Maloney (2019b)* results on
1877 the near-term detectability of the MJO precipitation amplitude increases with climate warming,
1878 especially since several previous studies have argued that trends in MJO precipitation and wind
1879 amplitude are already detectable in the observational record (e.g. *Slingo et al., 1999; Jones and*
1880 *Carvalho, 2006; Lee and Seo, 2011; Oliver and Thompson, 2012; Tao et al., 2015; Jones and*

1881 *Carvalho, 2011*). However, other studies have argued that natural variability may explain a large
1882 fraction of the recent changes in MJO activity (*Schubert et al., 2013*).

1883 Maloney et al. (2019a) also review other changes to MJO characteristics in a warmer climate
1884 that are projected by climate models. The depth of MJO convective heating and associated vertical
1885 motions are expected to increase with climate warming (e.g. *Chang et al., 2015; Wolding et al.,*
1886 *2017*). MJO propagation speed also tends to increase in models (e.g. *Arnold et al., 2013; Adames et*
1887 *al., 2017a; Liu et al., 2013; Caballero and Huber, 2010; Song and Seo, 2016; Rushley et al., 2019*),
1888 which shifts the MJO toward shorter period. The processes responsible for increased MJO
1889 propagation speed in a warmer climate remain unclear, although previous studies have invoked
1890 increased vertical and meridional moisture gradients as possible causes, particularly through their
1891 ability to hasten moistening through moisture advection to the east of the MJO convective center
1892 (e.g. *Arnold et al., 2015; Wolding et al., 2017; Chang et al., 2015; Adames et al., 2017a*). Many
1893 models also indicate an increase in the frequency of MJO events with warming, a result that is
1894 consistent with the decreased timescale of the MJO with warming (*Arnold et al., 2015; Adames et*
1895 *al., 2017a; Song and Seo, 2016*), although not all models demonstrate this behavior (*Subramanian*
1896 *et al., 2014*).

1897 Many outstanding questions about the effect of climate change on the MJO exist that deserve
1898 future emphasis by the scientific community. Changes in MJO precipitation amplitude in a warmer
1899 climate appear to be complicated by competing effects from basic state moisture profile changes,
1900 temperature profile changes, and MJO vertical structure changes (*Bui and Maloney, 2019a*), and
1901 more work is needed to understand these competing effects in single models and in the new CMIP6
1902 database. Processes responsible for changes in the strength of various feedbacks in warmer climate
1903 as they affect MJO amplitude require scrutiny, including potentially weaker cloud-radiative
1904 feedbacks and strengthened wind-evaporation feedbacks. The effect of the pattern of SST change
1905 on MJO amplitude needs further investigation, as MJO amplitude changes show substantial
1906 sensitivity to the pattern of SST change (*Takahashi et al., 2011; Maloney and Xie, 2013*). Many
1907 models do not reproduce the regional details of the tropical SST trend over the historical record
1908 (*Coats and Karnauskas, 2017*), which makes the SST pattern change a key uncertainty in future
1909 MJO projections. The processes responsible for increases in MJO propagation speed with climate
1910 warming remain relatively unclear. The separate contributions of SST warming and direct impact of

1911 increasing greenhouse gas concentrations on the MJO should be examined, as previous modeling
1912 studies have shown potentially important direct impacts of greenhouse gas changes on the tropical
1913 hydrologic cycle (*Allen and Ingram, 2002; Deser and Phillips, 2009*). How MJO teleconnections
1914 change in a warmer climate requires more scrutiny, including potentially confounding effects due to
1915 changes in the amplitude of MJO divergence anomalies and basic state changes such as the strength
1916 and extent of the north Pacific jet that affect the Rossby wave source and pathway of stationary
1917 Rossby wave propagation (e.g. *Hoskins and Ambrizzi, 1993*). Finally, the CMIP6 database presents
1918 an excellent opportunity to reassess the findings of *Rushley et al. (2019)* and *Bui and Maloney*
1919 *(2019b)* on when changes in MJO characteristics, including the relative strength of MJO
1920 precipitation and wind anomalies, become detectable relative to the historical record in the presence
1921 of substantial decadal variability in the climate system. If the change of the ratio of MJO wind to
1922 precipitation anomalies is as robust as suggested by models, evidence for a weakening ratio over
1923 the last few decades may already be present in the observational record.

1924 **4. Outlook and recommendations**

1925 In this section, we provide a brief outlook and recommendations of MJO research in the near
1926 future (e.g., the coming years or a decade) toward further improved understanding, modeling and
1927 prediction capability of the MJO and associated high-impact weather and climate extremes.

1928 ***4.1 New advanced observations of key processes associated with the MJO***

1929 Our understanding of many key processes of the MJO is hindered by a lack of accurate
1930 observations. For example, while TRMM rainfall products have been widely used to characterize
1931 convective activity associated with the MJO, the light rain and isolated convection associated with
1932 shallow and congestus cumuli during the MJO moisture preconditioning phase are largely
1933 underestimated by the TRMM precipitation radar (e.g., *Jiang et al., 2011; Berg et al., 2010; Short*
1934 *and Nakamura, 2000*). The sparse spatial and diurnal sampling of the TRMM measurements also
1935 precludes analysis of the evolution of individual MJO events. The vertical profiles of precipitation
1936 of the MJO can be significantly improved by the recent GPM Mission (*Hamada and Takayabu,*
1937 *2016; Skofronick-Jackson et al., 2018*). Observations of precipitation and clouds associated with the
1938 light rain regime can be complimented by CloudSat precipitation radar (CPR) (*Berg et al., 2010*),
1939 although the CPR has its own limitation in retrieving the intense rain over the MJO deep convection

1940 region, and lacks detailed information on the diurnal evolution of MJO convection owing to its sun-
1941 nynchronous orbit.

1942 Meanwhile, previous efforts on retrievals of vertical profiles of diabatic and radiative heating
1943 profiles from various satellites provided critical insights into the essential physics of the MJO (*Tao*
1944 *et al.*, 2006; *L'Ecuyer and McGarragh*, 2010; *Henderson et al.*, 2013; *Tao et al.*, 2016). However,
1945 these satellite-based vertical heating estimates are subject to considerable uncertainties due to
1946 limitations of satellite sensors, retrieval algorithms, as well as their dependence on reanalysis
1947 products and CRM simulations, which are further linked to physical parameterizations (*Ling and*
1948 *Zhang*, 2011; *Jiang et al.*, 2011; *Del Genio and Chen*, 2015).

1949 In the near future, new revolutionary remote-sensing technology and improved retrieval
1950 algorithms will provide an unprecedented opportunity to explore various processes crucial for the
1951 MJO as previously reviewed. For example, by employing the next-generation high-performance
1952 lidar and radar technology, the EarthCARE Mission (*Illingworth et al.*, 2015), to be launched in
1953 2021, will deliver comprehensive datasets that can be used to study the relationship among clouds,
1954 aerosols and radiation at accuracy levels that will significantly improve our understanding of MJO
1955 physics, including vertical profiles of aerosol, clouds, precipitation, and radiative cooling/heating
1956 associated with the MJO, and provides critical benchmark to constrain climate model development.
1957 The Doppler capability of the EarthCARE Project will also provide significantly improved
1958 characterization of convective motions and even entrainment processes associated with the MJO as
1959 has been explored based on CloudSat (*Luo et al.*, 2010), which have been shown to be highly
1960 sensitive to MJO behaviors in model simulations.

1961 Advanced observing technologies will also continue to boost our capability of making in situ
1962 observations critical to MJO studies. Autonomous underwater observing technologies (e.g.,
1963 seagliders, Wirewalkers, Prawlers) allow ocean profiles to be measured at spatial and temporal
1964 resolutions and locations not available from the global Argo array and the moored buoy networks
1965 (e.g., TAO, RAMA, PIRATA). The study on the diurnal cycle of the surface layer using seagliders
1966 (*Matthews et al.*, 2014) is one example. Robotic sea surface platforms (e.g., wavegliders,
1967 saildrones, and drifters) measure variables that are key to air-sea exchanges of energy and
1968 momentum but difficult to be observed by satellites. These robotic surface platforms serve to fill
1969 gaps in the moored buoy networks and are particularly useful in sampling regions of high spatial

1970 gradients (e.g., SST fronts, ocean eddies) and coastal regions. The quality of their observations of in
1971 situ state variables for bulk estimates of air-sea turbulent fluxes and radiation fluxes have proven
1972 comparable to those of standard platforms (*Thomson and Girton, 2017; Zhang et al., 2019*). It has
1973 been an even greater challenge to observe the atmospheric boundary layer over the tropical oceans
1974 than at and under the sea surface. Boundary-layer processes and their interaction with the free
1975 troposphere are deemed to play essential roles in MJO dynamics (Section 3.2). But in situ
1976 observations of the marine boundary layer are extremely rare. Traditional ways of measuring
1977 marine boundary layers using ships and airplanes are expensive, logistically difficult, and cover
1978 only limited space and time. Airdrones, which have been used widely for many purposes over land,
1979 can be an efficient and effective platform for observing the marine atmospheric boundary layer. The
1980 mobility of these platforms makes them well suited for adaptive observations for field campaign
1981 and targeted observations. Creative applications of existing and in-development technology would
1982 solve the issues of navigation, power supply, and data transmission to make a network of airdrones
1983 with moored docking devices to routinely sample the marine boundary layer over the tropical
1984 oceans for the study of the MJO and other tropical phenomena. These and other robotic or
1985 autonomous observing platforms should be widely used to fill the current observation gaps for
1986 improving understanding and predicting the MJO.

1987 ***4.2 Continuous improvement of MJO understanding***

1988 The availability of new reanalysis datasets, field observations, and model simulations,
1989 particularly from those based on CRMs, will help advance understanding of the role of multi-scale
1990 interaction among convective elements on the instability and propagation of the MJO. Remaining
1991 questions that can be addressed include whether the upscale transport of momentum, moisture, and
1992 heat from small-scale convective elements is crucial for the observed MJO, and whether these
1993 processes need to be fully resolved for realistic simulations and skillful prediction of the MJO.
1994 Additionally, how smaller-scale convective systems, including the CCEWs and MCSs, and their
1995 underlying physics are regulated by the dynamic and thermodynamic environment associated with
1996 the MJO needs to be fully characterized and understood in the context of two-way interactions
1997 between the MJO and smaller-scale convective systems.

1998 Meanwhile, despite significant progress in the most recent decade in understanding key
1999 processes of the MJO, knowledge gaps remain for explaining the observed year-to-year variability

2000 of the MJO. Many previous studies on the interannual variability of the MJO focused on the
2001 relationship between the MJO and the ENSO, but with controversial findings. While little
2002 relationship between the interannual variability of MJO and ENSO was reported in some studies
2003 (e.g., *Slingo et al.*, 1999; *Hendon et al.*, 1999; *Jones et al.*, 2004a; *Jones and Carvalho*, 2006; *Lin et*
2004 *al.*, 2015; *Son et al.*, 2016), modulations of ENSO-like large-scale environment on MJO amplitude
2005 and propagation were indicated in others (e.g., *Bellenger and Duvel*, 2012; *DeMott et al.*, 2018;
2006 *Gonzalez and Jiang*, 2019). The MJO-ENSO relationship is further complicated by its seasonal
2007 dependence (e.g., *Zhang and Gottschalck*, 2002; *Teng and Wang*, 2003; *Hendon et al.*, 2007) and
2008 the diversity of ENSO events (*Gushchina and Dewitte*, 2012; *Feng et al.*, 2015b).

2009 As discussed in Section 3.8, while strong modulation of the year-to-year MJO activity by the
2010 stratospheric QBO has been reported, our state-of-the-art climate models fail to capture this strong
2011 QBO-MJO connection. Also, although temperature stratification, wind shear, and cloud-radiative
2012 feedbacks associated with the QBO are proposed to play roles in regulating the MJO activity (*Son*
2013 *et al.*, 2016; *Hendon and Abhik*, 2018; *Martin et al.*, 2019), the mechanisms on the QBO-MJO
2014 connection remain largely elusive.

2015 ***4.3 New modeling strategies for improved MJO simulations and predictions***

2016 ***4.3.1 Cloud-permitting resolution***

2017 While the use of horizontal resolution fine enough to resolve convective systems is promising
2018 for improved MJO simulations by alleviating model uncertainties in cumulus processes, this
2019 approach requires significant computing resources, making it impractical for long-term climate
2020 simulations and operational prediction purposes. Therefore, new strategies for the super-
2021 parameterization application are under development. For example, encouraging results have been
2022 reported by using a so-called ultra-parameterization method (*Parishani et al.*, 2017), in which the
2023 grid spacing of the CRM is reduced to 250m to explicitly capture the BL turbulence, clouds, and
2024 entrainment in a global climate model. A quasi-three-dimensional super-parameterization has also
2025 been tested (*Jung and Arakawa*, 2014; *Jung*, 2016), in which 3D CRMs are applied to two mutually
2026 perpendicular channel domains that extend over GCM grid cells, allowing a representation of
2027 topographic effects that could not be implemented in the 2D CRMs in the earlier super-
2028 parameterization models.

2029 4.3.2 Stochastic convective parameterization

2030 Stochastic convective parameterization approach in GCMs (e.g., *Deng et al.*, 2015; *Wang et al.*, 2016b; *Deng et al.*, 2016; *Wang et al.*, 2016b; *Peters et al.*, 2017; *Goswami et al.*, 2017b; *Goswami et al.*, 2017a) is a less-expensive alternative to the CRM approach for representing subgrid cumulus variability. This approach is based on the earlier stochastic modeling concept of introducing subgrid cumulus variability to the deterministic parameterization of coarse resolution GCMs (e.g., *Buizza et al.*, 1999; *Lin and Neelin*, 2003). One of these stochastic convective schemes, the stochastic multi-cloud model (SMCM), has recently been implemented into several different GCMs, yielding improved simulations of both CCEWs and the MJO (*Goswami et al.*, 2017a; *Goswami et al.*, 2017b; *Peters et al.*, 2017). Compared to the conventional ways of tuning parameters in the convection schemes, one advantage of this SMCM approach is that the dominant parameters affecting model MJO variability are different from those controlling the model mean state (*Goswami et al.*, 2017b; *Peters et al.*, 2017). Therefore, unlike the known parameter tuning strategies that give an improved MJO at the expense of the mean state (c.f., Section 3.3.3). Stochastic parameterization has the potential to retain a model's realistic mean state while improving its MJO. A drawback of the SMCM implementation to GCMs is the complicated calibration process of the SMCM which involves many parameters for depicting the transition probability among different cloud types, and many of these parameters are subject to observational constraints. Additionally, plausible dependence of these parameters on the large-scale environment needs to be considered particularly for climate projection studies.

2049 4.3.3 Meso-scale convective system parameterization

2050 Despite the significant role of the MCSs as a building block of large-scale convective systems, the effects of organized convection associated with the MCSs in conventional GCMs are neither resolved nor represented in the cumulus parameterization scheme. A so-called MCS parameterization (MCSP) approach has been recently implemented to represent MCS impacts in climate models. For example, *Moncrieff et al.* (2017) proposed an additional parameterization to represent the layered overturning of MCSs over the conventional convective parameterization scheme. This additional parameterization consists of adding a top-heavy heating profile to the convective heating profile and a corresponding momentum transport profile associated with the layered flow as derived by observations and model simulations (e.g., *Houze et al.*, 2000; *Mechem et*

2059 *al.*, 2006; *Moncrieff and Klinker*, 1997). The profiles are applied when the convective
2060 parameterization is activated and their magnitudes are controlled by the large-scale shear. It has
2061 been shown that simulations of the MJO, CCEWs, and large-scale tropical precipitation patterns are
2062 improved by implementing a minimalist version of this MCSP approach in conventional GCMs
2063 (*Moncrieff et al.*, 2017; *Moncrieff*, 2019). A recent modeling study by Ahn et al. (2019) also
2064 highlighted the ability of MCSP in climate models to mitigate the aforementioned modeling
2065 dilemmas between MJO variability and mean state.

2066 While there is still room for improving MCSP approaches to represent MCS effects in climate
2067 models, the approach holds promise for improved representation of MCS effects in coarse-
2068 resolution models needed for climate projections of Earth's water cycle, rainfall, and severe
2069 weather.

2070 *4.3.4 Machine learning*

2071 Most recently, there is increasing interest in the use of machine learning (ML) approaches to
2072 create computationally efficient parameterizations for convective and BL processes. This approach
2073 involves fitting a statistical model to the output of relatively expensive physical models (e.g.,
2074 CRMs) that more faithfully represent the subgrid processes (*Brenowitz and Bretherton*, 2018;
2075 *Gentine et al.*, 2018; *Schneider et al.*, 2017; *O'Gorman and Dwyer*, 2018; *Rasp et al.*, 2018). In
2076 contrast to conventional parameterizations that incorporate simplified physical models, such as the
2077 entraining plum for convective parameterizations, an ML-based parameterization takes a statistical
2078 approach by minimizing the error between the ML model's predictions of the parameterized
2079 model's output. The resulting GCM is then a hybrid model consisting of a physically based
2080 component and one or more ML-based components.

2081 Rasp et al. (2018) applied a deep neural network to represent all atmospheric subgrid
2082 processes in the Community Atmosphere Model v3.0 (CAM3) by learning from a super-
2083 parameterized version of this GCM (SPCAM) in which convection is treated explicitly. The
2084 traditional subgrid parameterizations in CAM3 were then replaced with the trained neural network
2085 which freely interacted with the resolved dynamics and the surface-flux scheme. The prognostic
2086 multiyear simulations closely reproduced not only the mean climate of the cloud-resolving
2087 simulation but also key aspects of variability, including a realistic MJO and equatorial wave
2088 spectrum.

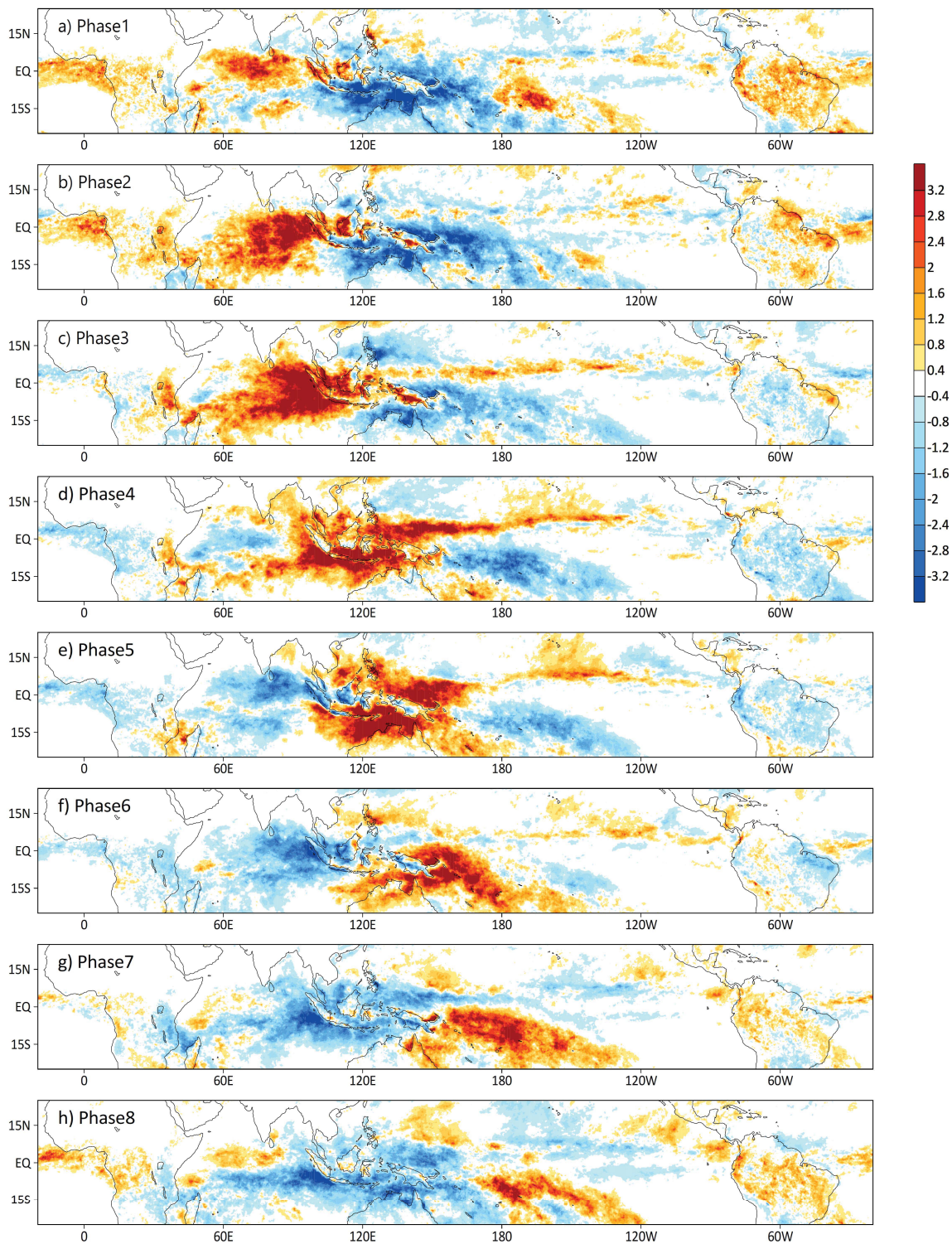
2089 As suggested by promising results from the recent studies, the coupling between the
2090 conventional GCMs and ML-trained statistical models is attractive if the most uncertain
2091 parameterizations in GCMs can be replaced with ML-based parameterizations that are trained
2092 systematically, and meanwhile greatly reduce the computational costs compared to CRMs. One
2093 caveat of this approach is that it may not be suitable for future climate projections based on training
2094 using a present-day mean state.

2095 **5. Concluding remarks**

2096 The crucial role of the MJO in the Earth's hydrological cycle has been well recognized since
2097 it was discovered five decades ago. Advanced understanding and skillful prediction of the MJO and
2098 its global influences have proven challenging, however, due to the complexity of the MJO physics
2099 which involve intricate feedbacks among clouds, circulation, moisture, and radiation. This article
2100 outlines several outstanding issues underlying fundamental MJO physics, and provides a
2101 comprehensive review of the recent progress in the observational, modeling, and theoretical study
2102 of the MJO, with a particular focus on the most recent decade since the publication of several
2103 previous review articles and books (e.g., Zhang, 2005; Lau and Waliser, 2012). Despite the exciting
2104 recent progress achieved in MJO research, significant efforts are warranted to further advance our
2105 understanding and prediction capability of the MJO. For example, our understanding remains poor
2106 on processes regulating the interannual variability of the MJO, the two-way interactions between
2107 the MJO and multi-scale convective elements, and the MJO-mean state trade-off issue in climate
2108 models. These near-future MJO research directions will be aided by the new observations and
2109 modeling strategies discussed in this review article.

2110 ***Acknowledgements:***

2114 We thank Chief Editor M. Zhang for inviting this contribution, H. Hendon and two other reviewers for their
2115 insightful comments on an earlier version of this manuscript, and W. Guan for helping produce several
2116 figures. We also wish to acknowledge WMO WGNE for supporting the MJO Task Force and its activities.
2117 XJ acknowledges support by the NOAA Climate Program Office under awards NA15OAR4310098,
2118 NA15OAR4310177, and NA17OAR4310261. HK was supported by NSF grant AGS-1652289. EDM was
2119 supported by NSF Grant AGS-1841754, NOAA CVP Grant NA18OAR4310299, and NASA CYGNSS
2120 Grant NNX17AH77G. DK was supported by the NASA Grant 80NSSC17K0227, NOAA Grant
2121 NA18OAR4310300, DOE Grant DE-SC0016223, and KMA Grant KMI2018-03110. This is PMEL
2122 contribution 5063. The MJO RMM index can be accessed from the website
2123 <http://www.bom.gov.au/climate/mjo/>. The TRMM 3B42 3-hourly rainfall data was downloaded from the
2124 https://disc.gsfc.nasa.gov/datasets/TRMM_3B42_7/summary, and the GPM IMERG Level-3 half hourly
2125 precipitation data was downloaded from
2126 https://disc.gsfc.nasa.gov/datasets/GPM_3IMERGHH_06/summary. The SubX reforecasts can be
2127 downloaded from <http://iridl.ldeo.columbia.edu/SOURCES/.Models/.SubX/>, and S2S reforecasts from
2128 <https://apps.ecmwf.int/datasets/data/s2s/>.



2129

2130

2131

2132

2133

2134

2135

Figure 1 Evolution of composite rainfall anomalies (mm day^{-1}) during boreal winter season from November to March for MJO Phases 1-8 as defined by Wheeler and Hendon (2004). The rainfall data is based on TRMM (Version 3B42; *Huffman et al.*, 2007) from 1998 to 2016. Before used in the composite analysis, daily rainfall anomalies are derived by removing the climatological annual cycle and then applying a 20-100day bandpass filtering.

2136
2137

2138
2139
2140
2141
2142
2143
2144
2145
2146
2147
2148
2149
2150
2151
2152
2153
2154
2155
2156
2157
2158
2159
2160

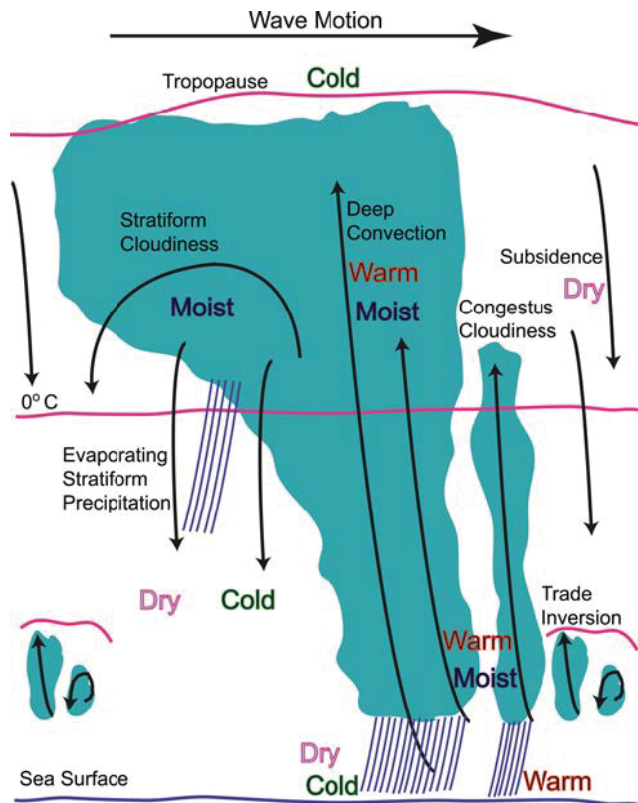
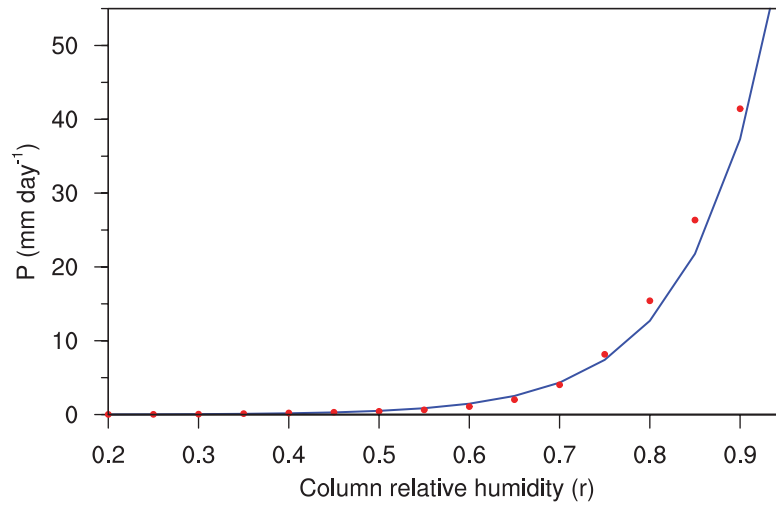


Fig. 2 Typical vertical structures in cloudiness, temperature, and humidity associated with multi-scale tropical convective systems including mesoscale convective systems (MCSs), convectively coupled equatorial waves (CCEWs), and the MJO. Wave movement is from left to right. Figure is reproduced courtesy of the American Geophysical Union from Kiladis et al. (2009).

2161
2162
2163
2164
2165

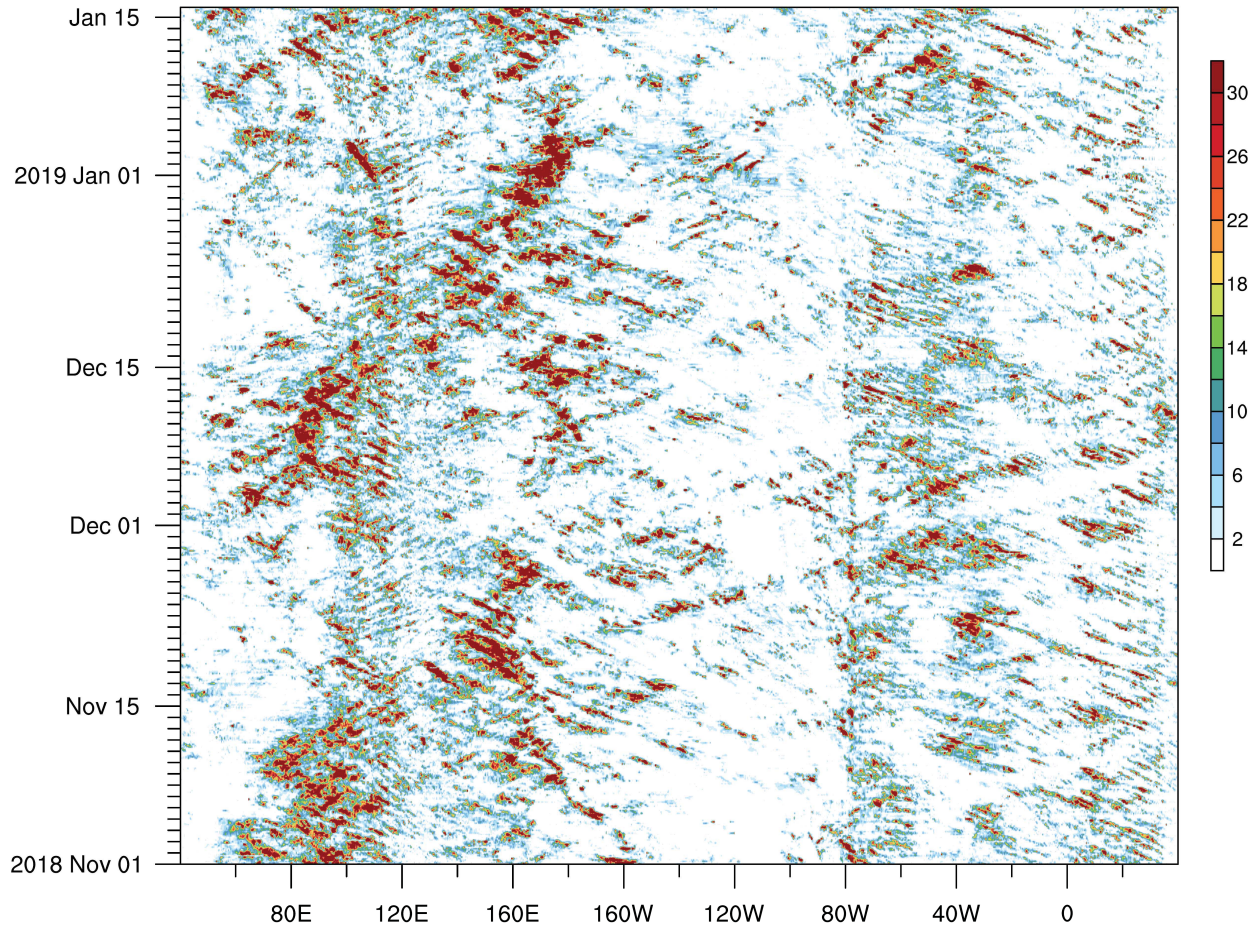


2166

2167 Fig. 3 Red dots: Distribution of daily precipitation P in 5% bins of column-relative humidity r over
2168 the Indian Ocean (15°S - 15°N , 50°E - 95°E) in all months of 1998–2016. The solid blue curve
2169 shows the exponential fit with $P = 0.00228 \exp(10.78 \cdot r)$ (mm day^{-1}). Precipitation and r data are
2170 based on TRMM 3B42 and ERA-Interim reanalysis (Dee *et al.*, 2011), respectively, and
2171 interpolated onto 2.5 by 2.5 degree grids.

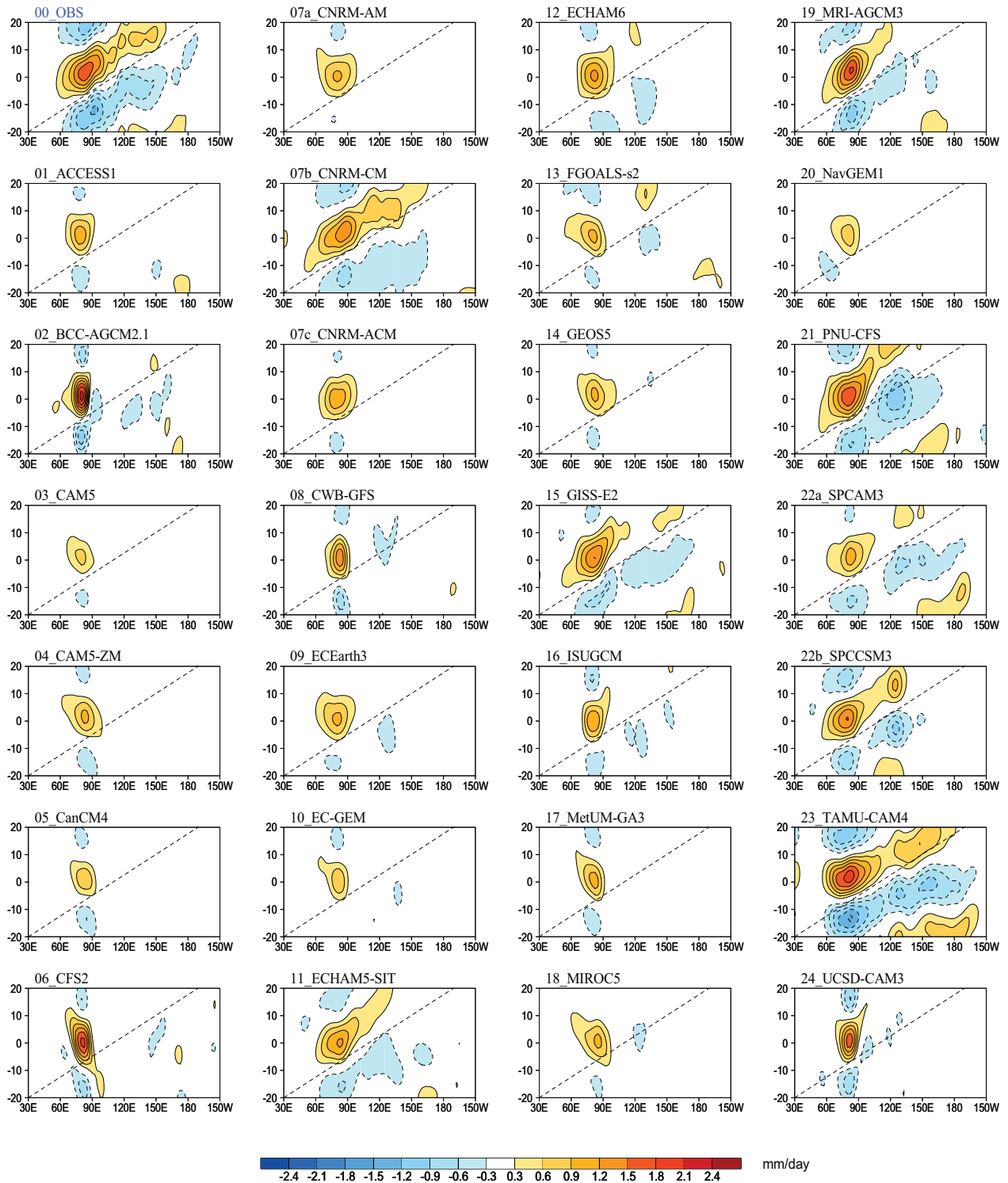
2172
2173
2174
2175
2176
2177
2178
2179
2180
2181
2182
2183
2184
2185
2186
2187
2188
2189
2190
2191
2192
2193
2194

2195
2196
2197
2198
2199



2200
2201
2202
2203
2204
2205
2206
2207
2208
2209
2210

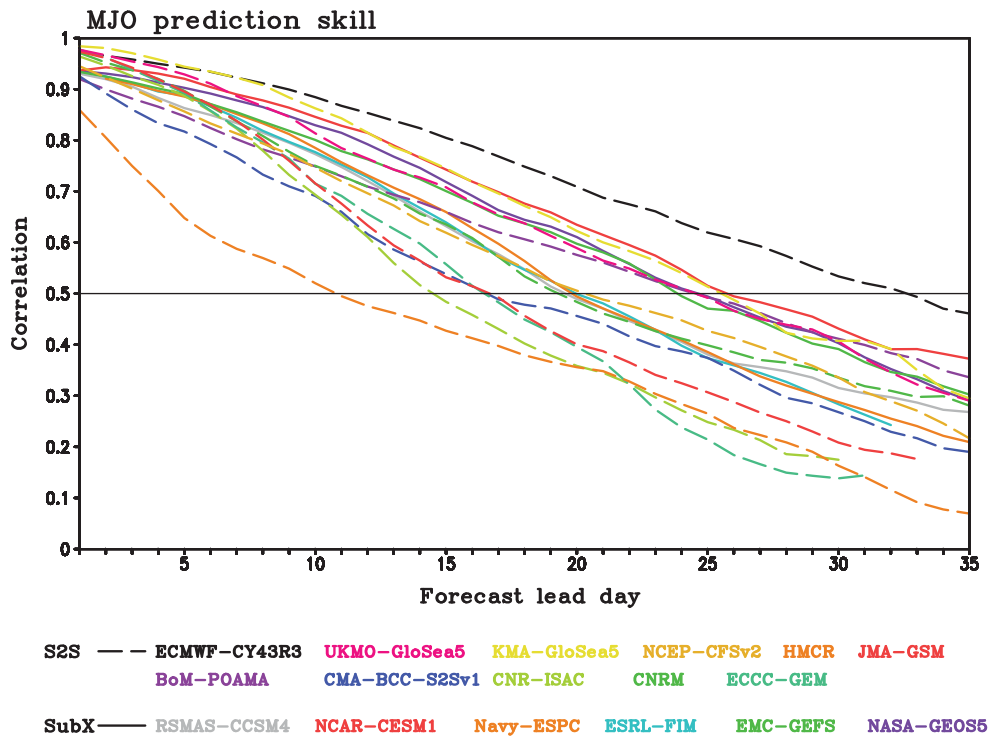
Figure 4. Time-longitude evolution of precipitation (mm day^{-1} ; averaged from 5°S to 7.5°N) from 1 November 2018 through 15 January 2019. Precipitation data is based on the NASA Global Precipitation Measurement (GPM) 0.5-hourly the Integrated Multi-satellitE Retrievals for GPM (IMERG, version 6; Huffman et al., 2019) with horizontal resolution of 0.1 by 0.1 degree.



2211

2212 Figure 5. MJO propagation in GCMs participated in the MJOTF/GASS model comparison project
 2213 represented by longitude-time evolution of rainfall anomalies (averaged over 10°S–10°N)
 2214 based on lag-regression of 20-100-day filtered anomalous rainfall against itself averaged over
 2215 the Eastern Indian Ocean (75–85°E; 5°S–5°N). Dashed lines in each panel denote the 5 m s⁻¹
 2216 eastward propagation phase speed. Reproduced courtesy of the American Geophysical Union
 2217 from Jiang et al. (2015).

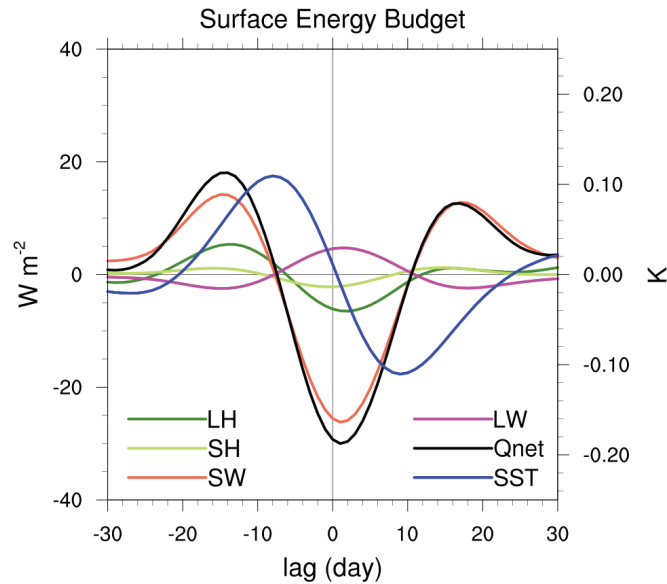
2218
 2219
 2220
 2221
 2222



2223
 2224
 2225
 2226
 2227
 2228
 2229
 2230
 2231
 2232
 2233
 2234
 2235
 2236
 2237
 2238
 2239
 2240
 2241
 2242
 2243
 2244
 2245

Figure 6. RMM prediction skill (bivariate correlation coefficient) for all days between the observation and ensemble means from S2S and SubX during Nov-March. Reforecasts are the same used in Lim et al. (2018) and Kim et al. (2019).

2246
2247
2248
2249



2250

2251

2252

2253

2254

2255

2256

2257

2258

Figure 7. November through April composite surface energy budget terms obtained by regressing 1986-2013 ERA-Interim individual surface heating anomalies onto 20-100 day filtered rainfall averaged over the eastern Indian Ocean (10°S-10°N, 85°E-95°E). Surface net heating (black), net shortwave (orange) and longwave (magenta) radiative fluxes, and latent (dark green) and sensible (light green) heat fluxes are plotted so that a positive flux heats the ocean (all units are (W m⁻²)/(mm day⁻¹) of base point rainfall). The composite SST ((K)/(mm day⁻¹); blue) is plotted on the right axis. The typical MJO rainfall perturbation is about 3 mm day⁻¹. Day 0 corresponds to maximum MJO precipitation.

2259

2260

2261

2262

2263

2264

2265

2266

2267

2268

2269

2270

2271

2272

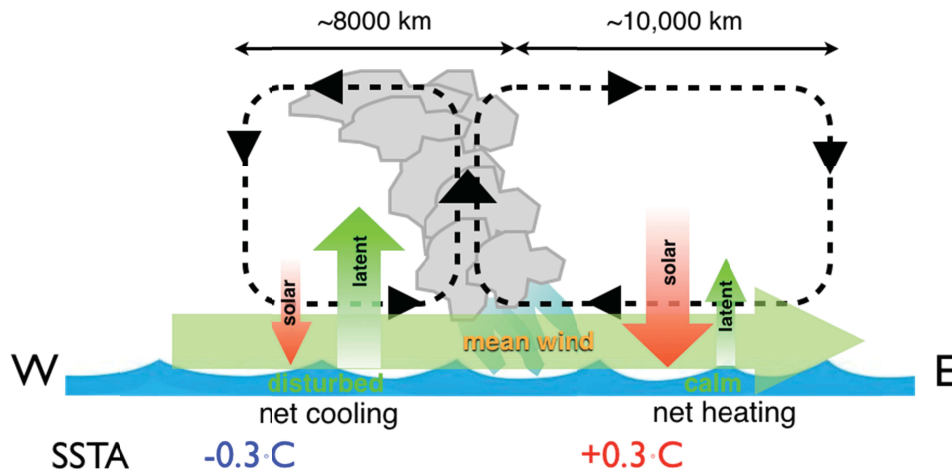
2273

2274

2275

2276

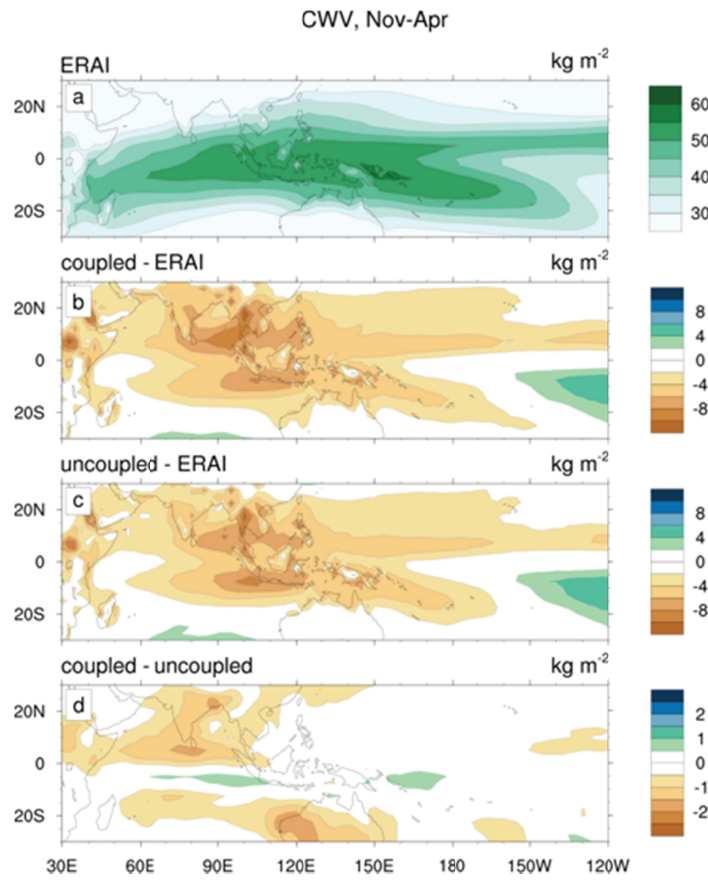
2277
2278
2279
2280



2281
2282
2283
2284
2285
2286
2287
2288
2289
2290
2291
2292
2293
2294
2295
2296
2297
2298
2299
2300
2301
2302
2303
2304
2305
2306
2307
2308
2309
2310
2311

Figure 8. Schematic zonal cross section illustration of MJO convection, circulation anomalies (black dashed arrows) imposed upon Warm Pool mean low-level winds (green horizontal arrow), anomalous surface latent heat flux (green upward arrows) and net surface solar flux (red downward arrows). East (west) of MJO convection, reduced (enhanced) winds and enhanced (reduced) solar heating promote calm (disturbed) ocean conditions and ocean warming (cooling).

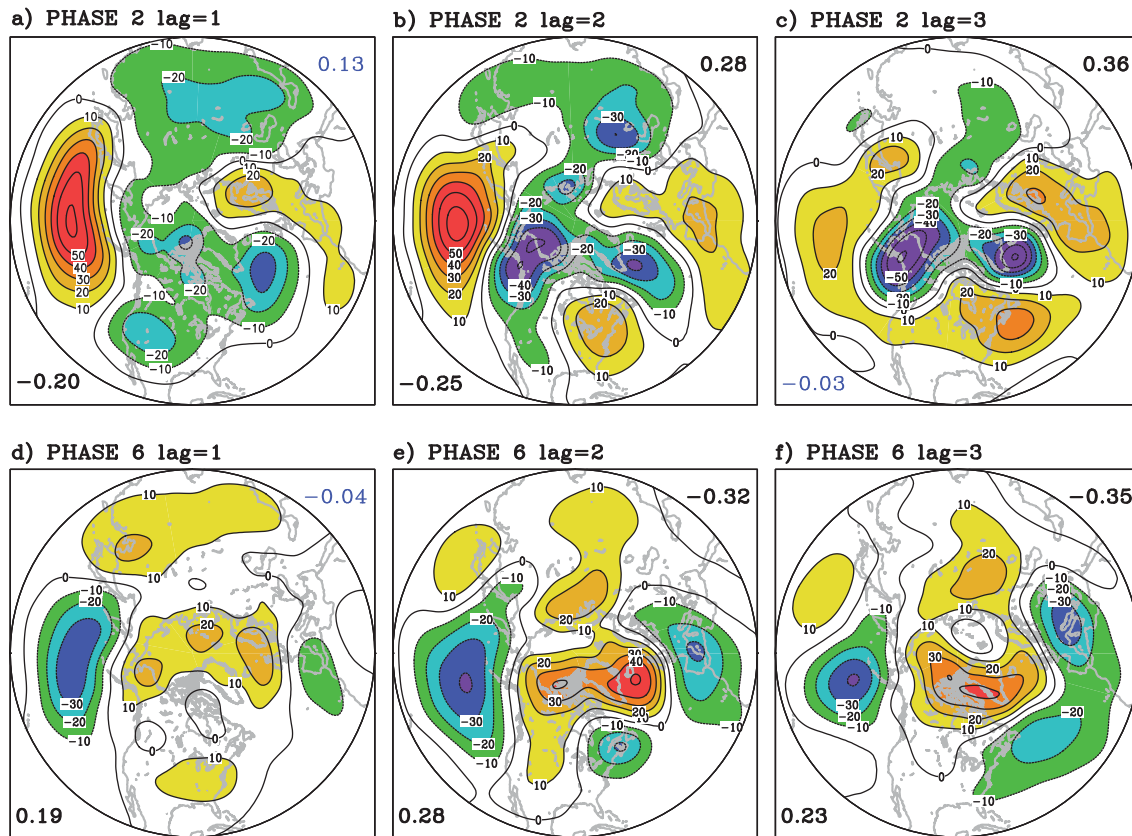
2312
2313
2314



2315
2316
2317
2318
2319
2320
2321
2322
2323
2324
2325
2326
2327
2328
2329
2330
2331
2332
2333
2334
2335
2336

Figure 9. a) November through April 1986-2013 mean column water vapor (CWV; kg m^{-2}) from ERA-Interim. b) coupled and c) uncoupled multi-model ensemble bias, and d) coupled-uncoupled CWV mean state differences for the four models analyzed in DeMott et al. (2019).

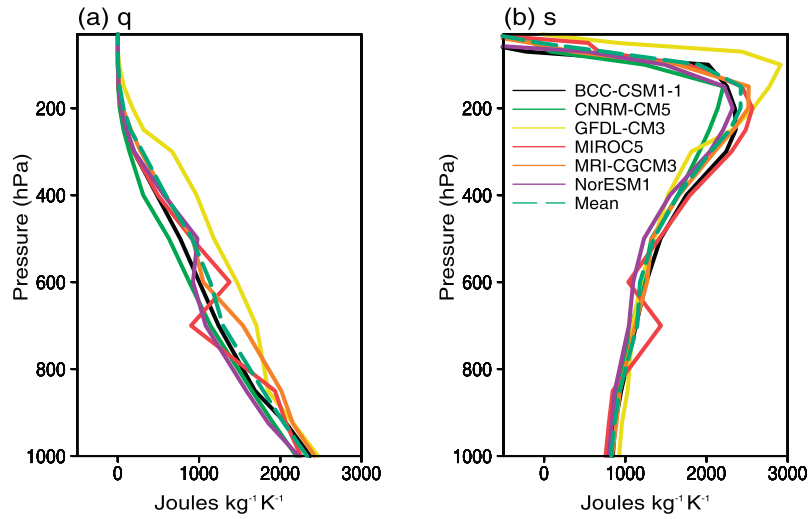
2337
2338
2339
2340



2341
2342
2343
2344
2345
2346
2347
2348
2349
2350
2351
2352
2353
2354
2355
2356
2357
2358
2359
2360

Figure 10. Lagged composites of 500-hPa geopotential height anomaly following MJO (a)-(c) phase 2 and (d)-(f) phase 6. Contour interval is 10 m. Lag= n means that the height anomaly lags the occurrence of MJO phase by n pentads. Detailed description of analysis method can be found in Lin et al. (2009). The number at the upper right (lower left) corner of each panel is the composite NAO (PNA) index which is calculated as projection to the NAO (PNA) pattern. Those in thick black font are different from zero at the 0.05 level according to a Student's t -test. 40 years of pentad data for extended winter from 1979/80 to 2018/19 are analyzed.

2361
2362
2363
2364

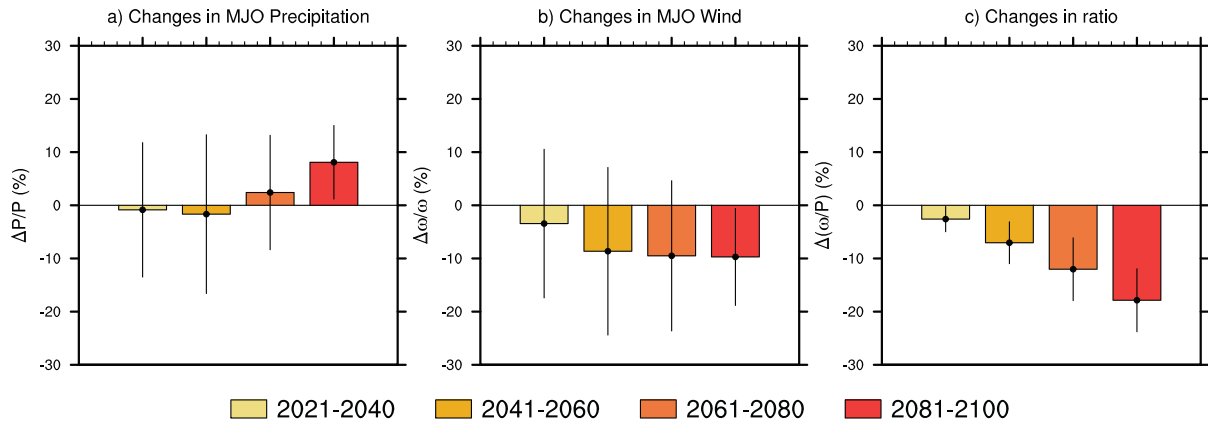


2365

2366 Figure 11. Changes as a function of pressure of November–April mean (a) specific humidity (q ,
2367 multiplied by latent heat of condensation) and (b) dry static energy s in RCP8.5 (2081-2100)
2368 relative to the historical simulations (1986-2005) of five CMIP5 models. Fields are averaged
2369 over the warm pool from 10°S – 0° , 90°E – 180° . Units are $\text{J kg}^{-1} \text{K}^{-1}$. This figure originally found
2370 in Bui and Maloney (2019a). © American Meteorological Society. Used with permission.

2371
2372
2373
2374
2375
2376
2377
2378
2379
2380
2381
2382
2383
2384
2385
2386
2387
2388
2389
2390
2391
2392
2393

2394
2395
2396
2397



2398

2399 Figure 12. Multi-model mean fractional changes in (a) MJO precipitation and (b) 500 hPa omega
2400 amplitude, and (c) changes in the ratio between the two in different decades of the 21st Century
2401 relative to the historical simulation averaged over the warm pool region (15°S-15°N, 60°E-180).
2402 The bars represent the standard deviation across models. Units are %. Before averaging across
2403 the warm pool, amplitude is defined at each location as the root mean squared anomaly across
2404 all eight composite phases of the MJO defined according to Wheeler and Hendon (2004). Figure
2405 is reproduced courtesy of the American Geophysical Union from Bui and Maloney (2019b).

2406
2407

2408

References

2409

- 2410 Abhik, S., and H. H. Hendon (2019), Influence of the QBO on the MJO During Coupled Model Multiweek
2411 Forecasts, *Geophys. Res. Lett.*, *46*, 10.1029/2019gl083152, 9213-9221.
- 2412 Abhik, S., H. H. Hendon, and M. C. Wheeler (2019), On the Sensitivity of Convectively Coupled Equatorial
2413 Waves to the Quasi-Biennial Oscillation, *J. Clim.*, *32*, 10.1175/jcli-d-19-0010.1, 5833-5847.
- 2414 Adames, Á. F., and J. M. Wallace (2014), Three-Dimensional Structure and Evolution of the Vertical
2415 Velocity and Divergence Fields in the MJO, *J. Atmos. Sci.*, *71*, 10.1175/jas-d-14-0091.1, 4661-4681.
- 2416 Adames, Á. F., and J. M. Wallace (2015), Three-Dimensional Structure and Evolution of the Moisture Field
2417 in the MJO, *J. Atmos. Sci.*, *72*, doi:10.1175/JAS-D-15-0003.1, 3733-3754.
- 2418 Adames, Á. F., and D. Kim (2016), The MJO as a Dispersive, Convectively Coupled Moisture Wave:
2419 Theory and Observations, *J. Atmos. Sci.*, *73*, doi:10.1175/JAS-D-15-0170.1, 913-941.
- 2420 Adames, Á. F. (2017), Precipitation Budget of the Madden–Julian Oscillation, *J. Atmos. Sci.*, *74*,
2421 10.1175/JAS-D-16-0242.1, 1799-1817.
- 2422 Adames, Á. F., D. Kim, A. H. Sobel, A. Del Genio, and J. Wu (2017a), Changes in the structure and
2423 propagation of the MJO with increasing CO₂, *Journal of Advances in Modeling Earth Systems*, *9*,
2424 10.1002/2017MS000913, 1251-1268.
- 2425 Adames, Á. F., D. Kim, A. H. Sobel, A. Del Genio, and J. Wu (2017b), Characterization of Moist Processes
2426 Associated With Changes in the Propagation of the MJO With Increasing CO₂, *Journal of Advances in
2427 Modeling Earth Systems*, *9*, 10.1002/2017MS001040, 2946-2967.
- 2428 Ahn, M.-S., D. Kim, K. R. Sperber, I.-S. Kang, E. Maloney, D. Waliser, and H. Hendon (2017), MJO
2429 simulation in CMIP5 climate models: MJO skill metrics and process-oriented diagnosis, *Climate
2430 Dyn.* 10.1007/s00382-017-3558-4, 1-23.
- 2431 Ahn, M.-S., D. Kim, S. Park, and Y.-G. Ham (2019), Do We Need to Parameterize Mesoscale Convective
2432 Organization to Mitigate the MJO-Mean State Trade-Off?, *Geophys. Res. Lett.*, *46*,
2433 10.1029/2018gl080314, 2293-2301.
- 2434 Ahn, M.-S., D. Kim, Y.-G. Ham, and S. Park (2020a), Role of Maritime Continent Land Convection on the
2435 Mean State and MJO Propagation, *J. Clim.*, *33*, 10.1175/jcli-d-19-0342.1, 1659-1675.
- 2436 Ahn, M.-S., D. Kim, D. Kang, J. Lee, K. R. Sperber, P. J. Glecker, X. Jiang, Y.-G. Ham, and H. Kim
2437 (2020b), MJO Propagation across the Maritime Continent: Are CMIP6 Models Better than CMIP5
2438 Models?, *Geophys Res Lett.*
- 2439 Aiyyer, A., and J. Molinari (2008), MJO and Tropical Cyclogenesis in the Gulf of Mexico and Eastern
2440 Pacific: Case Study and Idealized Numerical Modeling, *J. Atmos. Sci.*, *65*, 2691-2704.
- 2441 Allen, M. R., and W. J. Ingram (2002), Constraints on future changes in climate and the hydrologic cycle,
2442 *Nature*, *419*, 10.1038/nature01092, 228-232.

2443 Alvarez, M. S., C. S. Vera, G. N. Kiladis, and B. Liebmann (2016), Influence of the Madden Julian
2444 Oscillation on precipitation and surface air temperature in South America, *Climate Dyn.*, *46*,
2445 10.1007/s00382-015-2581-6, 245-262.

2446 Andersen, J. A., and Z. Kuang (2012), Moist Static Energy Budget of MJO-like Disturbances in the
2447 Atmosphere of a Zonally Symmetric Aquaplanet, *J. Clim.*, *25*, 10.1175/jcli-d-11-00168.1, 2782-2804.

2448 Anderson, S. P., R. A. Weller, and R. B. Lukas (1996), Surface Buoyancy Forcing and the Mixed Layer of
2449 the Western Pacific Warm Pool: Observations and 1D Model Results, *J. Clim.*, *9*, 10.1175/1520-
2450 0442(1996)009<3056:SBFATM>2.0.CO;2, 3056-3085.

2451 Arnold, N. P., Z. Kuang, and E. Tziperman (2013), Enhanced MJO-like Variability at High SST, *J. Clim.*,
2452 *26*, 10.1175/jcli-d-12-00272.1, 988-1001.

2453 Arnold, N. P., M. Branson, Z. Kuang, D. A. Randall, and E. Tziperman (2015), MJO Intensification with
2454 Warming in the Superparameterized CESM, *J. Clim.*, *28*, 10.1175/jcli-d-14-00494.1, 2706-2724.

2455 Arnold, N. P., and D. A. Randall (2015), Global-scale convective aggregation: Implications for the Madden-
2456 Julian Oscillation, *Journal of Advances in Modeling Earth Systems*, *7*, 10.1002/2015MS000498, 1499-
2457 1518.

2458 Baggett, C. F., E. A. Barnes, E. D. Maloney, and B. D. Mundhenk (2017), Advancing atmospheric river
2459 forecasts into subseasonal-to-seasonal time scales, *Geophys. Res. Lett.*, *44*, 10.1002/2017GL074434,
2460 7528-7536.

2461 Baggett, C. F., K. M. Nardi, S. J. Childs, S. N. Zito, E. A. Barnes, and E. D. Maloney (2018), Skillful
2462 Subseasonal Forecasts of Weekly Tornado and Hail Activity Using the Madden-Julian Oscillation,
2463 *Journal of Geophysical Research: Atmospheres*, *123*, 10.1029/2018JD029059, 12,661-612,675.

2464 Baldwin, M. P., and T. J. Dunkerton (2001), Stratospheric Harbingers of Anomalous Weather Regimes,
2465 *Science*, *294*, 10.1126/science.1063315, 581.

2466 Baldwin, M. P., L. J. Gray, T. J. Dunkerton, K. Hamilton, P. H. Haynes, W. J. Randel, J. R. Holton, M. J.
2467 Alexander, I. Hirota, T. Horinouchi, D. B. A. Jones, J. S. Kinnersley, C. Marquardt, K. Sato, and M.
2468 Takahashi (2001), The quasi-biennial oscillation, *Rev. Geophys.*, *39*, 10.1029/1999RG000073, 179-229.

2469 Baranowski, D. B., M. K. Flatau, P. J. Flatau, and A. J. Matthews (2016), Phase locking between
2470 atmospheric convectively coupled equatorial Kelvin waves and the diurnal cycle of precipitation over the
2471 Maritime Continent, *Geophys. Res. Lett.*, *43*, 10.1002/2016GL069602, 8269-8276.

2472 Baranowski, D. B., D. E. Waliser, X. Jiang, J. A. Ridout, and M. K. Flatau (2019), Contemporary GCM
2473 Fidelity in Representing the Diurnal Cycle of Precipitation Over the Maritime Continent, *Journal of*
2474 *Geophysical Research: Atmospheres*, *124*, 10.1029/2018JD029474, 747-769.

2475 Barnes, E. A., S. M. Samarasinghe, I. Ebert-Uphoff, and J. C. Furtado (2019), Tropospheric and
2476 Stratospheric Causal Pathways Between the MJO and NAO, *Journal of Geophysical Research:*
2477 *Atmospheres*, *124*, 10.1029/2019JD031024, 9356-9371.

2478 Barnes, H. C., and R. A. Houze (2013), The precipitating cloud population of the Madden-Julian Oscillation
2479 over the Indian and west Pacific Oceans, *Journal of Geophysical Research:*
2480 *Atmospheres*10.1002/jgrd.50375, n/a-n/a.

2481 Barnes, H. C., and R. A. Houze (2014), Precipitation hydrometeor type relative to the mesoscale airflow in
2482 mature oceanic deep convection of the Madden-Julian Oscillation, *Journal of Geophysical Research:*
2483 *Atmospheres*, 119, 10.1002/2014JD022241, 13,990-914,014.

2484 Barrett, B. S., J. F. Carrasco, and A. P. Testino (2011), Madden–Julian Oscillation (MJO) Modulation of
2485 Atmospheric Circulation and Chilean Winter Precipitation, *J. Clim.*, 25, 10.1175/JCLI-D-11-00216.1,
2486 1678-1688.

2487 Barrett, B. S., and V. A. Gensini (2013), Variability of central United States April–May tornado day
2488 likelihood by phase of the Madden-Julian Oscillation, *Geophys. Res. Lett.*, 40, 10.1002/grl.50522, 2790-
2489 2795.

2490 Baxter, S., S. Weaver, J. Gottschalck, and Y. Xue (2014), Pentad Evolution of Wintertime Impacts of the
2491 Madden–Julian Oscillation over the Contiguous United States, *J. Clim.*, 27, 10.1175/jcli-d-14-00105.1,
2492 7356-7367.

2493 Bechtold, P., M. Kohler, T. Jung, F. Doblas-Reyes, M. Leutbecher, M. J. Rodwell, F. Vitart, and G. Balsamo
2494 (2008), Advances in simulating atmospheric variability with the ECMWF model: From synoptic to
2495 decadal time-scales, *Quart. J. Roy. Meteor. Soc.*, 134, Doi 10.1002/Qj.289, 1337-1351.

2496 Becker, E. J., E. H. Berbery, and R. W. Higgins (2011), Modulation of Cold-Season U.S. Daily Precipitation
2497 by the Madden–Julian Oscillation, *J. Clim.*, 24, 10.1175/2011JCLI4018.1, 5157-5166.

2498 Bellenger, H., and J. P. Duvel (2009), An Analysis of Tropical Ocean Diurnal Warm Layers, *J. Clim.*, 22,
2499 Doi 10.1175/2008jcli2598.1, 3629-3646.

2500 Bellenger, H., and J. P. Duvel (2012), The event-to-event variability of the boreal winter MJO, *Geophys.*
2501 *Res. Lett.*, 39, 10.1029/2012GL051294, n/a-n/a.

2502 Bellenger, H., M. Katsumata, and K. Yoneyama (2015a), Turbulent mixing and its impact on lower
2503 tropospheric moisture over tropical ocean, *Geophys. Res. Lett.*, 42, 10.1002/2015GL063868, 3030-3037.

2504 Bellenger, H., K. Yoneyama, M. Katsumata, T. Nishizawa, K. Yasunaga, and R. Shirooka (2015b),
2505 Observation of Moisture Tendencies Related to Shallow Convection, *J. Atmos. Sci.*, 72, 10.1175/jas-d-14-
2506 0042.1, 641-659.

2507 Benedict, J. J., and D. A. Randall (2007), Observed Characteristics of the MJO Relative to Maximum
2508 Rainfall, *J. Atmos. Sci.*, 64, 2332-2354.

2509 Benedict, J. J., and D. A. Randall (2009), Structure of the Madden-Julian Oscillation in the
2510 Superparameterized CAM, *J. Atmos. Sci.*, 66, 3277-3296.

2511 Benedict, J. J., and D. A. Randall (2011), Impacts of Idealized Air–Sea Coupling on Madden–Julian
2512 Oscillation Structure in the Superparameterized CAM, *J. Atmos. Sci.*, *68*, 10.1175/JAS-D-11-04.1, 1990-
2513 2008.

2514 Benedict, J. J., E. D. Maloney, A. H. Sobel, and D. M. W. Frierson (2014), Gross Moist Stability and MJO
2515 Simulation Skill in Three Full-Physics GCMs, *J. Atmos. Sci.*, *71*, 10.1175/JAS-D-13-0240.1, 3327-3349.

2516 Benedict, J. J., M. S. Pritchard, and W. D. Collins (2015), Sensitivity of MJO propagation to a robust
2517 positive Indian Ocean dipole event in the superparameterized CAM, *Journal of Advances in Modeling
2518 Earth Systems*, *7*, 10.1002/2015MS000530, 1901-1917.

2519 Berg, W., T. L'Ecuyer, and J. M. Haynes (2010), The Distribution of Rainfall over Oceans from Spaceborne
2520 Radars, *Journal of Applied Meteorology and Climatology*, *49*, Doi 10.1175/2009jamc2330.1, 535-543.

2521 Bernie, D. J., S. J. Woolnough, J. M. Slingo, and E. Guilyardi (2005), Modeling diurnal and intraseasonal
2522 variability of the ocean mixed layer, *J. Clim.*, *18*, Doi 10.1175/Jcli3319.1, 1190-1202.

2523 Bessafi, M., and M. C. Wheeler (2006), Modulation of south Indian ocean tropical cyclones by the Madden-
2524 Julian oscillation and convectively coupled equatorial waves, *Mon. Weather Rev.*, *134*, 638-656.

2525 Biello, J. A., and A. J. Majda (2005), A new multiscale model for the Madden-Julian oscillation, *J. Atmos.
2526 Sci.*, *62*, 1694-1721.

2527 Birch, C. E., S. Webster, S. C. Peatman, D. J. Parker, A. J. Matthews, Y. Li, and M. E. E. Hassim (2016),
2528 Scale Interactions between the MJO and the Western Maritime Continent, *J. Clim.*, *29*, doi:10.1175/JCLI-
2529 D-15-0557.1, 2471-2492.

2530 Bond, N. A., and G. A. Vecchi (2003), The Influence of the Madden–Julian Oscillation on Precipitation in
2531 Oregon and Washington*, *Weather Forecasting*, *18*, 10.1175/1520-0434, 600-613.

2532 Bony, S., B. Stevens, D. M. W. Frierson, C. Jakob, M. Kageyama, R. Pincus, T. G. Shepherd, S. C.
2533 Sherwood, A. P. Siebesma, A. H. Sobel, M. Watanabe, and M. J. Webb (2015), Clouds, circulation and
2534 climate sensitivity, *Nature Geoscience*, *8*, 10.1038/ngeo2398, 261.

2535 Branstator, G. (1985), Analysis of General Circulation Model Sea-Surface Temperature Anomaly
2536 Simulations Using a Linear Model. Part I: Forced Solutions, *J. Atmos. Sci.*, *42*, 10.1175/1520-
2537 0469(1985)042<2225:AOGCMS>2.0.CO;2, 2225-2241.

2538 Brenowitz, N. D., and C. S. Bretherton (2018), Prognostic Validation of a Neural Network Unified Physics
2539 Parameterization, *Geophys. Res. Lett.*, *45*, 10.1029/2018gl078510, 6289-6298.

2540 Bretherton, C. S., M. E. Peters, and L. E. Back (2004), Relationships between water vapor path and
2541 precipitation over the tropical oceans, *J. Clim.*, *17*, 1517-1528.

2542 Bui, H. X., and E. D. Maloney (2018), Changes in Madden-Julian Oscillation Precipitation and Wind
2543 Variance Under Global Warming, *Geophys. Res. Lett.*, *45*, 10.1029/2018GL078504, 7148-7155.

2544 Bui, H. X., and E. D. Maloney (2019a), Mechanisms for Global Warming Impacts on Madden–Julian
2545 Oscillation Precipitation Amplitude, *J. Clim.*, *32*, 10.1175/jcli-d-19-0051.1, 6961-6975.

2546 Bui, H. X., and E. D. Maloney (2019b), Transient Response of MJO Precipitation and Circulation to
2547 Greenhouse Gas Forcing, *Geophys. Res. Lett.*, *46*, 10.1029/2019GL085328, 13546-13555.

2548 Buizza, R., M. Milleer, and T. N. Palmer (1999), Stochastic representation of model uncertainties in the
2549 ECMWF ensemble prediction system, *Quart. J. Roy. Meteor. Soc.*, *125*, 10.1002/qj.49712556006, 2887-
2550 2908.

2551 Caballero, R., and M. Huber (2010), Spontaneous transition to superrotation in warm climates simulated by
2552 CAM3, *Geophys. Res. Lett.*, *37*, 10.1029/2010GL043468, n/a-n/a.

2553 Carlson, H., and R. Caballero (2016), Enhanced MJO and transition to superrotation in warm climates,
2554 *Journal of Advances in Modeling Earth Systems*, *8*, 10.1002/2015MS000615, 304-318.

2555 Cassou, C. (2008), Intraseasonal interaction between the Madden-Julian Oscillation and the North Atlantic
2556 Oscillation, *Nature*, *455*, 523-527.

2557 Chang, C.-H., and N. C. Johnson (2015), The Continuum of Wintertime Southern Hemisphere Atmospheric
2558 Teleconnection Patterns, *J. Clim.*, *28*, 10.1175/JCLI-D-14-00739.1, 9507-9529.

2559 Chang, C.-P., and H. Lim (1988), Kelvin Wave-CISK: A Possible Mechanism for the 30-50 Day
2560 Oscillations, *J. Atmos. Sci.*, *45*, 1709-1720.

2561 Chang, C.-W. J., W.-L. Tseng, H.-H. Hsu, N. Keenlyside, and B.-J. Tsuang (2015), The Madden-Julian
2562 Oscillation in a warmer world, *Geophys. Res. Lett.*, *42*, 10.1002/2015GL065095, 6034-6042.

2563 Chang, C. P. (1977), Viscous Internal Gravity-Waves and Low-Frequency Oscillations in the Tropics, *J.*
2564 *Atmos. Sci.*, *34*, 901-910.

2565 Chao, W. C., and B. Chen (2001), The Role of Surface Friction in Tropical Intraseasonal Oscillation, *Mon.*
2566 *Weather Rev.*, *129*, 10.1175/1520-0493(2001)129<0896:TROSFI>2.0.CO;2, 896-904.

2567 Chen, B., and B. E. Mapes (2018), Effects of a Simple Convective Organization Scheme in a Two-Plume
2568 GCM, *Journal of Advances in Modeling Earth Systems*, *10*, 10.1002/2017MS001106, 867-880.

2569 Chen, G., and B. Wang (2017), Reexamination of the Wave Activity Envelope Convective Scheme in
2570 Theoretical Modeling of MJO, *J. Clim.*, *30*, 10.1175/JCLI-D-16-0325.1, 1127-1138.

2571 Chen, G., and B. Wang (2018a), Does the MJO Have a Westward Group Velocity?, *J. Clim.*, *31*,
2572 10.1175/JCLI-D-17-0446.1, 2435-2443.

2573 Chen, G., and B. Wang (2018b), Effects of Enhanced Front Walker Cell on the Eastward Propagation of the
2574 MJO, *J. Clim.*, *31*, 10.1175/jcli-d-17-0383.1, 7719-7738.

2575 Chen, S. S., and R. A. Houze (1997), Diurnal variation and life-cycle of deep convective systems over the
2576 Tropical Pacific warm pool, *Quart. J. Roy. Meteor. Soc.*, *123*, DOI 10.1002/qj.49712353806, 357-388.

2577 Chen, S. S., B. W. Kerns, N. Guy, D. P. Jorgensen, J. Delanoë, N. Viltard, C. J. Zappa, F. Judt, C.-Y. Lee,
2578 and A. Savarin (2016), Aircraft Observations of Dry Air, the ITCZ, Convective Cloud Systems, and Cold
2579 Pools in MJO during DYNAMO, *97*, 10.1175/bams-d-13-00196.1, 405-423.

2580 Chen, Y., and A. D. Del Genio (2009a), Evaluation of tropical cloud regimes in observations and a general
2581 circulation model, *Climate Dyn.*, *32*, 10.1007/s00382-008-0386-6, 355-369.

2582 Chen, Y. H., and A. D. Del Genio (2009b), Evaluation of tropical cloud regimes in observations and a
2583 general circulation model, *Climate Dyn.*, *32*, doi:10.1007/S00382-008-0386-6, 355-369.

2584 Chi, N.-H., R.-C. Lien, E. A. D'Asaro, and B. B. Ma (2014), The surface mixed layer heat budget from
2585 mooring observations in the central Indian Ocean during Madden–Julian Oscillation events, *Journal of*
2586 *Geophysical Research: Oceans*, *119*, 10.1002/2014JC010192, 4638-4652.

2587 Chikira, M., and M. Sugiyama (2010), A Cumulus Parameterization with State-Dependent Entrainment Rate.
2588 Part I: Description and Sensitivity to Temperature and Humidity Profiles, *J. Atmos. Sci.*, *67*, Doi
2589 10.1175/2010jas3316.1, 2171-2193.

2590 Chikira, M. (2014), Eastward-Propagating Intraseasonal Oscillation Represented by Chikira–Sugiyama
2591 Cumulus Parameterization. Part II: Understanding Moisture Variation under Weak Temperature Gradient
2592 Balance, *J. Atmos. Sci.*, *71*, 10.1175/JAS-D-13-038.1, 615-639.

2593 Ciesielski, P. E., R. H. Johnson, X. Jiang, Y. Zhang, and S. Xie (2017), Relationships Between Radiation,
2594 Clouds, and Convection During DYNAMO, *Journal of Geophysical Research:*
2595 *Atmospheres*10.1002/2016JD025965.

2596 Coats, S., and K. B. Karnauskas (2017), Are Simulated and Observed Twentieth Century Tropical Pacific
2597 Sea Surface Temperature Trends Significant Relative to Internal Variability?, *Geophys. Res. Lett.*, *44*,
2598 10.1002/2017GL074622, 9928-9937.

2599 Collimore, C. C., D. W. Martin, M. H. Hitchman, A. Huesmann, and D. Waliser (2003), On The
2600 Relationship between the QBO and Tropical Deep Convection, *J. Clim.*, *16*, 10.1175/1520-
2601 0442(2003)016<2552:otrbtq>2.0.co;2, 2552-2568.

2602 Crueger, T., B. Stevens, and R. Brokopf (2013), The Madden–Julian Oscillation in ECHAM6 and the
2603 Introduction of an Objective MJO Metric, *J. Clim.*, *26*, 10.1175/jcli-d-12-00413.1, 3241-3257.

2604 de Szoeke, S. P., J. B. Edson, J. R. Marion, C. W. Fairall, and L. Barteau (2015), The MJO and Air–Sea
2605 Interaction in TOGA COARE and DYNAMO, *J. Clim.*, *28*, 10.1175/jcli-d-14-00477.1, 597-622.

2606 de Szoeke, S. P., E. D. Skyllingstad, P. Zuidema, and A. S. Chandra (2017), Cold Pools and Their Influence
2607 on the Tropical Marine Boundary Layer, *J. Atmos. Sci.*, *74*, 10.1175/jas-d-16-0264.1, 1149-1168.

2608 de Szoeke, S. P. (2018), Variations of the Moist Static Energy Budget of the Tropical Indian Ocean
2609 Atmospheric Boundary Layer, *J. Atmos. Sci.*, *75*, 10.1175/jas-d-17-0345.1, 1545-1551.

2610 Dee, D. P., S. M. Uppala, A. J. Simmons, P. Berrisford, P. Poli, S. Kobayashi, U. Andrae, M. A. Balmaseda,
2611 G. Balsamo, P. Bauer, P. Bechtold, A. C. M. Beljaars, L. van de Berg, J. Bidlot, N. Bormann, C. Delsol,
2612 R. Dragani, M. Fuentes, A. J. Geer, L. Haimberger, S. B. Healy, H. Hersbach, E. V. Hólm, L. Isaksen, P.
2613 Kållberg, M. Köhler, M. Matricardi, A. P. McNally, B. M. Monge-Sanz, J. J. Morcrette, B. K. Park, C.
2614 Peubey, P. de Rosnay, C. Tavolato, J. N. Thépaut, and F. Vitart (2011), The ERA-Interim reanalysis:

2615 configuration and performance of the data assimilation system, *Quart. J. Roy. Meteor. Soc.*, *137*,
2616 10.1002/qj.828, 553-597.

2617 DeFlorio, M. J., D. E. Waliser, B. Guan, F. M. Ralph, and F. Vitart (2019), Global evaluation of atmospheric
2618 river subseasonal prediction skill, *Climate Dyn.*, *52*, 10.1007/s00382-018-4309-x, 3039-3060.

2619 Del Genio, A. D. (2012), Representing the Sensitivity of Convective Cloud Systems to Tropospheric
2620 Humidity in General Circulation Models, *Surveys in Geophysics*, *33*, 10.1007/s10712-011-9148-9, 637-
2621 656.

2622 Del Genio, A. D., Y. Chen, D. Kim, and M.-S. Yao (2012), The MJO Transition from Shallow to Deep
2623 Convection in CloudSat/CALIPSO Data and GISS GCM Simulations, *J. Clim.*, *25*, 10.1175/JCLI-D-11-
2624 00384.1, 3755-3770.

2625 Del Genio, A. D., and Y. Chen (2015), Cloud-radiative driving of the Madden-Julian oscillation as seen by
2626 the A-Train, *Journal of Geophysical Research: Atmospheres*, *120*, 10.1002/2015JD023278, 5344-5356.

2627 DeMott, C. A., C. Stan, D. A. Randall, and M. D. Branson (2014), Intraseasonal Variability in Coupled
2628 GCMs: The Roles of Ocean Feedbacks and Model Physics, *J. Clim.*, *27*, doi:10.1175/JCLI-D-13-00760.1,
2629 4970-4995.

2630 DeMott, C. A., N. P. Klingaman, and S. J. Woolnough (2015), Atmosphere-ocean coupled processes in the
2631 Madden-Julian oscillation, *Rev. Geophys.* 10.1002/2014RG000478, n/a-n/a.

2632 DeMott, C. A., J. J. Benedict, N. P. Klingaman, S. J. Woolnough, and D. A. Randall (2016), Diagnosing
2633 ocean feedbacks to the MJO: SST-modulated surface fluxes and the moist static energy budget, *Journal*
2634 *of Geophysical Research: Atmospheres*, *121*, 10.1002/2016JD025098, 8350-8373.

2635 DeMott, C. A., B. O. Wolding, E. D. Maloney, and D. A. Randall (2018), Atmospheric Mechanisms for
2636 MJO Decay Over the Maritime Continent, *Journal of Geophysical Research: Atmospheres*, *123*,
2637 10.1029/2017jd026979, 5188-5204.

2638 DeMott, C. A., N. P. Klingaman, W.-L. Tseng, M. A. Burt, Y. Gao, and D. A. Randall (2019), The
2639 convection connection: How ocean feedbacks affect tropical mean moisture and MJO propagation,
2640 *Journal of Geophysical Research: Atmospheres*, n/a, 10.1029/2019JD031015.

2641 Deng, L., and X. Wu (2010), Effects of Convective Processes on GCM Simulations of the Madden-Julian
2642 Oscillation, *J. Clim.*, *23*, 10.1175/2009jcli3114.1, 352-377.

2643 Deng, L., and X. Wu (2011), Physical Mechanisms for the Maintenance of GCM-Simulated Madden-Julian
2644 Oscillation over the Indian Ocean and Pacific, *J. Clim.*, *24*, 10.1175/2010JCLI3759.1, 2469-2482.

2645 Deng, Q., B. Khouider, and A. J. Majda (2015), The MJO in a Coarse-Resolution GCM with a Stochastic
2646 Multicloud Parameterization, *J. Atmos. Sci.*, *72*, 10.1175/jas-d-14-0120.1, 55-74.

2647 Deng, Q., B. Khouider, A. J. Majda, and R. S. Ajayamohan (2016), Effect of Stratiform Heating on the
2648 Planetary-Scale Organization of Tropical Convection, *J. Atmos. Sci.*, *73*, 10.1175/jas-d-15-0178.1, 371-
2649 392.

2650 Densmore, C. R., E. R. Sanabia, and B. S. Barrett (2019), QBO Influence on MJO Amplitude over the
2651 Maritime Continent: Physical Mechanisms and Seasonality, *Mon. Weather Rev.*, *147*, 10.1175/mwr-d-18-
2652 0158.1, 389-406.

2653 DePasquale, A., C. Schumacher, and A. Rapp (2014), Radar observations of MJO and Kelvin wave
2654 interactions during DYNAMO/CINDY2011/AMIE, *Journal of Geophysical Research: Atmospheres*, *119*,
2655 10.1002/2013JD021031, 6347-6367.

2656 Derbyshire, S. H., I. Beau, P. Bechtold, J.-Y. Grandpeix, J.-M. Piriou, J.-L. Redelsperger, and P. M. M.
2657 Soares (2004), Sensitivity of moist convection to environmental humidity, *Quart. J. Roy. Meteor. Soc.*,
2658 *130*, 3055-3079.

2659 Deser, C., and A. S. Phillips (2009), Atmospheric Circulation Trends, 1950–2000: The Relative Roles of Sea
2660 Surface Temperature Forcing and Direct Atmospheric Radiative Forcing, *J. Clim.*, *22*,
2661 10.1175/2008jcli2453.1, 396-413.

2662 DeWitt, L. H., D. J. Coffman, K. J. Schulz, W. Alan Brewer, T. S. Bates, and P. K. Quinn (2013),
2663 Atmospheric aerosol properties over the equatorial Indian Ocean and the impact of the Madden-Julian
2664 Oscillation, *Journal of Geophysical Research: Atmospheres*, *118*, 10.1002/jgrd.50419, 5736-5749.

2665 Dias, J., S. Leroux, S. N. Tulich, and G. N. Kiladis (2013), How systematic is organized tropical convection
2666 within the MJO?, *Geophys. Res. Lett.*, *40*, 10.1002/grl.50308, 1420-1425.

2667 Dias, J., N. Sakaeda, G. N. Kiladis, and K. Kikuchi (2017), Influences of the MJO on the space-time
2668 organization of tropical convection, *Journal of Geophysical Research: Atmospheres*, *122*,
2669 10.1002/2017JD026526, 8012-8032.

2670 Ding, R. Q., J. P. Li, and K. H. Seo (2010), Predictability of the Madden-Julian Oscillation Estimated Using
2671 Observational Data, *Mon. Weather Rev.*, *138*, Doi 10.1175/2009mwr3082.1, 1004-1013.

2672 Donald, A., H. Meinke, B. Power, A. d. H. N. Maia, M. C. Wheeler, N. White, R. C. Stone, and J. Ribbe
2673 (2006), Near-global impact of the Madden-Julian Oscillation on rainfall, *Geophys. Res. Lett.*, *33*,
2674 10.1029/2005GL025155, n/a-n/a.

2675 Drushka, K., J. Sprintall, S. T. Gille, and S. Wijffels (2012), In Situ Observations of Madden-Julian
2676 Oscillation Mixed Layer Dynamics in the Indian and Western Pacific Oceans, *J. Clim.*, *25*, 10.1175/jcli-
2677 d-11-00203.1, 2306-2328.

2678 Drushka, K., W. E. Asher, B. Ward, and K. Walesby (2016), Understanding the formation and evolution of
2679 rain-formed fresh lenses at the ocean surface, *Journal of Geophysical Research: Oceans*, *121*,
2680 10.1002/2015JC011527, 2673-2689.

2681 Dubey, S., T. N. Krishnamurti, and V. Kumar (2018), On scale interactions between the MJO and synoptic
2682 scale, *Quart. J. Roy. Meteor. Soc.*, *144*, 10.1002/qj.3400, 2727-2747.

2683 Emanuel, K. (2019), Inferences from Simple Models of Slow, Convectively Coupled Processes, *J. Atmos.*
2684 *Sci.*, *76*, 10.1175/JAS-D-18-0090.1, 195-208.

2685 Emanuel, K. A. (1987), An Air-Sea Interaction-Model of Intraseasonal Oscillations in the Tropics, *J. Atmos.*
2686 *Sci.*, *44*, 2324-2340.

2687 Emanuel, K. A. (1991), A Scheme for Representing Cumulus Convection in Large-Scale Models, *J. Atmos.*
2688 *Sci.*, *48*, 10.1175/1520-0469(1991)048<2313:ASFRCC>2.0.CO;2, 2313-2329.

2689 Emanuel, K. A. (1995), The Behavior of a Simple Hurricane Model Using a Convective Scheme Based on
2690 Subcloud-Layer Entropy Equilibrium, *J. Atmos. Sci.*, *52*, 10.1175/1520-
2691 0469(1995)052<3960:TBOASH>2.0.CO;2, 3960-3968.

2692 Fauchereau, N., B. Pohl, and A. Lorrey (2016), Extra-tropical impacts of the Madden-Julian Oscillation over
2693 New Zealand from a weather regime perspective, *J. Clim.*, *29*, 10.1175/JCLI-D-15-0152.1, 2161-2175.

2694 Feng, J., T. Li, and W. Zhu (2015a), Propagating and Nonpropagating MJO Events over Maritime Continent,
2695 *J. Clim.*, *28*, 10.1175/JCLI-D-15-0085.1, 8430-8449.

2696 Feng, J., P. Liu, W. Chen, and X. Wang (2015b), Contrasting Madden-Julian Oscillation activity during
2697 various stages of EP and CP El Niños, *Atmospheric Science Letters*, *16*, 10.1002/asl2.516, 32-37.

2698 Feng, P.-N., and H. Lin (2019), Modulation of the MJO-Related Teleconnections by the QBO, *Journal of*
2699 *Geophysical Research: Atmospheres*, *124*, 10.1029/2019jd030878, 12022-12033.

2700 Ferranti, L., T. N. Palmer, F. Molteni, and E. Klinker (1990), Tropical-Extratropical Interaction Associated
2701 with the 30-60 Day Oscillation and Its Impact on Medium and Extended Range Prediction, *J. Atmos. Sci.*,
2702 *47*, 2177-2199.

2703 Flatau, M., and Y.-J. Kim (2013), Interaction between the MJO and Polar Circulations, *J. Clim.*, *26*,
2704 10.1175/jcli-d-11-00508.1, 3562-3574.

2705 Franzke, C., S. Lee, and S. Feldstein (2004), Is the North Atlantic Oscillation a Breaking Wave, *J. Atmos.*
2706 *Sci.*, *61*, 10.1175/1520-0469(2004)061<0145:ITNAOA>2.0.CO;2, 145-160.

2707 Frederiksen, J. S. (1982), A Unified Three-Dimensional Instability Theory of the Onset of Blocking and
2708 Cyclogenesis, *J. Atmos. Sci.*, *39*, 10.1175/1520-0469(1982)039<0969:AUTDIT>2.0.CO;2, 969-982.

2709 Frederiksen, J. S. (1983), A Unified Three-Dimensional Instability Theory of the Onset of Blocking and
2710 Cyclogenesis. II. Teleconnection Patterns, *J. Atmos. Sci.*, *40*, 10.1175/1520-
2711 0469(1983)040<2593:AUTDIT>2.0.CO;2, 2593-2609.

2712 Frederiksen, J. S., and C. S. Frederiksen (1993), Monsoon Disturbances, Intraseasonal Oscillations,
2713 Teleconnection Patterns, Blocking, and Storm Tracks of the Global Atmosphere during January 1979 -
2714 Linear-Theory, *J. Atmos. Sci.*, *50*, 1349-1372.

2715 Frederiksen, J. S., and C. S. Frederiksen (1997), Mechanism of the formation of intraseasonal oscillations
2716 and Australian monsoon disturbances: The roles of convection, barotropic and baroclinic instability.
2717 *Contributions to Atmospheric Physics*, *70*, 39-56.

2718 Frederiksen, J. S. (2002), Genesis of Intraseasonal Oscillations and Equatorial Waves, *J. Atmos. Sci.*, *59*,
2719 10.1175/1520-0469(2002)059<2761:GOIOAE>2.0.CO;2, 2761-2781.

2720 Frederiksen, J. S., and H. Lin (2013), Tropical–Extratropical Interactions of Intraseasonal Oscillations, *J.*
2721 *Atmos. Sci.*, *70*, 10.1175/JAS-D-12-0302.1, 3180-3197.

2722 Fu, M., and E. Tziperman (2019), Essential Ingredients to the Dynamics of Westerly Wind Bursts, *J. Clim.*,
2723 *32*, 10.1175/JCLI-D-18-0584.1, 5549-5565.

2724 Fu, X., B. Wang, J.-Y. Lee, W. Wang, and L. Gao (2011), Sensitivity of Dynamical Intraseasonal Prediction
2725 Skills to Different Initial Conditions*, *Mon. Weather Rev.*, *139*, 10.1175/2011MWR3584.1, 2572-2592.

2726 Fu, X., W. Wang, J.-Y. Lee, B. Wang, K. Kikuchi, J. Xu, J. Li, and S. Weaver (2015), Distinctive Roles of
2727 Air–Sea Coupling on Different MJO Events: A New Perspective Revealed from the DYNAMO/CINDY
2728 Field Campaign, *Mon. Weather Rev.*, *143*, 10.1175/mwr-d-14-00221.1, 794-812.

2729 Fuchs, Z., and D. J. Raymond (2005), Large-Scale Modes in a Rotating Atmosphere with Radiative–
2730 Convective Instability and WISHE, *J. Atmos. Sci.*, *62*, 10.1175/JAS3582.1, 4084-4094.

2731 Fuchs, Ž., and D. J. Raymond (2007), A simple, vertically resolved model of tropical disturbances with a
2732 humidity closure, *Tellus A: Dynamic Meteorology and Oceanography*, *59*, 10.1111/j.1600-
2733 0870.2007.00230.x, 344-354.

2734 Fuchs, Ž., and D. J. Raymond (2017), A simple model of intraseasonal oscillations, *Journal of Advances in*
2735 *Modeling Earth Systems*, *9*, 10.1002/2017MS000963, 1195-1211.

2736 Garfinkel, C. I., S. B. Feldstein, D. W. Waugh, C. Yoo, and S. Lee (2012), Observed connection between
2737 stratospheric sudden warmings and the Madden-Julian Oscillation, *Geophys. Res. Lett.*, *39*,
2738 10.1029/2012GL053144, L18807.

2739 Garfinkel, C. I., J. J. Benedict, and E. D. Maloney (2014), Impact of the MJO on the boreal winter
2740 extratropical circulation, *Geophys. Res. Lett.*, *41*, 10.1002/2014gl061094, 6055-6062.

2741 Garfinkel, C. I., and C. Schwartz (2017), MJO-Related Tropical Convection Anomalies Lead to More
2742 Accurate Stratospheric Vortex Variability in Subseasonal Forecast Models, *Geophys. Res. Lett.*, *44*,
2743 10.1002/2017gl074470, 10,054-010,062.

2744 Gensini, V. A., D. Gold, J. T. Allen, and B. S. Barrett (2019), Extended U.S. Tornado Outbreak During Late
2745 May 2019: A Forecast of Opportunity, *Geophys. Res. Lett.*, *46*, 10.1029/2019gl084470, 10150-10158.

2746 Gentine, P., M. Pritchard, S. Rasp, G. Reinaudi, and G. Yacalis (2018), Could Machine Learning Break the
2747 Convection Parameterization Deadlock?, *Geophys. Res. Lett.*, *45*, 10.1029/2018gl078202, 5742-5751.

2748 Gonzalez, A. O., and X. Jiang (2017), Winter Mean Lower-Tropospheric Moisture over the Maritime
2749 Continent as a Climate Model Diagnostic Metric for the Propagation of the Madden-Julian Oscillation,
2750 *Geophys. Res. Lett.* 10.1002/2016GL072430.

2751 Gonzalez, A. O., and X. Jiang (2019), Distinct Propagation Characteristics of Intraseasonal Variability Over
2752 the Tropical West Pacific, *Journal of Geophysical Research: Atmospheres*, *0*, 10.1029/2018JD029884.

2753 Goswami, B. B., B. Khouider, R. Phani, P. Mukhopadhyay, and A. Majda (2017a), Improving synoptic and
2754 intraseasonal variability in CFSv2 via stochastic representation of organized convection, *Geophys. Res.*
2755 *Lett.*, *44*, 10.1002/2016GL071542, 1104-1113.

2756 Goswami, B. B., B. Khouider, R. Phani, P. Mukhopadhyay, and A. J. Majda (2017b), Implementation and
2757 calibration of a stochastic multicloud convective parameterization in the NCEP Climate Forecast System
2758 (CFSv2), *Journal of Advances in Modeling Earth Systems*, *9*, 10.1002/2017MS001014, 1721-1739.

2759 Gottschalck, J., M. Wheeler, K. Weickmann, F. Vitart, N. Savage, H. Lin, H. Hendon, D. Waliser, K.
2760 Sperber, M. Nakagawa, C. Prestrelo, M. Flatau, and W. Higgins (2010), A Framework for Assessing
2761 Operational Madden–Julian Oscillation Forecasts: A CLIVAR MJO Working Group Project, *Bull. Am.*
2762 *Meteorol. Soc.*, *91*, doi:10.1175/2010BAMS2816.1, 1247-1258.

2763 Gottschalck, J., P. E. Roundy, C. J. Schreck Iii, A. Vintzileos, and C. Zhang (2013), Large-Scale
2764 Atmospheric and Oceanic Conditions during the 2011–12 DYNAMO Field Campaign, *Mon. Weather*
2765 *Rev.*, *141*, 10.1175/MWR-D-13-00022.1, 4173-4196.

2766 Grabowski, W. W. (2001), Coupling Cloud Processes with the Large-Scale Dynamics Using the Cloud-
2767 Resolving Convection Parameterization (CRCP), *J. Atmos. Sci.*, *58*, 10.1175/1520-
2768 0469(2001)058<0978:Ccpwtl>2.0.Co;2, 978-997.

2769 Grabowski, W. W., and M. W. Moncrieff (2004), Moisture–convection feedback in the tropics, *Quart. J.*
2770 *Roy. Meteor. Soc.*, *130*, 10.1256/qj.03.135, 3081-3104.

2771 Gray, W. M., J. D. Sheaffer, and J. A. Knaff (1992), Influence of the Stratospheric QBO on ENSO
2772 Variability, *Journal of the Meteorological Society of Japan. Ser. II*, *70*, 10.2151/jmsj1965.70.5_975, 975-
2773 995.

2774 Greatbatch, R. J. (2000), The North Atlantic Oscillation, *Stochastic Environmental Research and Risk*
2775 *Assessment*, *14*, 10.1007/s004770000047, 213-242.

2776 Green, B. W., S. Sun, R. Bleck, S. G. Benjamin, and G. A. Grell (2017), Evaluation of MJO Predictive Skill
2777 in Multiphysics and Multimodel Global Ensembles, *Mon. Weather Rev.*, *145*, 10.1175/mwr-d-16-0419.1,
2778 2555-2574.

2779 Guan, B., D. E. Waliser, N. P. Molotch, E. J. Fetzer, and P. J. Neiman (2012), Does the Madden–Julian
2780 Oscillation Influence Wintertime Atmospheric Rivers and Snowpack in the Sierra Nevada?, *Mon.*
2781 *Weather Rev.*, *140*, 10.1175/MWR-D-11-00087.1, 325-342.

2782 Guo, Y., X. Jiang, and D. E. Waliser (2014), Modulation of the Convectively Coupled Kelvin Waves over
2783 South America and the Tropical Atlantic Ocean in Association with the Madden–Julian Oscillation, *J.*
2784 *Atmos. Sci.*, *71*, 10.1175/JAS-D-13-0215.1, 1371-1388.

2785 Guo, Y., D. E. Waliser, and X. Jiang (2015), A Systematic Relationship between the Representations of
2786 Convectively Coupled Equatorial Wave Activity and the Madden–Julian Oscillation in Climate Model
2787 Simulations, *J. Clim.*, *28*, 10.1175/JCLI-D-14-00485.1, 1881-1904.

2788 Gushchina, D., and B. Dewitte (2012), Intraseasonal Tropical Atmospheric Variability Associated with the
2789 Two Flavors of El Niño, *Mon. Weather Rev.*, *140*, 10.1175/mwr-d-11-00267.1, 3669-3681.

2790 Guy, N., and D. P. Jorgensen (2014), Kinematic and Precipitation Characteristics of Convective Systems
2791 Observed by Airborne Doppler Radar during the Life Cycle of a Madden–Julian Oscillation in the Indian
2792 Ocean, *Mon. Weather Rev.*, *142*, 10.1175/mwr-d-13-00252.1, 1385-1402.

2793 Haertel, P. (2018), Sensitivity of the Madden Julian Oscillation to Ocean Warming in a Lagrangian
2794 Atmospheric Model, *Climate*, *6*, 45.

2795 Haertel, P. T., and G. N. Kiladis (2004), Dynamics of 2-day equatorial waves, *J. Atmos. Sci.*, *61*, 2707-2721.

2796 Hagos, S., Z. Feng, C. D. Burleyson, K.-S. S. Lim, C. N. Long, D. Wu, and G. Thompson (2014), Evaluation
2797 of convection-permitting model simulations of cloud populations associated with the Madden-Julian
2798 Oscillation using data collected during the AMIE/DYNAMO field campaign, *Journal of Geophysical
2799 Research: Atmospheres*, *119*, 10.1002/2014JD022143, 12,052-012,068.

2800 Hagos, S. M., C. Zhang, Z. Feng, C. D. Burleyson, C. De Mott, B. Kerns, J. J. Benedict, and M. N. Martini
2801 (2016), The impact of the diurnal cycle on the propagation of Madden-Julian Oscillation convection
2802 across the Maritime Continent, *Journal of Advances in Modeling Earth Systems* 10.1002/2016MS000725.

2803 Hall, N. M. J., S. Thibaut, and P. Marchesiello (2017), Impact of the observed extratropics on climatological
2804 simulations of the MJO in a tropical channel model, *Climate Dyn.*, *48*, 10.1007/s00382-016-3221-5,
2805 2541-2555.

2806 Hamada, A., and Y. N. Takayabu (2016), Improvements in Detection of Light Precipitation with the Global
2807 Precipitation Measurement Dual-Frequency Precipitation Radar (GPM DPR), *Journal of Atmospheric
2808 and Oceanic Technology*, *33*, 10.1175/jtech-d-15-0097.1, 653-667.

2809 Han, W. (2005), Origins and Dynamics of the 90-Day and 30–60-Day Variations in the Equatorial Indian
2810 Ocean, *J. Phys. Oceanogr.*, *35*, 10.1175/jpo2725.1, 708-728.

2811 Han, Y., and B. Khouider (2010), Convectively Coupled Waves in a Sheared Environment, *J. Atmos. Sci.*,
2812 *67*, doi:10.1175/2010JAS3335.1, 2913-2942.

2813 Hannah, W. M., and E. D. Maloney (2011), The Role of Moisture–Convection Feedbacks in Simulating the
2814 Madden–Julian Oscillation, *J. Clim.*, *24*, 10.1175/2011jcli3803.1, 2754-2770.

2815 Hannah, W. M., and E. D. Maloney (2014), The moist static energy budget in NCAR CAM5 hindcasts
2816 during DYNAMO, *Journal of Advances in Modeling Earth Systems*, *6*, 10.1002/2013MS000272, 420-
2817 440.

2818 Hannah, W. M., E. D. Maloney, and M. S. Pritchard (2015), Consequences of systematic model drift in
2819 DYNAMO MJO hindcasts with SP-CAM and CAM5, *Journal of Advances in Modeling Earth Systems*,
2820 *7*, 10.1002/2014MS000423, 1051-1074.

2821 Hartmann, D. L., J. R. Holton, and Q. Fu (2001), The heat balance of the tropical tropopause, cirrus, and
2822 stratospheric dehydration, *Geophys. Res. Lett.*, *28*, 10.1029/2000GL012833, 1969-1972.

2823 Hayashi, M., and H. Itoh (2017), A New Mechanism of the Slow Eastward Propagation of Unstable
2824 Disturbances with Convection in the Tropics: Implications for the MJO, *J. Atmos. Sci.*, *74*, 10.1175/JAS-
2825 D-16-0300.1, 3749-3769.

2826 Hayes, S. P., L. J. Mangum, J. Picaut, A. Sumi, and K. Takeuchi (1991), TOGA-TAO: A Moored Array for
2827 Real-time Measurements in the Tropical Pacific Ocean, *Bull. Am. Meteorol. Soc.*, *72*, 10.1175/1520-
2828 0477(1991)072<0339:Ttamaf>2.0.Co;2, 339-347.

2829 Held, I. M., and B. J. Soden (2006), Robust Responses of the Hydrological Cycle to Global Warming, *J.*
2830 *Clim.*, *19*, 10.1175/JCLI3990.1, 5686-5699.

2831 Henderson, D. S., T. L'Ecuyer, G. Stephens, P. Partain, and M. Sekiguchi (2013), A Multisensor Perspective
2832 on the Radiative Impacts of Clouds and Aerosols, *Journal of Applied Meteorology and Climatology*, *52*,
2833 10.1175/JAMC-D-12-025.1, 853-871.

2834 Henderson, S. A., E. D. Maloney, and E. A. Barnes (2016), The Influence of the Madden–Julian Oscillation
2835 on Northern Hemisphere Winter Blocking, *J. Clim.*, *29*, 10.1175/jcli-d-15-0502.1, 4597-4616.

2836 Henderson, S. A., E. D. Maloney, and S.-W. Son (2017), Madden–Julian Oscillation Pacific
2837 Teleconnections: The Impact of the Basic State and MJO Representation in General Circulation Models,
2838 *J. Clim.*, *30*, 10.1175/jcli-d-16-0789.1, 4567-4587.

2839 Hendon, H. H., and B. Liebmann (1990), The Intraseasonal (30-50 day) Oscillation of the Australian
2840 Summer Monsoon, *J. Atmos. Sci.*, *47*, 2909-2924.

2841 Hendon, H. H., and B. Liebmann (1994), Organization of Convection within the Madden-Julian Oscillation,
2842 *J. Geophys. Res.*, *99*, 8073-8083.

2843 Hendon, H. H., and M. L. Salby (1994), The Life-Cycle of the Madden-Julian Oscillation, *J. Atmos. Sci.*, *51*,
2844 2225-2237.

2845 Hendon, H. H., and J. Glick (1997), Intraseasonal Air–Sea Interaction in the Tropical Indian and Pacific
2846 Oceans, *J. Clim.*, *10*, 10.1175/1520-0442(1997)010<0647:IASIIT>2.0.CO;2, 647-661.

2847 Hendon, H. H., C. Zhang, and J. D. Glick (1999), Interannual Variation of the Madden–Julian Oscillation
2848 during Austral Summer, *J. Clim.*, *12*, 10.1175/1520-0442(1999)012<2538:Ivotmj>2.0.Co;2, 2538-2550.

2849 Hendon, H. H. (2000), Impact of Air–Sea Coupling on the Madden–Julian Oscillation in a General
2850 Circulation Model, *J. Atmos. Sci.*, *57*, 10.1175/1520-0469(2001)058<3939:IOASCO>2.0.CO;2, 3939-
2851 3952.

2852 Hendon, H. H., M. C. Wheeler, and C. Zhang (2007), Seasonal Dependence of the MJO–ENSO
2853 Relationship, *J. Clim.*, *20*, 10.1175/jcli4003.1, 531-543.

2854 Hendon, H. H., and S. Abhik (2018), Differences in Vertical Structure of the Madden-Julian Oscillation
2855 Associated With the Quasi-Biennial Oscillation, *Geophys. Res. Lett.*, *45*, 10.1029/2018gl077207, 4419-
2856 4428.

2857 Higgins, R. W., J. K. E. Schemm, W. Shi, and A. Leetmaa (2000), Extreme precipitation events in the
2858 western United States related to tropical forcing, *J. Clim.*, *13*, 793-820.

2859 Higgins, R. W., and W. Shi (2001), Intercomparison of the Principal Modes of Interannual and Intraseasonal
2860 Variability of the North American Monsoon System, *J. Clim.*, *14*, 403-417.

2861 Holloway, C. E., and J. D. Neelin (2007), The Convective Cold Top and Quasi Equilibrium, *J. Atmos. Sci.*,
2862 *64*, 10.1175/jas3907.1, 1467-1487.

2863 Holloway, C. E., S. J. Woolnough, and G. M. S. Lister (2013), The Effects of Explicit versus Parameterized
2864 Convection on the MJO in a Large-Domain High-Resolution Tropical Case Study. Part I:
2865 Characterization of Large-Scale Organization and Propagation, *J. Atmos. Sci.*, *70*, 10.1175/jas-d-12-
2866 0227.1, 1342-1369.

2867 Hong, C.-C., H.-H. Hsu, W.-L. Tseng, M.-Y. Lee, C.-H. Chow, and L.-C. Jiang (2017a), Extratropical
2868 Forcing Triggered the 2015 Madden-Julian Oscillation-El Niño Event, *Scientific Reports*, *7*,
2869 10.1038/srep46692, 46692.

2870 Hong, X., C. A. Reynolds, J. D. Doyle, P. May, and L. O'Neill (2017b), Assessment of upper-ocean
2871 variability and the Madden-Julian Oscillation in extended-range air-ocean coupled mesoscale
2872 simulations, *Dynamics of Atmospheres and Oceans*, *78*, <https://doi.org/10.1016/j.dynatmoce.2017.03.002>,
2873 89-105.

2874 Hood, L. L. (2017), QBO/solar modulation of the boreal winter Madden-Julian oscillation: A prediction for
2875 the coming solar minimum, *Geophys. Res. Lett.*, *44*, 10.1002/2017GL072832, 3849-3857.

2876 Horel, J. D., and J. M. Wallace (1981), Planetary-Scale Atmospheric Phenomena Associated with the
2877 Southern Oscillation, *Mon. Weather Rev.*, *109*, 10.1175/1520-0493(1981)109<0813:Psapaw>2.0.Co;2,
2878 813-829.

2879 Hoskins, B. J., and T. Ambrizzi (1993), Rossby Wave Propagation on a Realistic Longitudinally Varying
2880 Flow, *J. Atmos. Sci.*, *50*, 10.1175/1520-0469(1993)050<1661:Rwpoar>2.0.Co;2, 1661-1671.

2881 Hoskins, B. J., and G.-Y. Yang (2000), The Equatorial Response to Higher-Latitude Forcing, *J. Atmos. Sci.*,
2882 *57*, 10.1175/1520-0469(2000)057<1197:Terthl>2.0.Co;2, 1197-1213.

2883 Houze, R. A., S. S. Chen, D. E. Kingsmill, Y. Serra, and S. E. Yuter (2000), Convection over the Pacific
2884 warm pool in relation to the atmospheric Kelvin-Rossby wave, *J. Atmos. Sci.*, *57*, 3058-3089.

2885 Hsu, H.-H. (1996), Global View of the intraseasonal Oscillation during Northern Winter, *J. Clim.*, *9*,
2886 10.1175/1520-0442(1996)009<2386:Gvotio>2.0.Co;2, 2386-2406.

2887 Hsu, H.-H., and M.-Y. Lee (2005), Topographic Effects on the Eastward Propagation and Initiation of the
2888 Madden-Julian Oscillation, *J. Clim.*, *18*, doi:10.1175/JCLI-3292.1, 795-809.

2889 Hsu, J.-Y., H. Hendon, M. Feng, and X. Zhou (2019), Magnitude and Phase of Diurnal SST Variations in the
2890 ACCESS-S1 Model During the Suppressed Phase of the MJOs, *Journal of Geophysical Research:
2891 Oceans*, *124*, 10.1029/2019JC015458, 9553-9571.

2892 Hsu, P. C., and T. Li (2012), Role of the Boundary Layer Moisture Asymmetry in Causing the Eastward
2893 Propagation of the Madden-Julian Oscillation, *J. Clim.*, *25*, Doi 10.1175/Jcli-D-11-00310.1, 4914-4931.

2894 Hu, Q., and D. A. Randall (1995), Low-Frequency Oscillations in Radiative Convective Systems .2. An
2895 Idealized Model, *J. Atmos. Sci.*, *52*, 478-490.

2896 Huffman, G., E. Stocker, D. T. Bolvin, E. J. Nelkin, and J. Tan (2019), GPM IMERG Final Precipitation L3
2897 1 day 0.1 degree x 0.1 degree V06, Edited by Andrey Savtchenko, Greenbelt, MD, Goddard Earth
2898 Sciences Data and Information Services Center (GES DISC), Accessed: [Data Access Date],
2899 10.5067/GPM/IMERGDF/DAY/06.

2900 Huffman, G. J., R. F. Adler, D. T. Bolvin, G. Gu, E. J. Nelkin, K. P. Bowman, Y. Hong, E. F. Stocker, and
2901 D. B. Wolff (2007), The TRMM Multisatellite Precipitation Analysis (TMPA): Quasi-Global, Multiyear,
2902 Combined-Sensor Precipitation Estimates at Fine Scales, *J. Hydrometeorol.*, *8*, 38-55.

2903 Hung, C.-S., and C.-H. Sui (2018), A Diagnostic Study of the Evolution of the MJO from Indian Ocean to
2904 Maritime Continent: Wave Dynamics versus Advective Moistening Processes, *J. Clim.*, *31*, 10.1175/jcli-
2905 d-17-0139.1, 4095-4115.

2906 Hung, M.-P., J.-L. Lin, W. Wang, D. Kim, T. Shinoda, and S. J. Weaver (2013), MJO and Convectively
2907 Coupled Equatorial Waves Simulated by CMIP5 Climate Models, *J. Clim.*, *26*, 10.1175/JCLI-D-12-
2908 00541.1, 6185-6214.

2909 Hurrell, J. W., Y. Kushnir, G. Ottersen, and M. Visbeck (2013), An Overview of the North Atlantic
2910 Oscillation, in *The North Atlantic Oscillation: Climatic Significance and Environmental Impact*, edited,
2911 pp. 1-35, American Geophysical Union.

2912 ICTP (2006), Workshop on the Organization and Maintenance of Tropical Convection and the Madden
2913 Julian Oscillation: Sponsors: ITCP, WCRP, Thorpex. Organizers: J. Slingo, F. Molteni, M. Moncrieff, M.
2914 Shapiro, edited by F.M. J. Slingo, M. Moncrieff, M. Shapiro, International Centre for Theoretical
2915 Physics, Trieste, Italy, March 13-17, 2006.

2916 Illingworth, A. J., H. W. Barker, A. Beljaars, M. Ceccaldi, H. Chepfer, N. Clerbaux, J. Cole, J. Delanoë, C.
2917 Domenech, D. P. Donovan, S. Fukuda, M. Hiraoka, R. J. Hogan, A. Huenerbein, P. Kollias, T. Kubota,
2918 T. Nakajima, T. Y. Nakajima, T. Nishizawa, Y. Ohno, H. Okamoto, R. Oki, K. Sato, M. Satoh, M. W.
2919 Shephard, A. Velázquez-Blázquez, U. Wandinger, T. Wehr, and G.-J. v. Zadelhoff (2015), The
2920 EarthCARE Satellite: The Next Step Forward in Global Measurements of Clouds, Aerosols,
2921 Precipitation, and Radiation, *Bull. Am. Meteorol. Soc.*, *96*, 10.1175/bams-d-12-00227.1, 1311-1332.

2922 Inness, P. M., and J. M. Slingo (2006), The interaction of the Madden-Julian Oscillation with the Maritime
2923 Continent in a GCM, *Quart. J. Roy. Meteor. Soc.*, *132*, 1645-1667.

2924 Inoue, K., and L. Back (2015a), Column-Integrated Moist Static Energy Budget Analysis on Various Time
2925 Scales during TOGA COARE, *J. Atmos. Sci.*, *72*, doi:10.1175/JAS-D-14-0249.1, 1856-1871.

2926 Inoue, K., and L. E. Back (2015b), Gross Moist Stability Assessment during TOGA COARE: Various
2927 Interpretations of Gross Moist Stability, *J. Atmos. Sci.*, *72*, doi:10.1175/JAS-D-15-0092.1, 4148-4166.

2928 Janiga, M. A., C. J. S. III, J. A. Ridout, M. Flatau, N. P. Barton, E. J. Metzger, and C. A. Reynolds (2018),
2929 Subseasonal Forecasts of Convectively Coupled Equatorial Waves and the MJO: Activity and Predictive
2930 Skill, *Mon. Weather Rev.*, *146*, 10.1175/mwr-d-17-0261.1, 2337-2360.

2931 Jeong, J.-H., C.-H. Ho, B.-M. Kim, and W.-T. Kwon (2005), Influence of the Madden-Julian Oscillation on
2932 wintertime surface air temperature and cold surges in east Asia, *Journal of Geophysical Research:*
2933 *Atmospheres*, *110*, 10.1029/2004JD005408, D11104.

2934 Jiang, X., T. Li, and B. Wang (2004), Structures and Mechanisms of the Northward Propagating Boreal
2935 Summer Intraseasonal Oscillation, *J. Clim.*, *17*, 1022-1039.

2936 Jiang, X., D. E. Waliser, W. S. Olson, W.-K. Tao, T. S. L'Ecuyer, J.-L. Li, B. Tian, Y. L. Yung, A. M.
2937 Tompkins, S. E. Lang, and M. Grecu (2009), Vertical Heating Structures Associated with the MJO as
2938 Characterized by TRMM Estimates, ECMWF Reanalyses, and Forecasts: A Case Study during 1998/99
2939 Winter, *J. Clim.*, *22*, doi:10.1175/2009JCLI3048.1, 6001-6020.

2940 Jiang, X., D. E. Waliser, W. S. Olson, W.-K. Tao, T. S. L'Ecuyer, K.-F. Li, Y. L. Yung, S. Shige, S. Lang,
2941 and Y. N. Takayabu (2011), Vertical Diabatic Heating Structure of the MJO: Intercomparison between
2942 Recent Reanalyses and TRMM Estimates, *Mon. Weather Rev.*, *139*, 10.1175/2011mwr3636.1, 3208-
2943 3223.

2944 Jiang, X., M. Zhao, and D. E. Waliser (2012), Modulation of Tropical Cyclones over the Eastern Pacific by
2945 the Intraseasonal Variability Simulated in an AGCM, *J. Clim.*, *25*, 10.1175/jcli-d-11-00531.1, 6524-6538.

2946 Jiang, X., D. E. Waliser, P. K. Xavier, J. Petch, N. P. Klingaman, S. J. Woolnough, B. Guan, G. Bellon, T.
2947 Crueger, C. DeMott, C. Hannay, H. Lin, W. Hu, D. Kim, C.-L. Lappen, M.-M. Lu, H.-Y. Ma, T.
2948 Miyakawa, J. A. Ridout, S. D. Schubert, J. Scinocca, K.-H. Seo, E. Shindo, X. Song, C. Stan, W.-L.
2949 Tseng, W. Wang, T. Wu, X. Wu, K. Wyser, G. J. Zhang, and H. Zhu (2015), Vertical structure and
2950 physical processes of the Madden-Julian oscillation: Exploring key model physics in climate simulations,
2951 *Journal of Geophysical Research: Atmospheres*, *120*, 10.1002/2014JD022375, 4718-4748.

2952 Jiang, X., M. Zhao, E. D. Maloney, and D. E. Waliser (2016), Convective moisture adjustment time scale as
2953 a key factor in regulating model amplitude of the Madden-Julian Oscillation, *Geophys. Res. Lett.*, *43*,
2954 10.1002/2016GL070898, 10,412-410,419.

2955 Jiang, X. (2017), Key processes for the eastward propagation of the Madden-Julian Oscillation based on
2956 multimodel simulations, *Journal of Geophysical Research: Atmospheres* 10.1002/2016JD025955.

2957 Jiang, X., Á. F. Adames, M. Zhao, D. Waliser, and E. Maloney (2018a), A Unified Moisture Mode
2958 Framework for Seasonality of the Madden-Julian Oscillation, *J. Clim.*, *31*, 10.1175/jcli-d-17-0671.1,
2959 4215-4224.

2960 Jiang, X., B. Xiang, M. Zhao, T. Li, S.-J. Lin, Z. Wang, and J.-H. Chen (2018b), Intraseasonal Tropical
2961 Cyclogenesis Prediction in a Global Coupled Model System, *J. Clim.*, *31*, 10.1175/JCLI-D-17-0454.1,
2962 6209-6227.

2963 Jiang, X., H. Su, and D. E. Waliser (2019), A Damping Effect of the Maritime Continent for the Madden-
2964 Julian Oscillation, *Journal of Geophysical Research: Atmospheres* 10.1029/2019JD031503.

2965 Jiang, X., D. Kim, and E. Maloney (2020), Progress and Status of MJO Simulation in Climate Models and
2966 Process-Oriented Diagnostics, Chapter 25 in *The Multiscale Global Monsoon System*, eds :C.P. Chang,
2967 K.J. Ha, R. H. Johnson, D. Kim, G.N. Lau, B. Wang. World Scientific Series on Asia-Pacific Weather
2968 and Climate, Vol. 11. World Scientific, Singapore., edited.

2969 Johnson, R. H., T. M. Rickenbach, S. A. Rutledge, P. E. Ciesielski, and W. H. Schubert (1999), Trimodal
2970 Characteristics of Tropical Convection, *J. Clim.*, *12*, 2397-2418.

2971 Johnson, R. H., and P. E. Ciesielski (2013), Structure and Properties of Madden–Julian Oscillations Deduced
2972 from DYNAMO Sounding Arrays, *J. Atmos. Sci.*, *70*, 10.1175/JAS-D-13-065.1, 3157-3179.

2973 Johnson, R. H., P. E. Ciesielski, J. H. Ruppert, and M. Katsumata (2015), Sounding-Based Thermodynamic
2974 Budgets for DYNAMO, *J. Atmos. Sci.*, *72*, 10.1175/JAS-D-14-0202.1, 598-622.

2975 Jones, C., L. M. V. Carvalho, R. Wayne Higgins, D. E. Waliser, and J. K. E. Schemm (2004a), Climatology
2976 of Tropical Intraseasonal Convective Anomalies: 1979–2002, *J. Clim.*, *17*, 10.1175/1520-
2977 0442(2004)017<0523:COTICA>2.0.CO;2, 523-539.

2978 Jones, C., D. E. Waliser, K. M. Lau, and W. Stern (2004b), Global occurrences of extreme precipitation and
2979 the Madden-Julian oscillation: Observations and predictability, *J. Clim.*, *17*, 4575-4589.

2980 Jones, C., and L. M. V. Carvalho (2006), Changes in the Activity of the Madden–Julian Oscillation during
2981 1958–2004, *J. Clim.*, *19*, 10.1175/JCLI3972.1, 6353-6370.

2982 Jones, C., and L. M. V. Carvalho (2011), Will global warming modify the activity of the Madden–Julian
2983 Oscillation?, *Quart. J. Roy. Meteor. Soc.*, *137*, 10.1002/qj.765, 544-552.

2984 Jones, C., and L. M. V. Carvalho (2012), Spatial–Intensity Variations in Extreme Precipitation in the
2985 Contiguous United States and the Madden–Julian Oscillation, *J. Clim.*, *25*, 10.1175/jcli-d-11-00278.1,
2986 4898-4913.

2987 Judt, F., and S. S. Chen (2014), An explosive convective cloud system and its environmental conditions in
2988 MJO initiation observed during DYNAMO, *Journal of Geophysical Research: Atmospheres*, *119*,
2989 10.1002/2013JD021048, 2781-2795.

2990 Kacimi, A., and B. Khouider (2018), The transient response to an equatorial heat source and its convergence
2991 to steady state: implications for MJO theory, *Climate Dyn.*, *50*, 10.1007/s00382-017-3807-6, 3315-3330.

2992 Kalnay, E., M. Kanamitsu, R. Kistler, W. Collins, D. Deaven, L. Gandin, M. Iredell, S. Saha, G. White, J.
2993 Woollen, Y. Zhu, M. Chelliah, W. Ebisuzaki, W. Higgins, J. Janowiak, K. C. Mo, C. Ropelewski, J.

2994 Wang, A. Leetmaa, R. Reynolds, R. Jenne, and D. Joseph (1996), The NCEP/NCAR 40-year reanalysis
2995 project, *Bull. Am. Meteorol. Soc.*, *77*, 437-471.

2996 Kang, W., and E. Tziperman (2017), More Frequent Sudden Stratospheric Warming Events due to Enhanced
2997 MJO Forcing Expected in a Warmer Climate, *J. Clim.*, *30*, 10.1175/jcli-d-17-0044.1, 8727-8743.

2998 Kang, W., and E. Tziperman (2018a), The Role of Zonal Asymmetry in the Enhancement and Suppression
2999 of Sudden Stratospheric Warming Variability by the Madden-Julian Oscillation, *J. Clim.*, *31*,
3000 10.1175/jcli-d-17-0489.1, 2399-2415.

3001 Kang, W., and E. Tziperman (2018b), The MJO-SSW Teleconnection: Interaction Between MJO-Forced
3002 Waves and the Midlatitude Jet, *Geophys. Res. Lett.*, *45*, 10.1029/2018GL077937, 4400-4409.

3003 Kapur, A., and C. Zhang (2012), Multiplicative MJO Forcing of ENSO, *J. Clim.*, *25*, 10.1175/jcli-d-11-
3004 00609.1, 8132-8147.

3005 Kemball-Cook, S. R., and B. C. Weare (2001), The onset of convection in the Madden-Julian oscillation, *J.*
3006 *Clim.*, *14*, 780-793.

3007 Kerns, B. W., and S. S. Chen (2014), Equatorial Dry Air Intrusion and Related Synoptic Variability in MJO
3008 Initiation during DYNAMO, *Mon. Weather Rev.*, *142*, 10.1175/MWR-D-13-00159.1, 1326-1343.

3009 Kerns, B. W., and S. S. Chen (2016), Large-scale precipitation tracking and the MJO over the Maritime
3010 Continent and Indo-Pacific warm pool, *Journal of Geophysical Research: Atmospheres*, *121*,
3011 10.1002/2015JD024661, 8755-8776.

3012 Kessler, W. S., and R. Kleeman (2000), Rectification of the Madden-Julian Oscillation into the ENSO Cycle,
3013 *J. Clim.*, *13*, 3560-3575.

3014 Khairoutdinov, M., D. Randall, and C. DeMott (2005), Simulations of the atmospheric general circulation
3015 using a cloud-resolving model as a superparameterization of physical processes, *J. Atmos. Sci.*, *62*, 2136-
3016 2154.

3017 Khairoutdinov, M. F., and D. A. Randall (2003), Cloud resolving modeling of the ARM summer 1997 IOP:
3018 Model formulation, results, uncertainties, and sensitivities, *J. Atmos. Sci.*, *60*, 607-625.

3019 Khairoutdinov, M. F., and K. Emanuel (2018), Intraseasonal Variability in a Cloud-Permitting Near-Global
3020 Equatorial Aquaplanet Model, *J. Atmos. Sci.*, *75*, 10.1175/jas-d-18-0152.1, 4337-4355.

3021 Khouider, B., and A. J. Majda (2006), A Simple Multicloud Parameterization for Convectively Coupled
3022 Tropical Waves. Part I: Linear Analysis, *J. Atmos. Sci.*, *63*, 1308-1323.

3023 Khouider, B., Y. Han, A. J. Majda, and S. N. Stechmann (2012), Multiscale Waves in an MJO Background
3024 and Convective Momentum Transport Feedback, *J. Atmos. Sci.*, *69*, 10.1175/JAS-D-11-0152.1, 915-933.

3025 Kikuchi, K., and Y. N. Takayabu (2004), The development of organized convection associated with the MJO
3026 during TOGA COARE IOP: Trimodal characteristics, *Geophys. Res. Lett.*, *31*.

3027 Kikuchi, K., and B. Wang (2008), Diurnal Precipitation Regimes in the Global Tropics, *J. Clim.*, *21*,
3028 doi:10.1175/2007JCLI2051.1, 2680-2696.

3029 Kikuchi, K. (2014), An introduction to combined Fourier–wavelet transform and its application to
3030 convectively coupled equatorial waves, *Climate Dyn.*, *43*, 10.1007/s00382-013-1949-8, 1339-1356.

3031 Kiladis, G. N., and K. M. Weickmann (1992), Extratropical Forcing of Tropical Pacific Convection during
3032 Northern Winter, *Mon. Weather Rev.*, *120*, 1924-1938.

3033 Kiladis, G. N., K. H. Straub, and P. T. Haertel (2005), Zonal and Vertical Structure of the Madden-Julian
3034 Oscillation, *J. Atmos. Sci.*, *62*, 2790-2809.

3035 Kiladis, G. N., M. C. Wheeler, P. T. Haertel, K. H. Straub, and P. E. Roundy (2009), Convectively Coupled
3036 Equatorial Waves, *Rev. Geophys.*, *47*, RG2003, DOI:10.1029/2008RG000266

3037 Kiladis, G. N., J. Dias, K. H. Straub, M. C. Wheeler, S. N. Tulich, K. Kikuchi, K. M. Weickmann, and M. J.
3038 Ventrice (2014), A Comparison of OLR and Circulation-Based Indices for Tracking the MJO, *Mon.*
3039 *Weather Rev.*, *142*, 10.1175/mwr-d-13-00301.1, 1697-1715.

3040 Kim, D., K. Sperber, W. Stern, D. Waliser, I. S. Kang, E. Maloney, W. Wang, K. Weickmann, J. Benedict,
3041 M. Khairoutdinov, M. I. Lee, R. Neale, M. Suarez, K. Thayer-Calder, and G. Zhang (2009), Application
3042 of MJO Simulation Diagnostics to Climate Models, *J. Clim.*, *22*, Doi 10.1175/2009jcli3063.1, 6413-6436.

3043 Kim, D., A. H. Sobel, and I.-S. Kang (2011a), A mechanism denial study on the Madden-Julian Oscillation,
3044 *Journal of Advances in Modeling Earth Systems*, *3*, 10.1029/2011MS000081, n/a-n/a.

3045 Kim, D., A. H. Sobel, E. D. Maloney, D. M. W. Frierson, and I. S. Kang (2011b), A Systematic Relationship
3046 between Intraseasonal Variability and Mean State Bias in AGCM Simulations, *J. Clim.*, *24*, Doi
3047 10.1175/2011jcli4177.1, 5506-5520.

3048 Kim, D., and I.-S. Kang (2012), A bulk mass flux convection scheme for climate model: description and
3049 moisture sensitivity, *Climate Dyn.*, *38*, 10.1007/s00382-010-0972-2, 411-429.

3050 Kim, D., A. H. Sobel, A. D. Del Genio, Y. Chen, S. J. Camargo, M.-S. Yao, M. Kelley, and L. Nazarenko
3051 (2012), The Tropical Subseasonal Variability Simulated in the NASA GISS General Circulation Model,
3052 *J. Clim.*, *25*, 10.1175/JCLI-D-11-00447.1, 4641-4659.

3053 Kim, D., J.-S. Kug, and A. H. Sobel (2014a), Propagating versus Nonpropagating Madden–Julian Oscillation
3054 Events, *J. Clim.*, *27*, 10.1175/JCLI-D-13-00084.1, 111-125.

3055 Kim, D., P. Xavier, E. Maloney, M. Wheeler, D. Waliser, K. Sperber, H. Hendon, C. Zhang, R. Neale, Y.-T.
3056 Hwang, and H. Liu (2014b), Process-Oriented MJO Simulation Diagnostic: Moisture Sensitivity of
3057 Simulated Convection, *J. Clim.*, *27*, 10.1175/jcli-d-13-00497.1, 5379-5395.

3058 Kim, D., M.-S. Ahn, I.-S. Kang, and A. D. D. Genio (2015), Role of Longwave Cloud–Radiation Feedback
3059 in the Simulation of the Madden–Julian Oscillation, *J. Clim.*, *28*, doi:10.1175/JCLI-D-14-00767.1, 6979-
3060 6994.

3061 Kim, D., H. Kim, and M.-I. Lee (2017), Why does the MJO detour the Maritime Continent during austral
3062 summer?, *Geophys. Res. Lett.* 10.1002/2017GL072643, n/a-n/a.

3063 Kim, D., and E. Maloney (2017), Simulation of the Madden-Julian Oscillation Using General Circulation
3064 Models, in *The Global Monsoon System*, edited, pp. 161-172, World Scientific.

3065 Kim, D., E. Maloney, and C. Zhang (2020a), Review: MJO propagation over the Maritime Continent. The
3066 Multiscale Global Monsoon System, C. P. Chang et al., Eds., Vol. 11, World Scientific Series on Asia-
3067 Pacific Weather and Climate, World Scientific.

3068 Kim, H.-M., P. J. Webster, V. E. Toma, and D. Kim (2014c), Predictability and Prediction Skill of the MJO
3069 in Two Operational Forecasting Systems, *J. Clim.*, 27, doi:10.1175/JCLI-D-13-00480.1, 5364-5378.

3070 Kim, H.-M., D. Kim, F. Vitart, V. E. Toma, J.-S. Kug, and P. J. Webster (2016), MJO Propagation across the
3071 Maritime Continent in the ECMWF Ensemble Prediction System, *J. Clim.*, 29, doi:10.1175/JCLI-D-15-
3072 0862.1, 3973-3988.

3073 Kim, H.-M. (2017), The Impact of the Mean Moisture Bias on the Key Physics of MJO Propagation in the
3074 ECMWF Reforecast, *Journal of Geophysical Research: Atmospheres* 10.1002/2017JD027005,
3075 2017JD027005.

3076 Kim, H., F. Vitart, and D. E. Waliser (2018), Prediction of the Madden-Julian Oscillation: A Review, *J.*
3077 *Clim.*, 31, 10.1175/JCLI-D-18-0210.1, 9425-9443.

3078 Kim, H., M. A. Janiga, and K. Pegion (2019), MJO Propagation Processes and Mean Biases in the SubX and
3079 S2S Reforecasts, *Journal of Geophysical Research: Atmospheres*, 124, 10.1029/2019JD031139, 9314-
3080 9331.

3081 Kim, H., J. M. Caron, J. H. Richter, and I. R. Simpson (2020b), The lack of QBO-MJO connection in
3082 CMIP6 models, *Geophys. Res. Lett.*, n/a, 10.1029/2020GL087295, e2020GL087295.

3083 Kim, H., J. H. Richter, and Z. Martin (2020c), Insignificant QBO-MJO Prediction Skill Relationship in the
3084 SubX and S2S Subseasonal Reforecasts, *Journal of Geophysical Research: Atmospheres*, 124,
3085 10.1029/2019jd031416, 12655-12666.

3086 Kim, J., and S.-W. Son (2012), Tropical Cold-Point Tropopause: Climatology, Seasonal Cycle, and
3087 Intraseasonal Variability Derived from COSMIC GPS Radio Occultation Measurements, *J. Clim.*, 25,
3088 10.1175/jcli-d-11-00554.1, 5343-5360.

3089 Kiranmayi, L., and E. D. Maloney (2011), Intraseasonal moist static energy budget in reanalysis data,
3090 *Journal of Geophysical Research: Atmospheres*, 116, 10.1029/2011JD016031, D21117.

3091 Kirtman, B., and coauthors (2013), Near-term Climate Change: Projections and Predictability. In: Climate
3092 Change 2013: The Physical Science Basis. Contribution of Working Group I to the Fifth Assessment
3093 Report of the Intergovernmental Panel on Climate Change [Stocker, T.F., D. Qin, G.-K. Plattner, M.
3094 Tignor, S.K. Allen, J. Boschung, A. Nauels, Y. Xia, V. Bex and P.M. Midgley (eds.)]. Cambridge
3095 University Press, Cambridge, United Kingdom and New York, NY, USA. , edited.

3096 Klingaman, N. P., and S. J. Woolnough (2014), The role of air-sea coupling in the simulation of the
3097 Madden-Julian oscillation in the Hadley Centre model, *Quart. J. Roy. Meteor. Soc.* 10.1002/qj.2295.

3098 Klingaman, N. P., X. Jiang, P. K. Xavier, J. Petch, D. Waliser, and S. J. Woolnough (2015a), Vertical
3099 structure and physical processes of the Madden-Julian oscillation: Synthesis and summary, *Journal of*
3100 *Geophysical Research: Atmospheres*, *120*, 10.1002/2015JD023196, 4671-4689.

3101 Klingaman, N. P., S. J. Woolnough, X. Jiang, D. Waliser, P. K. Xavier, J. Petch, M. Caian, C. Hannay, D.
3102 Kim, H.-Y. Ma, W. J. Merryfield, T. Miyakawa, M. Pritchard, J. A. Ridout, R. Roehrig, E. Shindo, F.
3103 Vitart, H. Wang, N. R. Cavanaugh, B. E. Mapes, A. Shelly, and G. J. Zhang (2015b), Vertical structure
3104 and physical processes of the Madden-Julian oscillation: Linking hindcast fidelity to simulated diabatic
3105 heating and moistening, *Journal of Geophysical Research: Atmospheres*, *120*, 10.1002/2014JD022374,
3106 4690-4717.

3107 Klingaman, N. P., and C. A. Demott (2020), Mean State Biases and Interannual Variability Affect Perceived
3108 Sensitivities of the Madden-Julian Oscillation to Air-Sea Coupling, *Journal of Advances in Modeling*
3109 *Earth Systems*, *12*, 10.1029/2019MS001799, e2019MS001799.

3110 Klotzbach, P., S. Abhik, H. H. Hendon, M. Bell, C. Lucas, A. G. Marshall, and E. C. J. Oliver (2019), On the
3111 emerging relationship between the stratospheric Quasi-Biennial oscillation and the Madden-Julian
3112 oscillation, *Scientific Reports*, *9*, 10.1038/s41598-019-40034-6, 2981.

3113 Klotzbach, P. J. (2010), On the Madden-Julian Oscillation-Atlantic Hurricane Relationship, *J. Clim.*, *23*,
3114 doi:10.1175/2009JCLI2978.1, 282-293.

3115 Knutson, T. R., and S. Manabe (1995), Time-Mean Response over the Tropical Pacific to Increased CO₂ in a
3116 Coupled Ocean-Atmosphere Model, *J. Clim.*, *8*, 10.1175/1520-0442(1995)008<2181:Tmrott>2.0.Co;2,
3117 2181-2199.

3118 Kodama, Y.-M., M. Tokuda, and F. Murata (2006), Convective Activity Over the Indonesian Maritime
3119 Continent During CPEA-I as Evaluated by Lightning Activity and Q1 and Q2 Profiles, *Journal of the*
3120 *Meteorological Society of Japan. Ser. II*, *84A*, 10.2151/jmsj.84A.133, 133-149.

3121 Krishnamurti, T. N., D. K. Oosterhof, and A. V. Mehta (1988), Air-Sea Interaction on the Time Scale of 30
3122 to 50 Days, *J. Atmos. Sci.*, *45*, 10.1175/1520-0469(1988)045<1304:Aiotts>2.0.Co;2, 1304-1322.

3123 Kuang, Z. (2008), A moisture-stratiform instability for convectively coupled waves, *J. Atmos. Sci.*, *65*, Doi
3124 10.1175/2007jas2444.1, 834-854.

3125 Kubokawa, H., M. Satoh, J. Suzuki, and M. Fujiwara (2016), Influence of topography on temperature
3126 variations in the tropical tropopause layer, *Journal of Geophysical Research: Atmospheres*, *121*,
3127 10.1002/2016JD025569, 11,556-511,574.

3128 Kubota, H., K. Yoneyama, J.-I. Hamada, P. Wu, A. Sudaryanto, and I. B. Wahyono (2015), Role of
3129 Maritime Continent Convection during the Preconditioning Stage of the Madden-Julian Oscillation
3130 Observed in CINDY2011/DYNAMO, *Journal of the Meteorological Society of Japan. Ser. II*, *93A*,
3131 10.2151/jmsj.2015-050, 101-114.

3132 Kuo, Y.-H., J. D. Neelin, C.-C. Chen, W.-T. Chen, L. J. Donner, A. Gettelman, X. Jiang, K.-T. Kuo, E.
3133 Maloney, C. R. Mechoso, Y. Ming, K. A. Schiro, C. J. Seman, C.-M. Wu, and M. Zhao (2019),
3134 Convective transition statistics over tropical oceans for climate model diagnostics: GCM evaluation, *J.*
3135 *Atmos. Sci.*, *0*, 10.1175/jas-d-19-0132.1, null.

3136 L'Ecuyer, T. S., and G. McGarragh (2010), A 10-Year Climatology of Tropical Radiative Heating and Its
3137 Vertical Structure from TRMM Observations, *J. Clim.*, *23*, Doi 10.1175/2009jcli3018.1, 519-541.

3138 L'Heureux, M. L., and R. W. Higgins (2008), Boreal winter links between the Madden-Julian oscillation and
3139 the Arctic oscillation, *J. Clim.*, *21*, Doi 10.1175/2007jcli1955.1, 3040-3050.

3140 L'Heureux, M. L., and R. W. Higgins (2008), Boreal Winter Links between the Madden–Julian Oscillation
3141 and the Arctic Oscillation, *J. Clim.*, *21*, 10.1175/2007jcli1955.1, 3040-3050.

3142 Lau, K.-M., and P. H. Chan (1986), Aspects of the 40-50 Day Oscillation during the Northern Summer as
3143 Inferred from Outgoing Longwave Radiation, *Mon. Weather Rev.*, *114*, 1354-1367.

3144 Lau, K.-M., and T. J. Phillips (1986), Coherent Fluctuations of Extratropical Geopotential Height and
3145 Tropical Convection in Intraseasonal Time Scales, *J. Atmos. Sci.*, *43*, 10.1175/1520-
3146 0469(1986)043<1164:Cfogh>2.0.Co;2, 1164-1181.

3147 Lau, K.-M., and L. Peng (1987), Origin of Low-Frequency (Intraseasonal) Oscillations in the Tropical
3148 Atmosphere. Part I: Basic Theory, *J. Atmos. Sci.*, *44*, 950-972.

3149 Lau, W. K.-M., and D. E. Waliser (2012), *Intraseasonal Variability in the Atmosphere-Ocean Climate*
3150 *System*, Second ed., Springer, 613p, Heidelberg, Germany.

3151 Lee, C.-Y., S. J. Camargo, F. Vitart, A. H. Sobel, and M. K. Tippett (2018), Sub-seasonal tropical cyclone
3152 genesis prediction and MJO in the S2S dataset, *Weather Forecasting*, *33*, 10.1175/waf-d-17-0165.1.

3153 Lee, H.-J., and K.-H. Seo (2019), Impact of the Madden-Julian oscillation on Antarctic sea ice and its
3154 dynamical mechanism, *Scientific Reports*, *9*, 10.1038/s41598-019-47150-3, 10761.

3155 Lee, J.-E., B. R. Lintner, J. D. Neelin, X. Jiang, P. Gentine, C. K. Boyce, J. B. Fisher, J. T. Perron, T. L.
3156 Kubar, J. Lee, and J. Worden (2012), Reduction of tropical land region precipitation variability via
3157 transpiration, *Geophys. Res. Lett.*, *39*, 10.1029/2012GL053417, n/a-n/a.

3158 Lee, J. C. K., and N. P. Klingaman (2018), The effect of the quasi-biennial oscillation on the Madden–Julian
3159 oscillation in the Met Office Unified Model Global Ocean Mixed Layer configuration, *Atmospheric*
3160 *Science Letters*, *19*, 10.1002/asl.816, e816.

3161 Lee, M. I., I. S. Kang, J. K. Kim, and B. E. Mapes (2001), Influence of cloud-radiation interaction on
3162 simulating tropical intraseasonal oscillation with an atmospheric general circulation model, *J. Geophys.*
3163 *Res.*, *106*, 14219-14233.

3164 Lee, M. I., I. S. Kang, and B. E. Mapes (2003), Impacts of cumulus convection parameterization on aqua-
3165 planet AGCM Simulations of tropical intraseasonal variability, *J. Meteorol. Soc. Japan*, *81*, 963-992.

3166 Lee, S.-H., and K.-H. Seo (2011), A multi-scale analysis of the interdecadal change in the Madden-Julian
3167 Oscillation, *Atmosphere*, 21.

3168 Lee, S., T. Gong, N. Johnson, S. B. Feldstein, and D. Pollard (2011), On the Possible Link between Tropical
3169 Convection and the Northern Hemisphere Arctic Surface Air Temperature Change between 1958 and
3170 2001, *J. Clim.*, 24, 10.1175/2011jcli4003.1, 4350-4367.

3171 Leutbecher, M., S.-J. Lock, P. Ollinaho, S. T. K. Lang, G. Balsamo, P. Bechtold, M. Bonavita, H. M.
3172 Christensen, M. Diamantakis, E. Dutra, S. English, M. Fisher, R. M. Forbes, J. Goddard, T. Haiden, R. J.
3173 Hogan, S. Juricke, H. Lawrence, D. MacLeod, L. Magnusson, S. Malardel, S. Massart, I. Sandu, P. K.
3174 Smolarkiewicz, A. Subramanian, F. Vitart, N. Wedi, and A. Weisheimer (2017), Stochastic
3175 representations of model uncertainties at ECMWF: state of the art and future vision, *Quart. J. Roy.
3176 Meteor. Soc.*, 143, 10.1002/qj.3094, 2315-2339.

3177 Li, K.-F., B. Tian, D. E. Waliser, and Y. L. Yung (2010), Tropical mid-tropospheric CO₂ variability driven
3178 by the Madden-Julian oscillation, *Proceedings of the National Academy of Sciences*, 107,
3179 10.1073/pnas.1008222107, 19171-19175.

3180 Li, Y., and R. E. Carbone (2012), Excitation of Rainfall over the Tropical Western Pacific, *J. Atmos. Sci.*, 69,
3181 10.1175/jas-d-11-0245.1, 2983-2994.

3182 Li, Y., W. Han, T. Shinoda, C. Wang, R.-C. Lien, J. N. Moum, and J.-W. Wang (2013), Effects of the
3183 diurnal cycle in solar radiation on the tropical Indian Ocean mixed layer variability during wintertime
3184 Madden-Julian Oscillations, *Journal of Geophysical Research: Oceans*, 118, 10.1002/jgrc.20395, 4945-
3185 4964.

3186 Liebmann, B., and D. L. Hartmann (1984), An Observational Study of Tropical-Midlatitude Interaction on
3187 Intraseasonal Time Scales during Winter, *J. Atmos. Sci.*, 41, 3333-3350.

3188 Liebmann, B., H. H. Hendon, and J. D. Glick (1994), The Relationship between Tropical Cyclones of the
3189 Western Pacific and Indian Oceans and the Madden-Julian Oscillation, *J. Meteorol. Soc. Japan*, 72, 401-
3190 412.

3191 Liebmann, B., H. H. Hendon, and J. D. Glick (1997), On the generation of two-day convective disturbances
3192 across the western equatorial Pacific, *J. Meteorol. Soc. Japan*, 75, 939-946.

3193 Liess, S., and M. A. Geller (2012), On the relationship between QBO and distribution of tropical deep
3194 convection, *Journal of Geophysical Research: Atmospheres*, 117, 10.1029/2011JD016317.

3195 Lim, Y., S.-W. Son, and D. Kim (2018), MJO Prediction Skill of the Subseasonal-to-Seasonal Prediction
3196 Models, *J. Clim.*, 31, 10.1175/JCLI-D-17-0545.1, 4075-4094.

3197 Lim, Y., S.-W. Son, A. G. Marshall, H. H. Hendon, and K.-H. Seo (2019), Influence of the QBO on MJO
3198 prediction skill in the subseasonal-to-seasonal prediction models, *Climate Dyn.*, 53, 10.1007/s00382-019-
3199 04719-y, 1681-1695.

3200 Limpasuvan, V., and D. L. Hartmann (1999), Eddies and the annular modes of climate variability, *Geophys.*
3201 *Res. Lett.*, *26*, 10.1029/1999GL010478, 3133-3136.

3202 Lin, H., G. Brunet, and J. Derome (2007), Intraseasonal Variability in a Dry Atmospheric Model, *J. Atmos.*
3203 *Sci.*, *64*, 10.1175/JAS3955.1, 2422-2441.

3204 Lin, H., and G. Brunet (2009), The Influence of the Madden–Julian Oscillation on Canadian Wintertime
3205 Surface Air Temperature, *Mon. Weather Rev.*, *137*, 10.1175/2009mwr2831.1, 2250-2262.

3206 Lin, H., G. Brunet, and J. Derome (2009), An Observed Connection between the North Atlantic Oscillation
3207 and the Madden-Julian Oscillation, *J. Clim.*, *22*, Doi 10.1175/2008jcli2515.1, 364-380.

3208 Lin, H., G. Brunet, and R. Mo (2010), Impact of the Madden–Julian Oscillation on Wintertime Precipitation
3209 in Canada, *Mon. Weather Rev.*, *138*, 10.1175/2010MWR3363.1, 3822-3839.

3210 Lin, H., and G. Brunet (2011), Impact of the North Atlantic Oscillation on the forecast skill of the Madden-
3211 Julian Oscillation, *Geophys. Res. Lett.*, *38*, 10.1029/2010GL046131.

3212 Lin, H., G. Brunet, and B. Yu (2015), Interannual variability of the Madden-Julian Oscillation and its impact
3213 on the North Atlantic Oscillation in the boreal winter, *Geophys. Res. Lett.*, *42*, 10.1002/2015GL064547,
3214 5571-5576.

3215 Lin, H. (2018), Predicting the Dominant Patterns of Subseasonal Variability of Wintertime Surface Air
3216 Temperature in Extratropical Northern Hemisphere, *Geophys. Res. Lett.*, *45*, 10.1029/2018GL077509,
3217 4381-4389.

3218 Lin, H., and G. Brunet (2018), Extratropical Response to the MJO: Nonlinearity and Sensitivity to the Initial
3219 State, *J. Atmos. Sci.*, *75*, 10.1175/jas-d-17-0189.1, 219-234.

3220 Lin, H., J. S. Frederiksen, D. M. Straus, and C. Stan (2019a), Tropical-extratropical interactions and
3221 teleconnections. Chapter 7, Pages 143-164, Sub-Seasonal to Seasonal Prediction: The Gap Between
3222 Weather and Climate Forecasting, Editor(s): Andrew W. Robertson, Frederic Vitart, Elsevier, 2019.,
3223 edited.

3224 Lin, H., R. Mo, F. Vitart, and C. Stan (2019b), Eastern Canada Flooding 2017 and its Subseasonal
3225 Predictions, *Atmosphere-Ocean*, *57*, 10.1080/07055900.2018.1547679, 195-207.

3226 Lin, H. (2020), Subseasonal Forecast Skill over the Northern Polar Region in Boreal Winter, *J. Clim.*, *33*,
3227 10.1175/jcli-d-19-0408.1, 1935-1951.

3228 Lin, J.-L., G. N. Kiladis, B. E. Mapes, K. M. Weickmann, K. R. Sperber, W. Lin, M. C. Wheeler, S. D.
3229 Schubert, A. Del Genio, L. J. Donner, S. Emori, J.-F. Gueremy, F. Hourdin, P. J. Rasch, E. Roeckner, and
3230 J. F. Scinocca (2006), Tropical Intraseasonal Variability in 14 IPCC AR4 Climate Models. Part I:
3231 Convective Signals, *J. Clim.*, *19*, 2665-2690.

3232 Lin, J.-L., M.-I. Lee, D. Kim, I.-S. Kang, and D. M. W. Frierson (2008), The Impacts of Convective
3233 Parameterization and Moisture Triggering on AGCM-Simulated Convectively Coupled Equatorial
3234 Waves, *J. Clim.*, *21*, 10.1175/2007jcli1790.1, 883-909.

3235 Lin, J., B. Mapes, M. Zhang, and M. Newman (2004), Stratiform Precipitation, Vertical Heating Profiles,
3236 and the Madden-Julian Oscillation, *J. Atmos. Sci.*, *61*, 296-309.

3237 Lin, J. L., and B. E. Mapes (2004), Radiation budget of the tropical intraseasonal oscillation, *J. Atmos. Sci.*,
3238 *61*, 2050-2062.

3239 Lin, J. W.-B., and J. D. Neelin (2003), Toward stochastic deep convective parameterization in general
3240 circulation models, *Geophys. Res. Lett.*, *30*, 10.1029/2002GL016203, n/a-n/a.

3241 Lin, X., and R. H. Johnson (1996), Kinematic and thermodynamic characteristics of the flow over the
3242 western Pacific warm pool during TOGA COARE, *J. Atmos. Sci.*, *53*, 695-715.

3243 Ling, J., C. Li, and X. Jia (2009), Impacts of cumulus momentum transport on MJO simulation, *Advances in*
3244 *Atmospheric Sciences*, *26*, 10.1007/s00376-009-8016-8, 864-876.

3245 Ling, J., and C. Zhang (2011), Structural Evolution in Heating Profiles of the MJO in Global Reanalyses and
3246 TRMM Retrievals, *J. Clim.*, *24*, 10.1175/2010jcli3826.1, 825-842.

3247 Ling, J., Y. Zhao, and G. Chen (2019), Barrier Effect on MJO Propagation by the Maritime Continent in the
3248 MJO Task Force/GEWEX Atmospheric System Study Models, *J. Clim.*, *32*, 10.1175/jcli-d-18-0870.1,
3249 5529-5547.

3250 Liu, C., B. Tian, K.-F. Li, G. L. Manney, N. J. Livesey, Y. L. Yung, and D. E. Waliser (2014), Northern
3251 Hemisphere mid-winter vortex-displacement and vortex-split stratospheric sudden warmings: Influence
3252 of the Madden-Julian Oscillation and Quasi-Biennial Oscillation, *Journal of Geophysical Research:*
3253 *Atmospheres*, *119*, 10.1002/2014JD021876, 12,599-512,620.

3254 Liu, P., M. Satoh, B. Wang, H. Fudeyasu, T. Nasuno, T. Li, H. Miura, H. Taniguchi, H. Masunaga, X. Fu,
3255 and H. Annamalai (2009), An MJO Simulated by the NICAM at 14- and 7-km Resolutions, *Mon.*
3256 *Weather Rev.*, *137*, 10.1175/2009mwr2965.1, 3254-3268.

3257 Liu, P., T. Li, B. Wang, M. Zhang, J.-j. Luo, Y. Masumoto, X. Wang, and E. Roeckner (2013), MJO change
3258 with A1B global warming estimated by the 40-km ECHAM5, *Climate Dyn.*, *41*, 10.1007/s00382-012-
3259 1532-8, 1009-1023.

3260 Liu, X., T. Wu, S. Yang, T. Li, W. Jie, L. Zhang, Z. Wang, X. Liang, Q. Li, Y. Cheng, H. Ren, Y. Fang, and
3261 S. Nie (2017), MJO prediction using the sub-seasonal to seasonal forecast model of Beijing Climate
3262 Center, *Climate Dyn.*, *48*, 10.1007/s00382-016-3264-7, 3283-3307.

3263 Long, C. N., S. A. McFarlane, A. D. Genio, P. Minnis, T. P. Ackerman, J. Mather, J. Comstock, G. G. Mace,
3264 M. Jensen, and C. Jakob (2013), ARM Research In The Equatorial Western Pacific: A Decade And
3265 Counting, *Bull. Am. Meteorol. Soc.*, *94*, 10.1175/BAMS-D-11-00137.1, 695-708.

3266 Lopez, H., B. P. Kirtman, E. Tziperman, and G. Gebbie (2013), Impact of interactive westerly wind bursts
3267 on CCSM3, *Dynamics of Atmospheres and Oceans*, *59*, <https://doi.org/10.1016/j.dynatmoce.2012.11.001>,
3268 24-51.

3269 Lorenz, D. J., and D. L. Hartmann (2006), The Effect of the MJO on the North American Monsoon, *J. Clim.*,
3270 *19*, 333-343.

3271 Love, B. S., A. J. Matthews, and G. M. S. Lister (2011), The diurnal cycle of precipitation over the Maritime
3272 Continent in a high-resolution atmospheric model, *Quart. J. Roy. Meteor. Soc.*, *137*, 10.1002/qj.809, 934-
3273 947.

3274 Luo, Z. J., G. Y. Liu, and G. L. Stephens (2010), Use of A-Train data to estimate convective buoyancy and
3275 entrainment rate, *Geophys. Res. Lett.*, *37*, 10.1029/2010gl042904.

3276 Ma, D., and Z. M. Kuang (2011), Modulation of radiative heating by the Madden-Julian Oscillation and
3277 convectively coupled Kelvin waves as observed by CloudSat, *Geophys. Res. Lett.*, *38*, Doi
3278 10.1029/2011gl049734.

3279 Ma, D., and Z. Kuang (2016), A mechanism-denial study on the Madden-Julian Oscillation with reduced
3280 interference from mean state changes, *Geophys. Res. Lett.*, *43*, 10.1002/2016GL067702, 2989-2997.

3281 Madden, R. A., and P. R. Julian (1971), Detection of a 40-50 Day Oscillation in Zonal Wind in Tropical
3282 Pacific, *J. Atmos. Sci.*, *28*, 702-&.

3283 Madden, R. A., and P. R. Julian (1972), Description of Global-Scale Circulation Cells in Tropics with a 40-
3284 50 Day Period, *J. Atmos. Sci.*, *29*, 1109-&.

3285 Madden, R. A., and P. R. Julian (1994), Observations of the 40-50-Day Tropical Oscillation: A Review,
3286 *Mon. Weather Rev.*, *122*, 814-837.

3287 Majda, A. J., and J. A. Biello (2004), A multiscale model for tropical intraseasonal oscillations, *Proc. Natl.*
3288 *Acad. Sci.*, *101*, 4736-4741.

3289 Majda, A. J., and S. N. Stechmann (2009), A Simple Dynamical Model with Features of Convective
3290 Momentum Transport, *J. Atmos. Sci.*, *66*, 373-392.

3291 Majda, A. J., and S. N. Stechmann (2011), Nonlinear Dynamics and Regional Variations in the MJO
3292 Skeleton, *J. Atmos. Sci.*, *68*, 10.1175/JAS-D-11-053.1, 3053-3071.

3293 Majda, A. J., and S. N. Stechmann (2012), Multi-scale theories for the MJO, in *Intraseasonal Variability in*
3294 *the Atmosphere-Ocean Climate System*, edited by W. K. M. Lau and D. E. Waliser, Springer, Heidelberg,
3295 Germany.

3296 Majda, A. J., and Q. Yang (2016), A Multiscale Model for the Intraseasonal Impact of the Diurnal Cycle
3297 over the Maritime Continent on the Madden-Julian Oscillation, *J. Atmos. Sci.*, *73*, doi:10.1175/JAS-D-
3298 15-0158.1, 579-604.

3299 Maloney, E. D., and D. L. Hartmann (1998), Frictional Moisture Convergence in a Composite Life Cycle of
3300 the Madden-Julian Oscillation, *J. Clim.*, *11*, 2387-2403.

3301 Maloney, E. D., and D. L. Hartmann (2000), Modulation of Eastern North Pacific Hurricanes by the
3302 Madden-Julian Oscillation, *J. Clim.*, *13*, 1451-1460.

3303 Maloney, E. D., and D. L. Hartmann (2001), The sensitivity of intraseasonal variability in the NCAR CCM3
3304 to changes in convective parameterization, *J. Clim.*, *14*, 2015-2034.

3305 Maloney, E. D., and A. H. Sobel (2004), Surface Fluxes and Ocean Coupling in the Tropical Intraseasonal
3306 Oscillation, *J. Clim.*, *17*, 4368-4386.

3307 Maloney, E. D. (2009), The Moist Static Energy Budget of a Composite Tropical Intraseasonal Oscillation in
3308 a Climate Model, *J. Clim.*, *22*, 711-729.

3309 Maloney, E. D., A. H. Sobel, and W. M. Hannah (2010), Intraseasonal variability in an aquaplanet general
3310 circulation model, *Journal of Advances in Modeling Earth Systems*, *2*, 10.3894/james.2010.2.5.

3311 Maloney, E. D., and S.-P. Xie (2013), Sensitivity of tropical intraseasonal variability to the pattern of climate
3312 warming, *Journal of Advances in Modeling Earth Systems*, *5*, 10.1029/2012MS000171, 32-47.

3313 Maloney, E. D., Á. F. Adames, and H. X. Bui (2019a), Madden–Julian oscillation changes under
3314 anthropogenic warming, *Nature Climate Change*, *9*, 10.1038/s41558-018-0331-6, 26-33.

3315 Maloney, E. D., A. Gettelman, Y. Ming, J. D. Neelin, D. Barrie, A. Mariotti, C. C. Chen, D. R. B. Coleman,
3316 Y.-H. Kuo, B. Singh, H. Annamalai, A. Berg, J. F. Booth, S. J. Camargo, A. Dai, A. Gonzalez, J. Hafner,
3317 X. Jiang, X. Jing, D. Kim, A. Kumar, Y. Moon, C. M. Naud, A. H. Sobel, K. Suzuki, F. Wang, J. Wang,
3318 A. A. Wing, X. Xu, and M. Zhao (2019b), Process-Oriented Evaluation of Climate and Weather
3319 Forecasting Models, *Bull. Am. Meteorol. Soc.*, *100*, 10.1175/BAMS-D-18-0042.1, 1665-1686.

3320 Mapes, B., S. Tulich, J. Lin, and P. Zuidema (2006), The mesoscale convection life cycle: Building block or
3321 prototype for large-scale tropical waves?, *Dynamics of Atmospheres and Oceans*, *42*, Doi
3322 10.1016/J.Dynatmoce.2006.03.003, 3-29.

3323 Mapes, B., and R. Neale (2011a), Parameterizing Convective Organization to Escape the Entrainment
3324 Dilemma, *Journal of Advances in Modeling Earth Systems*, *3*, 10.1029/2011ms000042.

3325 Mapes, B. E. (2000), Convective Inhibition, Subgrid-Scale Triggering Energy, and Stratiform Instability in a
3326 Toy Tropical Wave Model, *J. Atmos. Sci.*, *57*, 1515-1535.

3327 Mapes, B. E., and R. B. Neale (2011b), Parameterizing convective organization, *Journal of Advances in*
3328 *Modeling Earth Systems*, *3*, 10.1029/2011ms000042, 20 pp.

3329 Marshall, A. G., O. Alves, and H. H. Hendon (2008), An Enhanced Moisture Convergence–Evaporation
3330 Feedback Mechanism for MJO Air–Sea Interaction, *J. Atmos. Sci.*, *65*, 10.1175/2007jas2313.1, 970-986.

3331 Marshall, A. G., D. Hudson, M. C. Wheeler, O. Alves, H. H. Hendon, M. J. Pook, and J. S. Risbey (2014),
3332 Intra-seasonal drivers of extreme heat over Australia in observations and POAMA-2, *Climate Dyn.*, *43*,
3333 10.1007/s00382-013-2016-1, 1915-1937.

3334 Marshall, A. G., H. H. Hendon, and G. Wang (2016), On the role of anomalous ocean surface temperatures
3335 for promoting the record Madden-Julian Oscillation in March 2015, *Geophys. Res. Lett.*, *43*,
3336 10.1002/2015GL066984, 472-481.

3337 Marshall, A. G., H. H. Hendon, S.-W. Son, and Y. Lim (2017), Impact of the quasi-biennial oscillation on
3338 predictability of the Madden–Julian oscillation, *Climate Dyn.* 10.1007/s00382-016-3392-0, 1-13.

3339 Martin, Z., S. Wang, J. Nie, and A. Sobel (2019), The Impact of the QBO on MJO Convection in Cloud-
3340 Resolving Simulations, *J. Atmos. Sci.*, 76, 10.1175/jas-d-18-0179.1, 669-688.

3341 Masunaga, H., T. S. L'Ecuyer, and C. D. Kummerow (2006), The Madden-Julian oscillation recorded in
3342 early observations from the Tropical Rainfall Measuring Mission (TRMM), *J. Atmos. Sci.*, 63, 2777-
3343 2794.

3344 Matsuno, T. (1966), Quasi-Geostrophic Motions in the Equatorial Area, *J. Meteorol. Soc. Japan*, 44, 25-42.

3345 Matthews, A. J., and G. N. Kiladis (1999), The Tropical–Extratropical Interaction between High-Frequency
3346 Transients and the Madden–Julian Oscillation, *Mon. Weather Rev.*, 127, 10.1175/1520-0493, 661-677.

3347 Matthews, A. J., B. J. Hoskins, and M. Masutani (2004), The global response to tropical heating in the
3348 Madden–Julian oscillation during the northern winter, *Quart. J. Roy. Meteor. Soc.*, 130,
3349 10.1256/qj.02.123, 1991-2011.

3350 Matthews, A. J., D. B. Baranowski, K. J. Heywood, P. J. Flatau, and S. Schmidtko (2014), The Surface
3351 Diurnal Warm Layer in the Indian Ocean during CINDY/DYNAMO, *J. Clim.*, 27, 10.1175/jcli-d-14-
3352 00222.1, 9101-9122.

3353 McPhaden, M. J. (1999), Genesis and evolution of the 1997-98 El Nino, *Science*, 283, 950-954.

3354 McPhaden, M. J. (2004), Evolution of the 2002/03 El Niño*, *Bull. Am. Meteorol. Soc.*, 85, 10.1175/bams-
3355 85-5-677, 677-696.

3356 Mechem, D. B., S. S. Chen, and R. A. Houze Jr. (2006), Momentum transport processes in the stratiform
3357 regions of mesoscale convective systems over the western Pacific warm pool, *Quart. J. Roy. Meteor.*
3358 *Soc.*, 132, 10.1256/qj.04.141, 709-736.

3359 Miura, H., M. Satoh, T. Nasuno, A. T. Noda, and K. Oouchi (2007), A Madden-Julian Oscillation event
3360 realistically simulated by a global cloud-resolving model, *Science*, 318, Doi 10.1126/Science.1148443,
3361 1763-1765.

3362 Miyakawa, T., M. Satoh, H. Miura, H. Tomita, H. Yashiro, A. T. Noda, Y. Yamada, C. Kodama, M. Kimoto,
3363 and K. Yoneyama (2014), Madden–Julian Oscillation prediction skill of a new-generation global model
3364 demonstrated using a supercomputer, *Nat Commun*, 5, 10.1038/ncomms4769.

3365 Miyakawa, T., and K. Kikuchi (2018), CINDY2011/DYNAMO Madden-Julian oscillation successfully
3366 reproduced in global cloud/cloud-system resolving simulations despite weak tropical wavelet power,
3367 *Scientific Reports*, 8, 10.1038/s41598-018-29931-4, 11664.

3368 Mo, K. C., and R. W. Higgins (1998), Tropical Convection and Precipitation Regimes in the Western United
3369 States, *J. Clim.*, 11, 2404-2423.

3370 Mo, K. C. (2000), Intraseasonal Modulation of Summer Precipitation over North America, *Mon. Weather*
3371 *Rev.*, 128, 1490-1505.

3372 Mo, K. C., C. Jones, and J. Nogues-Paegle (2012), Pan-America, in *Intraseasonal Variability in the*
3373 *Atmosphere-Ocean Climate System*, edited by W. K. M. Lau and D. E. Waliser, pp. 111-145, Springer,
3374 Heidelberg, Germany.

3375 Moncrieff, M. W. (1992), Organized Convective Systems - Archetypal Dynamic-Models, Mass and
3376 Momentum Flux Theory, and Parametrization, *Quart. J. Roy. Meteor. Soc.*, *118*, 819-850.

3377 Moncrieff, M. W., and E. Klinker (1997), Organized convective systems in the tropical western Pacific as a
3378 process in general circulation models: A TOGA COARE case-study, *Quart. J. Roy. Meteor. Soc.*, *123*,
3379 10.1002/qj.49712354002, 805-827.

3380 Moncrieff, M. W., D. E. Waliser, M. J. Miller, M. A. Shapiro, G. R. Asrar, and J. Caughey (2012),
3381 Multiscale Convective Organization and the YOTC Virtual Global Field Campaign, *Bull. Am. Meteorol.*
3382 *Soc.*, *93*, 10.1175/bams-d-11-00233.1, 1171-1187.

3383 Moncrieff, M. W. (2019), Toward a Dynamical Foundation for Organized Convection Parameterization in
3384 GCMs, *Geophys. Res. Lett.* 10.1029/2019gl085316.

3385 Monier, E., B. C. Weare, and W. I. Gustafson (2010), The Madden-Julian oscillation wind-convection
3386 coupling and the role of moisture processes in the MM5 model, *Climate Dyn.*, *35*, 10.1007/s00382-009-
3387 0626-4, 435-447.

3388 Mori, M., and M. Watanabe (2008), The Growth and Triggering Mechanisms of the PNA: A MJO-PNA
3389 Coherence, *Journal of the Meteorological Society of Japan. Ser. II*, *86*, 10.2151/jmsj.86.213, 213-236.

3390 Mori, S., H. Jun-Ichi, Y. I. Tauhid, M. D. Yamanaka, N. Okamoto, F. Murata, N. Sakurai, H. Hashiguchi,
3391 and T. Sribimawati (2004), Diurnal Land-Sea Rainfall Peak Migration over Sumatera Island, Indonesian
3392 Maritime Continent, Observed by TRMM Satellite and Intensive Rawinsonde Soundings, *Mon. Weather*
3393 *Rev.*, *132*, doi:10.1175/1520-0493(2004)132<2021:DLRPMO>2.0.CO;2, 2021-2039.

3394 Morita, J., Y. N. Takayabu, S. Shige, and Y. Kodama (2006), Analysis of rainfall characteristics of the
3395 Madden-Julian oscillation using TRMM satellite data, *Dynamics of Atmospheres and Oceans*, *42*,
3396 <https://doi.org/10.1016/j.dynatmoce.2006.02.002>, 107-126.

3397 Moteki, Q., M. Katsumata, K. Yoneyama, K. Ando, and T. Hasegawa (2018), Drastic thickening of the
3398 barrier layer off the western coast of Sumatra due to the Madden-Julian oscillation passage during the
3399 Pre-Years of the Maritime Continent campaign, *Progress in Earth and Planetary Science*, *5*,
3400 10.1186/s40645-018-0190-9, 35.

3401 Moulin, A. J., J. N. Moum, and E. L. Shroyer (2018), Evolution of Turbulence in the Diurnal Warm Layer,
3402 *J. Phys. Oceanogr.*, *48*, 10.1175/jpo-d-17-0170.1, 383-396.

3403 Moum, J. N., S. P. de Szoeke, W. D. Smyth, J. B. Edson, H. L. DeWitt, A. J. Moulin, E. J. Thompson, C. J.
3404 Zappa, S. A. Rutledge, R. H. Johnson, and C. W. Fairall (2014a), Air-Sea Interactions from Westerly
3405 Wind Bursts during the November 2011 MJO in the Indian Ocean, *Bull. Am. Meteorol.*
3406 *Soc.* 10.1175/BAMS-D-12-00225.1.

3407 Moum, J. N., S. P. d. Szoeke, W. D. Smyth, J. B. Edson, H. L. DeWitt, A. J. Moulin, E. J. Thompson, C. J.
3408 Zappa, S. A. Rutledge, R. H. Johnson, and C. W. Fairall (2014b), Air–Sea Interactions from Westerly
3409 Wind Bursts During the November 2011 MJO in the Indian Ocean, *Bull. Am. Meteorol. Soc.*, *95*,
3410 10.1175/bams-d-12-00225.1, 1185-1199.

3411 Moum, J. N., K. Pujiana, R.-C. Lien, and W. D. Smyth (2016), Ocean feedback to pulses of the Madden–
3412 Julian Oscillation in the equatorial Indian Ocean, *Nature Communications*, *7*, 10.1038/ncomms13203,
3413 13203.

3414 Mundhenk, B. D., E. A. Barnes, E. D. Maloney, and C. F. Baggett (2018), Skillful empirical subseasonal
3415 prediction of landfalling atmospheric river activity using the Madden–Julian oscillation and quasi-
3416 biennial oscillation, *npj Climate and Atmospheric Science*, *1*, 10.1038/s41612-017-0008-2, 20177.

3417 Muraleedharan, P. M., S. Prasanna Kumar, K. Mohana kumar, S. Sijikumar, K. U. Sivakumar, and T.
3418 Mathew (2015), Observational evidence of Mixed Rossby Gravity waves at the central equatorial Indian
3419 Ocean, *Meteorol. Atmos. Phys.*, *127*, 10.1007/s00703-015-0376-2, 407-417.

3420 Nagura, M., and M. J. McPhaden (2012), The dynamics of wind-driven intraseasonal variability in the
3421 equatorial Indian Ocean, *Journal of Geophysical Research: Oceans*, *117*, 10.1029/2011JC007405.

3422 Nakazawa, T. (1988), Tropical Super Clusters within Intraseasonal Variations over the Western Pacific, *J.*
3423 *Meteorol. Soc. Japan*, *66*, 823-839.

3424 NAS (2010), Assessment of Intraseasonal to Interannual Climate Prediction and Predictability. The National
3425 Academies Press, Washington, D.C. ISBN-0-309-15184-8, 192 pages.

3426 NASEM (2016), Next Generation Earth System Prediction: Strategies for Subseasonal to Seasonal Forecasts,
3427 *National Research Council, National Academy of Sciences*, Washington DC, ISBN-978-0-309-38880-1,
3428 290 pages.

3429 Nasuno, T., H. Miura, M. Satoh, A. T. Noda, and K. Oouchi (2009), Multi-scale Organization of Convection
3430 in a Global Numerical Simulation of the December 2006 MJO Event Using Explicit Moist Processes,
3431 *Journal of the Meteorological Society of Japan. Ser. II*, *87*, 10.2151/jmsj.87.335, 335-345.

3432 Naumann, G., and W. M. Vargas (2010), Joint Diagnostic of the Surface Air Temperature in Southern South
3433 America and the Madden–Julian Oscillation, *Weather Forecasting*, *25*, 10.1175/2010waf2222418.1,
3434 1275-1280.

3435 Neale, R., and J. Slingo (2003), The Maritime Continent and Its Role in the Global Climate: A GCM Study,
3436 *J. Clim.*, *16*, 10.1175/1520-0442(2003)016<0834:TMCAIR>2.0.CO;2, 834-848.

3437 Neelin, J. D., and I. M. Held (1987), Modeling Tropical Convergence Based on the Moist Static Energy
3438 Budget, *Mon. Weather Rev.*, *115*, 3-12.

3439 Neelin, J. D., I. M. Held, and K. H. Cook (1987), Evaporation-Wind Feedback and Low-Frequency
3440 Variability in the Tropical Atmosphere, *J. Atmos. Sci.*, *44*, 2341-2348.

3441 Neelin, J. D., and J. Y. Yu (1994), Modes of Tropical Variability under Convective Adjustment and the
3442 Madden-Julian Oscillation .1. Analytical Theory, *J. Atmos. Sci.*, *51*, 1876-1894.

3443 Neena, J. M., J. Y. Lee, D. Waliser, B. Wang, and X. Jiang (2014), Predictability of the Madden-Julian
3444 Oscillation in the Intraseasonal Variability Hindcast Experiment (ISVHE), *J. Clim.*, *27*, 10.1175/JCLI-D-
3445 13-00624.1, 4531-4543.

3446 Nesbitt, S. W., and E. J. Zipser (2003), The Diurnal Cycle of Rainfall and Convective Intensity according to
3447 Three Years of TRMM Measurements, *J. Clim.*, *16*, doi:10.1175/1520-
3448 0442(2003)016<1456:TDCORA>2.0.CO;2, 1456-1475.

3449 Nie, J., and A. H. Sobel (2015), Responses of Tropical Deep Convection to the QBO: Cloud-Resolving
3450 Simulations, *J. Atmos. Sci.*, *72*, doi:10.1175/JAS-D-15-0035.1, 3625-3638.

3451 Nishimoto, E., and S. Yoden (2017), Influence of the Stratospheric Quasi-Biennial Oscillation on the
3452 Madden-Julian Oscillation during Austral Summer, *J. Atmos. Sci.*, *74*, 10.1175/JAS-D-16-0205.1, 1105-
3453 1125.

3454 O'Gorman, P. A., and J. G. Dwyer (2018), Using Machine Learning to Parameterize Moist Convection:
3455 Potential for Modeling of Climate, Climate Change, and Extreme Events, *Journal of Advances in*
3456 *Modeling Earth Systems*, *10*, 10.1029/2018ms001351, 2548-2563.

3457 Oh, J.-H., B.-M. Kim, K.-Y. Kim, H.-J. Song, and G.-H. Lim (2013), The impact of the diurnal cycle on the
3458 MJO over the Maritime Continent: a modeling study assimilating TRMM rain rate into global analysis,
3459 *Climate Dyn.*, *40*, 10.1007/s00382-012-1419-8, 893-911.

3460 Oh, J.-H., X. Jiang, D. E. Waliser, M. W. Moncrieff, and R. H. Johnson (2015a), Convective Momentum
3461 Transport Associated with the Madden-Julian Oscillation Based on a Reanalysis Dataset, *J. Clim.*, *28*,
3462 10.1175/JCLI-D-14-00570.1, 5763-5782.

3463 Oh, J.-H., X. Jiang, D. E. Waliser, M. W. Moncrieff, R. H. Johnson, and P. Ciesielski (2015b), A
3464 Momentum Budget Analysis of Westerly Wind Events Associated with the Madden-Julian Oscillation
3465 during DYNAMO, *J. Atmos. Sci.*, *72*, 10.1175/JAS-D-15-0044.1, 3780-3799.

3466 Oh, J. H., K. Y. Kim, and G. H. Lim (2012), Impact of MJO on the diurnal cycle of rainfall over the western
3467 Maritime Continent in the austral summer, *Climate Dyn.*, *38*, DOI 10.1007/s00382-011-1237-4, 1167-
3468 1180.

3469 Oliver, E. C. J., and K. R. Thompson (2012), A Reconstruction of Madden-Julian Oscillation Variability
3470 from 1905 to 2008, *J. Clim.*, *25*, 10.1175/jcli-d-11-00154.1, 1996-2019.

3471 Palmer, T., R. Buizza, F. Doblas-Reyes, T. Jung, M. Leutbecher, G. Shutts, M. Steinheimer, and A.
3472 Weisheimer (2009), Stochastic parametrization and model uncertainty. Tech. Memo. 598, ECMWF,
3473 Reading, UK, edited.

3474 Parishani, H., M. S. Pritchard, C. S. Bretherton, M. C. Wyant, and M. Khairoutdinov (2017), Toward low-
3475 cloud-permitting cloud superparameterization with explicit boundary layer turbulence, *Journal of*
3476 *Advances in Modeling Earth Systems*, *9*, 10.1002/2017ms000968, 1542-1571.

3477 Park, C. K., D. M. Straus, and K. M. Lau (1990), An Evaluation of the Structure of Tropical Intraseasonal
3478 Oscillations in 3 General-Circulation Models, *J. Meteorol. Soc. Japan*, *68*, 403-417.

3479 Park, S. (2014), A Unified Convection Scheme (UNICON). Part I: Formulation, *J. Atmos. Sci.*, *71*,
3480 10.1175/jas-d-13-0233.1, 3902-3930.

3481 Park, T.-W., C.-H. Ho, S. Yang, and J.-H. Jeong (2010), Influences of Arctic Oscillation and Madden-Julian
3482 Oscillation on cold surges and heavy snowfalls over Korea: A case study for the winter of 2009–2010,
3483 *Journal of Geophysical Research: Atmospheres*, *115*, 10.1029/2010JD014794, D23122.

3484 Peatman, S. C., A. J. Matthews, and D. P. Stevens (2014), Propagation of the Madden–Julian Oscillation
3485 through the Maritime Continent and scale interaction with the diurnal cycle of precipitation, *Quart. J.*
3486 *Roy. Meteor. Soc.*, *140*, 10.1002/qj.2161, 814-825.

3487 Peatman, S. C., A. J. Matthews, and D. P. Stevens (2015), Propagation of the Madden–Julian Oscillation and
3488 scale interaction with the diurnal cycle in a high-resolution GCM, *Climate Dyn.*, *45*, 10.1007/s00382-
3489 015-2513-5, 2901-2918.

3490 Pegion, K., and B. P. Kirtman (2008), The Impact of Air–Sea Interactions on the Simulation of Tropical
3491 Intraseasonal Variability, *J. Clim.*, *21*, 10.1175/2008jcli2180.1, 6616-6635.

3492 Pegion, K., B. P. Kirtman, E. Becker, D. C. Collins, E. LaJoie, R. Burgman, R. Bell, T. DelSole, D. Min, Y.
3493 Zhu, W. Li, E. Sinsky, H. Guan, J. Gottschalek, E. J. Metzger, N. P. Barton, D. Achuthavarier, J.
3494 Marshak, R. D. Koster, H. Lin, N. Gagnon, M. Bell, M. K. Tippett, A. W. Robertson, S. Sun, S. G.
3495 Benjamin, B. W. Green, R. Bleck, and H. Kim (2019), The Subseasonal Experiment (SubX): A
3496 Multimodel Subseasonal Prediction Experiment, *Bull. Am. Meteorol. Soc.*, *100*, 10.1175/bams-d-18-
3497 0270.1, 2043-2060.

3498 Pei, S., T. Shinoda, A. Soloviev, and R.-C. Lien (2018), Upper Ocean Response to the Atmospheric Cold
3499 Pools Associated With the Madden-Julian Oscillation, *Geophys. Res. Lett.*, *45*, 10.1029/2018GL077825,
3500 5020-5029.

3501 Petch, J., D. Waliser, X. Jiang, P. Xavier, and S. Woolnough (2011), A global model inter-comparison of the
3502 physical processes associated with the MJO, *GEWEX News*, August. .

3503 Peters, K., T. Crueger, C. Jakob, and B. Möbis (2017), Improved MJO-simulation in ECHAM6.3 by
3504 coupling a Stochastic Multicloud Model to the convection scheme, *Journal of Advances in Modeling*
3505 *Earth Systems*, *9*, 10.1002/2016MS000809, 193-219.

3506 Peters, O., and J. D. Neelin (2006), Critical phenomena in atmospheric precipitation, *Nat Phys*, *2*, 393-396.

3507 Pohl, B., and A. J. Matthews (2007), Observed Changes in the Lifetime and Amplitude of the Madden–
3508 Julian Oscillation Associated with Interannual ENSO Sea Surface Temperature Anomalies, *J. Clim.*, *20*,
3509 10.1175/jcli4230.1, 2659-2674.

3510 Powell, S. W., and R. A. Houze (2013), The cloud population and onset of the Madden-Julian Oscillation
3511 over the Indian Ocean during DYNAMO-AMIE, *Journal of Geophysical Research: Atmospheres*, *118*,
3512 10.1002/2013JD020421, 2013JD020421.

3513 Powell, S. W., and R. A. Houze (2015), Effect of dry large-scale vertical motions on initial MJO convective
3514 onset, *Journal of Geophysical Research: Atmospheres*, *120*, 10.1002/2014JD022961, 4783-4805.

3515 Pritchard, M. S., and C. S. Bretherton (2014), Causal Evidence that Rotational Moisture Advection is
3516 Critical to the Superparameterized Madden–Julian Oscillation, *J. Atmos. Sci.*, *71*, 10.1175/JAS-D-13-
3517 0119.1, 800-815.

3518 Pritchard, M. S., and D. Yang (2016), Response of the Superparameterized Madden–Julian Oscillation to
3519 Extreme Climate and Basic-State Variation Challenges a Moisture Mode View, *J. Clim.*, *29*, 10.1175/jcli-
3520 d-15-0790.1, 4995-5008.

3521 Pujiana, K., J. N. Moum, W. D. Smyth, and S. J. Warner (2015), Distinguishing ichthyogenic turbulence
3522 from geophysical turbulence, *Journal of Geophysical Research: Oceans*, *120*, 10.1002/2014JC010659,
3523 3792-3804.

3524 Pujiana, K., J. N. Moum, and W. D. Smyth (2018), The Role of Turbulence in Redistributing Upper-Ocean
3525 Heat, Freshwater, and Momentum in Response to the MJO in the Equatorial Indian Ocean, *J. Phys.*
3526 *Oceanogr.*, *48*, 10.1175/jpo-d-17-0146.1, 197-220.

3527 Puy, M., J. Vialard, M. Lengaigne, and E. Guilyardi (2016), Modulation of equatorial Pacific
3528 westerly/easterly wind events by the Madden–Julian oscillation and convectively-coupled Rossby waves,
3529 *Climate Dyn.*, *46*, 10.1007/s00382-015-2695-x, 2155-2178.

3530 Qian, J.-H. (2008), Why Precipitation Is Mostly Concentrated over Islands in the Maritime Continent, *J.*
3531 *Atmos. Sci.*, *65*, doi:10.1175/2007JAS2422.1, 1428-1441.

3532 Ramage, C. S. (1968), ROLE OF A TROPICAL “MARITIME CONTINENT” IN THE ATMOSPHERIC
3533 CIRCULATION, *Mon. Weather Rev.*, *96*, doi:10.1175/1520-0493(1968)096<0365:ROATMC>2.0.CO;2,
3534 365-370.

3535 Randall, D., M. Khairoutdinov, A. Arakawa, and W. Grabowski (2003), Breaking the Cloud
3536 Parameterization Deadlock, *Bull. Am. Meteorol. Soc.*, *84*, 10.1175/BAMS-84-11-1547, 1547-1564.

3537 Rashid, H. A., H. H. Hendon, M. C. Wheeler, and O. Alves (2011), Prediction of the Madden-Julian
3538 oscillation with the POAMA dynamical prediction system, *Climate Dyn.*, *36*, 10.1007/s00382-010-0754-
3539 x, 649-661.

3540 Rasp, S., M. S. Pritchard, and P. Gentine (2018), Deep learning to represent subgrid processes in climate
3541 models, *Proceedings of the National Academy of Sciences*, *115*, 10.1073/pnas.1810286115, 9684-9689.

3542 Rauniyar, S. P., and K. J. E. Walsh (2011), Scale Interaction of the Diurnal Cycle of Rainfall over the
3543 Maritime Continent and Australia: Influence of the MJO, *J. Clim.*, *24*, doi:10.1175/2010JCLI3673.1, 325-
3544 348.

3545 Rauniyar, S. P., and K. J. E. Walsh (2013), Influence of ENSO on the Diurnal Cycle of Rainfall over the
3546 Maritime Continent and Australia, *J. Clim.*, *26*, 10.1175/jcli-d-12-00124.1, 1304-1321.

3547 Ray, P., and C. Zhang (2010), A Case Study of the Mechanics of Extratropical Influence on the Initiation of
3548 the Madden–Julian Oscillation, *J. Atmos. Sci.*, *67*, 10.1175/2009jas3059.1, 515-528.

3549 Ray, P., and T. Li (2013), Relative Roles of Circumnavigating Waves and Extratropics on the MJO and Its
3550 Relationship with the Mean State, *J. Atmos. Sci.*, *70*, 10.1175/jas-d-12-0153.1, 876-893.

3551 Raymond, D. J. (1995), Regulation of Moist Convection over the West Pacific Warm Pool, *J. Atmos. Sci.*,
3552 *52*, 3945-3959.

3553 Raymond, D. J. (2001), A new model of the Madden-Julian oscillation, *J. Atmos. Sci.*, *58*, 2807-2819.

3554 Raymond, D. J., and Ž. Fuchs (2009), Moisture Modes and the Madden–Julian Oscillation, *J. Clim.*, *22*,
3555 10.1175/2008jcli2739.1, 3031-3046.

3556 Raymond, D. J., S. Sessions, A. Sobel, and Z. Fuchs (2009), The Mechanics of Gross Moist Stability,
3557 *Journal of Advances in Modeling Earth Systems*, *1*, 10.3894/james.2009.1.9, 20 pp.

3558 Reed, R. J., W. J. Campbell, L. A. Rasmussen, and D. G. Rogers (1961), Evidence of a downward-
3559 propagating, annual wind reversal in the equatorial stratosphere, *Journal of Geophysical Research (1896-
3560 1977)*, *66*, 10.1029/JZ066i003p00813, 813-818.

3561 Riley Dellaripa, E. M., and E. Maloney (2015), Riley Dellaripa, E. M., and E. D. Maloney, 2014: Analysis
3562 of MJO Wind-Flux Feedbacks in the Indian Ocean Using RAMA Buoy Observations. *J. Meteor. Soc.
3563 Japan*, doi:10.2151/jmsj.2015-021.

3564 Riley, E. M., B. E. Mapes, and S. N. Tulich (2011), Clouds Associated with the Madden–Julian Oscillation:
3565 A New Perspective from CloudSat, *J. Atmos. Sci.*, *68*, 10.1175/JAS-D-11-030.1, 3032-3051.

3566 Rostami, M., and V. Zeitlin (2019), Eastward-moving convection-enhanced modons in shallow water in the
3567 equatorial tangent plane, *Physics of Fluids*, *31*, 10.1063/1.5080415, 021701.

3568 Roundy, P. E., K. MacRitchie, J. Asuma, and T. Melino (2010), Modulation of the Global Atmospheric
3569 Circulation by Combined Activity in the Madden–Julian Oscillation and the El Niño–Southern
3570 Oscillation during Boreal Winter, *J. Clim.*, *23*, 10.1175/2010JCLI3446.1, 4045-4059.

3571 Rowe, A. K., and R. A. Houze (2015), Cloud organization and growth during the transition from suppressed
3572 to active MJO conditions, *Journal of Geophysical Research: Atmospheres*, *120*, 10.1002/2014JD022948,
3573 10,324-310,350.

3574 Ruppert, J. H., and R. H. Johnson (2015), Diurnally Modulated Cumulus Moistening in the Pre-Onset Stage
3575 of the Madden–Julian Oscillation during DYNAMO, *J. Atmos. Sci.* 10.1175/JAS-D-14-0218.1.

3576 Rushley, S. S., D. Kim, C. S. Bretherton, and M. S. Ahn (2018), Reexamining the Nonlinear Moisture -
3577 Precipitation Relationship Over the Tropical Oceans, *Geophys. Res. Lett.*, *45*,
3578 doi:10.1002/2017GL076296, 1133-1140.

3579 Rushley, S. S., D. Kim, and Á. F. Adames (2019), Changes in the MJO under Greenhouse Gas-Induced
3580 Warming in CMIP5 Models, *J. Clim.*, *32*, 10.1175/jcli-d-18-0437.1, 803-821.

3581 Rydbeck, A. V., and T. G. Jensen (2017), Oceanic Impetus for Convective Onset of the Madden-Julian
3582 Oscillation in the Western Indian Ocean, *J. Clim.*, *30*, 10.1175/jcli-d-16-0595.1, 4299-4316.

3583 Sakaeda, N., G. Kiladis, and J. Dias (2017), The Diurnal Cycle of Tropical Cloudiness and Rainfall
3584 Associated with the Madden-Julian Oscillation, *J. Clim.*, *30*, 10.1175/jcli-d-16-0788.1, 3999-4020.

3585 Salby, M. L., and H. H. Hendon (1994), Intraseasonal Behavior of Clouds, Temperature, and Motion in the
3586 Tropics, *J. Atmos. Sci.*, *51*, 2207-2224.

3587 Salby, M. L., H. H. Hendon, and R. R. Garcia (1994), Planetary-Scale Circulations in the Presence of
3588 Climatological and Wave-Induced Heating, *J. Atmos. Sci.*, *51*, 3365-3365.

3589 Sardeshmukh, P. D., and B. J. Hoskins (1988), The Generation of Global Rotational Flow by Steady
3590 Idealized Tropical Divergence, *J. Atmos. Sci.*, *45*, 10.1175/1520-0469(1988)045<1228:Tgogrf>2.0.Co;2,
3591 1228-1251.

3592 Schneider, T., J. Teixeira, C. S. Bretherton, F. Brient, K. G. Pressel, C. Schär, and A. P. Siebesma (2017),
3593 Climate goals and computing the future of clouds, *Nature Climate Change*, *7*, 10.1038/nclimate3190, 3-5.

3594 Schubert, J. J., B. Stevens, and T. Crueger (2013), Madden-Julian oscillation as simulated by the MPI Earth
3595 System Model: Over the last and into the next millennium, *Journal of Advances in Modeling Earth*
3596 *Systems*, *5*, 10.1029/2012MS000180, 71-84.

3597 Schwartz, M. J., D. E. Waliser, B. Tian, D. L. Wu, J. H. Jiang, and W. G. Read (2008), Characterization of
3598 MJO-related upper tropospheric hydrological processes using MLS, *Geophys. Res. Lett.*, *35*, Doi
3599 10.1029/2008gl033675.

3600 Seo, H., A. C. Subramanian, A. J. Miller, and N. R. Cavanaugh (2014), Coupled Impacts of the Diurnal
3601 Cycle of Sea Surface Temperature on the Madden-Julian Oscillation, *J. Clim.*, *27*, 10.1175/jcli-d-14-
3602 00141.1, 8422-8443.

3603 Seo, K.-H., W. Wang, J. Gottschalck, Q. Zhang, J.-K. E. Schemm, W. R. Higgins, and A. Kumar (2009),
3604 Evaluation of MJO Forecast Skill from Several Statistical and Dynamical Forecast Models, *J. Clim.*, *22*,
3605 doi:10.1175/2008JCLI2421.1, 2372-2388.

3606 Seo, K.-H., H.-J. Lee, and D. M. W. Frierson (2016), Unraveling the Teleconnection Mechanisms that
3607 Induce Wintertime Temperature Anomalies over the Northern Hemisphere Continents in Response to the
3608 MJO, *J. Atmos. Sci.*, *73*, 10.1175/JAS-D-16-0036.1, 3557-3571.

3609 Seo, K.-H., and H.-J. Lee (2017), Mechanisms for a PNA-Like Teleconnection Pattern in Response to the
3610 MJO, *J. Atmos. Sci.*, *74*, 10.1175/jas-d-16-0343.1, 1767-1781.

3611 Seo, K. H., and K. Y. Kim (2003), Propagation and initiation mechanisms of the Madden-Julian oscillation,
3612 *J. Geophys. Res.*, *108*, Doi 10.1029/2002jd002876, -.

3613 Seo, K. H., and W. Q. Wang (2010), The Madden-Julian Oscillation Simulated in the NCEP Climate
3614 Forecast System Model: The Importance of Stratiform Heating, *J. Clim.*, *23*, Doi 10.1175/2010jcli2983.1,
3615 4770-4793.

3616 Seo, K. H., and S. W. Son (2012), The Global Atmospheric Circulation Response to Tropical Diabatic
3617 Heating Associated with the Madden-Julian Oscillation during Northern Winter, *J. Atmos. Sci.*, *69*, Doi
3618 10.1175/2011jas3686.1, 79-96.

3619 Shi, X., D. Kim, Á. F. Adames-Corraliza, and J. Sukhatme (2018), WISHE-moisture mode in an aquaplanet
3620 simulation, *Journal of Advances in Modeling Earth Systems*, *0*, 10.1029/2018MS001441.

3621 Shinoda, T., H. H. Hendon, and J. Glick (1998), Intraseasonal Variability of Surface Fluxes and Sea Surface
3622 Temperature in the Tropical Western Pacific and Indian Oceans, *J. Clim.*, *11*, 10.1175/1520-
3623 0442(1998)011<1685:Ivosfa>2.0.Co;2, 1685-1702.

3624 Shinoda, T., W. Han, L. Zamudio, R.-C. Lien, and M. Katsumata (2017), Remote Ocean Response to the
3625 Madden–Julian Oscillation during the DYNAMO Field Campaign: Impact on Somali Current System and
3626 the Seychelles–Chagos Thermocline Ridge, *Atmosphere*, *8*, 171.

3627 Short, D. A., and K. Nakamura (2000), TRMM radar observations of shallow precipitation over the tropical
3628 oceans, *J. Clim.*, *13*, 4107-4124.

3629 Simmons, A. J., J. M. Wallace, and G. W. Branstator (1983), Barotropic Wave Propagation and Instability,
3630 and Atmospheric Teleconnection Patterns, *J. Atmos. Sci.*, *40*, 10.1175/1520-
3631 0469(1983)040<1363:Bwpaia>2.0.Co;2, 1363-1392.

3632 Skofronick-Jackson, G., D. Kirschbaum, W. Petersen, G. Huffman, C. Kidd, E. Stocker, and R. Kakar
3633 (2018), The Global Precipitation Measurement (GPM) mission's scientific achievements and societal
3634 contributions: reviewing four years of advanced rain and snow observations, *Quart. J. Roy. Meteor. Soc.*,
3635 *144*, 10.1002/qj.3313, 27-48.

3636 Slingo, J., P. Inness, R. Neale, S. Woolnough, and G. Y. Yang (2003), Scale interactions on diurnal to
3637 seasonal timescales and their relevance to model systematic errors, *Annals of Geophysics*, *46*, 139-155.

3638 Slingo, J. M., K. R. Sperber, J. S. Boyle, J. P. Ceron, M. Dix, B. Dugas, W. Ebisuzaki, J. Fyfe, D. Gregory,
3639 J. F. Gueremy, J. Hack, A. Harzallah, P. Inness, A. Kitoh, W. K. M. Lau, B. McAvaney, R. Madden, A.
3640 Matthews, T. N. Palmer, C. K. Park, D. Randall, and N. Renno (1996), Intraseasonal oscillations in 15
3641 atmospheric general circulation models: Results from an AMIP diagnostic subproject, *Climate Dyn.*, *12*,
3642 325-357.

3643 Slingo, J. M., D. P. Rowell, K. R. Sperber, and F. Nortley (1999), On the predictability of the interannual
3644 behaviour of the Madden-Julian oscillation and its relationship with el Niño, *Quart. J. Roy. Meteor. Soc.*,
3645 *125*, 10.1002/qj.49712555411, 583-609.

3646 Sobel, A., and E. Maloney (2012), An Idealized Semi-Empirical Framework for Modeling the Madden–
3647 Julian Oscillation, *J. Atmos. Sci.*, *69*, 10.1175/jas-d-11-0118.1, 1691-1705.

3648 Sobel, A., and E. Maloney (2013), Moisture Modes and the Eastward Propagation of the MJO, *J. Atmos.*
3649 *Sci.*, *70*, Doi 10.1175/Jas-D-12-0189.1, 187-192.

3650 Sobel, A., S. Wang, and D. Kim (2014), Moist Static Energy Budget of the MJO during DYNAMO, *J.*
3651 *Atmos. Sci.*, *71*, 10.1175/JAS-D-14-0052.1, 4276-4291.

3652 Sobel, A. H., J. Nilsson, and L. M. Polvani (2001), The weak temperature gradient approximation and
3653 balanced tropical moisture waves, *J. Atmos. Sci.*, *58*, 3650-3665.

3654 Sobel, A. H., and H. Gildor (2003), A simple time-dependent model of SST hot spots, *J. Clim.*, *16*, 3978-
3655 3992.

3656 Sobel, A. H., E. D. Maloney, G. Bellon, and D. M. Frierson (2008), The role of surface heat fluxes in
3657 tropical intraseasonal oscillations, *Nature Geoscience*, *1*, Doi 10.1038/Ngeo312, 653-657.

3658 Sobel, A. H., E. D. Maloney, G. Bellon, and D. M. Frierson (2010), Surface Fluxes and Tropical
3659 Intraseasonal Variability: a Reassessment, *Journal of Advances in Modeling Earth Systems*, *2*,
3660 10.3894/JAMES.2010.2.2, 2.

3661 Son, S.-W., Y. Lim, C. Yoo, H. H. Hendon, and J. Kim (2016), Stratospheric Control of the Madden–Julian
3662 Oscillation, *J. Clim.*, *30*, 10.1175/JCLI-D-16-0620.1, 1909-1922.

3663 Son, S.-W., Y. Lim, C. Yoo, H. H. Hendon, and J. Kim (2017), Stratospheric Control of the Madden–Julian
3664 Oscillation, *J. Clim.*, *30*, 10.1175/jcli-d-16-0620.1, 1909-1922.

3665 Song, E.-J., and K.-H. Seo (2016), Past- and present-day Madden-Julian Oscillation in CNRM-CM5,
3666 *Geophys. Res. Lett.*, *43*, 10.1002/2016GL068771, 4042-4048.

3667 Sperber, K., J. Slingo, and P. Inness (2012), Modeling intraseasonal variability, in *Intraseasonal Variability*
3668 *in the Atmosphere-Ocean Climate System*, edited by W. K. M. Lau and D. E. Waliser, Springer,
3669 Heidelberg, Germany.

3670 Sperber, K. R. (2003), Propagation and the vertical structure of the Madden-Julian oscillation, *Mon. Weather*
3671 *Rev.*, *131*, 3018-3037.

3672 Sprintall, J., and M. Tomczak (1992), Evidence of the barrier layer in the surface layer of the tropics,
3673 *Journal of Geophysical Research: Oceans*, *97*, 10.1029/92JC00407, 7305-7316.

3674 Stan, C., D. M. Straus, J. S. Frederiksen, H. Lin, E. D. Maloney, and C. Schumacher (2017), Review of
3675 Tropical-Extratropical Teleconnections on Intraseasonal Time Scales, *Rev. Geophys.*, *55*,
3676 10.1002/2016RG000538, 902-937.

3677 Stephens, G. L., P. J. Webster, R. H. Johnson, R. Engelen, and T. L'Ecuyer (2004), Observational evidence
3678 for the mutual regulation of the tropical hydrological cycle and tropical sea surface temperatures, *J.*
3679 *Clim.*, *17*, 2213-2224.

3680 Stevens, B. (2002), Entrainment in stratocumulus-topped mixed layers, *Quart. J. Roy. Meteor. Soc.*, *128*,
3681 10.1256/qj.01.202, 2663-2690.

3682 Stolz, D. C., S. A. Rutledge, W. Xu, and J. R. Pierce (2017), Interactions between the MJO, Aerosols, and
3683 Convection over the Central Indian Ocean, *J. Atmos. Sci.*, *74*, 10.1175/jas-d-16-0054.1, 353-374.

3684 Straub, K. H., and G. N. Kiladis (2003), The observed structure of convectively coupled Kelvin waves:
3685 Comparison with simple models of coupled wave instability, *J. Atmos. Sci.*, *60*, 1655-1668.

3686 Straub, K. H. (2013), MJO Initiation in the Real-Time Multivariate MJO Index, *J. Clim.*, *26*, 10.1175/JCLI-
3687 D-12-00074.1, 1130-1151.

3688 Subramanian, A., M. Jochum, A. J. Miller, R. Neale, H. Seo, D. Waliser, and R. Murtugudde (2014), The
3689 MJO and global warming: a study in CCSM4, *Climate Dyn.*, *42*, 10.1007/s00382-013-1846-1, 2019-
3690 2031.

3691 Subramanian, A. C., and T. N. Palmer (2017), Ensemble superparameterization versus stochastic
3692 parameterization: A comparison of model uncertainty representation in tropical weather prediction,
3693 *Journal of Advances in Modeling Earth Systems*, *9*, 10.1002/2016MS000857, 1231-1250.

3694 Sui, C.-H., and K.-M. Lau (1992), Multiscale Phenomena in the Tropical Atmosphere over the Western
3695 Pacific, *Mon. Weather Rev.*, *120*, 10.1175/1520-0493(1992)120<0407:Mpitta>2.0.Co;2, 407-430.

3696 Sultan, B., S. Janicot, and A. Diedhiou (2003), The West African monsoon dynamics. Part I: Documentation
3697 of intraseasonal variability, *J. Clim.*, *16*, 3389-3406.

3698 Takahashi, C., N. Sato, A. Seiki, K. Yoneyama, and R. Shirooka (2011), Projected Future Change of MJO
3699 and its Extratropical Teleconnection in East Asia during the Northern Winter Simulated in IPCC AR4
3700 Models, *SOLA*, *7*, 10.2151/sola.2011-051, 201-204.

3701 Takasuka, D., M. Satoh, and S. Yokoi (2019), Observational Evidence of Mixed Rossby-Gravity Waves as a
3702 Driving Force for the MJO Convective Initiation and Propagation, *Geophys. Res. Lett.*, *46*,
3703 10.1029/2019GL083108, 5546-5555.

3704 Takayabu, Y. N. (1994), Large-Scale Cloud Disturbances Associated with Equatorial Waves .2. Westward-
3705 Propagating Inertio-Gravity Waves, *J. Meteorol. Soc. Japan*, *72*, 451-465.

3706 Takayabu, Y. N., T. Iguchi, M. Kachi, A. Shibata, and H. Kanzawa (1999), Abrupt termination of the 1997-
3707 98 El Nino in response to a Madden-Julian oscillation, *Nature*, *402*, 279-282.

3708 Tao, L., J. Zhao, and T. Li (2015), Trend analysis of tropical intraseasonal oscillations in the summer and
3709 winter during 1982–2009, *International Journal of Climatology*, *35*, 10.1002/joc.4258, 3969-3978.

3710 Tao, W.-K., E. A. Smith, R. F. Adler, Z. S. Haddad, A. Y. Hou, T. Iguchi, R. Kakar, T. N. Krishnamurti, C.
3711 D. Kummerow, S. Lang, R. Meneghini, K. Nakamura, T. Nakazawa, K. Okamoto, W. S. Olson, S. Satoh,
3712 S. Shige, J. Simpson, Y. Takayabu, G. J. Tripoli, and S. Yang (2006), Retrieval of Latent Heating from
3713 TRMM Measurements, *Bull. Am. Meteorol. Soc.*, *87*, 1555-1572.

3714 Tao, W.-K., Y. N. Takayabu, S. Lang, S. Shige, W. Olson, A. Hou, G. Skofronick-Jackson, X. Jiang, C.
3715 Zhang, W. Lau, T. Krishnamurti, D. Waliser, M. Grecu, P. E. Ciesielski, R. H. Johnson, R. Houze, R.
3716 Kakar, K. Nakamura, S. Braun, S. Hagos, R. Oki, and A. Bhardwaj (2016), TRMM Latent Heating
3717 Retrieval: Applications and Comparisons with Field Campaigns and Large-Scale Analyses,
3718 *Meteorological Monographs*, 56, doi:10.1175/AMSMONOGRAPHS-D-15-0013.1, 2.1-2.34.

3719 Teng, H. Y., and B. Wang (2003), Interannual variations of the boreal summer intraseasonal oscillation in
3720 the Asian-Pacific region, *J. Clim.*, 16, 3572-3584.

3721 Thayer-Calder, K., and D. A. Randall (2009), The Role of Convective Moistening in the Madden-Julian
3722 Oscillation, *J. Atmos. Sci.*, 66, Doi 10.1175/2009jas3081.1, 3297-3312.

3723 Thompson, D. W. J., and J. M. Wallace (1998), The Arctic oscillation signature in the wintertime
3724 geopotential height and temperature fields, *Geophys. Res. Lett.*, 25, 10.1029/98GL00950, 1297-1300.

3725 Thompson, D. W. J., and J. M. Wallace (2000), Annular modes in the extratropical circulation. Part I:
3726 Month-to-month variability, *J. Clim.*, 13, 1000-1016.

3727 Thompson, E. J., S. A. Rutledge, B. Dolan, and M. Thurai (2015), Drop Size Distributions and Radar
3728 Observations of Convective and Stratiform Rain over the Equatorial Indian and West Pacific Oceans, *J.*
3729 *Atmos. Sci.*, 72, 10.1175/jas-d-14-0206.1, 4091-4125.

3730 Thomson, J., and J. Girton (2017), Sustained Measurements of Southern Ocean Air-Sea Coupling from a
3731 Wave Glider Autonomous Surface Vehicle, *Oceanography*, 30, 10.5670/oceanog.2017.228, 104-109.

3732 Thual, S., A. J. Majda, and S. N. Stechmann (2014), A Stochastic Skeleton Model for the MJO, *J. Atmos.*
3733 *Sci.*, 71, 10.1175/JAS-D-13-0186.1, 697-715.

3734 Tian, B., Y. L. Yung, D. E. Waliser, T. Tyranowski, L. Kuai, E. J. Fetzer, and F. W. Irion (2007),
3735 Intraseasonal variations of the tropical total ozone and their connection to the Madden-Julian Oscillation,
3736 *Geophys. Res. Lett.*, 34, 10.1029/2007GL029451.

3737 Tian, B., D. E. Waliser, E. J. Fetzer, and Y. L. Yung (2010), Vertical Moist Thermodynamic Structure of the
3738 Madden-Julian Oscillation in Atmospheric Infrared Sounder Retrievals: An Update and a Comparison to
3739 ECMWF Interim Re-Analysis, *Mon. Weather Rev.*, 138, doi:10.1175/2010MWR3486.1, 4576-4582.

3740 Tian, B., D. E. Waliser, R. A. Kahn, and S. Wong (2011), Modulation of Atlantic aerosols by the Madden-
3741 Julian Oscillation, *Journal of Geophysical Research: Atmospheres*, 116, 10.1029/2010JD015201.

3742 Tian, B., C. O. Ao, D. E. Waliser, E. J. Fetzer, A. J. Mannucci, and J. Teixeira (2012), Intraseasonal
3743 temperature variability in the upper troposphere and lower stratosphere from the GPS radio occultation
3744 measurements, *Journal of Geophysical Research: Atmospheres*, 117, 10.1029/2012JD017715.

3745 Tian, B. J., D. E. Waliser, and E. J. Fetzer (2006a), Modulation of the diurnal cycle of tropical deep
3746 convective clouds by the MJO, *Geophys. Res. Lett.*, 33, Doi 10.1029/2006gl027752.

3747 Tian, B. J., D. E. Waliser, E. J. Fetzer, B. H. Lambrigtsen, Y. L. Yung, and B. Wang (2006b), Vertical moist
3748 thermodynamic structure and spatial-temporal evolution of the MJO in AIRS observations, *J. Atmos. Sci.*,
3749 *63*, 2462-2485.

3750 Ting, M., and P. D. Sardeshmukh (1993), Factors Determining the Extratropical Response to Equatorial
3751 Diabatic Heating Anomalies, *J. Atmos. Sci.*, *50*, 10.1175/1520-0469(1993)050<0907:Fdtert>2.0.Co;2,
3752 907-918.

3753 Tippet, M. K. (2018), Robustness of Relations between the MJO and U.S. Tornado Occurrence, *Mon.*
3754 *Weather Rev.*, *146*, 10.1175/mwr-d-18-0207.1, 3873-3884.

3755 Tokioka, T., K. Yamazaki, A. Kitoh, and T. Ose (1988), The Equatorial 30-60 Day Oscillation and the
3756 Arakawa-Schubert Penetrative Cumulus Parameterization, *J. Meteorol. Soc. Japan*, *66*, 883-901.

3757 Toms, B. A., E. A. Barnes, E. D. Maloney, and S. C. van den Heever (2020), The Global Teleconnection
3758 Signature of the Madden-Julian Oscillation and Its Modulation by the Quasi-Biennial Oscillation, *Journal*
3759 *of Geophysical Research: Atmospheres*, *125*, 10.1029/2020JD032653, e2020JD032653.

3760 Tromeur, E., and W. B. Rossow (2010), Interaction of Tropical Deep Convection with the Large-Scale
3761 Circulation in the MJO, *J. Clim.*, *23*, Doi 10.1175/2009jcli3240.1, 1837-1853.

3762 Tseng, K.-C., E. Maloney, and E. Barnes (2019), The Consistency of MJO Teleconnection Patterns: An
3763 Explanation Using Linear Rossby Wave Theory, *J. Clim.*, *32*, 10.1175/jcli-d-18-0211.1, 531-548.

3764 Tseng, W.-L., H.-H. Hsu, N. Keenlyside, C.-W. J. Chang, B.-J. Tsuang, C.-Y. Tu, and L.-C. Jiang (2017),
3765 Effects of Surface Orography and Land–Sea Contrast on the Madden–Julian Oscillation in the Maritime
3766 Continent: A Numerical Study Using ECHAM5-SIT, *J. Clim.*, *30*, 10.1175/jcli-d-17-0051.1, 9725-9741.

3767 Tung, W. W., and M. Yanai (2002a), Convective momentum transport observed during the TOGA COARE
3768 IOP. Part II: Case studies, *J. Atmos. Sci.*, *59*, 2535-2549.

3769 Tung, W. W., and M. Yanai (2002b), Convective momentum transport observed during the TOGA COARE
3770 IOP. Part I: General features, *J. Atmos. Sci.*, *59*, 1857-1871.

3771 Vecchi, G. A., and N. A. Bond (2004), The Madden-Julian Oscillation (MJO) and northern high latitude
3772 wintertime surface air temperatures, *Geophys. Res. Lett.*, *31*, L04104, Doi 10.1029/2003gl018645, -.

3773 Virts, K. S., and J. M. Wallace (2010), Annual, Interannual, and Intraseasonal Variability of Tropical
3774 Tropopause Transition Layer Cirrus, *J. Atmos. Sci.*, *67*, doi:10.1175/2010JAS3413.1, 3097-3112.

3775 Virts, K. S., and J. M. Wallace (2014), Observations of Temperature, Wind, Cirrus, and Trace Gases in the
3776 Tropical Tropopause Transition Layer during the MJO, *J. Atmos. Sci.*, *71*, 10.1175/jas-d-13-0178.1,
3777 1143-1157.

3778 Virts, K. S., and R. A. Houze (2015), Variation of Lightning and Convective Rain Fraction in Mesoscale
3779 Convective Systems of the MJO, *J. Atmos. Sci.*, *72*, 10.1175/jas-d-14-0201.1, 1932-1944.

3780 Vitart, F., S. Woolnough, M. A. Balmaseda, and A. M. Tompkins (2007), Monthly forecast of the Madden-
3781 Julian oscillation using a coupled GCM, *Mon. Weather Rev.*, *135*, Doi 10.1175/Mwr3415.1, 2700-2715.

3782 Vitart, F., and T. Jung (2010), Impact of the Northern Hemisphere extratropics on the skill in predicting the
3783 Madden Julian Oscillation, *Geophys. Res. Lett.*, *37*, 10.1029/2010GL045465.

3784 Vitart, F., and F. Molteni (2010), Simulation of the Madden-Julian Oscillation and its teleconnections in the
3785 ECMWF forecast system, *Quart. J. Roy. Meteor. Soc.*, *136*, Doi 10.1002/Qj.623, 842-855.

3786 Vitart, F., A. Robertson, A. Kumar, H. Hendon, Y. Takaya, H. Lin, A. Arribas, J.-Y. Lee, D. Waliser, B.
3787 Kirtman, and H.-K. Kim (2012), Subseasonal To Seasonal Prediction: Research Implementation Plan,
3788 WWRP/THORPEX-WCRP Report.

3789 Vitart, F., A. Robertson, and S2S Steering Group (2015), Sub-seasonal to seasonal prediction: Linking
3790 weather and climate. Seamless Prediction of the Earth System: From Minutes to Months, G. Brunet, S.
3791 Jones, and P. M. Ruti, Eds., WMO-1156, World Meteorological Organization, 385–401. [Available
3792 online at http://library.wmo.int/pmb_ged/wmo_1156_en.pdf.].

3793 Vitart, F. (2017), Madden—Julian Oscillation prediction and teleconnections in the S2S database, *Quart. J.*
3794 *Roy. Meteor. Soc.*, *143*, 10.1002/qj.3079, 2210-2220.

3795 Vitart, F., C. Ardilouze, A. Bonet, A. Brookshaw, M. Chen, C. Codorean, M. Déqué, L. Ferranti, E. Fucile,
3796 M. Fuentes, H. Hendon, J. Hodgson, H.-S. Kang, A. Kumar, H. Lin, G. Liu, X. Liu, P. Malguzzi, I.
3797 Mallas, M. Manoussakis, D. Mastrangelo, C. MacLachlan, P. McLean, A. Minami, R. Mladek, T.
3798 Nakazawa, S. Najm, Y. Nie, M. Rixen, A. W. Robertson, P. Ruti, C. Sun, Y. Takaya, M. Tolstykh, F.
3799 Venuti, D. Waliser, S. Woolnough, T. Wu, D.-J. Won, H. Xiao, R. Zaripov, and L. Zhang (2017), The
3800 Subseasonal to Seasonal (S2S) Prediction Project Database, *Bull. Am. Meteorol. Soc.*, *98*, 10.1175/bams-
3801 d-16-0017.1, 163-173.

3802 Vitart, F., and A. W. Robertson (2018), The sub-seasonal to seasonal prediction project (S2S) and the
3803 prediction of extreme events, *npj Climate and Atmospheric Science*, *1*, 10.1038/s41612-018-0013-0, 3.

3804 Waliser, D., K. Sperber, H. Hendon, D. Kim, M. Wheeler, K. Weickmann, C. Zhang, L. Donner, J.
3805 Gottschalck, W. Higgins, I. S. Kang, D. Legler, M. Moncrieff, F. Vitart, B. Wang, W. Wang, S.
3806 Woolnough, E. Maloney, S. Schubert, W. Stern, and C. M.-J. Oscillation (2009), MJO Simulation
3807 Diagnostics, *J. Clim.*, *22*, Doi 10.1175/2008jcli2731.1, 3006-3030.

3808 Waliser, D. E., W. Stern, S. Schubert, and K. M. Lau (2003), Dynamic predictability of intraseasonal
3809 variability associated with the Asian summer monsoon, *Quart. J. Roy. Meteor. Soc.*, *129*, Doi
3810 10.1256/Qj.02.51, 2897-2925.

3811 Waliser, D. E., R. Murtugudde, P. Strutton, and J.-L. Li (2005), Subseasonal organization of ocean
3812 chlorophyll: Prospects for prediction based on the Madden-Julian Oscillation, *Geophys. Res. Lett.*, *32*,
3813 10.1029/2005GL024300.

3814 Waliser, D. E. (2012), Predictability and Forecasting, in *Intraseasonal Variability in the Atmosphere-Ocean*
3815 *Climate System*, edited by W. K. M. Lau and D. E. Waliser, Springer, Heidelberg, Germany.

3816 Waliser, D. E., M. W. Moncrieff, D. Burridge, A. H. Fink, D. Gochis, B. N. Goswami, B. Guan, P. Harr, J.
3817 Heming, H.-H. Hsu, C. Jakob, M. Janiga, R. Johnson, S. Jones, P. Knippertz, J. Marengo, H. Nguyen, M.
3818 Pope, Y. Serra, C. Thorncroft, M. Wheeler, R. Wood, and S. Yuter (2012), The “Year” of Tropical
3819 Convection (May 2008–April 2010): Climate Variability and Weather Highlights, *Bull. Am. Meteorol.*
3820 *Soc.*, *93*, doi:10.1175/2011BAMS3095.1, 1189-1218.

3821 Wallace, J. M., and D. S. Gutzler (1981), Teleconnections in the Geopotential Height Field during the
3822 Northern Hemisphere Winter, *Mon. Weather Rev.*, *109*, 10.1175/1520-
3823 0493(1981)109<0784:TITGHF>2.0.CO;2, 784-812.

3824 Wang, B. (1988), Dynamics of Tropical Low-Frequency Waves - an Analysis of the Moist Kelvin Wave, *J.*
3825 *Atmos. Sci.*, *45*, 2051-2065.

3826 Wang, B., and H. Rui (1990), Dynamics of the Coupled Moist Kelvin-Rossby Wave on an Equatorial Beta-
3827 Plane, *J. Atmos. Sci.*, *47*, 397-413.

3828 Wang, B., and T. M. Li (1994), Convective Interaction with Boundary-Layer Dynamics in the Development
3829 of a Tropical Intraseasonal System, *J. Atmos. Sci.*, *51*, 1386-1400.

3830 Wang, B., and X. S. Xie (1998), Coupled modes of the warm pool climate system. Part 1: The role of air-sea
3831 interaction in maintaining Madden-Julian oscillation, *J. Clim.*, *11*, 2116-2135.

3832 Wang, B. (2006), *The Asian Monsoon*, Springer, Heidelberg, Germany.

3833 Wang, B., and F. Liu (2011), A Model for Scale Interaction in the Madden–Julian Oscillation, *J. Atmos. Sci.*,
3834 *68*, 10.1175/2011jas3660.1, 2524-2536.

3835 Wang, B., F. Liu, and G. Chen (2016a), A trio-interaction theory for Madden–Julian oscillation, *Geoscience*
3836 *Letters*, *3*, 10.1186/s40562-016-0066-z, 34.

3837 Wang, B., and S.-S. Lee (2017), MJO Propagation Shaped by Zonal Asymmetric Structures: Results from 24
3838 GCM Simulations, *J Clim*, *30*, 10.1175/jcli-d-16-0873.1, 7933-7952.

3839 Wang, B., S.-S. Lee, D. E. Waliser, C. Zhang, A. Sobel, E. Maloney, T. Li, X. Jiang, and K.-J. Ha (2018a),
3840 Dynamics-Oriented Diagnostics for the Madden–Julian Oscillation, *J. Clim.*, *31*, 10.1175/jcli-d-17-
3841 0332.1, 3117-3135.

3842 Wang, B., G. Chen, and F. Liu (2019a), Diversity of the Madden-Julian Oscillation, *Science Advances*, *5*,
3843 10.1126/sciadv.aax0220, eaax0220.

3844 Wang, D., J.-I. Yano, and Y. Lin (2019b), Madden–Julian Oscillations Seen in the Upper-Troposphere
3845 Vorticity Field: Interactions with Rossby Wave Trains, *J. Atmos. Sci.*, *76*, 10.1175/JAS-D-18-0172.1,
3846 1785-1807.

3847 Wang, J., H.-M. Kim, E. K. M. Chang, and S.-W. Son (2018b), Modulation of the MJO and North Pacific
3848 Storm Track Relationship by the QBO, *Journal of Geophysical Research: Atmospheres*, *123*,
3849 10.1029/2017JD027977, 3976-3992.

3850 Wang, L., T. Li, E. Maloney, and B. Wang (2017), Fundamental Causes of Propagating and Nonpropagating
3851 MJOs in MJOTF/GASS Models, *J. Clim.*, *30*, 10.1175/jcli-d-16-0765.1, 3743-3769.

3852 Wang, L., T. Li, L. Chen, S. K. Behera, and T. Nasuno (2018c), Modulation of the MJO intensity over the
3853 equatorial western Pacific by two types of El Niño, *Climate Dyn.*, *51*, 10.1007/s00382-017-3949-6, 687-
3854 700.

3855 Wang, S., A. H. Sobel, A. Fridlind, Z. Feng, J. M. Comstock, P. Minnis, and M. L. Nordeen (2015),
3856 Simulations of cloud-radiation interaction using large-scale forcing derived from the CINDY/DYNAMO
3857 northern sounding array, *Journal of Advances in Modeling Earth Systems*, *7*, 10.1002/2015MS000461,
3858 1472-1498.

3859 Wang, S., A. H. Sobel, M. K. Tippett, and F. Vitart (2019c), Prediction and predictability of tropical
3860 intraseasonal convection: seasonal dependence and the Maritime Continent prediction barrier, *Climate*
3861 *Dyn.*, *52*, 10.1007/s00382-018-4492-9, 6015-6031.

3862 Wang, S., M. K. Tippett, A. H. Sobel, Z. K. Martin, and F. Vitart (2019d), Impact of the QBO on Prediction
3863 and Predictability of the MJO Convection, *Journal of Geophysical Research: Atmospheres*, *124*,
3864 10.1029/2019jd030575, 11766-11782.

3865 Wang, W., M.-P. Hung, S. Weaver, A. Kumar, and X. Fu (2014), MJO prediction in the NCEP Climate
3866 Forecast System version 2, *Climate Dyn.* 10.1007/s00382-013-1806-9, 1-12.

3867 Wang, W. Q., and M. E. Schlesinger (1999), The dependence on convection parameterization of the tropical
3868 intraseasonal oscillation simulated by the UIUC 11-layer atmospheric GCM, *J. Clim.*, *12*, 1423-1457.

3869 Wang, Y., G. J. Zhang, and G. C. Craig (2016b), Stochastic convective parameterization improving the
3870 simulation of tropical precipitation variability in the NCAR CAM5, *Geophys. Res. Lett.*, *43*,
3871 10.1002/2016GL069818, 6612-6619.

3872 Wang, Z., W. Li, M. S. Peng, X. Jiang, R. McTaggart-Cowan, and C. A. Davis (2018d), Predictive Skill and
3873 Predictability of North Atlantic Tropical Cyclogenesis in Different Synoptic Flow Regimes, *J. Atmos.*
3874 *Sci.*, *75*, 10.1175/jas-d-17-0094.1, 361-378.

3875 Weber, N. J., and C. F. Mass (2017), Evaluating CFSv2 Subseasonal Forecast Skill with an Emphasis on
3876 Tropical Convection, *Mon. Weather Rev.*, *145*, 10.1175/MWR-D-17-0109.1, 3795-3815.

3877 Weber, N. J., and C. F. Mass (2019), Subseasonal Weather Prediction in a Global Convection-Permitting
3878 Model, *Bull. Am. Meteorol. Soc.*, *100*, 10.1175/bams-d-18-0210.1, 1079-1089.

3879 Webster, P. J., and J. R. Holton (1982), Cross-Equatorial Response to Middle-Latitude Forcing in a Zonally
3880 Varying Basic State, *J. Atmos. Sci.*, *39*, 10.1175/1520-0469(1982)039<0722:Certml>2.0.Co;2, 722-733.

3881 Webster, P. J., and R. Lukas (1992), TOGA COARE: The Coupled Ocean–Atmosphere Response
3882 Experiment, *Bull. Am. Meteorol. Soc.*, *73*, 1377-1416.

3883 Webster, P. J., V. O. Magana, T. N. Palmer, J. Shukla, R. A. Tomas, M. Yanai, and T. Yasunari (1998),
3884 Monsoons: Processes, predictability, and the prospects for prediction, *J. Geophys. Res.*, *103*, 14451-
3885 14510.

3886 Weisheimer, A., S. Corti, T. Palmer, and F. Vitart (2014), Addressing model error through atmospheric
3887 stochastic physical parametrizations: impact on the coupled ECMWF seasonal forecasting system,
3888 *Philosophical Transactions of the Royal Society A: Mathematical, Physical and Engineering Sciences*,
3889 *372*, 10.1098/rsta.2013.0290, 20130290.

3890 Wheeler, M., and G. N. Kiladis (1999), Convectively coupled equatorial waves: Analysis of clouds and
3891 temperature in the wavenumber-frequency domain, *J. Atmos. Sci.*, *56*, 374-399.

3892 Wheeler, M., and E. Maloney (2013), Madden-Julian Oscillation (MJO) Task Force: a joint effort of the
3893 climate and weather communities, *CLIVAR Exchanges*. No. 61 (Vol 18 No.1).

3894 Wheeler, M. C., and H. H. Hendon (2004), An All-Season Real-Time Multivariate MJO Index:
3895 Development of an Index for Monitoring and Prediction, *Mon. Weather Rev.*, *132*, 1917-1932.

3896 Wheeler, M. C., H. H. Hendon, S. Cleland, H. Meinke, and A. Donald (2009), Impacts of the Madden-Julian
3897 Oscillation on Australian Rainfall and Circulation, *J. Clim.*, *22*, 10.1175/2008jcli2595.1, 1482-1498.

3898 Whelan, J., and J. S. Frederiksen (2017), Dynamics of the perfect storms: La Niña and Australia's extreme
3899 rainfall and floods of 1974 and 2011, *Climate Dyn.*, *48*, 10.1007/s00382-016-3312-3, 3935-3948.

3900 Wilson, E. A., A. L. Gordon, and D. Kim (2013), Observations of the Madden Julian Oscillation during
3901 Indian Ocean Dipole events, *Journal of Geophysical Research: Atmospheres*, *118*, 10.1002/jgrd.50241,
3902 2588-2599.

3903 Wolding, B. O., and E. D. Maloney (2015), Objective Diagnostics and the Madden-Julian Oscillation. Part
3904 II: Application to Moist Static Energy and Moisture Budgets, *J. Clim.*, *28*, 10.1175/jcli-d-14-00689.1,
3905 7786-7808.

3906 Wolding, B. O., E. D. Maloney, S. Henderson, and M. Branson (2017), Climate change and the Madden-
3907 Julian oscillation: A vertically resolved weak temperature gradient analysis, *Journal of Advances in*
3908 *Modeling Earth Systems* 10.1002/2016MS000843, n/a-n/a.

3909 Woolnough, S. J., J. M. Slingo, and B. J. Hoskins (2000), The Relationship between Convection and Sea
3910 Surface Temperature on Intraseasonal Timescales, *J. Clim.*, *13*, 2086-2104.

3911 Woolnough, S. J., F. Vitart, and M. A. Balmaseda (2007), The role of the ocean in the Madden-Julian
3912 Oscillation: Implications for MJO prediction, *Quart. J. Roy. Meteor. Soc.*, *133*, 10.1002/qj.4, 117-128.

3913 Wu, C.-H., and H.-H. Hsu (2009), Topographic Influence on the MJO in the Maritime Continent, *J. Clim.*,
3914 *22*, doi:10.1175/2009JCLI2825.1, 5433-5448.

3915 Wu, P., D. Ardiansyah, S. Yokoi, S. Mori, F. Syamsudin, and K. Yoneyama (2017), Why Torrential Rain
3916 Occurs on the Western Coast of Sumatra Island at the Leading Edge of the MJO Westerly Wind Bursts,
3917 *SOLA*, *13*, 10.2151/sola.2017-007, 36-40.

3918 Wu, P., S. Mori, and F. Syamsudin (2018), Land-sea surface air temperature contrast on the western coast of
3919 Sumatra Island during an active phase of the Madden-Julian Oscillation, *Progress in Earth and Planetary*
3920 *Science*, *5*, 10.1186/s40645-017-0160-7, 4.

3921 Xavier, P. K., J. C. Petch, N. P. Klingaman, S. J. Woolnough, X. Jiang, D. E. Waliser, M. Caian, J. Cole, S.
3922 M. Hagos, C. Hannay, D. Kim, T. Miyakawa, M. S. Pritchard, R. Roehrig, E. Shindo, F. Vitart, and H.
3923 Wang (2015), Vertical structure and physical processes of the Madden-Julian Oscillation: Biases and
3924 uncertainties at short range, *Journal of Geophysical Research: Atmospheres*, *120*,
3925 10.1002/2014JD022718, 4749-4763.

3926 Xiang, B., S.-J. Lin, M. Zhao, S. Zhang, G. Vecchi, T. Li, X. Jiang, L. Harris, and J.-H. Chen (2015a),
3927 Beyond Weather Time-Scale Prediction for Hurricane Sandy and Super Typhoon Haiyan in a Global
3928 Climate Model, *Mon. Weather Rev.*, *143*, 10.1175/MWR-D-14-00227.1, 524-535.

3929 Xiang, B., M. Zhao, X. Jiang, S.-J. Lin, T. Li, X. Fu, and G. Vecchi (2015b), 3-4 week MJO prediction skill
3930 in a GFDL Coupled Model, *J. Clim.* 10.1175/JCLI-D-15-0102.1.

3931 Xiang, B., Q. Sun, J.-H. Chen, N. C. Johnson, and X. Jiang (2020), Subseasonal prediction of land cold
3932 extremes in boreal wintertime, *Journal of Geophysical Research: Atmospheres*.

3933 Xie, S.-P., C. Deser, G. A. Vecchi, J. Ma, H. Teng, and A. T. Wittenberg (2010), Global Warming Pattern
3934 Formation: Sea Surface Temperature and Rainfall, *J. Clim.*, *23*, 10.1175/2009jcli3329.1, 966-986.

3935 Xu, W., and S. A. Rutledge (2014), Convective Characteristics of the Madden-Julian Oscillation over the
3936 Central Indian Ocean Observed by Shipborne Radar during DYNAMO, *J. Atmos. Sci.*, *71*, 10.1175/JAS-
3937 D-13-0372.1, 2859-2877.

3938 Xu, W., and S. A. Rutledge (2015), Morphology, Intensity, and Rainfall Production of MJO Convection:
3939 Observations from DYNAMO Shipborne Radar and TRMM, *J. Atmos. Sci.*, *72*, 10.1175/jas-d-14-0130.1,
3940 623-640.

3941 Xu, W., S. A. Rutledge, C. Schumacher, and M. Katsumata (2015), Evolution, Properties, and Spatial
3942 Variability of MJO Convection near and off the Equator during DYNAMO, *J. Atmos. Sci.*, *72*,
3943 10.1175/jas-d-15-0032.1, 4126-4147.

3944 Xu, W., and S. A. Rutledge (2016), Time scales of shallow-to-deep convective transition associated with the
3945 onset of Madden-Julian Oscillations, *Geophys. Res. Lett.*, *43*, 10.1002/2016GL068269, 2880-2888.

3946 Yadav, P., and D. M. Straus (2017), Circulation Response to Fast and Slow MJO Episodes, *Mon. Weather*
3947 *Rev.*, *145*, 10.1175/mwr-d-16-0352.1, 1577-1596.

3948 Yanai, M., and M.-M. Lu (1983), Equatorially Trapped Waves at the 200 mb Level and Their Association
3949 with Meridional Convergence of Wave Energy Flux, *J. Atmos. Sci.*, *40*, 10.1175/1520-
3950 0469(1983)040<2785:Etwatm>2.0.Co;2, 2785-2803.

3951 Yang, D., and A. P. Ingersoll (2013), Triggered Convection, Gravity Waves, and the MJO: A Shallow-Water
3952 Model, *J. Atmos. Sci.*, *70*, 10.1175/JAS-D-12-0255.1, 2476-2486.

3953 Yang, D., and A. P. Ingersoll (2014), A theory of the MJO horizontal scale, *Geophys. Res. Lett.*, *41*,
3954 10.1002/2013GL058542, 1059-1064.

3955 Yang, D., Á. F. Adames-Corraliza, B. Khouider, B. Wang, and C. Zhang (2020), A Review of MJO
3956 Theories. Chap. 19 in *The Multiscale Global Monsoon System*, eds: C.P. Chang, K.J. Ha, R. H. Johnson,
3957 D. Kim, G.N. Lau, B. Wang. World Scientific Series on Asia-Pacific Weather and Climate, Vol. 11.
3958 World Scientific, Singapore., edited.

3959 Yang, G.-Y., and J. Slingo (2001a), The Diurnal Cycle in the Tropics, *Mon. Weather Rev.*, *129*,
3960 10.1175/1520-0493(2001)129<0784:Tdcitt>2.0.Co;2, 784-801.

3961 Yang, G. Y., and J. Slingo (2001b), The diurnal cycle in the Tropics, *Mon. Weather Rev.*, *129*, 784-801.

3962 Yang, Q., Q. Fu, and Y. Hu (2010), Radiative impacts of clouds in the tropical tropopause layer, *Journal of*
3963 *Geophysical Research: Atmospheres*, *115*, 10.1029/2009JD012393.

3964 Yang, Q., A. J. Majda, and M. W. Moncrieff (2019), Upscale Impact of Mesoscale Convective Systems and
3965 Its Parameterization in an Idealized GCM for an MJO Analog above the Equator, *J. Atmos. Sci.*, *76*,
3966 10.1175/jas-d-18-0260.1, 865-892.

3967 Yano, J.-I., and J. J. Tribbia (2017), Tropical Atmospheric Madden–Julian Oscillation: A Strongly Nonlinear
3968 Free Solitary Rossby Wave?, *J. Atmos. Sci.*, *74*, 10.1175/JAS-D-16-0319.1, 3473-3489.

3969 Yasunaga, K., and B. Mapes (2012), Differences between More Divergent and More Rotational Types of
3970 Convectively Coupled Equatorial Waves. Part II: Composite Analysis based on Space–Time Filtering, *J.*
3971 *Atmos. Sci.*, *69*, 10.1175/jas-d-11-034.1, 17-34.

3972 Yokoi, S., M. Katsumata, and K. Yoneyama (2014), Variability in surface meteorology and air-sea fluxes
3973 due to cumulus convective systems observed during CINDY/DYNAMO, *Journal of Geophysical*
3974 *Research: Atmospheres*, *119*, 10.1002/2013JD020621, 2013JD020621.

3975 Yokoi, S., and A. H. Sobel (2015), Intraseasonal Variability and Seasonal March of the Moist Static Energy
3976 Budget over the Eastern Maritime Continent during CINDY2011/DYNAMO, *Journal of the*
3977 *Meteorological Society of Japan. Ser. II*, *93A*, 10.2151/jmsj.2015-041, 81-100.

3978 Yokoi, S., S. Mori, M. Katsumata, B. Geng, K. Yasunaga, F. Syamsudin, Nurhayati, and K. Yoneyama
3979 (2017), Diurnal Cycle of Precipitation Observed in the Western Coastal Area of Sumatra Island: Offshore
3980 Preconditioning by Gravity Waves, *Mon. Weather Rev.*, *145*, 10.1175/mwr-d-16-0468.1, 3745-3761.

3981 Yokoi, S., S. Mori, F. Syamsudin, U. Haryoko, and B. Geng (2019), Environmental Conditions for
3982 Nighttime Offshore Migration of Precipitation Area as Revealed by In Situ Observation off Sumatra
3983 Island, *Mon. Weather Rev.*, *147*, 10.1175/mwr-d-18-0412.1, 3391-3407.

3984 Yoneyama, K., C. Zhang, and C. N. Long (2013), Tracking Pulses of the Madden–Julian Oscillation, *Bull.*
3985 *Am. Meteorol. Soc.*, *94*, 10.1175/BAMS-D-12-00157.1, 1871-1891.

3986 Yoneyama, K., and C. Zhang (2020), Years of the Maritime Continent, *Geophys. Res. Lett.*, *47*,
3987 10.1029/2020GL087182, e2020GL087182.

3988 Yoo, C., S. Feldstein, and S. Lee (2011), The impact of the Madden-Julian Oscillation trend on the Arctic
3989 amplification of surface air temperature during the 1979–2008 boreal winter, *Geophys. Res. Lett.*, *38*,
3990 10.1029/2011GL049881, L24804.

3991 Yoo, C., S. Lee, and S. B. Feldstein (2012), Mechanisms of Arctic Surface Air Temperature Change in
3992 Response to the Madden–Julian Oscillation, *J. Clim.*, *25*, 10.1175/JCLI-D-11-00566.1, 5777-5790.

3993 Yoo, C., and S.-W. Son (2016), Modulation of the boreal wintertime Madden-Julian oscillation by the
3994 stratospheric quasi-biennial oscillation, *Geophys. Res. Lett.*, *43*, 10.1002/2016GL067762, 1392-1398.

3995 Yu, J. Y., and J. D. Neelin (1994), Modes of Tropical Variability under Convective Adjustment and the
3996 Madden-Julian Oscillation .2. Numerical Results, *J. Atmos. Sci.*, *51*, 1895-1914.

3997 Yuan, J., and R. A. Houze (2010), Global Variability of Mesoscale Convective System Anvil Structure from
3998 A-Train Satellite Data, *J. Clim.*, *23*, 10.1175/2010jcli3671.1, 5864-5888.

3999 Yuan, J., and R. A. Houze (2012), Deep Convective Systems Observed by A-Train in the Tropical Indo-
4000 Pacific Region Affected by the MJO, *J. Atmos. Sci.*, *70*, 10.1175/jas-d-12-057.1, 465-486.

4001 Zadra, A., K. Williams, A. Frassoni, M. Rixen, Á. F. Adames, J. Berner, F. Bouysse, B. Casati, H.
4002 Christensen, M. B. Ek, G. Flato, Y. Huang, F. Judt, H. Lin, E. Maloney, W. Merryfield, A. V. Niekerk, T.
4003 Rackow, K. Saito, N. Wedi, and P. Yadav (2018), Systematic Errors in Weather and Climate Models:
4004 Nature, Origins, and Ways Forward, *Bull. Am. Meteorol. Soc.*, *99*, 10.1175/bams-d-17-0287.1, ES67-
4005 ES70.

4006 Zeng, Z., S.-P. Ho, S. Sokolovskiy, and Y.-H. Kuo (2012), Structural evolution of the Madden-Julian
4007 Oscillation from COSMIC radio occultation data, *Journal of Geophysical Research: Atmospheres*, *117*,
4008 10.1029/2012JD017685, D22108.

4009 Zermeño-Díaz, D. M., C. Zhang, P. Kollias, and H. Kalesse (2015), The Role of Shallow Cloud Moistening
4010 in MJO and Non-MJO Convective Events over the ARM Manus Site, *J. Atmos. Sci.*, *72*, 10.1175/jas-d-
4011 14-0322.1, 4797-4820.

4012 Zhang, C., and P. J. Webster (1989), Effects of Zonal Flows on Equatorially Trapped Waves, *J. Atmos. Sci.*,
4013 *46*, 10.1175/1520-0469(1989)046<3632:Eozfoe>2.0.Co;2, 3632-3652.

4014 Zhang, C. (1996), Atmospheric Intraseasonal Variability at the Surface in the Tropical Western Pacific
4015 Ocean, *J. Atmos. Sci.*, *53*, 739-758.

4016 Zhang, C., and H. H. Hendon (1997), Propagating and Standing Components of the Intraseasonal
4017 Oscillation in Tropical Convection, *J. Atmos. Sci.*, *54*, doi:10.1175/1520-
4018 0469(1997)054<0741:PASCOT>2.0.CO;2, 741-752.

4019 Zhang, C., and J. Gottschalck (2002), SST Anomalies of ENSO and the Madden–Julian Oscillation in the
4020 Equatorial Pacific, *J. Clim.*, *15*, 10.1175/1520-0442(2002)015<2429:SAOEAT>2.0.CO;2, 2429-2445.

4021 Zhang, C., J. Ling, S. Hagos, W.-K. Tao, S. Lang, Y. N. Takayabu, S. Shige, M. Katsumata, W. S. Olson,
4022 and T. L'Ecuyer (2010), MJO Signals in Latent Heating: Results from TRMM Retrievals, *J. Atmos. Sci.*,
4023 67, 10.1175/2010jas3398.1, 3488-3508.

4024 Zhang, C. (2012), Vertical structure from recent observations, in *Intraseasonal Variability in the*
4025 *Atmosphere-Ocean Climate System*, edited by W. K. M. Lau and D. E. Waliser, Springer, Heidelberg,
4026 Germany.

4027 Zhang, C., and J. Ling (2012), Potential Vorticity of the Madden–Julian Oscillation, *J. Atmos. Sci.*, 69,
4028 10.1175/JAS-D-11-081.1, 65-78.

4029 Zhang, C. (2013), Madden–Julian Oscillation: Bridging Weather and Climate, *Bull. Am. Meteorol. Soc.*, 94,
4030 10.1175/bams-d-12-00026.1, 1849-1870.

4031 Zhang, C., J. Gottschalck, E. D. Maloney, M. W. Moncrieff, F. Vitart, D. E. Waliser, B. Wang, and M. C.
4032 Wheeler (2013), Cracking the MJO nut, *Geophys. Res. Lett.*, 40, 10.1002/grl.50244, 1223-1230.

4033 Zhang, C., and J. Ling (2017), Barrier Effect of the Indo-Pacific Maritime Continent on the MJO:
4034 Perspectives from Tracking MJO Precipitation, *J. Clim.*, 30, 10.1175/JCLI-D-16-0614.1, 3439-3459.

4035 Zhang, C., and B. Zhang (2018), QBO-MJO Connection, *Journal of Geophysical Research: Atmospheres*,
4036 123, 10.1002/2017jd028171, 2957-2967.

4037 Zhang, C., Á. F. Adames, B. Khouider, B. Wang, and D. Yang (2020), FOUR THEORIES OF THE
4038 MADDEN-JULIAN OSCILLATION, *Rev. Geophys.* 10.1029/2019RG000685, e2019RG000685.

4039 Zhang, C. D., and M. J. McPhaden (2000), Intraseasonal surface cooling in the equatorial western Pacific, *J.*
4040 *Clim.*, 13, 2261-2276.

4041 Zhang, C. D., and M. Dong (2004), Seasonality in the Madden-Julian oscillation, *J. Clim.*, 17, 3169-3180.

4042 Zhang, C. D. (2005), Madden-Julian oscillation, *Rev. Geophys.*, 43, RG2003, DOI: 10.1029/2004RG000158,
4043 36.

4044 Zhang, C. D., M. Dong, S. Gualdi, H. H. Hendon, E. D. Maloney, A. Marshall, K. R. Sperber, and W. Q.
4045 Wang (2006), Simulations of the Madden-Julian oscillation in four pairs of coupled and uncoupled global
4046 models, *Climate Dyn.*, 27, 573-592.

4047 Zhang, D., M. F. Cronin, C. Meinig, J. T. Farrar, R. Jenkins, D. Peacock, J. Keene, A. Sutton, and Q. Yang
4048 (2019), Comparing Air-Sea Flux Measurements from a New Unmanned Surface Vehicle and Proven
4049 Platforms During the SPURS-2 Field Campaign, *Oceanography*, 32,
4050 <https://doi.org/10.5670/oceanog.2019.220>, 122-133.

4051 Zhang, G. J., and M. Mu (2005), Simulation of the Madden–Julian Oscillation in the NCAR CCM3 Using a
4052 Revised Zhang–McFarlane Convection Parameterization Scheme, *J. Clim.*, 18, 10.1175/jcli3508.1, 4046-
4053 4064.

4054 Zhang, G. J., and X. L. Song (2009), Interaction of deep and shallow convection is key to Madden-Julian
4055 Oscillation simulation, *Geophys. Res. Lett.*, 36, Doi 10.1029/2009gl037340.

4056 Zhao, N., and T. Nasuno (2020), How Does the Air-Sea Coupling Frequency Affect Convection During the
4057 MJO Passage?, *Journal of Advances in Modeling Earth Systems*, *12*, 10.1029/2020MS002058,
4058 e2020MS002058.

4059 Zheng, C., E. K.-M. Chang, H.-M. Kim, M. Zhang, and W. Wang (2018), Impacts of the Madden–Julian
4060 Oscillation on Storm-Track Activity, Surface Air Temperature, and Precipitation over North America, *J.*
4061 *Clim.*, *31*, 10.1175/jcli-d-17-0534.1, 6113-6134.

4062 Zhou, L., R. B. Neale, M. Jochum, and R. Murtugudde (2012a), Improved Madden-Julian Oscillations with
4063 Improved Physics: The Impact of Modified Convection Parameterizations, *J. Clim.*, *25*, Doi
4064 10.1175/2011jcli4059.1, 1116-1136.

4065 Zhou, L., and R. Murtugudde (2020), Oceanic Impacts on MJOs Detouring near the Maritime Continent, *J.*
4066 *Clim.*, *33*, 10.1175/jcli-d-19-0505.1, 2371-2388.

4067 Zhou, S., M. L’Heureux, S. Weaver, and A. Kumar (2012b), A composite study of the MJO influence on the
4068 surface air temperature and precipitation over the Continental United States, *Climate Dyn.*, *38*,
4069 10.1007/s00382-011-1001-9, 1459-1471.

4070 Zhu, C., T. Nakazawa, J. Li, and L. Chen (2003), The 30–60 day intraseasonal oscillation over the western
4071 North Pacific Ocean and its impacts on summer flooding in China during 1998, *Geophys. Res. Lett.*, *30*,
4072 10.1029/2003GL017817, 1952.

4073 Zhu, H., and H. H. Hendon (2015), Role of large-scale moisture advection for simulation of the MJO with
4074 increased entrainment, *Quart. J. Roy. Meteor. Soc.*, *141*, 10.1002/qj.2510, 2127-2136.

4075 Zhu, H. Y., H. Hendon, and C. Jakob (2009), Convection in a Parameterized and Superparameterized Model
4076 and Its Role in the Representation of the MJO, *J. Atmos. Sci.*, *66*, Doi 10.1175/2009jas3097.1, 2796-
4077 2811.

4078 Zuluaga, M. D., and R. A. Houze (2013), Evolution of the Population of Precipitating Convective Systems
4079 over the Equatorial Indian Ocean in Active Phases of the Madden–Julian Oscillation, *J. Atmos. Sci.*, *70*,
4080 10.1175/JAS-D-12-0311.1, 2713-2725.

4081

Figure 01.

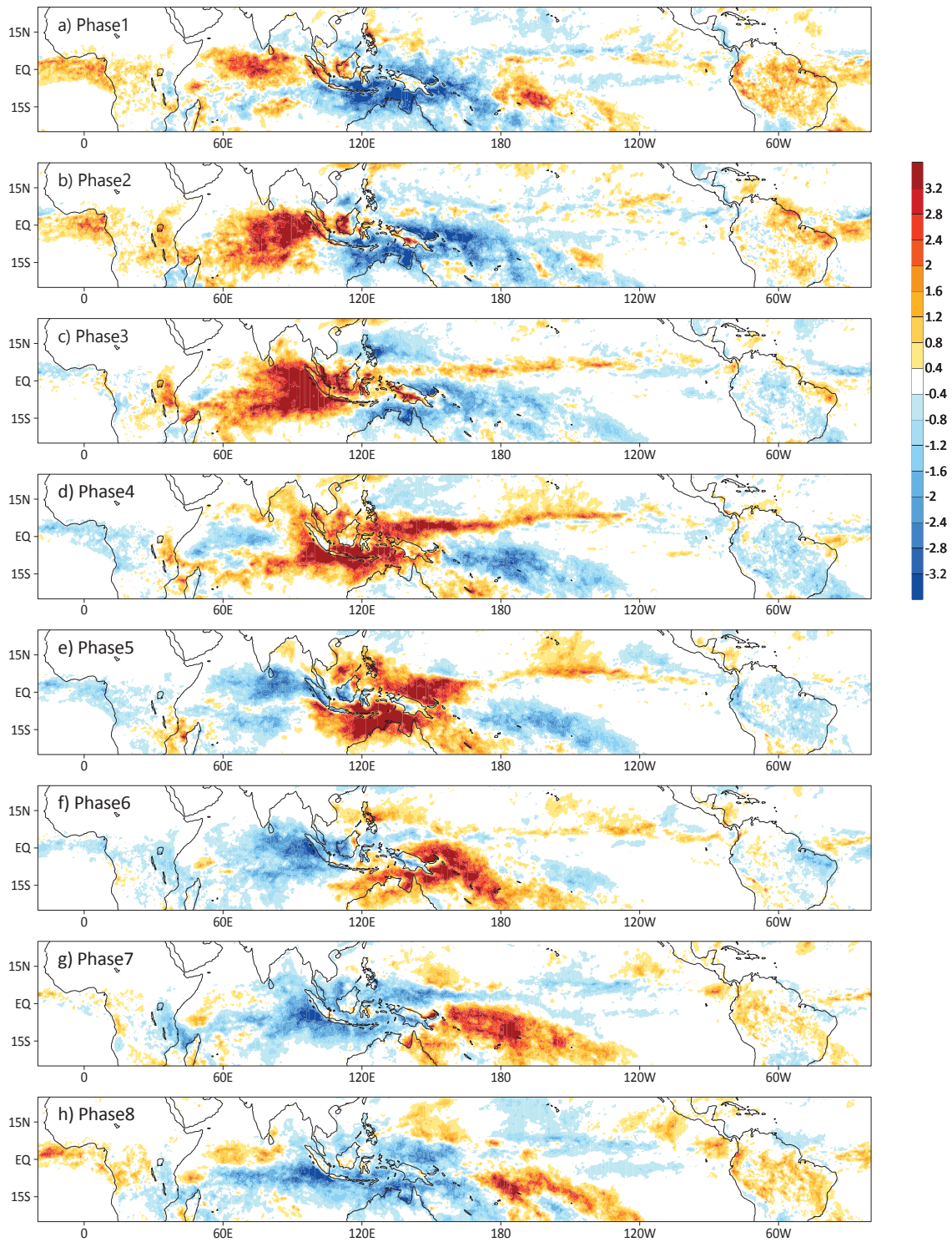


Figure 02.

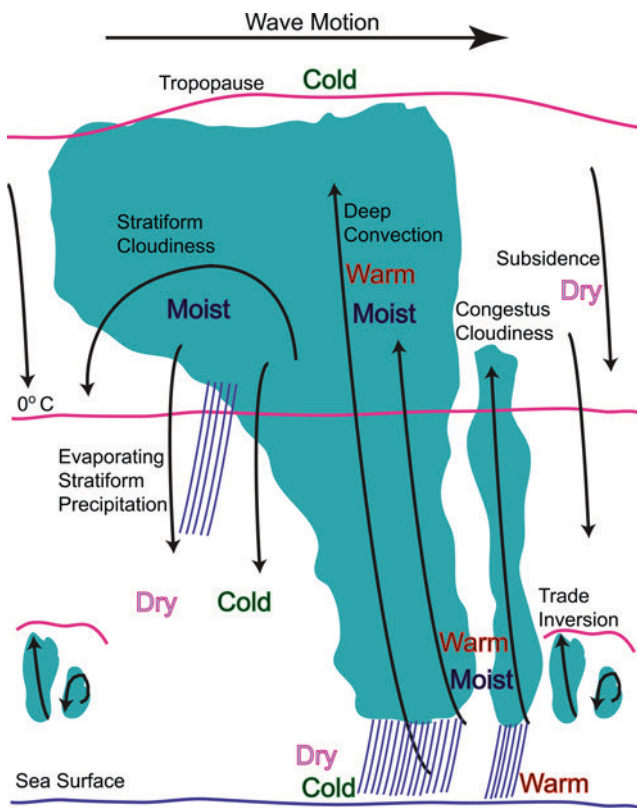


Figure 03.

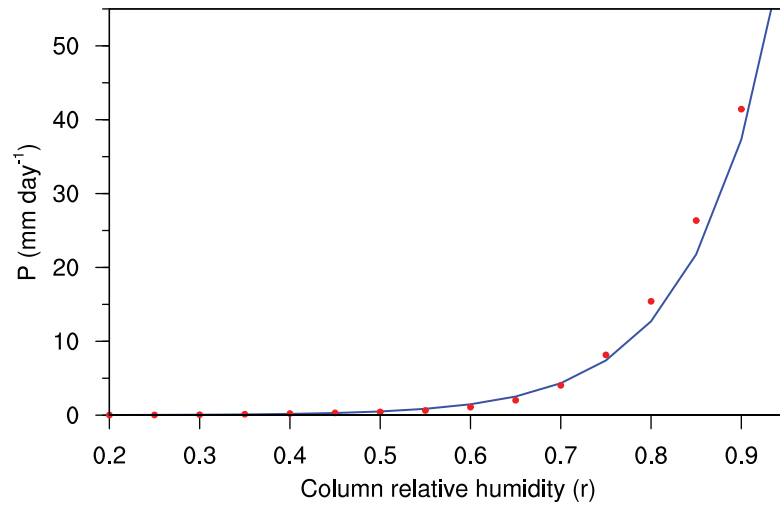


Figure 04.

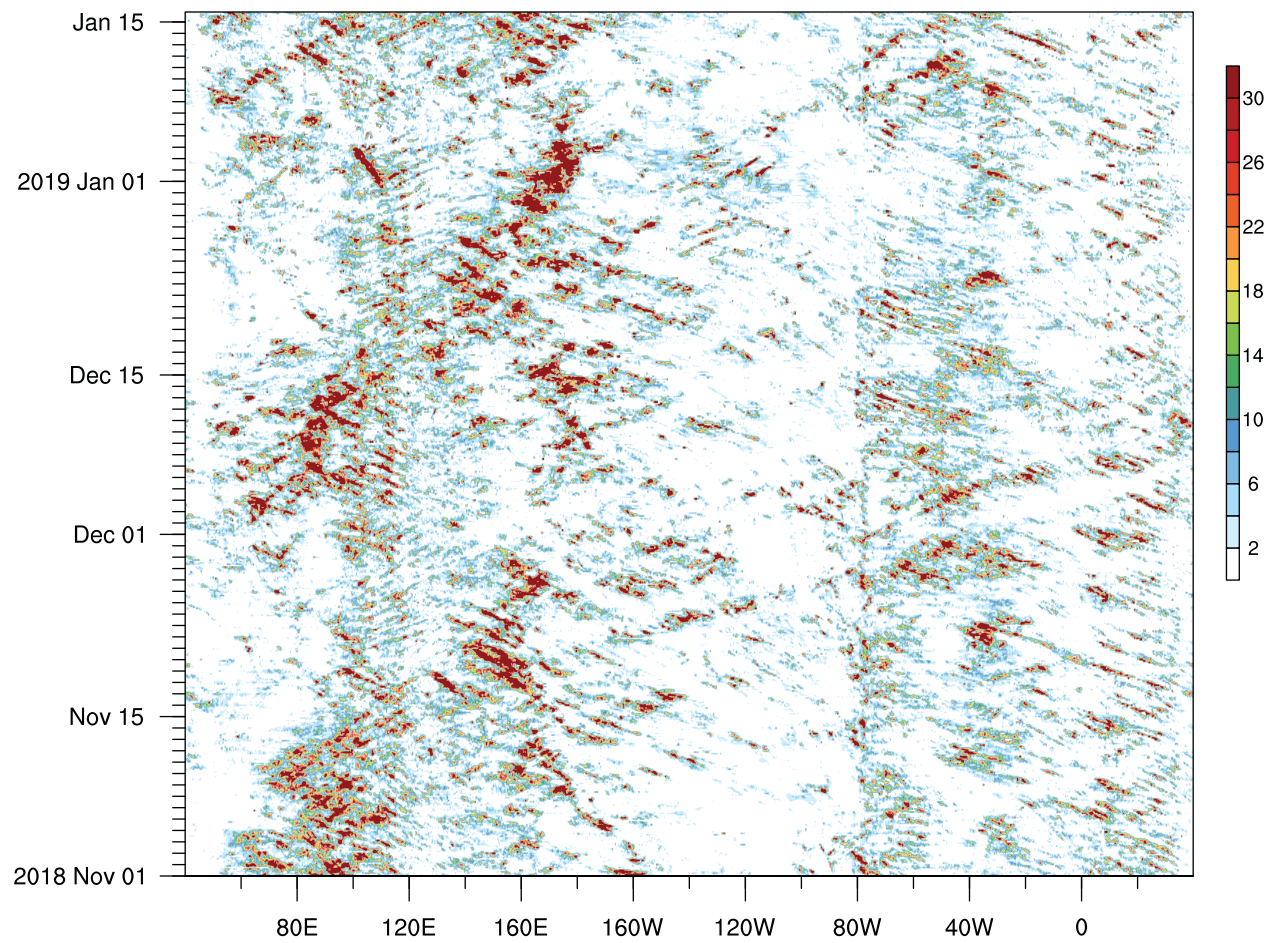
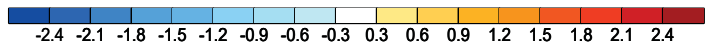
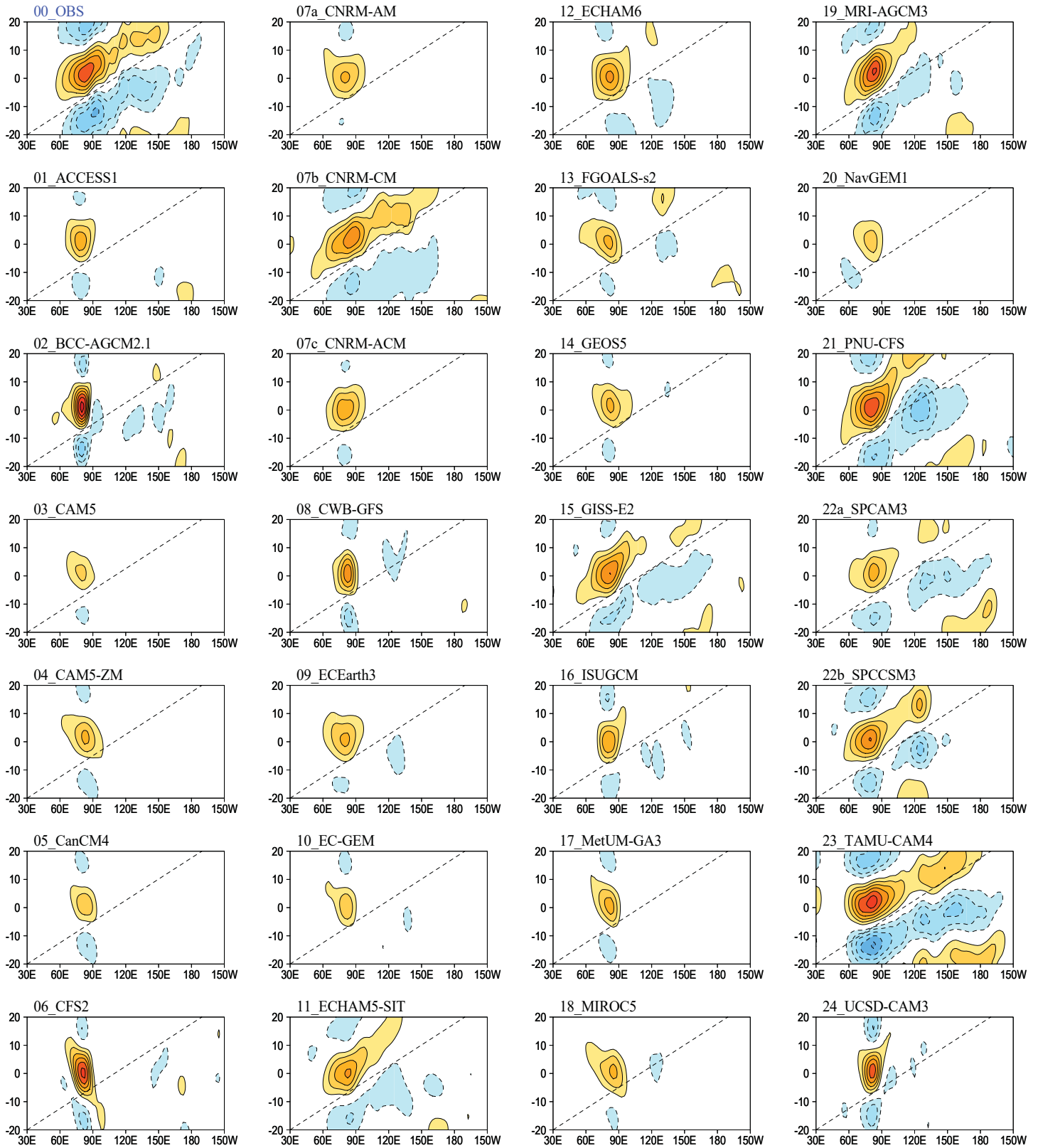
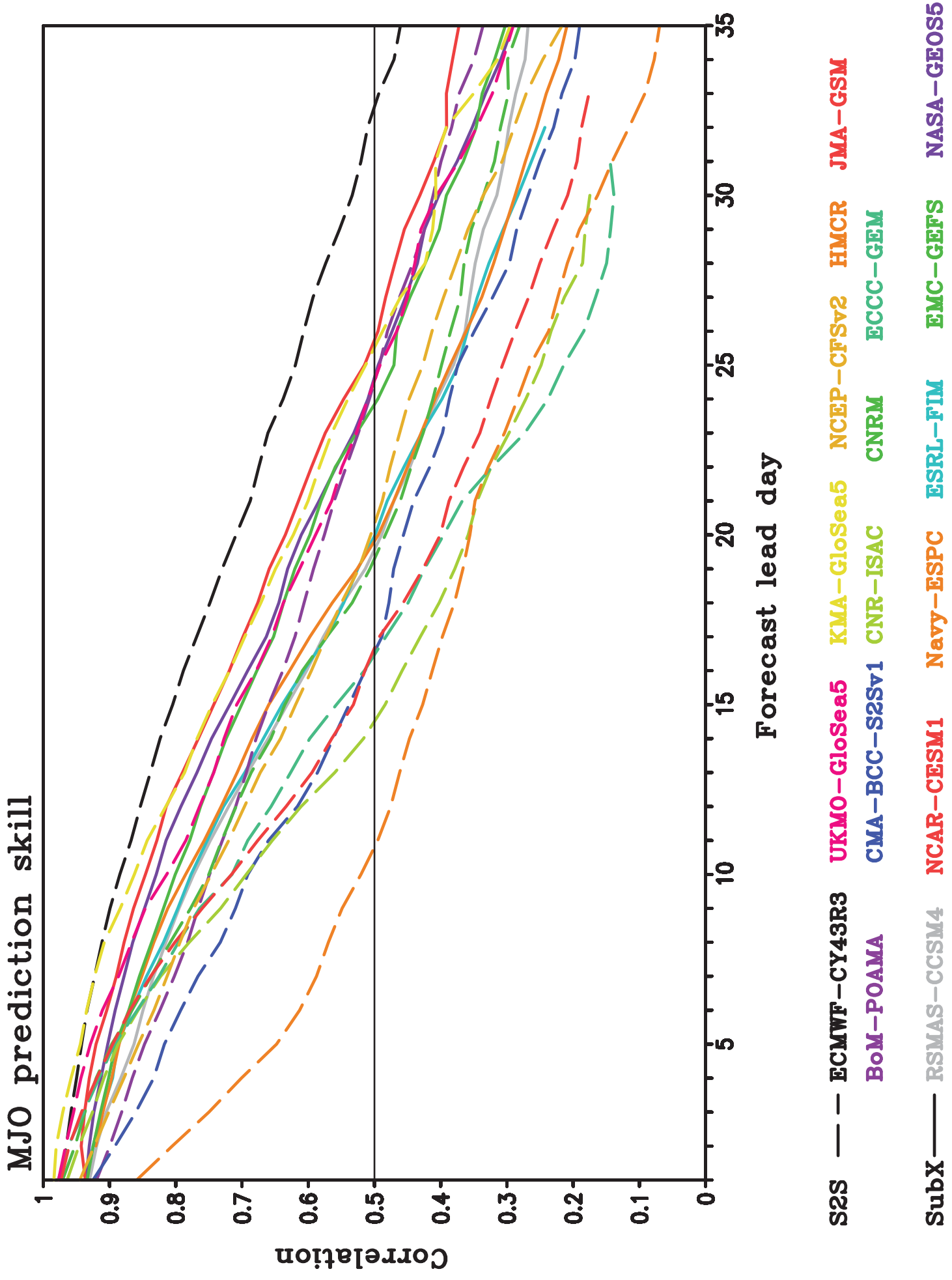


Figure 05.



mm/day

Figure 06.



MJO prediction skill

Correlation

Forecast lead day

- S2S --- ECMWF-CY43R3 UKMO-GloSea5 KMA-GloSea5 NCEP-CFSv2 HMCR JMA-GSM
- BoM-POAMA CMA-BCC-S2Sv1 CNR-ISAC CNRM ECCC-GEM
- SubX — RSMAS-CCSM4 NCAR-CESM1 Navy-ESPC ESRL-FIM EMC-GEFS NASA-GEOS5

Figure 07.

ERA-Interim Nov-Apr

Surface Energy Budget

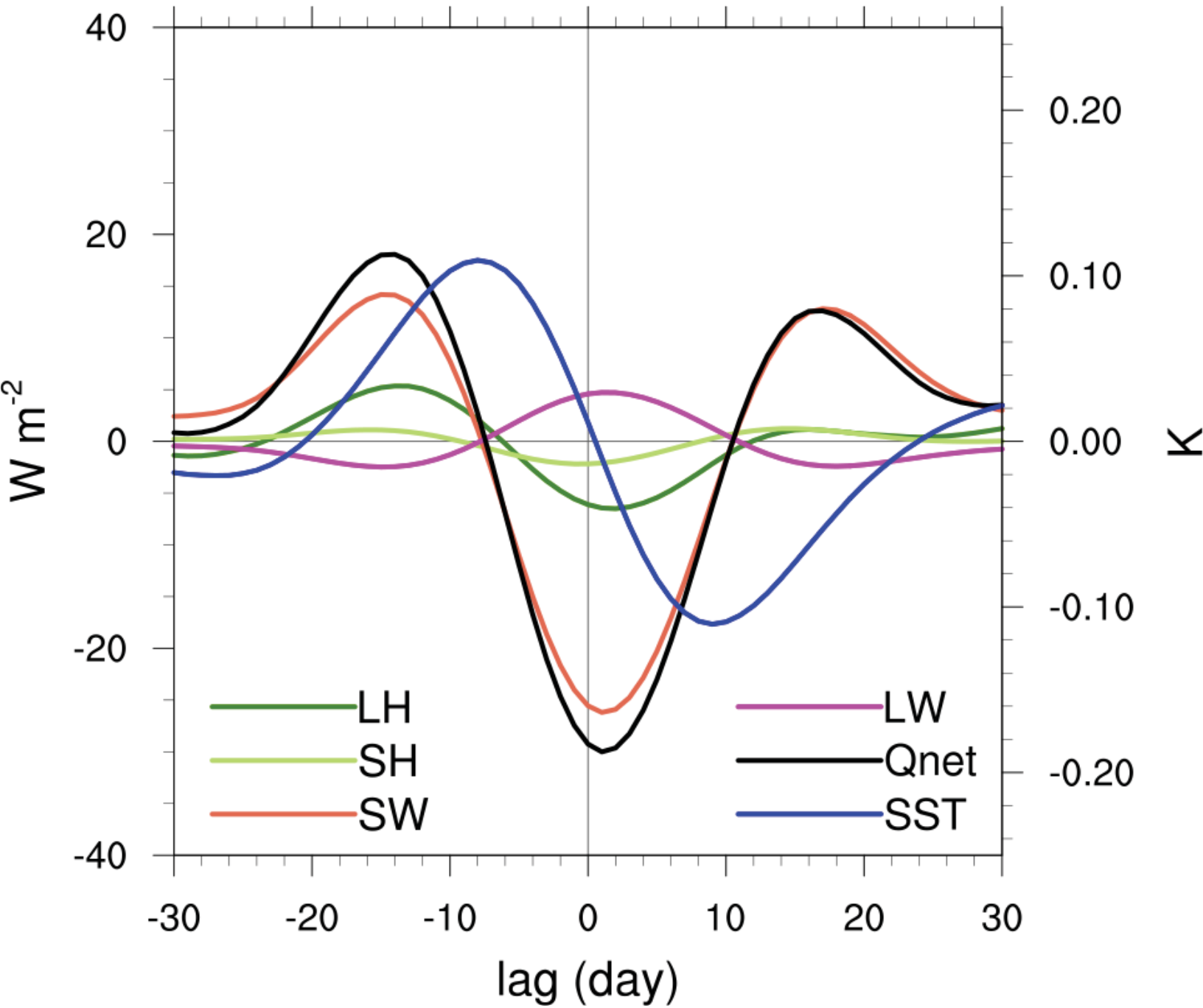


Figure 08.

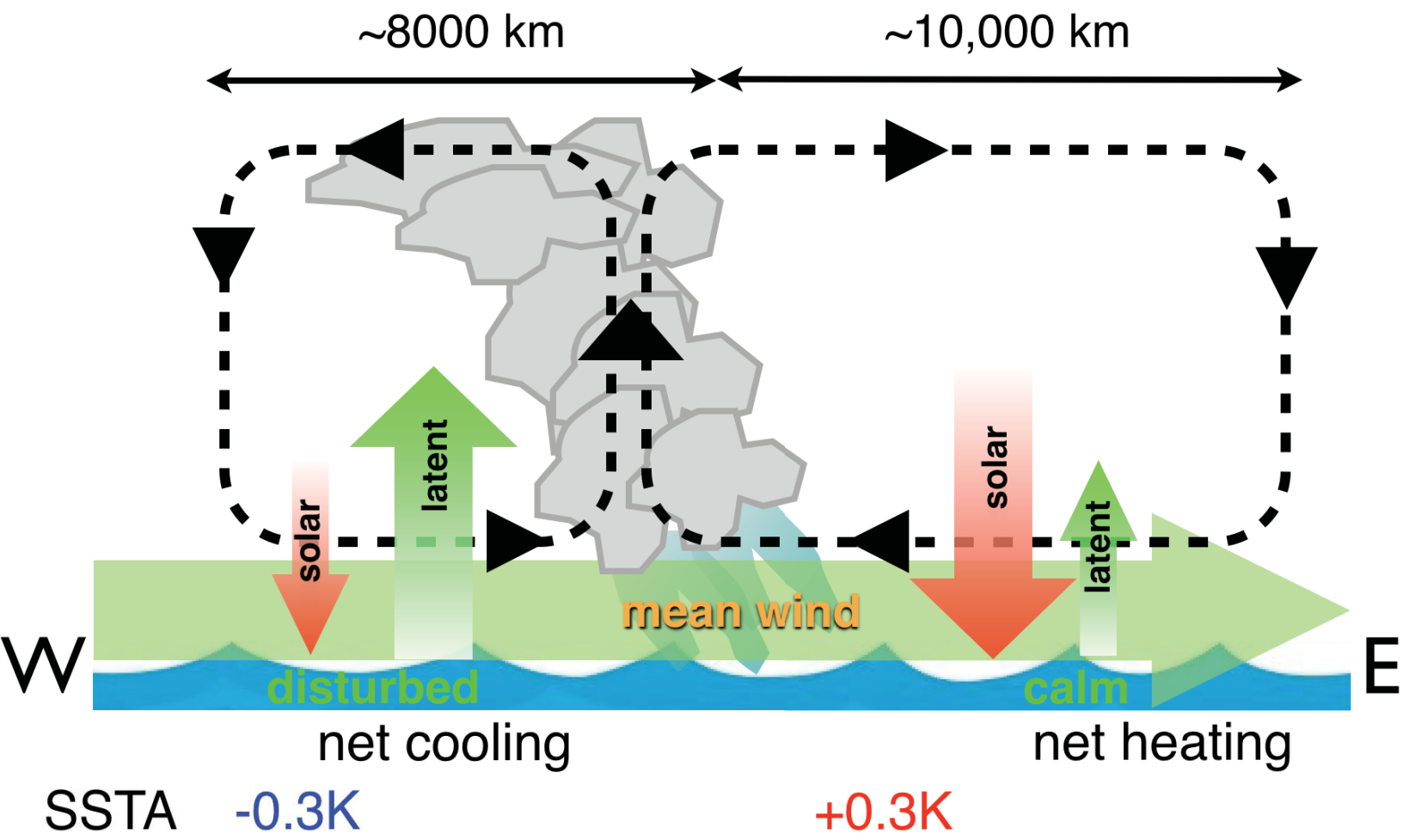


Figure 09.

CWV, Nov-Apr

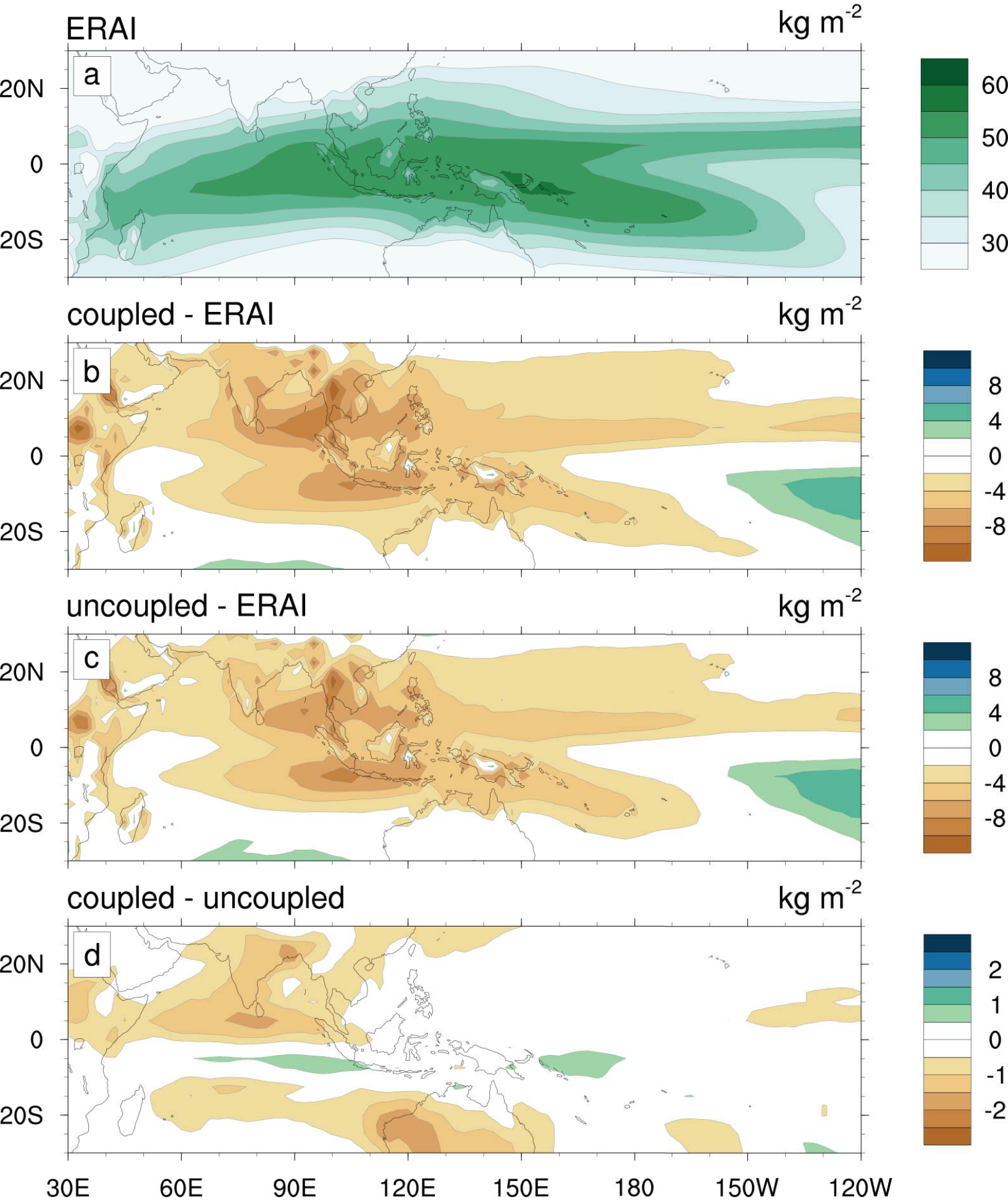
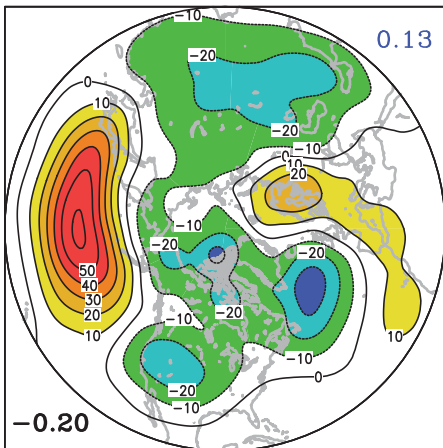
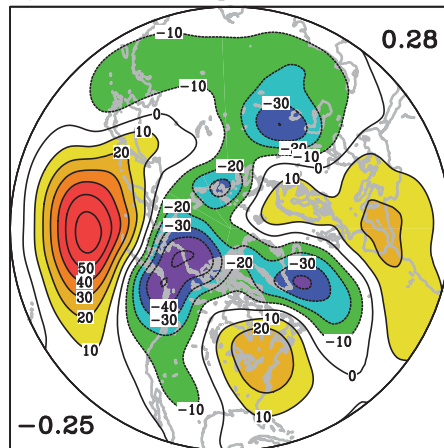


Figure 01.

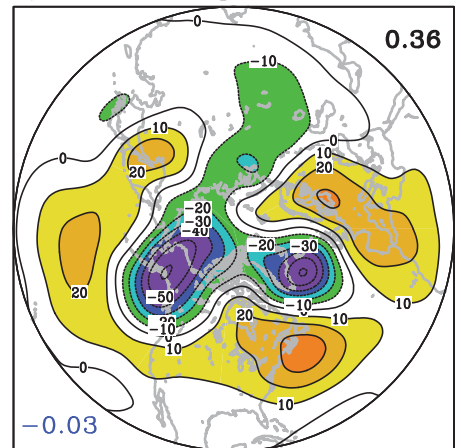
a) PHASE 2 lag=1



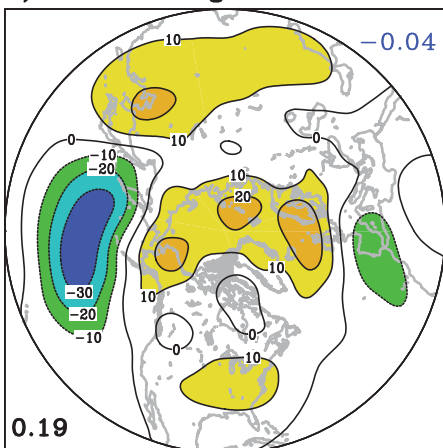
b) PHASE 2 lag=2



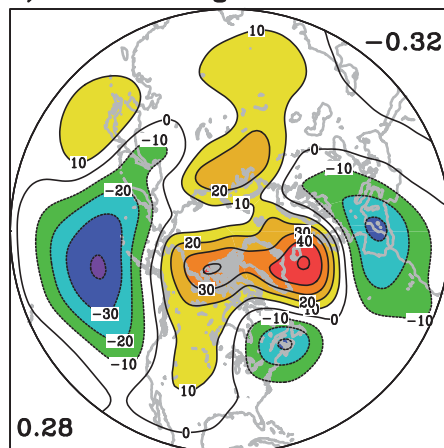
c) PHASE 2 lag=3



d) PHASE 6 lag=1



e) PHASE 6 lag=2



f) PHASE 6 lag=3

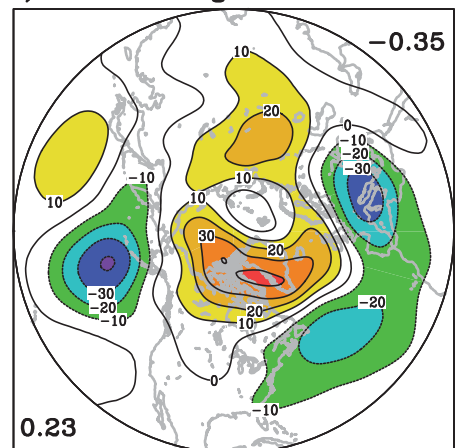


Figure 11.

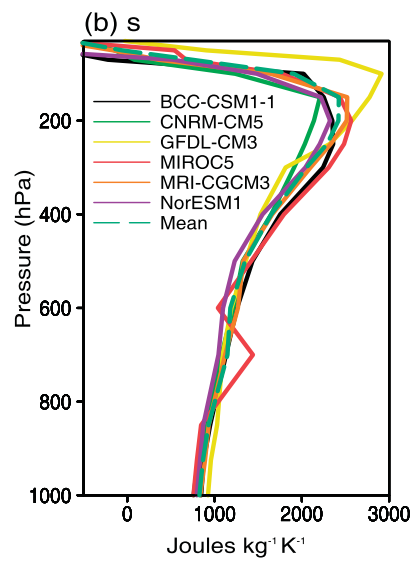
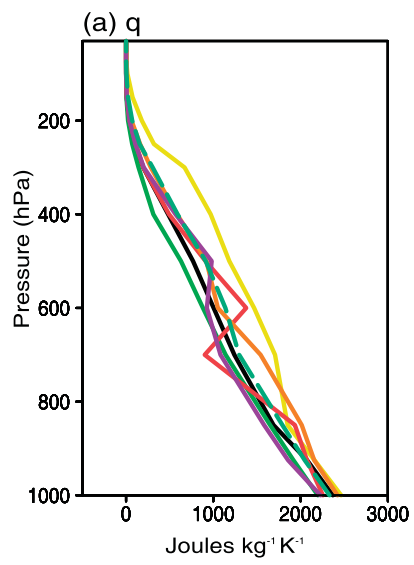


Figure 12.

